

PEDESTRIAN PROTECTION USING A SHOCK ABSORBING LIQUID (SALi) BASED BUMPER SYSTEM

Huw Davies

Karen Holford

Cardiff University School of Engineering

United Kingdom

Alexandre Assoune

Bastien Trioulier

L'institut Français De Mécanique Avancée

France

Bill Courtney

Cheshire Innovation

United Kingdom

Paper Number 09-0027

ABSTRACT

Improving pedestrian protection in vehicle impacts is achieved by the combination of proper shapes and materials in vehicle front end design. This may however conflict with other priorities regarding vehicle impact performance, such as damageability. It would be advantageous to have a single bumper system design that meets global legislative impact requirements. Alternative materials may provide the solution.

The composite material described in this paper is a blend of elastomeric capsules or beads in a matrix of Newtonian fluid. The material, which can be considered as a liquid analogy to elastomeric foams, is referred to as shock absorbing liquid or SALi.

SALi based shock absorbers have the ability to change their energy absorbing properties depending on the type of impact (velocity and size of the impacting body) that they are cushioning. Based on this ability, SALi based shock absorber devices could be beneficial for impact energy management applications because of their attendant response tailorability. However, prior to adopting SALi based devices for impact energy management applications several key issues need to be resolved.

The present study was focused on one of the most significant of these: the verification of the tunability of the response of such devices at different stroking velocities. Impact tests using an assisted drop tower facility were conducted on SALi based energy absorbers for a range of impact velocities. The results of the experimental tests conducted on SALi based shock absorbers are encouraging. The material shows innovative energy absorbing properties. Interpretation of the results described here provide for a better understanding of the fundamental behaviour of SALi based energy absorbers and provide a first step tool in optimising the design of energy absorbing bumper systems.

INTRODUCTION

Pedestrian safety is now a high profile issue within the automotive industry. All new passenger cars are required to provide an effective level of protection for pedestrians and other vulnerable road users in the event of contact. It is therefore prudent to set these standards high so that a larger number of pedestrians are protected in cases where no emergency braking takes place and to focus on the development of technologies that can meet this challenge.

Shock Absorbing Liquid (SALi) [1][2] is an innovative technology that has the potential to deliver a car bumper design that would enhance pedestrian protection without either sacrificing vehicle damageability or significantly increasing the depth of the bumper system. SALi is a mixture of elastomeric capsules – which compress to absorb impact energy – and a viscous matrix fluid – which absorbs energy as the fluid shears when the capsules compress. When packaged correctly, the result is a material that when subject to impact loading is highly efficient in absorbing impact energy and offers smart properties – soft for pedestrian impacts yet stiff for vehicle damageability. The above properties also lend SALi to other pedestrian and occupant safety applications.

However, the effective utilisation of SALi will require the correct combination of materials (with the right elastic and viscous damping properties) and mixture proportions (to minimise weight, volume and cost) to solve the impact absorbing problems of pedestrian protection. Towards this end, initial verification of the tunability of the response of such devices at different stroking velocities was undertaken. Impact tests were conducted on SALi shock absorbers at various velocities. Newtonian matrix fluids with different viscous damping properties were used with expanded polystyrene beads or polymeric

microspheres. The role of the capsules to the side of the impact zone in absorbing impact energy will be highlighted. The objective is to move towards a set of design rules for constructing SALi based impact absorbers.

The results presented provide a better understanding of the fundamental behaviour of SALi based energy absorbers and provide a useful tool for optimising the design of energy absorbing bumper systems.

BACKGROUND

Every year 1.7 million people are injured and 38 thousand people are killed on European roads [3]. Pedestrians form a large proportion of road accident casualties impacted by the front of a passenger car [4].

As pedestrians constitute a significant proportion of all road user casualties, the Commission of the European Communities (EC) has set itself the target of reducing the figure of fatalities by 30% and the injured pedestrian by 17%.

Measures were introduced by the Commission to improve the safety of vulnerable road users in case of injuries resulting from a collision with a motor vehicle [5]. The EC Directive 2003/102/EC proposed performance requirements for the frontal structures of certain categories of motor vehicles to reduce their aggressiveness [6]. It established tests and limit values based on the EEVC proposals to be complied with by new vehicles. The introduction was to be in two phases, with proposed European Enhanced Vehicle Safety Committee (EEVC) test procedure being mandatory in 2010.

Most of the current solutions designed for pedestrian protection aim at absorbing energy by deformation after impact (passive systems) [7]. A pedestrian friendly vehicle involves three requirements:

- A sufficient crush depth established by keeping adequate space between the bumper or the bonnet and the hard elements like the engine [8];
- An appropriate deformation stiffness of the crushing elements generated by energy absorbing materials to decelerate progressively the leg and the head of the pedestrian during the impact;
- An appropriate force distribution on the leg introduced by small changes in vehicle front designs.

The goal is to make the vehicle front end less injurious to pedestrian by preventing and reducing the severity of the impact.

However, there is a conflict between these goals and those for crash management as a whole. The purpose of crash management is to minimise damages at the front of the vehicle and reduce pedestrian injuries. Reducing repair costs in order to achieve a favourable insurance classification is one of the key drivers for OEMs. The level of damage is assessed in the Research Council for Automobile Repairs (RCAR) crash repair test [9]. In this test, the vehicle is crashed against a non-deformable barrier at a speed of 15km/h with 40 % overlap. It would therefore be advantageous to have a single bumper system design that meets global legislative impact requirements.

A brief discussion of the pedestrian leg impact requirements will be helpful before proceeding. The purpose of the pedestrian leg impact test procedure is to reduce the occurrence of lower limb injuries in pedestrian accidents. In the pedestrian leg impact test, a 'leg-form' impactor is propelled toward a stationary vehicle at a velocity of 40 km/h parallel to the vehicle's longitudinal axis. The test can be performed at any location across the face of the vehicle, between the 30° bumper corners. The acceptance criteria are illustrated in Figure 1. The limit values given are those used by EuroNCAP (the European New Car Assessment Programme) [10] and proposed as phase II of EC Directive 2003/102/EC [6]. The maximum tibia acceleration criterion is intended to prevent tibia fractures. The knee bend angle and shear deformation criteria are intended to prevent knee joint injuries such as ligament ruptures and intra-articular bone fractures.

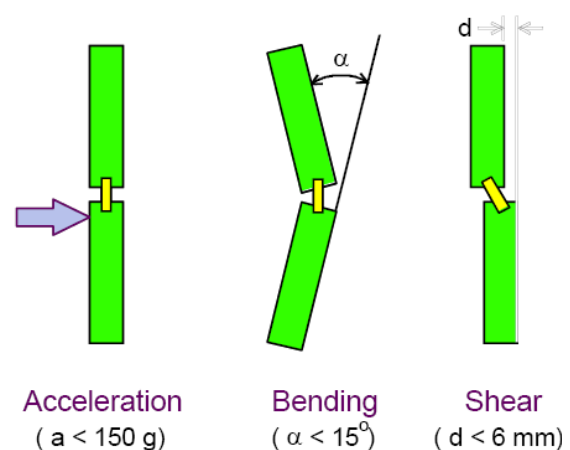


Figure 1: Pedestrian 'leg-form' injury criteria as specified by EuroNCAP and originally proposed as phase II of EC Directive 2003/102/EC.

The Commission adopted a new Proposal for a Regulation on Pedestrian Safety (and repealing the Directive) in October 2007, which forms the basis for a combination of feasible requirements with active safety measures [5]. The limit values for the

lower legform to bumper test are proposed as 170g (acceleration), 19° (bending angle) and 6mm (shearing displacement).

The front bumper is a key part in any discussion regarding lower leg impact, and - more specifically - the energy management of the bumper energy absorbing system [10][11]. In order to pass the leg impact tests, the first requirement is that the acceleration should be less than limit value. This is governed by the crush strength and depth of the bumper material [12]. Currently, plastic foams, such as expanded polystyrene (EPS) or expanded polypropylene (EPP), are the most common material used to provide energy management. The most important mechanical property these foams as an impact material are their resistance to compressive stresses. Plastic foam bumpers have been proven to perform well in single impact scenarios, but in order to prevent bottoming-out (contact and crushing occurring between opposing cell walls), there must be sufficient depth of material. The problem with increasing the depth is that it adds cost and weight to the design. In addition, like most impact materials, EPS and EPP foams absorb the impact energy by plastic deformation, resulting in permanent damage. The softer, deeper foam recommended for leg protection will adversely affect the vehicle's ability to survive low speed collisions without damage [13].

SHOCK ABSORBING LIQUID (SALi)

Shock Absorbing Liquid (SALi) is an innovative technology that has the potential to deliver a car bumper design that would enhance pedestrian protection without either sacrificing vehicle damageability or significantly increasing the depth of the bumper system.

What is SALi?

The SALi based shock absorber is a composite material designed to absorb the energy of impacts, vibrations and shock waves. It consists of a large number of small elastomeric capsules surrounded by an incompressible matrix liquid retained in a flexible low stretch packaging (Figure 2).

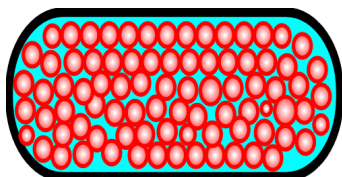


Figure 2: SALi based shock absorber showing the elastomeric capsules in red surrounded by an incompressible matrix fluid and contained within a flexible low stretch packaging.

Many different materials can be used to make SALi impact absorbers. The small capsules may be closed or open gas filled capsules, expanded polystyrene beads or polymeric microspheres for example. For the matrix fluid, any liquid which can hydraulically transfer pressure changes is potentially usable. The size and the shape of the container affect the impact energy absorbing performance. The container must be leak proof and deform easily under impact but not stretch significantly. This is to enable the capsules under and adjacent to the impact zone to rearrange themselves in the package whose front face takes the shape of the impactor.

How does SALi work?

SALi provides high impact absorbing performance, because the matrix fluid transmits pressure changes. When subject to an impact, the SALi based shock absorber combines the elastomeric properties of closed cell foams with the viscous damping and pressure equalization properties of a liquid. The matrix fluid acts as a lubricant, transmitting the stresses between adjacent capsules in the container and damping the movement of the capsules. The gas pressure inside closed capsules changes in response to pressure changes in the surrounding fluid. Before the impact, the elastomeric capsules are in close contact and incompressible matrix fluid fills all of the void space between the capsules (Figure 2). During the impact the ratio of fluid to capsule volume increases as the capsules are compressed (Figure 3).

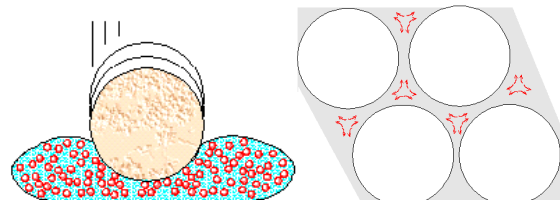


Figure 3: Hydraulic pressure causes all of the elastomeric capsules inside the bag to be compressed. The viscous liquid swirls around the shrinking capsules, contributing viscous damping to the energy absorbing effect.

What are the advantages of SALi?

The shock absorber has the ability to change its energy absorbing properties depending on the type of impact (velocity and size of the impacting body) it is cushioning. With a small impacting body, the elastic fluid is shifted sideways of the impact zone (Figure 4). The impacting body would "see" the SALi filled package as a wide, soft cushion. The matrix fluid transmits pressure changes, allowing the elastomeric material to the sides of the impact zone to also participate in absorbing impact energy.

A larger object involves a wider contact area during an impact. There would be no movement of the elastic material sideways from the impact zone (Figure 5). The rate at which the SALi material is crushed will be higher. The SALi material will have a higher stiffness. The material only exhibits these characteristics if it is packed in a stout, high tensile strength bag.

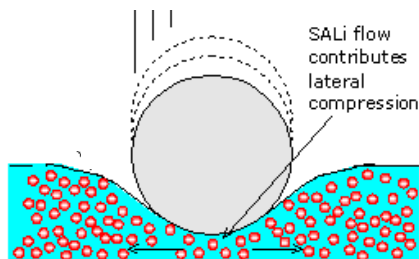


Figure 4: For a small impacting body, the elastic fluid would move sideways from the impact zone.

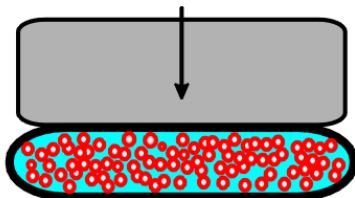


Figure 5: For a large impacting body there would be no movement of the elastic material sideways from the impact zone.

The stiffness of any foam energy absorber needs to be chosen such that the stress in the plateau region is less than the specified stress. Damaging levels of impact stress travel through the foam, to the underlying surface when the foam is compressed more than about 65%. For SALi, compression, in terms of thickness change can reach 100% without leaving the plateau region, because elastomeric material flows to the side, during the impact.

At higher impact speed, energy absorption by viscous damping increases, effectively, stiffening the SALi based absorber. The use of a highly viscous matrix fluid allows the compression impulse travelling to the sides of the impact zone to be damped rapidly.

The forces applied to the impactor are fairly uniform over the contact area, which is a strong advantage against rigid foams. When correctly packaged, the hydraulic properties of SALi allow the impact loads to be transmitted over the femur and adjacent soft tissue.

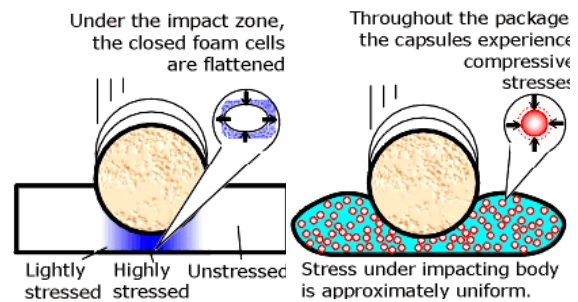


Figure 6: Stress distribution within SALi (RHS) compared with elastomeric foam (LHS).

What are the potential applications for SALi?

When looking at pedestrian protection in isolation, we can achieve the desired level of protection with traditional methods. It is a question of specifying a material with the appropriate stress / strain properties and defining the optimal geometry of the vehicle front structure. However, the manufacturer always has to balance pedestrian protection with other competing interests, such as damageability and design space constraints.

What SALi can do is offer a material that manages to balance competing interests far better than traditional solutions. The “smart properties” of SALi can resolve the “conflict of stiffness” problem. The variable uniaxial stiffness optimizes the impact absorbing abilities to provide a high degree of protection for a wide range of pedestrian sizes (from small child to larger adult body), and an adequate cushioning in impacts with other vehicles or street furniture. The SALi filled impact absorber is reusable and can accept many impacts as the capsules are uniformly compressed on all sides, take minimal damage and make a fairly recovery in volume with little residual compression when load is removed. Its energy absorbing behaviour does not change radically with the form of the impacting body, as the hydraulic pressure equalization characteristics of the absorbers allow them to absorb uniaxial impacts as a bulk compression phenomenon. It can efficiently protect occupants, pedestrians and other vulnerable road users, and minimize vehicle repair costs.

Beyond bumper systems, SALi also has potential application in:

Head Impact

- Pillar trim
- Side rail and roof lining
- Side curtain airbag attachment

Side Impact

- Upper arm & thoracic protection
- Pelvis and leg protection

Pedestrian Protection

- Under hood attachment

APPROACH

It was identified that prior to adopting SALi based devices for impact energy management applications several key issues needed to be addressed. The present study focused on one of the most significant of these, the verification of the tunability of the response of such devices at different stroking velocities (representative of the difference between pedestrian to vehicle and vehicle to vehicle impacts). This represents one of five key phases building towards the development of a SALi based bumper system:

- Phase 1: Characterisation of SALi Properties
- Phase 2: Further Characterisation / Simulation
- Phase 3: Complex SALi Simulation
- Phase 4: Real Car Simulation
- Phase 5: Car Maker Tests

CHARACTERISATION OF SALi PROPERTIES

Phase one of the Cardiff University research was recently completed. The main purpose of the Phase one work was to validate our theoretical predictions of how SALi type devices work.

TEST PROGRAMME

Many formulations are possible for a SALi based impact absorber. The combination of materials and mixture proportions with the right elastic and viscous damping properties have to be found to solve the impact absorbing problems of pedestrian protection. The shock absorber should minimize acceleration and displacement during impacts with pedestrians as well as with other vehicles or street furniture. The weight, thickness and cost of the SALi filled bumper must also be at the minimum.

Phase one was concerned with mechanical testing of SALi shock absorbers. The primary objective of the experimental programme was to attest SALi Technology shock absorbing properties. Physical experiments were conducted on SALi shock absorbers to verify the innovative properties of the material and to establish its potential for pedestrian protection. Several series of tests were established with different formulations at various impact velocities.

Sample Composition and Preparation

The formulation of SALi consists of elastomeric beads and a viscous matrix fluid. Two types of beads were used for the preparation of the SALi shock absorbers: expanded polystyrene beads (diameter: 4-7mm) or polymeric microspheres (diameter: 60-90 μ m). The blending of the two

constituent parts by volume was as shown in Table 1.

Table 1: Component part in the blending of SALi shock absorbers

Parts by volume	EPS beads	Matrix fluid
True parts	66	34
Measured parts	100	34

A third set of beads was also prepared; this consisted of the above expanded polystyrene beads blended with the polymeric microspheres. Shock absorbers using this mix of beads were referred to as nested SALi shock absorbers as the small polymeric microsphere effectively 'nest' between the larger beads. The blending of the constituent parts by volume was as shown in Table 2

Table 2: Component parts in the blending of nested SALi shock absorbers

Parts by volume	EPS beads	Polymeric microspheres	Matrix fluid
True parts	66	22.5	11.5
Measured parts	100	34	11.5

The difference between the true and actual volume (parts) is due to the volume occupied by void spaces between the spherical particles. The true volume of elastomeric material when expressed as a proportion of the measured volume is referred to as packing fraction. The volume of SALi is evaluated, and then considering that the true volume of EPS beads corresponds to 66% of the measured one, the volume is fulfilled with EPS beads and then completed with 34% extra volume of silicone oil. For instance, for a 1L sample, 340mL of oil will be added to measure 1L of EPS beads. For a nested version, 115mL of matrix fluid will be mixed with 340mL of microspheres and 1L of EPS beads. The liquid fraction is reduced from 35% to about 12%.

Every set of SALi was tested with different matrix fluids. BluStar silicone oils of 100cSt, 1000cSt and 12500cSt were used [15].

The blended mixture of elastomeric beads and matrix fluid are placed in strong polythene tubing. This tubing is heat sealed at either end (Figure 7).



Figure 7: Elastomeric material (EPS beads) blended with viscous matrix fluid. The polythene tubing retains the mixture. This is then wrapped in a low stretch outer sheath.

Test Apparatus and Procedure

Experiments were performed on an Instron Dynatup® 9250 HV Impact Test System equipped with a 15kN tup load cell and software for continuous data acquisition.

In each of the test, the SALi sample was fixed onto a steel plate as shown in Figure 8. The SALi material within the centre section was retained inside a strong, low stretch outer sheath. Without the low stretch sheath, the packaging would stretch during an impact allowing the elastomeric capsules to be displaced without suffering significant compression. The main energy absorbing mechanism would be the work done in stretching the polythene – which is fairly low, compared with the work done compressing SALi.

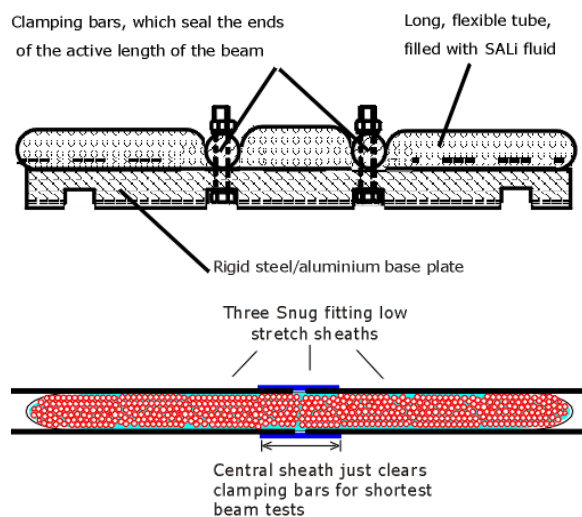


Figure 8: A holder was designed to contain the SALi absorber. The spacing of the clamping bars was adjustable to allow samples of different length to be tested.

Test Series 1

The first series of tests investigated the involvement of SALi material beyond the immediate impact zone. The impactor was a cylinder of 25mm diameter and of mass 5.2kg (Figure 9).

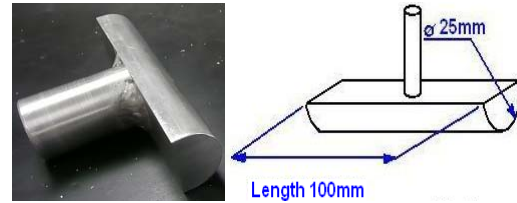


Figure 9: Cylinder shaped impactor

The longitudinal axis of the cylinder was aligned across the SALi pad. The cross section of the SALi pad was 70mm in the direction of the cylinder longitudinal axis by 50mm in the direction of the impact axis (Figure 10). The length of the pad (shown as dimension A) was varied from 70mm to 170mm in increments of 50mm. This type of impact is analogous to a pedestrian type impact described previously.

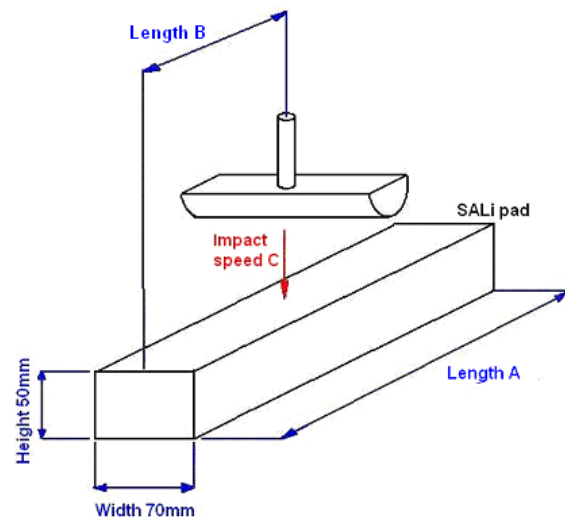


Figure 10: The alignment of the impactor and SALi sample (Length A = 2 x Length B).

The impact conditions were the same for each of the samples; the only change was the length of the pad perpendicular to the longitudinal axis of the impactor.

Fixed Parameters

- Impactor mass: 5.2 kg
- Striker shape: cylinder (25mm diameter)
- Package: polythene tubing
- Sample cross sectional area: 70x50mm
- Fluid viscosity: 1000cSt
- Capsules: EPS beads

Variable Parameters

- Impact velocity: 0.8-2.4m/s
- Sample length: 70-320mm

Test Series 2

The second series of tests investigated changes in viscosity of the matrix fluid. The experimental set-up from test series one was replicated. The change was that the sample length was a fixed parameter and the fluid viscosity was a variable parameter. The choice of sample length was based on assessment of test series 1 result.

Fixed Parameters

- Impactor mass: 5.2 kg
- Striker shape: cylinder (25mm diameter)
- Package: polythene tubing
- Sample cross sectional area: 70x50mm
- Capsules: EPS beads
- Sample length: 170mm

Variable Parameters

- Impact velocity: 0.8-2.4m/s
- Fluid viscosity: 100cSt, 1000cSt and 12500cSt

Test Series 3

The third series of test investigated a change to the capsule size. The experimental set-up from test series one was replicated. With the exception of the change in bead size, the fixed and variable parameters remained as for test series two.

Test Series 4

The fourth series of tests investigated blending EPS beads with polymeric microspheres. The experimental set-up from test series one was replicated. With the exception of the change in bead size, the fixed and variable parameters remained as for test series two.

Additional Test Series

Although not reported within the following sections, a number of additional test series were undertaken. These investigated repeatability of SALi type absorbers at various stages of the investigation, the response of EPS foam blocks and the response of SALi type absorbers to change in impactor (size and mass).

RESULTS AND DISCUSSION

Force against deflection was recorded from each of the tests. The test data was then evaluated based on what is required from a manufacturer's perspective for a pedestrian friendly bumper system. This is to limit peak acceleration (to pass the leg impact tests, the first requirement is that the acceleration should

be less than limit value) and increase efficiency (the more efficient the energy management, the smaller the depth of space needed to absorb the energy from the event).

The peak load measured during the impact test was used to investigate peak acceleration (force is analogous to acceleration as impact mass was fixed).

The efficiency was investigated using the following relationship:

$$\int F(x)dx = F\Delta x\eta$$

Where:

- F = Peak Force
- Δx = Deflection
- η = Waveform efficiency

Influence of Shock Absorber Length

The initial series of tests investigated change in absorber length upon peak load and absorber efficiency. The peak load for each of the test results is compared against change in velocity in Figure 11 and the efficiency in Figure 12.

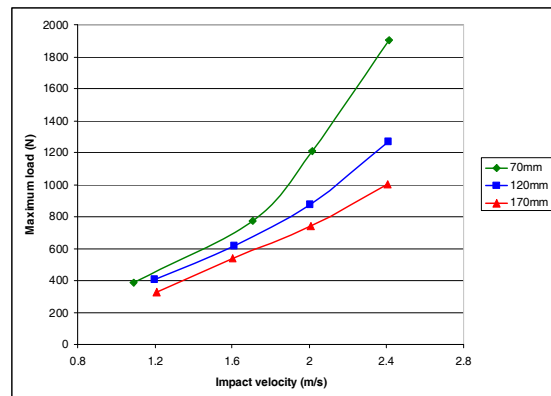


Figure 11: Maximum load variation against impact velocity with the 25mm diameter impactor and for the three SALi pad sample lengths tested.

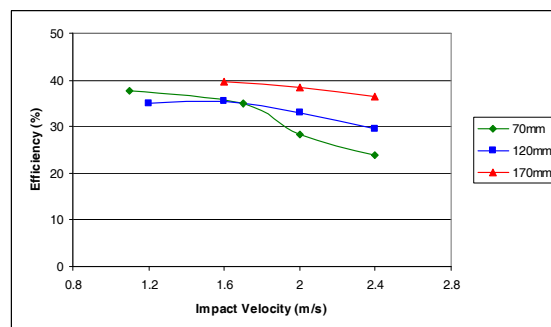


Figure 12: Efficiency with change in impact velocity with the 25mm diameter impactor and for the three SALi pad sample lengths tested.

A number of observations can be made regarding the peak load change and change in efficiency:

- Peak load decreased with pad length.
- Peak load increased with impact velocity.
- Rate of change in peak load with velocity was greater for the 70mm length sample for impact velocities $>1.6\text{m/s}$.
- Efficiency was highest for the 170mm length sample.

To explain these observations, it is necessary to look at the energy absorption process.

Energy absorption by a SALi composite material occurs by two mechanisms. One is the work done in compressing the elastomeric material. The other is work done by the matrix fluid as it shears. Looking at these contributions individually:

- For a given deflection, within a larger volume of SALi, the strain-rate of the individual EPS beads is reduced. Experimental work on EPS foams [17] has shown that EPS is strain rate dependent and that stress increases at higher strain rates. Therefore for a larger volume of SALi the work done in compressing the elastomeric material is reduced.
- If the strain-rate of the individual beads is less within a larger volume of SALi, then the shear rate of the matrix fluid would also change i.e. for a larger volume of SALi the state may change from i to ii in Figure 13 compared to a change from i to iii for a smaller volume. For a Newtonian fluid, the shear rate is directly proportional to shear stress. Therefore the contribution to the work done by shearing of the matrix fluid would therefore be less as SALi volume is increased.

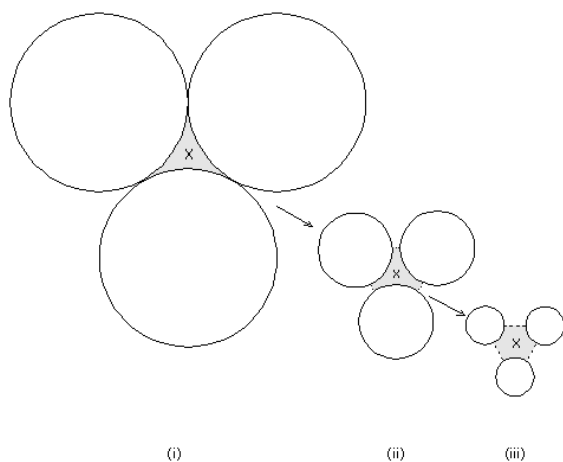


Figure 13: A two dimensional simplification of bead compression within a SALi composite fluid. The neutral point about which the fluid flows is shown as X.

The result is of the above is a reduction in work done and hence a lowering of the peak load for the same stiffness of beads and same matrix fluid viscosity. The above assumes that the pressure change is not localised, but that pressure change is distributed through the SALi fluid (this assumption will be investigated in more detail in the second series of tests).

A further observation was that the peak load increased for each of the samples at higher impact velocities. This is not unreasonable given that strain rate dependency of the EPS material mentioned earlier and that shear rate of the matrix fluid would increase (and hence shear stress).

The final observation was that whilst the change in peak load for increasing velocity was approximately linear for the 120mm and 170mm samples, this was not the case for the shorter 70mm sample.

Higher velocities considerably increase the amount of impact energy that requires dissipation. Doubling the impact speed from 1.2 to 2.4m/s increased the energy to be dissipated by a factor of 4. The higher energy impacts for the 70mm samples are compressing of the EPS beads into the densification region (region in the stress strain curve in which stress rises steeply due to contact and crushing of the cell walls). Strain hardening of EPS foam has been shown to occur at approximately 55%-65% strain region [17]. The effect of entering the densification region is a fall in the efficiency of the absorber.

Influence of Matrix Fluid Viscosity

The second series of test investigated changes in viscosity of the matrix fluid upon peak load and absorber efficiency. The length of absorber was chosen as 170mm based on observation of efficiency in the previous series of tests that showed this length of absorber to be the most efficient of the three lengths tested.

The peak load for each of the test results was compared against change in velocity in Figure 14 and the efficiency in Figure 15.

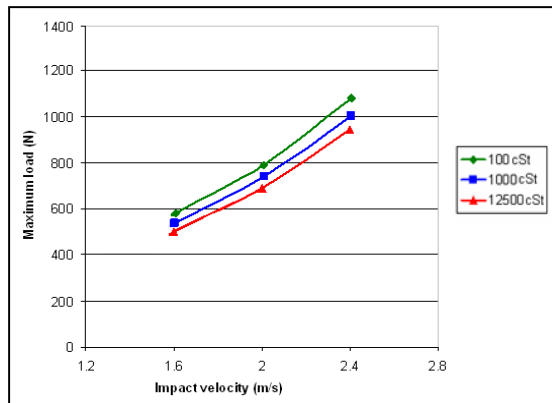


Figure 14: Maximum load variation against impact velocity with the 25mm diameter impactor and for the three matrix fluid viscosities tested.

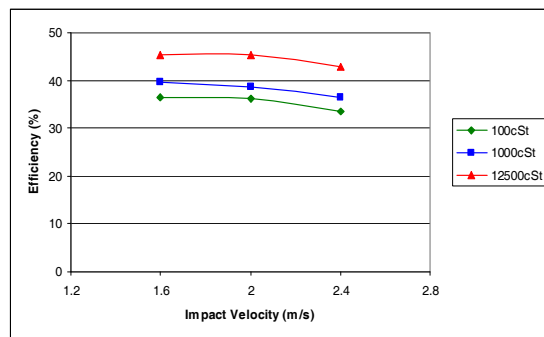


Figure 15: Efficiency against impact velocity with the 25mm diameter impactor and for the three matrix fluid viscosities tested.

A number of observations can be made regarding the peak load change and change in efficiency:

- Peak load increased with velocity.
- Peak load decreased with viscosity
- Efficiency increased with viscosity.
- Efficiency decreased with velocity.

As for the previous test series it would be reasonable to expect an increase in peak load at higher impact velocity due to the strain rate dependency of the elastomeric material (stress increases with strain-rate) and the higher shear rate of the matrix fluid (shear stress increases with shear rate).

However, as viscosity of the matrix fluid is increased, the shear stress is far greater and hence pressure change is more localised. This results in greater differential compression of the EPS beads (those nearer the impact zone suffer proportionally higher strain than those further away). This can be observed by comparing the respective force deflection curves for the different viscosities at each impact velocity.

The force deflection curves exhibit hysteresis i.e. the energy dissipation during the impact results in smaller compliance during unloading (restitution) than was present during loading (compression). The area under the unloading curve equals the elastic strain energy released from the deforming region during restitution. As can be observed from the force deflection curves presented here (Figure 16), the elastic strain energy released is less for the higher viscosity matrix fluid. EPS foam is known to exhibit linear behaviour for strains less than 0.05 [17]. Therefore the greater the volume of EPS material under strain the greater the elastic strain energy released. Put succinctly, the greater the number of beads subject to compression the greater the elastic strain energy stored.

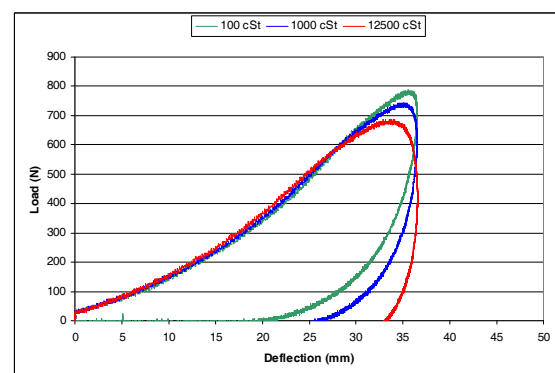


Figure 16: Force against deflection curves for 2.0m/s impact against the 100cs, 1000cs and 12500cs SALi shock absorber pads. The compliance is less for the higher viscosity matrix fluid.

Increasing the viscosity of the matrix fluid increases the efficiency of the absorber as shearing of the matrix fluid lowers the peak load

Influence of Bead Size

The third series of tests investigated changes in elastomeric beads upon peak load and absorber efficiency. The EPS beads (diameter: 4-7mm) were replaced with Expancel polymeric microspheres (diameter: 60-90 μm). The peak load for each of the test results is compared against change in velocity in Figure 17 and the efficiency in Figure 18.

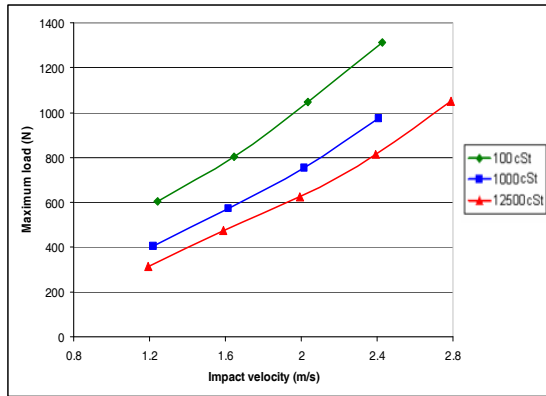


Figure 17: Maximum load variation against impact velocity with the 25mm diameter impactor and for the three matrix fluid viscosities tested.

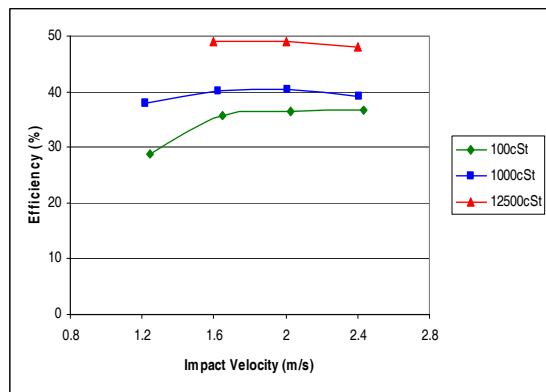


Figure 18: Efficiency against impact velocity with the 25mm diameter impactor and for the three matrix fluid viscosities tested.

Similar observations to those made for the EPS beads can be made regarding peak load and efficiency. The exceptions are that the difference in peak load at different viscosities was greater and that efficiency was maintained with increase in impact velocity. Indeed, efficiency was observed to initially increase (from 1.2m/s to 1.6m/s).

The rationale for the change in load is that the contribution to the work done from shearing of the matrix fluid was greater. This follows from the fact that the total solid-liquid interface surface is higher (greater potential for shear of the matrix fluid). However, for a given level of compression the beads remain closer and therefore the mean displacement of elements of the liquid, and hence the shear rate (and hence shear stress) of the matrix fluid is reduced.

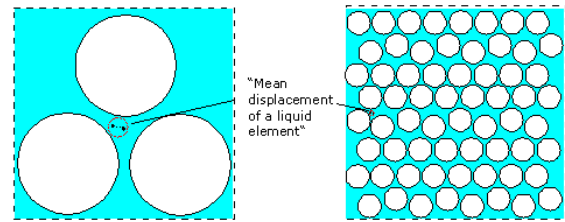


Figure 19: Comparison of SALi with different bead size. The solid-liquid interface area is higher, but for a given compression of the total volume the displacement of the fluid would be less.

The principal advantage of the polymeric microspheres over EPS beads used in the previous tests is in creating a low weight version of SALi. A mixture of liquid and polymeric microspheres used to fill the void spaces between the larger spheres would reduce the weight of the matrix fluid in the SALi shock absorber.

Combing Polymeric Microspheres and EPS Beads

The fourth series of tests investigated blending of the EPS and polymeric microspheres upon peak load and absorber efficiency. The peak load for the test with the 1000cSt matrix fluid is compared against the tests with the EPS beads and microspheres in Figure 20 and the efficiency in Figure 21.

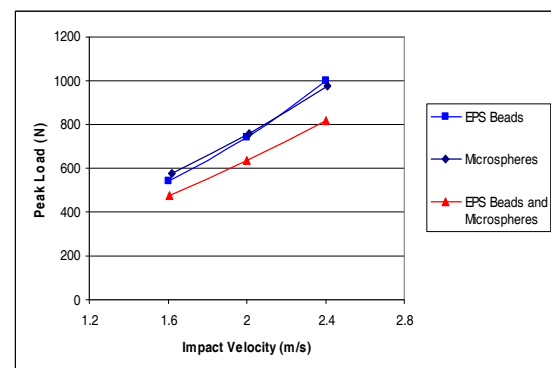


Figure 20: Maximum load variation against impact velocity for the SALi absorber using the 1000cSt matrix fluid.

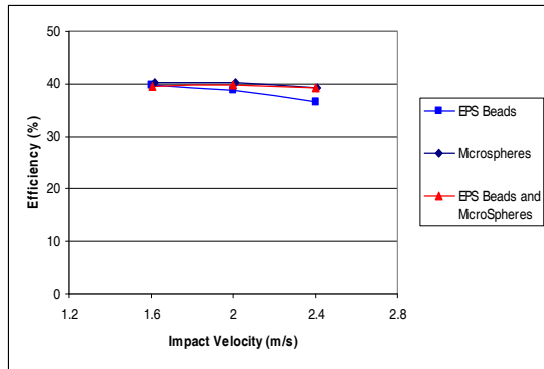


Figure 21: Efficiency against impact velocity for the SALi absorber using the 1000cSt matrix fluid.

Peak loads were lower compared to equivalent tests with just EPS or microspheres. However, the efficiency of the absorber is similar to the previous test at lower velocities and is more efficient than EPS alone at higher velocities.

This difference can be explained by assuming that the EPS beads are effectively immersed in an elastic matrix liquid. Consequently, from the perspective of the EPS beads, there is no need for the bead-to-liquid geometry to change as depicted previously (Figure 22).

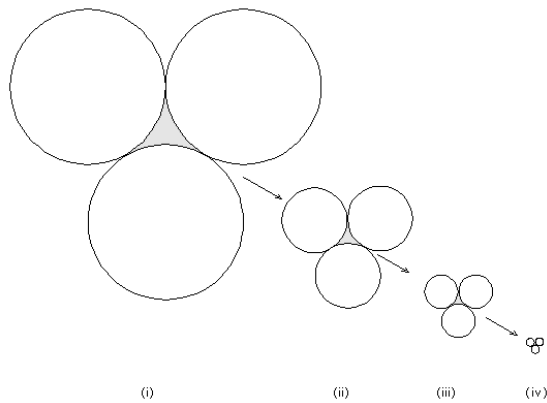


Figure 22: If the matrix fluid filling the void spaces between the EPS beads shrinks at the same rate as the beads, then there is no need for the fluid to swirl round the beads, as suggested.

For this explanation to be valid, the Microspheres and EPS beads would need to exhibit similar levels of compressive stiffness over the compression range tested.

IMPLICATIONS FOR BUMPER DESIGN

From the perspective of vehicle damageability it is necessary to have a stiff bumper to improve the vehicle's ability to survive low speed collisions without damage. The stiffness of the SALi bumper in vehicle damageability type impacts is taken to be

a function of stiffness of the elastomeric material (when compared to pedestrian impacts, these are low speed events so viscous damping rate and hence viscous stress would be lower than in a pedestrian impact). Conversely, from the perspective of pedestrian protection it is necessary to have a lower stiffness. In addition, designing a bumper to fit within the packaging space typical of today's vehicle styling it is necessary to maximise the efficiency of the absorber.

The results of the experimental investigation have shown that stiffness of the SALi absorber can be lowered for small body impacts (representative of leg form impacts) without compromising the stiffness of the elastomeric material (necessary for vehicle damageability). For the same elastomeric material:

- Lengthening of the impact absorber lowered the peak load.
- Increasing the viscosity of the matrix fluid lowered the peak load.

However, the efficiency of the absorber was observed to decrease at higher impact velocities. Altering the formulation of SALi by the blending of EPS beads with polymeric microspheres was shown to maximise the efficiency of the absorber over the range of impact velocities investigated.

In addition to the above it is necessary to ensure that the strain of the elastomeric material does not reach the densification stage (strain hardening). For SALi absorbers it was shown that strain hardening could be avoided without resort to increasing the depth of the energy absorber. This provides a distinct advantage when it comes to packaging a SALi energy absorber.

Schuler et al [10] calculated the minimum energy absorber thickness for a leg impact. For foam systems it was found that a thickness of 100mm was required. A similar calculation based on the nested version of the SALi absorber (assuming similar efficiencies at higher impact speeds) would see the minimum thickness reduced to less than 60mm.

In addition, the weight of the absorber is critical. The matrix liquid is the highest density component of any SALi formulation. A mixture of liquid and polymeric microspheres can be used to fill the void spaces between the larger spheres. This would have the two advantages of (1) reducing the weight of the matrix fluid in the SALi shock absorber and (2) for a small body impact it reduces the effective stiffness. However, as long as the crush strength of the blended matrix liquid was equal to or higher than the larger spheres then the bumper stiffness for vehicle damageability would not be compromised

(the large spheres would always compress in preference to the matrix fluid).

FURTHER RESEARCH

The basic SALi formulations investigated were close packed expanded polystyrene (EP) beads, 4 to 7 mm in diameter, with the void space between them filled with a viscous liquid. This formulation is useful for helping us to understand how SALi works, but too heavy for commercial applications. A low weight version of SALi, using a mixture of liquid and polymeric microspheres to fill the void spaces between the larger spheres was also investigated.

They all shared a basic idea: to use the available package space in the most efficient manner. It means: the fast response of the energy absorbing structure to the impact event (shape force – intrusion curve close to rectangular shape), the more efficient the energy management and, therefore, the smaller the thickness of space needed to absorb the energy from the event. An important feature of the further research work will be to investigate various blends of stiff and soft microspheres, in order to increase impact energy absorbing performance.

In addition, stiff particles can be added to Newtonian liquids to convert them into shear thickening fluids. If the particle density is sufficiently high and the applied stress increases sufficiently rapidly, the fluid can lock up, to transiently mimic the properties of a solid.

SUMMARY

The purpose of crash management is to minimize damages at the front of the vehicle - reducing repair costs in order to achieve a favourable insurance classification is one of the key drivers for OEMs – and reducing pedestrian injuries – pedestrian safety is now a high profile issue within the automotive industry.

In summary, the experimental work has shown that the shock absorbing liquid composite transmits impact energy from the impact zone and through a much greater bulk of the material than would be expected of conventional solid dry foams. The result is that the stiffness of the SALi absorber can be lowered for small body impacts (representative of leg form impacts) without compromising the stiffness of the elastomeric material (necessary for vehicle damageability). The result is that forces at the impact zone that are smaller than those produced in conventional solid dry foams. Therefore, it is expected that vehicle bumpers produced from the shock absorbing liquid composite will produce comparatively less impact

forces on pedestrians and will therefore be more pedestrian friendly. Key points from this work are outlined below:

- It was found that SALi provided high impact absorbing performance, because the matrix fluid transmits pressure changes, allowing the elastomeric material at the sides of the impact zone to also participate in absorbing impact energy. The investigation showed a significantly increasing performance up to 170mm (compared to 70mm and 120mm length absorbers). The forces applied to the impactor decrease with the shock absorber length, which is advantageous for pedestrian impacts. The SALi impact absorber has better energy absorbing characteristics with a higher length, which is advantageous for reducing packaging space requirement. For vehicle application, the actual values (for pad length in relation to a particular SALi composite) will depend on the size and shape of the contact area, the fluid viscosity, the impact speed and energy (these will need to be determined in the follow-up phases of the investigation).
- A highly viscous fluid was found to provide a better shock absorbing performance as loads and deflections decrease significantly with increasing viscosity. A more viscous fluid can absorb more impact energy within a smaller crush depth. The upper amount of compressible material provided by the use of very smaller polymeric microspheres instead of polystyrene beads increases the performance of SALi shock absorbers. Both loads and deflections are lower with the combination of high viscous fluid and microspheres.
- Based on observations made in this experimental investigation, a reduction in packaging space of 33% against traditional foam based systems is theoretically possible.
- The work presented here characterises SALi based absorbers in a particular impact configuration. Based on the above investigation, further possibilities have been put forward for increasing the efficiency of the absorber. Further investigation is also required in order to define design rules for SALi absorbers that seek to maximise the benefits of SALi as a crash management instrument in vehicle applications.

REFERENCES

- [1] W.A. Courtney, Device incorporating elastic fluids and viscous damping, *World Intellectual Property Organisation, WO 97/25551* (1997).
- [2] W.A. Courtney, Improved impact absorber with viscous damping, *World Intellectual Property Organisation, PCT/GB98/03594* (1998).
- [3] Communication from the European Commission, European road safety action programme - Halving the number of road accident victims in the European Union by 2010: a shared responsibility; COM/2003/0311 final, June 2003.
- [4] EEVC Working Group 17 Report, Improved test methods to evaluate pedestrian protection afforded by passenger cars, December 1998 with September 2002 updates.
- [5] European Commission, Proposal for a Regulation of the European Parliament and of the council on the protection of pedestrians and other vulnerable road users, October 2007.
- [6] European Union, Directive 2003/102/EC of the European Parliament and of the Council of 17 November 2003 relating to the protection of pedestrians and other vulnerable road users before and in the event of a collision with a motor vehicle and amending Council Directive 70/156/EEC. Official Journal of the European Union, L 321, 06/12/2003 P. 0015 – 0025.
- [7] G J L Lawrence, B J Hardy, J A Carroll, W M S Donaldson, C Visvikis and D A Peel, A study on the feasibility of measures relating to the protection of pedestrians, Project report, TRL Limited, June 2004.
- [8] Christian Pinecki, Richard Zeitouni, Technical solutions for enhancing the pedestrian protection, PSA Peugeot Citroën, Paper number 07-0307.
- [9] RCAR Bumper Test, Issue 1.02, Research Council for Automobile Repairs, November 2008,
- [10] European New Car Assessment Programme (Euro NCAP) Pedestrian Testing Protocol, February 2009. <http://www.euroncap.com>
- [11] Stephen Shuler, Frank Mooijman and Alok Nanda, Bumper Systems Design for Both Pedestrian Protection and FMVSS Requirements, SAE International Conference, Paper Number 2003-01-0214.
- [12] Svoboda Jiri and Kuklik Martin, Influence of Bumper Design to Lower Leg Impact Response, Czech Technical University in Prague, Faculty of Mechanical Engineering, Department of Automotive and Aerospace Engineering, Czech Republic.
- [13] B Shah, R Sturt and A Kasparian. Effect of pedestrian protection on styling and engineering of vehicles. Vehicle Safety 2000 Conference, London. Paper C567/032/2000
- [14] <http://www.cheshire-innovation.com>. Accessed August 2008.
- [15] Rhodorsil® Oils 47. Technical information. Available from Bluestar Silicones France SAS 21, avenue Georges Pompidou F-69486 Lyon Cedex 03 – France.
- [16] Guinehut Sebastien, Salin Laurent, Marcelo Fonseca Barbosa and Lenti Frederic. Car Over Hang Reduction With Innovative Bumper System, Valeo, France.
- [17] Liu D, Chang C, Fan C and Hsu S. Influence of environmental factors on energy absorption degradation of polystyrene foam in protective helmets. Engineering Failure Analysis 10 (2003) pg 581-591.

ACKNOWLEDGEMENTS

The above work was undertaken by students of L'institut Français De Mécanique Avancée working in partnership with Cheshire Innovation and under the supervision of academic staff at Cardiff University. Dr Huw Davies at Cardiff University is the corresponding author.

DEVELOPMENT OF A NEW FLEX-PLI LS-DYNA MODEL AND INVESTIGATIONS OF INJURY FROM VEHICLE IMPACT

Masahiro Awano

Isamu Nishimura

Mitsubishi Motors Corporation

Shinya Hayashi

JSOL Corporation

Japan

Paper Number 09-0088

ABSTRACT

A new flexible pedestrian legform impactor (Flex-PLI) has been developed by Japan Automobile Manufacturers Association, Inc. (JAMA) and Japan Automobile Research Institute (JARI).

The new Flex-PLI has good biofidelity as well as several knee ligament elongation measurement capabilities, three femur and four tibia bending moment measurement capabilities. For these reasons Flex-PLI is likely to be adopted for the future pedestrian Global Technical Regulation.

This presentation introduces a finite element model of the Flex-PLI for LS-DYNA and presents a CAE (Computer Aided Engineering) study that investigates Flex-PLI kinematic behaviour caused by impact with a vehicle. The new Flex-PLI LS-DYNA model was carefully created to ensure that every important detail was included. Geometries, masses and material properties of all parts were reproduced from drawings and inspection of the real components. Connectivity and component interaction within the model were determined by thorough experiments. Accurate prediction of injury indices and kinematic behaviour was achieved by correlation to JARI's static and dynamic calibration tests. A fine mesh was used while reasonable calculation cost assured by imposing an analysis time step of 0.9 micro seconds.

In this report, investigations by computer simulation of Flex-PLI deformation behaviour mechanisms during vehicle impact are presented.

INTRODUCTION

The increase of traffic accidents between pedestrians and vehicles is recognized as an ongoing serious problem. One approach to reduce pedestrian injuries is to improve the front structure of vehicles.

Pedestrian injury statistics from traffic accident databases accumulated in the USA, Germany, Japan and Australia show that pedestrian AIS 2-6 injuries occurred to the head in 31.4% of the cases and to the legs in 32.6% [1][2]. In the EU, protection of pedestrian lower legs has already been regulated in EEC2003/102 and assessed by EuroNCAP. These

use a rigid-bone type lower leg impactor produced by TRL.

JAMA and JARI have developed a new **Flexible Pedestrian Legform Impactor** (Flex-PLI) with improved biofidelity as well as more appropriate injury measurement capabilities. The 1st version of Flex-PLI was created in 2002 [3] and since then various technical evaluations have been carried out by the Flex-TEG (Flexible Pedestrian legform Impactor Technical Evaluation Group), conducted under GRSP/INF-PS-GR of the United Nations. JAMA and JARI have continued to improve and upgrade Flex-PLI, and in 2007 the 5th version, called Type GT (Flex-GT) was produced [4]. The Flex-GT has been verified worldwide to have excellent test repeatability and be sufficiently practical for use as a certification test tool [5][6].

From 2008 to 2009 the Flex-GT was upgraded to the 6th version, Type GTR (Flex-GTR) [7]. Flex-GTR is expected to have the same performance as Type GT and is planned to be the final design. It is likely to be used for the future pedestrian Global Technical Regulation.

In order to develop vehicles using Flex-PLI, the application of CAE is essential and must be very efficient. Therefore, in 2008, a Flex-GT LS-DYNA model development was started. In a second phase continuing to 2009, the Flex-GT model was further validated in real-vehicle impact scenarios and proven to be a highly accurate yet numerically stable model.

FLEX-GT LS-DYNA MODEL DEVELOPMENT

Model General Outline

Figure 1 shows the whole view of Flex-GT LS-DYNA model. The Flex-GT comprises an internal skeleton structure covered with a flesh material made up of layered neoprene and rubber sheets.

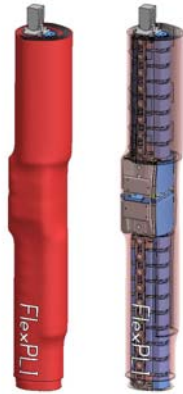


Figure 1. Flex-GT model whole view.

The mesh size and distribution in the Flex-GT model was developed over a series of concept phases in order to achieve sufficient accuracy at minimal calculation cost. The minimum mesh size of deformable parts was limited by imposing a 0.9micro second time step. Total elements amount to around 540,000 but deformable elements only to 220,000.

The geometry of the model was created not only from 2D drawings but also from long and detailed inspection of a physical impactor. The physical impactor was completely disassembled to measure accurately the size and weight of all components. The Flex-GT model is thus set up carefully to have the exact same mass distribution as the physical impactor.

Figure 2 shows the internal structure of Flex-GT. On the left is the LS-DYNA model, on the right is the physical impactor [8]. The internal structure is composed of three portions: femur, knee and tibia.

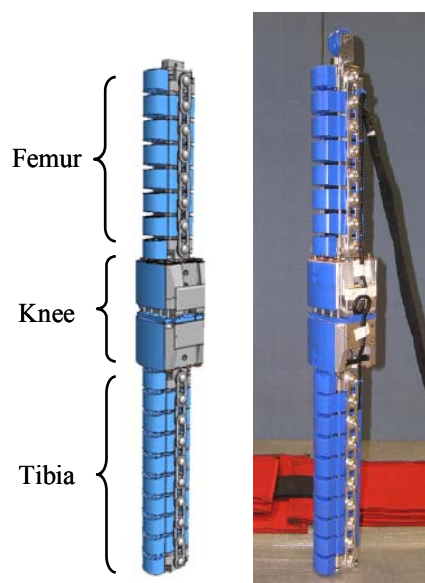


Figure 2. Flex-GT internal structure: LS-DYNA model and a physical impactor.

Bone cores form the fundamental structure inside the femur and tibia, and provide the flexibility and stiffness in those areas.

The knee joint is made up of two blocks connected by steel cables and springs which replicate ligaments in the real human knee. With this system, good biofidelic behaviour can be achieved without requiring replacement parts. The ligament layout is asymmetric because it represents a human right leg hit from the right side.

The Flex-GT model was developed using LS-DYNA Version 971 R3.2.1 [9].

Model Detailed Description

Bone Core Model - Figure 3 shows the femur and tibia bone cores. They were modelled using a purely elastic material because the real parts are made of strong glass fiber reinforced plastic (FRP) and assumed not to incur any permanent deformation (plastic strain) under normal loads. Young's Modulus was determined from 3-point bending static calibrations. Strain gauges, which in the real device are glued on the bone cores, were modelled by very weak spring elements attached using tied contacts. Three spring elements were attached to each side of the femur bone (at the same height on the tension and compression surfaces) and four to each side of the tibia, according to the specification of Flex-GT.

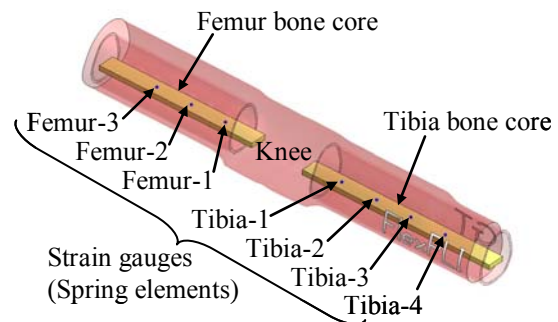


Figure 3. Bone cores and strain gauges.

Femur and Tibia Models - Figure 4 shows a section through the tibia model. The femur model has the same structure. The bone core lies down the middle of square section exterior housings which were are chained together by links down their flanks. The MC-nylon exterior housings were modelled using an elastic material and the aluminium core binders and connection bolts by a rigid material. Friction coefficients of the core binders and the connection bolts contacting on the bone cores were estimated from surface conditions of the real parts and then further tuned in the later calibration studies. Connection plates tie the exterior housing structures together and link together around connection bolts.

Accurate connectivity of the links was determined from detailed observation of the physical impactor.

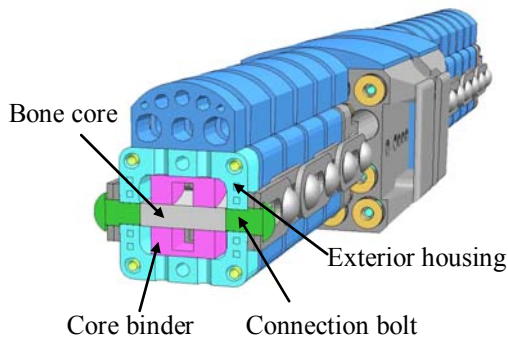


Figure 4. Exterior housing.

Figure 5 shows the connection between the femur and knee condyle model. The tibia is connected in a similar manner. The core binder at the end of the femur was attached to the knee condyle using a discrete beam element. The connection stiffness was set with reference to the physical components, and later revised in a correlation study during dynamic calibration.

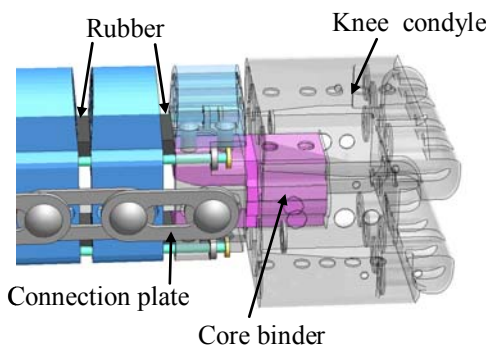


Figure 5. Connection of core binder and knee condyle.

Figure 6 shows the bending stopper cable model. This was modelled explicitly to behave in the same way as the physical impactor: the cable limits the total bend when the stopper contacts the exterior housings.

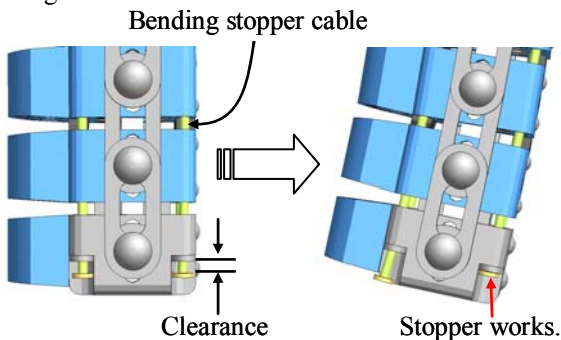


Figure 6. Bending stopper cable.

Knee Model - Figure 7 shows the model of the knee. The upper and lower knee condyles were modelled using a rigid material. The area contacting

the ligament cables was modelled with very fine mesh for accurate and stable interaction with the ligament cables. The MC-nylon contact face between upper and lower knee condyles was modelled using an elastic material. The convex impact faces were also modelled in a similar way.

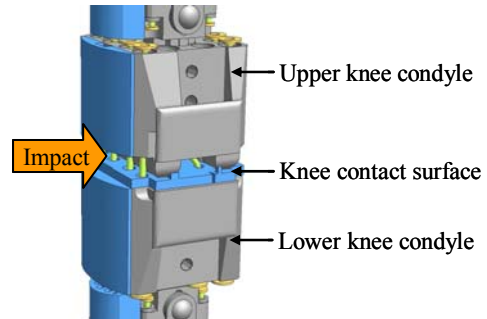


Figure 7. Knee whole view.

Figure 8 shows the knee ligament model. Four kinds of ligament cables: ACL (Anterior Cruciate Ligament), MCL (Medial Collateral Ligament, PCL (Posterior Cruciate Ligament) and LCL (Lateral Collateral Ligament), were created using very detailed and complicated modelling techniques. Ligament spring stiffness was determined from specifications and later calibrated during the correlation phase. The completed knee model was found to have good performance in predicting the varied kinematic behaviour of the real device.

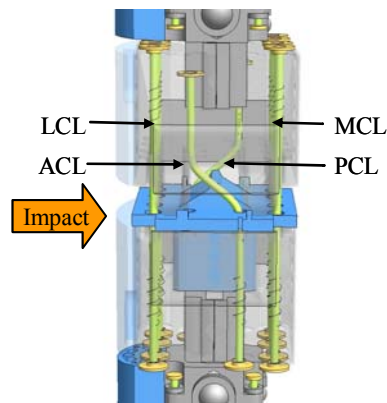


Figure 8. Knee ligament structure.

Figure 9 shows the model of the three knee potentiometers measuring extensions at ACL, MCL and PCL locations. These were modelled using weak spring elements: their deflections measure the same distance as the real wire potentiometers.

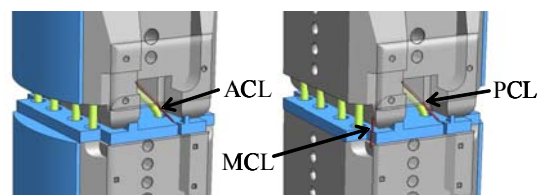


Figure 9. Knee potentiometers.

The knee joint system can flex in complicated kinematic modes: not only in bending but also in shear and torsion. It is designed to behave in the same way as a human knee. In particular, when it hits a curved area of the vehicle, a combined twist, shear and bend mode can often occur. Accurate realisation of all kinematic modes is vital for correct injury prediction and this has been achieved using detailed modelling techniques and thorough validation stages.

Flesh - Figure 10 shows the layered structure of neoprene and rubber sheets that form the flesh in the same way as the physical impactor (see also Figures 11, 12). Wide adhesive tape is used to hold the rubber sheets to the femur and this was modelled by membrane elements with realistic stiffness. Rate sensitive material properties of the neoprene and rubber were developed from accurate static and dynamic tests of production sheets.

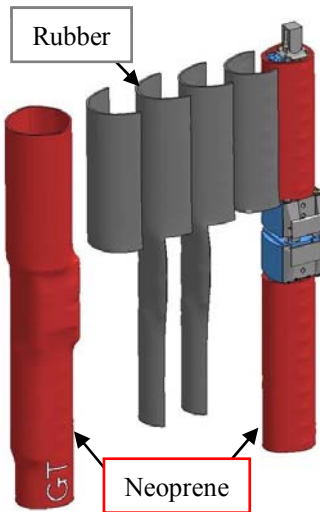


Figure 10. Layered sheets of flesh construction.



Figure 11. Flesh construction of Flex-GT model and physical impactor (Top).



Figure 12. Flesh construction of Flex-GT model and physical impactor (Bottom).

Model Calibrations

Bone Core Static Calibration - Simulations of 3-point bending static calibration tests for the femur and tibia bone cores [10] were performed and the Young's Modulus of the core adjusted to achieve the correct calibration stiffness (see Figures 13, 14).

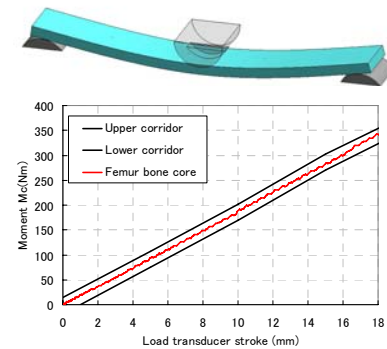


Figure 13. Femur bone core calibration result.

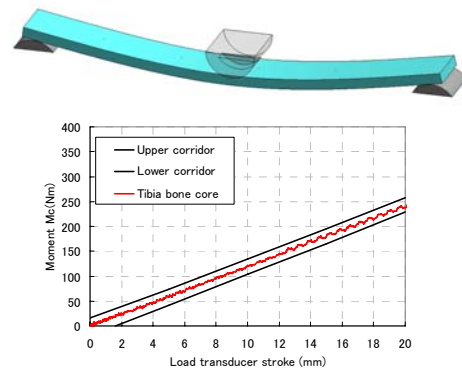


Figure 14. Tibia bone core calibration result.

The Flex-GT model is designed to be analyzed using explicit LS-DYNA, so these simulations were analyzed using the quasi-static method in explicit code. In this method the loading occurs over a very short period of time but care is taken to ensure that inertia effects are kept to a minimum and do not influence the result. It was found that correct geometries of the load transducer and support jigs were very important to get precise results. These methods were also used in the other quasi-static calibration studies.

During this stage, factors to convert strain gauge output (spring elements) into bending moments were calculated and set in the model.

Femur and Tibia Static Calibration – Figures 15 to 18 show the results of the 3-point bending static calibration analysis for the femur and tibia model assemblies [10]. The models were adjusted to satisfy calibration stiffness requirements, and the deflection modes compared to photos of the real tests (Figures 17, 18).

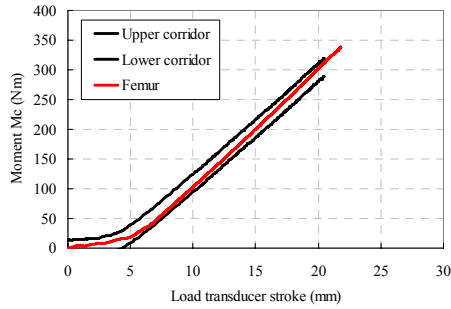


Figure 15. Femur static calibration result.

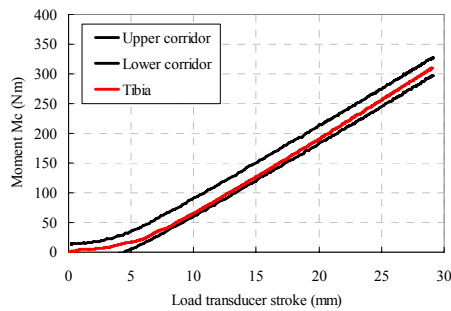


Figure 16. Tibia static calibration result.

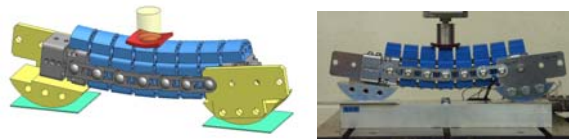


Figure 17. Femur deflection in static calibration

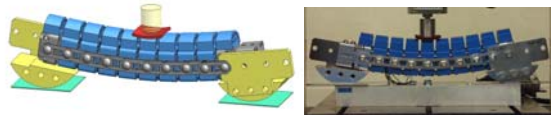


Figure 18. Tibia deflection in static calibration

Complicated support jigs attached to the both sides of the femur and tibia were modelled carefully since they influence the results.

According to the test specification, one sheet of neoprene is inserted between the load transducer and leg assembly. This deformed significantly because of its low stiffness and was often a cause of calculation instability. To avoid this problem, contact definitions and element size were modified many times. These stability modelling methods for the neoprene were also applied to the final flesh model.

Knee Static Calibration - Figures 19 and 20 show the results of the 3-point bending static calibration analysis for the knee model [10]. The model was adjusted to satisfy calibration stiffness

requirements, and the deflection mode compared to photos of the real test (Figure 20).

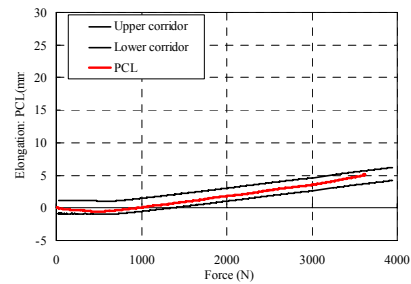
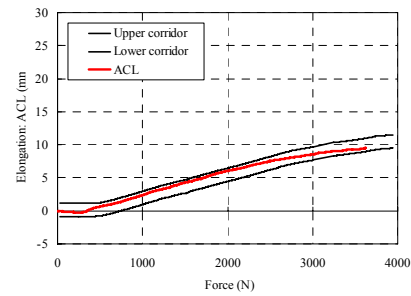
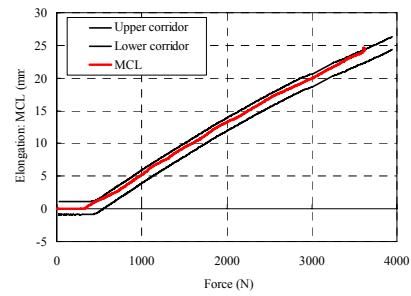
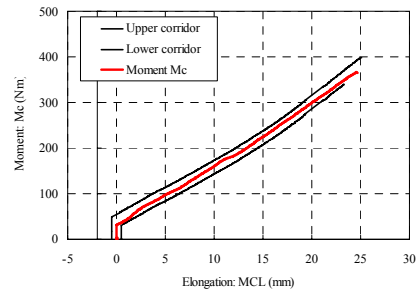


Figure 19. Knee static calibration result.

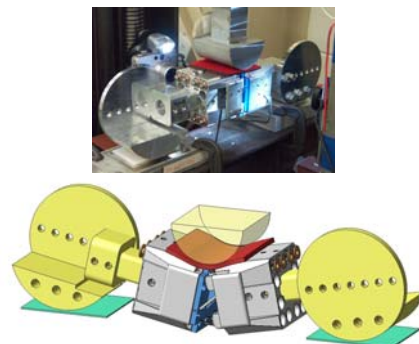


Figure 20. Knee deflection in static calibration

Assembly Dynamic Calibration – The whole internal structure of the Flex-GT was assembled from the calibrated femur, tibia and knee models and a model of the test jig created according to the dynamic calibration test specification. As shown in Figure 21, the top of the femur is connected to the jig via a pin joint and the leg is released to freely swing down from a position 15 degrees above horizontal.

Calibration requirements are defined by a corridor for peak injury of knee MCL, PCL and ACL elongations, three femur bending moments and four tibia bending moments [10]. The graphs in Figure 22 show that the Flex-GT model not only satisfies all calibration requirements but also predicts the rise and fall of injury over time with great accuracy. Figure 23 shows the model deformation at maximum MCL injury (maximum bend).

During this phase the femur, tibia and knee models were modified slightly so each static calibration test was reanalyzed and model recalibrated.

In the dynamic analysis set up, the Flex-GT leg initial position was set to be just impacting the jig and given an initial velocity. This method saves much calculation time by omitting the free drop phase. However the angular velocity at impact was not defined in the calibration specification. At first an attempt was made to calculate this theoretically but in the end a free drop simulation was performed to obtain the correct angular velocity.

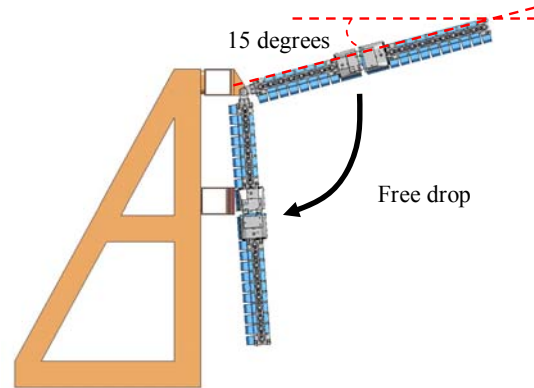


Figure 21. Dynamic calibration specification.

- Calibration corridor
- Test
- Simulation (LS-DYNA)

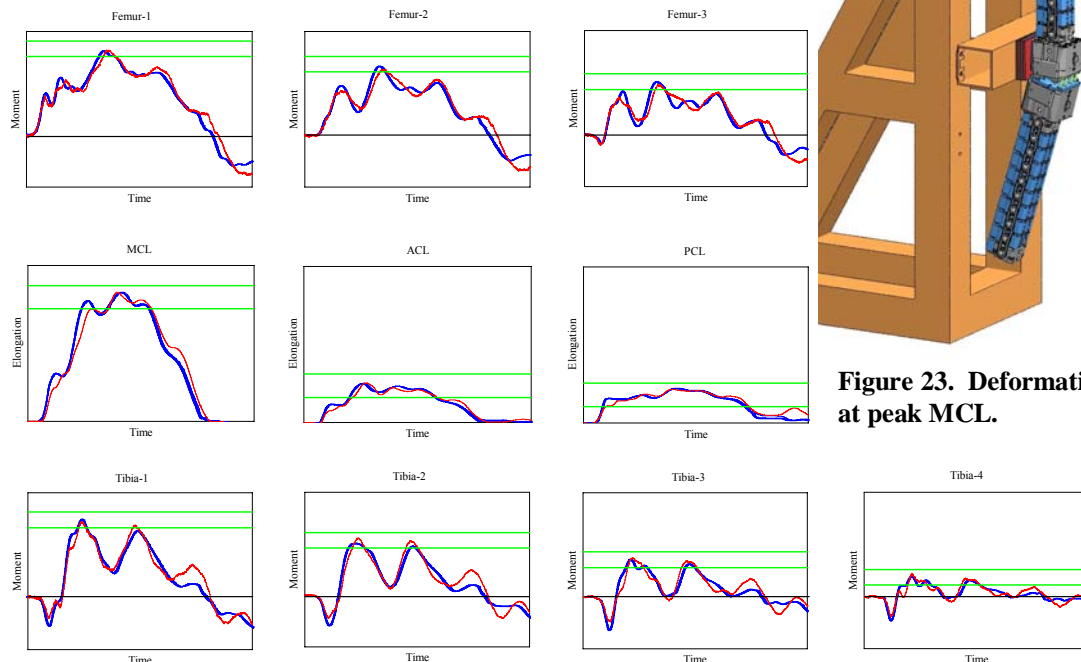


Figure 23. Deformation at peak MCL.

Figure 22. Dynamic calibration result: comparison of simulation and test.

FLEX-GT SIMPLIFIED CAR RIG IMPACT

In this study, a series of simplified car rig impacts were performed to validate the accuracy of the Flex-GT model. Figure 24 shows the simplified car rig test just before impact.



Figure 24. Simplified car rig test.

The simplified car rig was designed to represent the front structure of a vehicle. It comprises a BLE (Bonnet Leading Edge) plate, bumper and spoiler. The BLE is bent steel plate; the bumper and spoiler are PP(polypropylene) expanded foam blocks (see Figure 25).

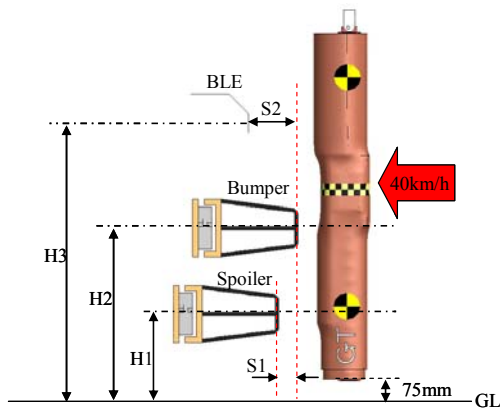


Figure 25. Simplified car rig setback and height.

The BLE, bumper and spoiler were positioned with setback and height as shown in Table.1. This represents a Type A sedan vehicle. The test was performed at an impact velocity of 40km/h and ground clearance of 75mm.

Table 1.
Setback and height conditions (mm)

TEST ID	S1	S2	H1	H2	H3
B02	50	130	Sedan type A		

A high accuracy simplified car rig model was created. A detailed mesh model of the BLE plate and PP foam blocks was made and their structural response correlated to dynamic impact tests. The model was set up as shown in Figure 26 so that the impact velocity, ground clearance and impactor position

were exactly like test conditions. In this test, four accelerometers (femur upper, knee upper, knee lower and tibia lower) were specially added on the internal structure of the Flex-GT (see Figure 27).

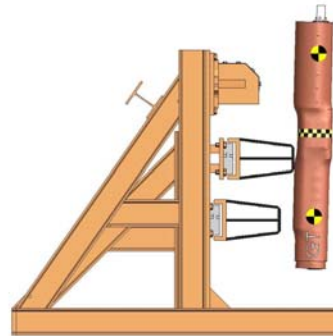


Figure 26. Simplified car rig LS-DYNA model.

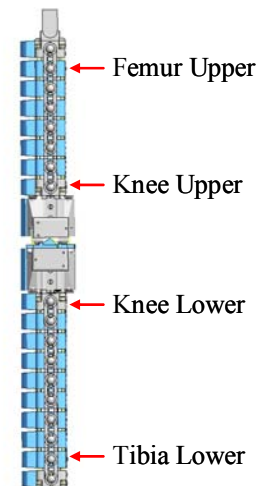


Figure 27. Accelerometers added on Flex-GT.

Figure 28 shows injury graphs of test and the simulation results. The peak values and graphical trends are well correlated. However, the simulation predicted peak femur moments 5-10msec earlier than the test. This is thought to be caused by a small difference in BLE mounting stiffness or deformation mode.

Figure 29 shows a comparison of Flex-GT kinematics. The test result was taken from high-speed film.

Figure 30 shows the acceleration pulses and graphs of acceleration vs. stroke. The kinematics of the model is nearly identical to test. The femur upper acceleration predicted from 25-32msec was a little higher than test. As described above, this is thought to be related to the accuracy of the BLE fitting model.

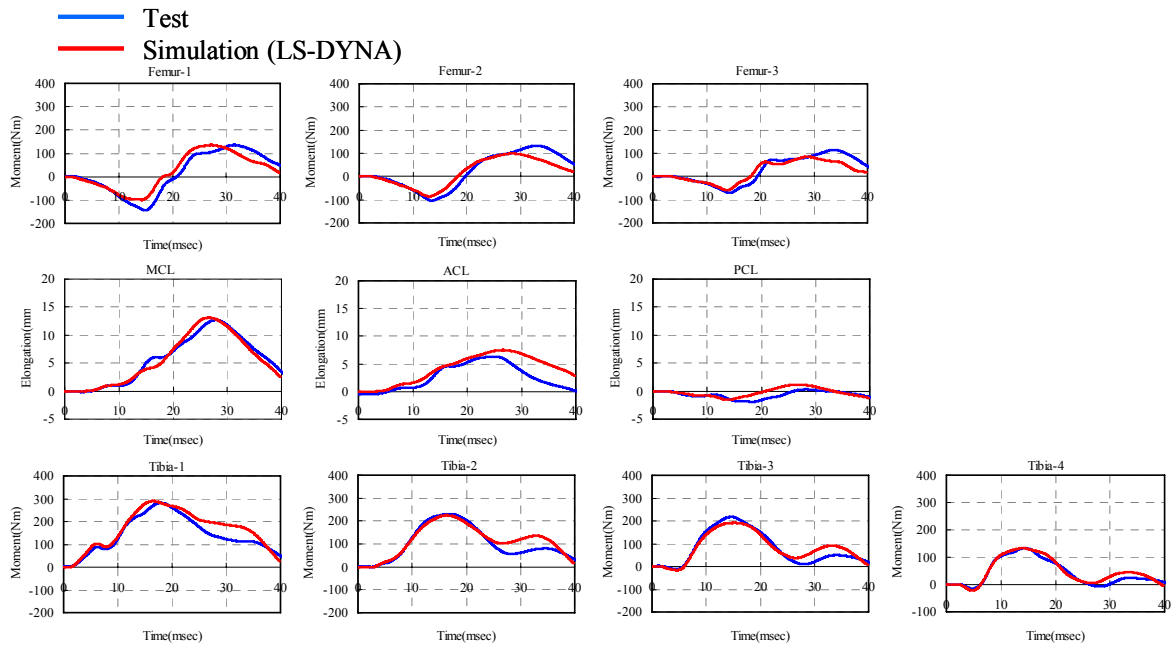


Figure 28. Flex-GT injury time history curves.

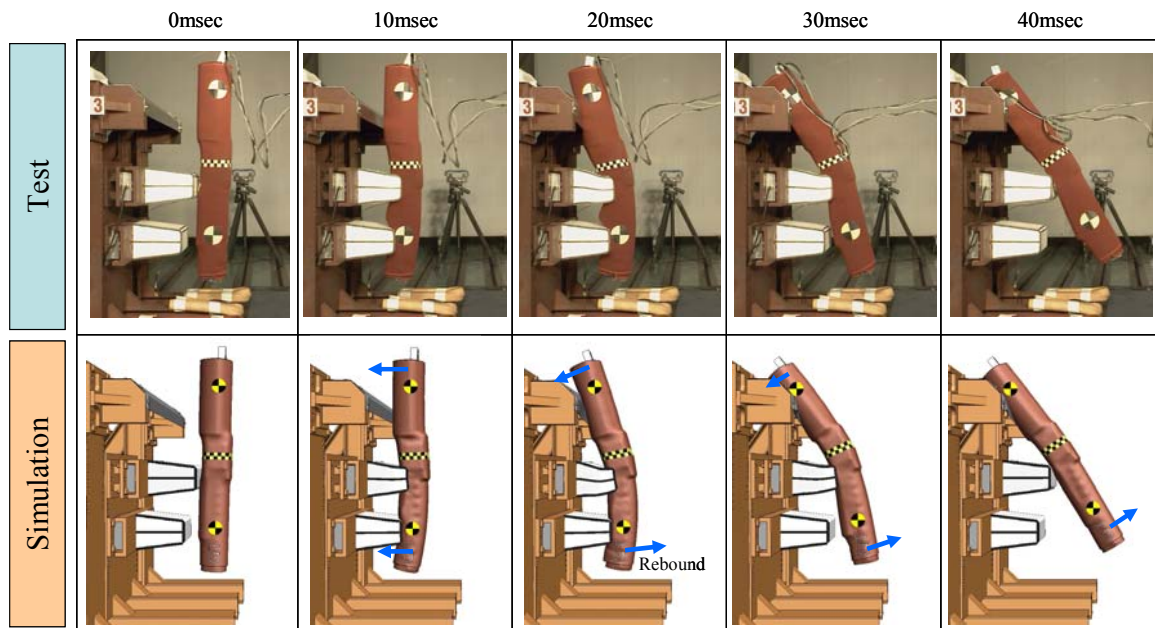


Figure 29. Flex-GT deformation mode.

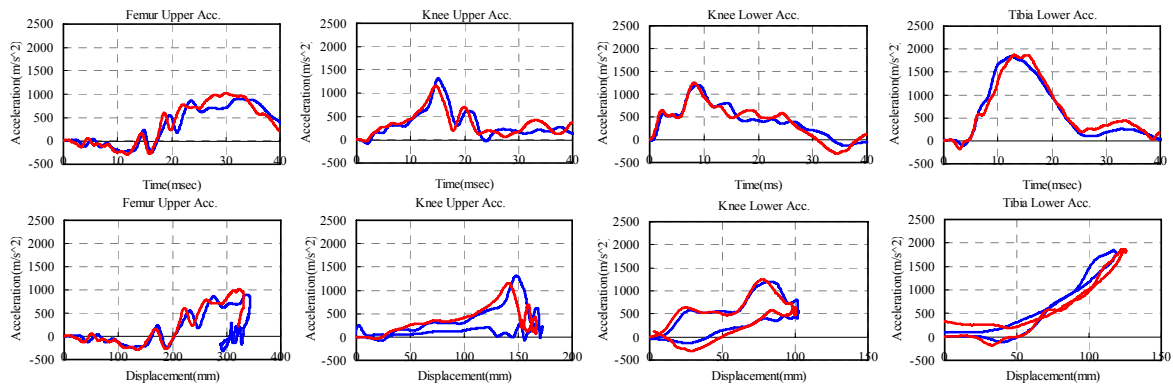


Figure 30. Flex-GT acceleration and displacement curves.

Flex-GT Injury Investigation

In this study, the Flex-GT injury mechanisms which occur in the simplified car rig test (see Figures 28 to 30) are investigated and some ideas for reducing these injuries are studied.

First, the lower knee contacts the bumper and the knee lower acceleration rises sharply. Soon after, the tibia contacts the spoiler which is located 50mm back from the bumper. At just 15msec the tibia starts to rebound by unloading forces from the bumper and the spoiler. At this time the lower tibia is moving like the curl of a whip and the tibia lower acceleration reaches a maximum.

The femur starts to contact the BLE at around 15msec, and the peak knee upper acceleration happens at that time. The BLE is positioned 150mm backward from the bumper. At 30msec the femur starts to rebound from the BLE and the femur upper acceleration reaches a maximum. Overall, the Flex-GT rotates forward and finally leans on the BLE. This is mainly caused by the setback differences of the BLE and the spoiler.

The peak MCL occurs at approximately 27msec while Flex-GT is still rotating forward. The maximum tibia moment, 289Nm, occurs at Tibia-1 near the bumper, at 15msec when the bumper reaction force becomes greatest. The maximum femur moment, 136Nm, occurs at Femur-1 at 30msec, when the BLE reaction force reaches its peak.

Ways to reduce Flex-GT injuries are discussed in the following section. As described above, the peak MCL occurs during the overall rotation of Flex-GT. It is considered likely that MCL is related to the rebounding properties of the bumper and spoiler and the stiffness of BLE.

There are two simple ideas to reduce the MCL.

- Control the kinematic behaviour of Flex-GT.
- Absorb more energy within the vehicle front structure (without adversely affecting performance in other crashes).

Better kinematic behaviour means less femur forward displacement, achieved using a stiff BLE, and/or greater tibia rearward motion by a larger rebound off the spoiler. Also, the rebounding stiffness of the bumper should be less than the spoiler because reaction forces from the bumper contribute more to knee bending.

However, these countermeasures require raising forces on the femur and tibia and might lead to increase in bending moments. The bending moments are measured all along the femur and tibia (see Figure 3), so any countermeasure loads must be distributed

carefully.

This problem suggests that it is necessary to carefully control load balance and timing on the femur and tibia as well as the distribution of energy absorption within the vehicle structure and Flex-GT.

In order to solve such a complicated problem with so many input parameters, an optimization method is recommended. CAE is a very efficient way to obtain an optimized solution in a short period of time and at reasonable cost. Also, CAE is able to provide a lot of detailed data: reaction force time histories, visualisation of load paths through the vehicle structure, insight into the Flex-GT kinematic modes and detailed knee bending behaviour (See Figure 31). This data is needed to clearly understand the mechanisms that cause leg injury. It is impossible to get such data relying only on real experiments. Furthermore, this method can be used on vehicles in the early design stages, before any real prototypes exist.

The Flex-GT model is considered an essential tool in the development of effective pedestrian protection technologies.

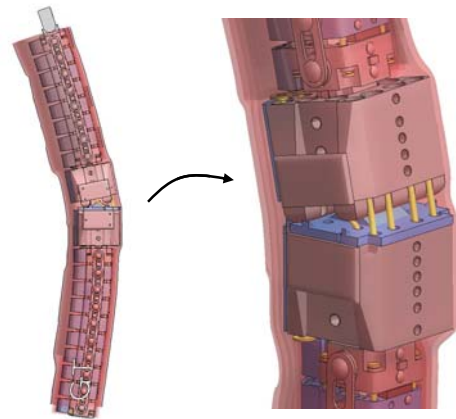


Figure 31. Flex-GT deformation mode.

Further Simplified Car Rig Tests

As shown in Table 2, a total of 6 impact cases were performed using the simplified car rig in various setback and height configurations. In all cases, the model showed excellent agreement with tests. The Flex-GT model was thus validated to a high accuracy level under similar impact conditions with real vehicles. Also, these results themselves were very useful to investigate the influence of vehicle front structure layout upon the Flex-GT kinematic behaviour.

Table 2.
All test case conditions (mm)

CASE ID	S1	S2	H1	H2	H3
B01	0	130	Sedan type A		
B02	50	130			
B03	100	130			
B04	0	130	SUV type A		
B05	50	130			
B07	50	130	SUV type B		

FULL VEHICLE MODEL FLEX-GT IMPACT

Figures 32 and 33 show two impact simulations with a full vehicle and the resulting stress distribution.

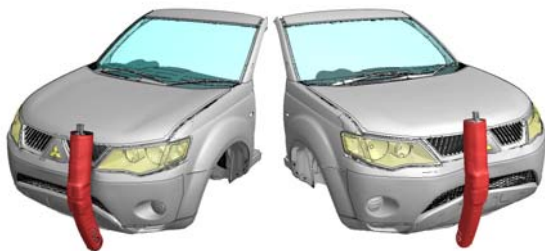


Figure 32. Full vehicle model results.

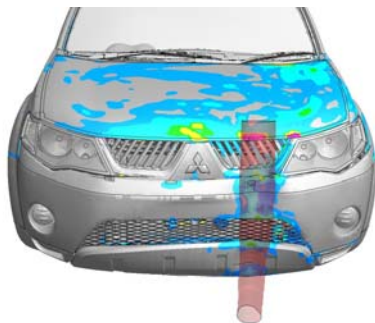


Figure 33. Stress distribution in vehicle.

The Flex-GT LS-DYNA model was confirmed to be highly robust under several full vehicle impact conditions and the calculation cost deemed very reasonable at current computing standards. Overall, the Flex-GT model is considered highly suited to CAE vehicle development.

FLEX-GTR MODEL DEVELOPMENT PLAN

An effort to upgrade Flex-GT LS-DYNA model into Flex-GTR is currently underway. Part of the upgrade includes changes to the knee ligament system [11], but most of structure and performance of Flex-GTR is reported to be similar to the Flex-GT. Therefore the modelling techniques and methods employed in developing Flex-GT model can be directly applied to Flex-GTR, ensuring the same high level of accuracy and realism.

CONCLUSION

A Flex-GT LS-DYNA model has been successfully developed and the following results were obtained:

- 1) A high accuracy Flex-GT LS-DYNA model was developed that satisfies all calibration requirements. In particular, excellent correlation of injury graphs was achieved in the dynamic calibration test.
- 2) Thorough validation was achieved using a series of simplified car rig impacts at 40km/h. By accurately predicting the same trends as test, the Flex-GT model is confirmed to have sufficient accuracy and high performance for use in vehicle development analysis.

ACKNOWLEDGEMENT

The authors would like to show grateful appreciation to the engineers at JARI for their cooperation and help in understanding the physical Flex-GT impactor, and also for executing the precise calibration and simplified car rig tests used in this study. They would also like to thank Richard Taylor of Arup for advice and support.

REFERENCES

- [1] Mizuno Y.: "Summary of IHRA Pedestrian Safety WG Activities (2005) – Proposed Test Methods to Evaluate Pedestrian Protection Afforded by Passenger Cars", Paper Number 05-0138 ESV (2005)
- [2] Konosu A.: "Development of Flexible Pedestrian Legform Impactor (Flex-PLI) and Introduction of Flex-PLI Technical Evaluation Group (Flex-TEG) Activities", <http://www.sae.org/events/gim/presentations/2008konosu1.pdf>, SAE Government/Industry Meeting (2008)
- [3] Konosu A. and Tanahashi M.: "Development of a biofidelic pedestrian legform impactor: Introduction of JAMA-JARI legform impactor ver. 2002. Proc", 18th International Technical Conference on the Enhanced Safety of Vehicle, Paper No. 378 (2003)
- [4] UN/ECE/WP29/GRSP/INF-GR-PS/Flex-TEG: "Information on Flexible Pedestrian Legform Impactor Type GT (Flex-GT)", TEG-033 (2007)
- [5] UN/ECE/WP29/GRSP/INF-GR-PS/Flex-TEG: "Flex GT Testing of US Vehicles", TEG-063 (2008)
- [6] UN/ECE/WP29/GRSP/INF-GR-PS/Flex-TEG: "Flex-GT: Repeatability and reproducibility of assembly certification and inverse test results",

TEG-051 (2007)

[7] UN/ECE/WP29/GRSP/INF-DOC: “Status Report on Flexible Pedestrian Legform Impactor Technical Evaluation Group (Flex-TEG) Activities”, GRSP-44-28 (2008)

[8] UN/ECE/WP29/GRSP/INF-GR-PS/Flex-TEG: “Report on Tests with the Flexible Pedestrian Legform Impactor Flex GT α and Flex GT”, TEG-043 (2007)

[9] Hallquist J. O.: “LS-DYNA Keyword User’s Manual Version 971” (2007)

[10] UN/ECE/WP29/GRSP/INF-GR-PS/Flex-TEG: “Flex-GT Full Calibration Test Procedures”, TEG-047 (2007)

[11] UN/ECE/WP29/GRSP/INF-GR-PS/Flex-TEG: “FLEX-PLI-GTR Development Mechanical Design”, TEG-054 (2008)

DEVELOPMENT OF A BIOFIDELIC FLEXIBLE PEDESTRIAN LEGFORM IMPACTOR TYPE GTR PROTOTYPE

PART2: TECHNICAL DETAILS

Bernard Been and Mark Burleigh

First Technology Safety Systems
The Netherlands and the United Kingdom

Atsuhiko Konosu and Takahiro Issiki

Japan Automobile Research Institute
Japan

Yukou Takahashi and Hideki Suzuki

Japan Automobile Manufacturers Association, Inc
Japan

Paper Number 09-0146

ABSTRACT

In 1998 the European Enhanced Vehicle-Safety Committee (EEVC) proposed a test procedure to assess the protection vehicles provide to the lower extremity of a pedestrian during a collision. This procedure utilizes a legform impactor composed of rigid long bones. In order to improve biofidelity of the legform impactor, the Japan Automobile Research Institute (JARI) and the Japan Automobile Manufacturers Association, Inc. (JAMA) have been developing a biofidelic flexible pedestrian legform impactor (Flex-PLI) since 2002.

The Flex-PLI has high biofidelity especially for its long bone parts, which have human-like bending characteristics under a car impact condition, compared to other types of legform impactors, which have rigid long bone parts. The Flex-PLI also provides extended injury assessment capability, including long bone bending moment at multiple locations and knee ligament elongations in comparison to other pedestrian legforms.

In 2005, the Flex-PLI Technical Evaluation Group (Flex-TEG) was settled under the UN/ECE/WP29/GRSP/Informal Group on Pedestrian Safety in order to evaluate its performance to adopt the impactor as a regulatory purpose test tool for a Global Technical Regulation on Pedestrian Safety (PS-GTR: gtr 9). The Flex-PLI was evaluated and improved its performance under the Flex-TEG activity, and then its design of the final version, type GTR (Flex-GTR), was agreed by the Flex-TEG members in April 2008.

This paper provides technical details of the Flexible Pedestrian Legform Impactor GTR prototype (Flex-GTR prototype). Technical specifications on all important aspects of the Flex-GTR prototype are given: dimensions and mass at (sub-) assembly level; biomechanical responses of main components of the femur, knee and tibia; calibration procedures

and corridors; standard and optional instrumentation channels, their capacity and position; handling; including details of electrical systems and data acquisition. The paper will present results of calibration testing, repeatability and reproducibility of three prototypes which are evaluated at First Technology Safety Systems (FTSS) before their release from the FTSS factory.

INTRODUCTION

In 1998, the European Enhanced Vehicle-Safety Committee proposed a test procedure to assess the protection vehicles provide to the lower extremity of a pedestrian during a collision [1]. This procedure utilizes a legform impactor composed of rigid long bones. In order to improve biofidelity of the legform impactor, the Japan Automobile Research Institute (JARI) and the Japan Automobile Manufacturers Association, Inc. (JAMA) have been developing a biofidelic flexible pedestrian legform impactor (Flex-PLI) since 2002 [2]. The Flex-PLI has high biofidelity especially for its long bone parts, which have human-like bending characteristics under a car impact condition, compared to other types of legform impactors, which have rigid long bone parts [3]. The Flex-PLI also provides extended injury assessment capability, including long bone bending moment at multiple locations and knee ligament elongations in comparison to other pedestrian legforms [3].

In 2005, the Flex-PLI Technical Evaluation Group (Flex-TEG) was settled under the ECE/WP29/GRSP/ Informal Group on Pedestrian Safety in order to evaluate its performance to adopt the impactor as a regulatory purpose test tool for a Global Technical Regulation on Pedestrian Safety (PS-GTR). The Ministry of Land, Infrastructure, Transport, and Tourism of Japan (J-MLIT) has been supporting this Flex-TEG activity, taking a task of a chair country of the group and conducting technical evaluation tests on the Flex-PLI. After the

settlement of the Flex-TEG, the Flex-PLI was evaluated and improved its performance under the Flex-TEG activity, and then its design of the final version, type GTR (Flex-GTR), was agreed by the Flex-TEG members in April 2008 [4], and its prototype (Flex-GTR-PROTO) was released in November 2008. In the Flex-GTR development, First Technology Safety Systems (FTSS) is involved as a dummy development specialist company. This paper provides technical details of the Flex-GTR prototype and changes that were made with respect to the previous version, the Flex-GT. Technical evaluation test results on them under several impact conditions are presented separately in Paper Number 09-0145.

DESIGN IMPROVEMENTS

Methodology

As part of the Flex-TEG activities a design review of the Flex-GT version was completed. This activity highlighted a number of changes necessary to improve sensitivity, handling and durability. The recommendations resulting from the design review were the starting point for the Flex-GTR development. The most important issues found were:

1. The cruciate ligaments in the Flex-GT knee exert a twist moment causing misalignment between the femur and the tibia. It was recommended to balance these ligaments with an additional set of cruciate ligament springs.
2. The position of the ligament elongation sensors on the outside of the Flex-GT would cause a difference in sensitivity to left and right oblique loading. It was recommended to position ligament sensors at the centreline of the tool.
3. The high channel count of the Flex-PLI and associated larger umbilical cable might cause a higher influence on the free flight trajectory and reduced accuracy of hitting the target impact location. It was recommended to integrate an on-board data acquisition system (DAS).
4. Some umbilical cable damage was experienced during the Flex-GT evaluation and caused significant downtime of the Flex-PLI because of necessary repairs. It was recommended to provide better cable protection and to make a quick disconnect of the umbilical cable to off board possible. This would help continuation of testing and repair of spare cable simultaneously.
5. It was recommended to update the dynamic calibration procedure, to obtain a loading level closer to the injury tolerance level and loading during vehicle testing.

An important boundary condition for the Flex-GTR development was that the performance of the Flex-GT version should be maintained, as not to invalidate what was achieved with the GT version in the Flex-TEG. Therefore existing size, mass and

materials were to be maintained as much as possible. Numerous smaller changes were recommended and integrated into the Flex-GTR design to improve handling and durability.

Design improvements

To balance the twist moment, additional springs were added in the knee. The distribution of the load required smaller springs and thinner ligaments to be used. The spring rate and the stroke of the springs were adapted to maintain the original response. Bronze bushes were introduced and plastic cable sleeves were omitted to reduce friction and wear.

To address sensitivity to oblique load, new and smaller ligament elongation sensors were positioned on the centreline of the knee (see Figure 1). Also for ligament sensors, bronze bushes were introduced to reduce friction and wear.

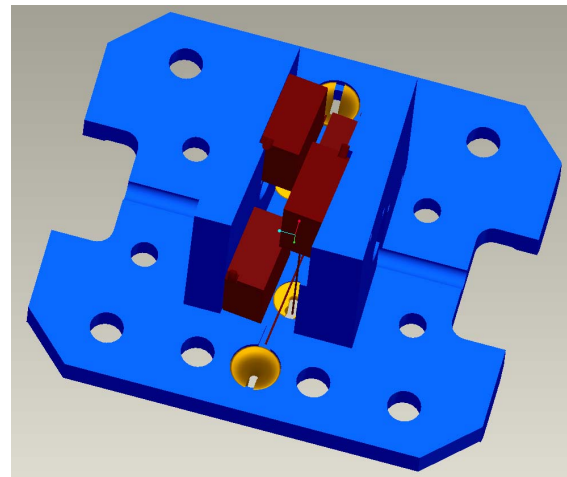


Figure 1: Ligament sensor arrangement at centreline

The addition of optional on-board data acquisition systems was achieved within the dimensions of the Flex-GT specifications. The smaller cruciate springs gave additional space in the front and rear sides for integration of on-board DAS. Two systems from different DAS equipment manufacturers were integrated: DTS-SLICE and MESSRING M=BUS. As off-board DAS is also considered, three different version prototypes were manufactured: with off-board, 'M=BUS' and 'SLICE' data acquisition systems.

The Flex-GTR is standard equipped with a connector system that allows quick disconnection of umbilical cables to the various data acquisition systems and for sensor exchange.

The dynamic calibration procedure was enhanced by running the test with the leg upside down, the addition of a 5 kg mass at the femur end, addition of an accelerometer to the knee and introduction of a stopper block performance test.

Further enhancements were introduced especially to improve handling and durability. To name a few: to protect the ends of the leg after rebound from a test, moulded polymer bumpers were added to the tibia base and femur top; locking nuts were used on the knee ligaments and bone cables to better maintain adjustment settings; to improve free flight stability, the umbilical cable exit locations were brought closer to the centre of gravity of the leg; to enhance the assembly of the tight fitting Neoprene outer covers, a larger plastic zipper was selected and hook and loop flaps were added to protect the zipper.

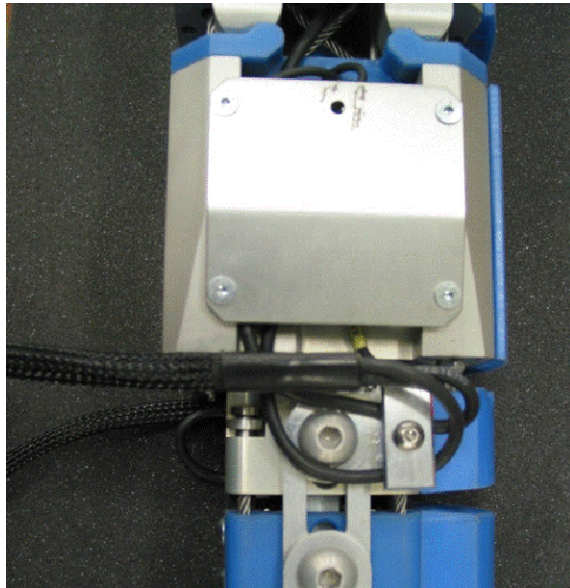


Figure 2: Off board cable clamp arrangement

ANTHROPOMETRY

Figure 3 shows the Flex-GTR from the rear identifying the knee joint position and the bone lengths next to a picture of the human right leg for orientation purpose. Also the co-ordinate system convention for automotive testing [5] is shown, with x –direction, forward away from the observer.

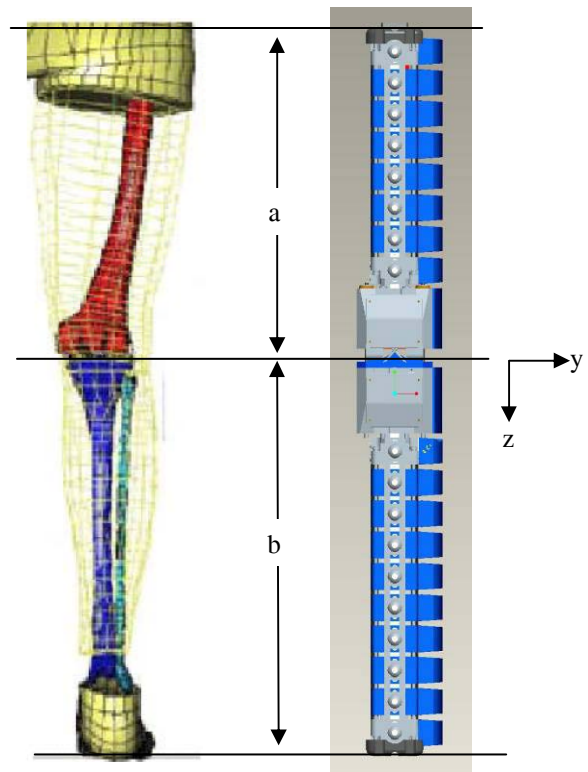


Figure 3: Human bone dimensions and Flex GTR

Figure 4 shows the position of ligament elongation sensors in a plan view of the tibia knee side (femur knee side removed). Refer to legend for identification.

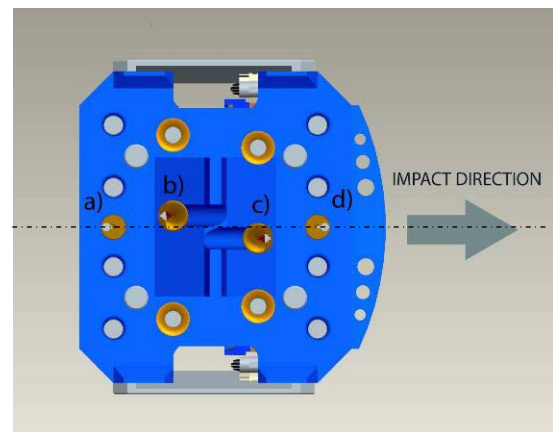


Figure 4: Ligament sensor positions in knee joint

- a) Medial Collateral Ligament, MCL
- b) Posterior Cruciate Ligament, PCL
- c) Anterior Cruciate Ligament, ACL
- d) Lateral Collateral Ligament, LCL

Table 1: Comparison of human leg to GTR

Length, C.G. Location [mm], and Mass [kg]	50th percentile male [6]	Flex-GTR
a) Thigh length	428	433
b) Leg length	493	495
C.G. location of thigh**	218	195
C.G. location of leg **	233	188
Total legform impactor mass	13.4	12.94
Thigh mass	8.6	7.16
Leg mass	4.8	5.78

** From the knee joint centre; Flex-GTR C.G values are estimates from CAD.

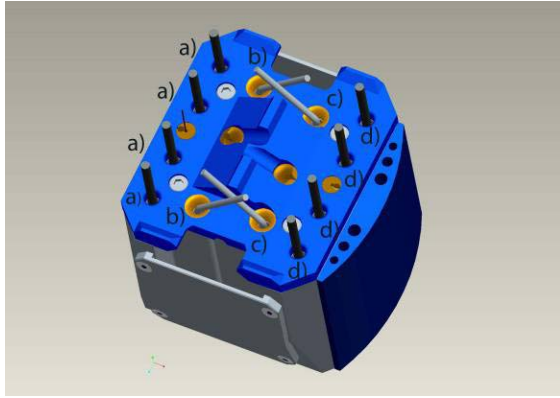


Figure 5: Ligament wire positions

Figure 5 shows the tibia knee block with ligament wires cut through to help identification.

INSTRUMENTATION

Standard Instrumentation

The standard instrumentation channels are listed in Table 2. The table also gives details on the sensor vertical distance from the knee centre. Channel numbers are proposed for a standard sensor numbering for the Flex-GTR. To obtain control over the dynamic calibration deceleration pulse, an accelerometer was added to sensor list in the GTR version.

The strain gages on the bones, measuring bone bending moments in the impact direction ‘Y’ (X bending moment) were made into a half bridge configuration incorporating both the tension and compression sides of the bone in one channel, two resistors per each set of gages complete the full bridge. The bridge completion resistors and sensor identification (ID) chips are encapsulated in a PCB located on each bone. The completed full bridge configuration makes the output of the sensor insensitive to elongation due to tension in the bone and length variation due to thermal expansion and also increases the voltage output compared to application of single strain gages per the GT version.

The durability of the gage bonding was confirmed in a production test submitting the gages to 50 quasi-static deflections to check bonding process.

Table 2: Standard instrumentation and the sensor distance from the knee joint

Channel Number	Channel	Distance (mm)
1	Femur moment 3	297
2	Femur moment 2	217
3	Femur moment 1	137
4	LCL elongation	0
5	ACL elongation	0
6	PCL elongation	0
7	MCL elongation	0
8	Tibia moment 1	134
9	Tibia moment 2	214
10	Tibia moment 3	294
11	Tibia moment 4	374
12	Lower knee acceln.	47

Optional Instrumentation

FTSS was requested by JAMA to consider the addition of optional sensors for research and development purpose. The optional sensors are listed in Table 3. It is recommended to use the additional sensors only for research purpose and not to deviate from standard during tests for official purpose (future legislation or consumer rating) to assure proper test mass and inertial properties.

Figure 6 shows the optional sensor positions in the tibia. Item 1 in green shows the tri-axial accelerometer inside an Aluminium mount. Item 2 shows the single axis a_y accelerometer mounted inside a dedicated impact segment. The segment y -accelerometer can be positioned at any of the inner segments if required. Item 3 shows the subassembly with a tri-axial linear accelerometer and the three angular rate sensors inside a mount and its dedicated impact segment. The optional sensors on the femur are the mirror image of that shown in Figure 6 and share the same components.

Table 3: optional sensors position and parameters

Sensor location	Measurement Parameter
Femur top	Acceleration a_x, a_y, a_z
Knee top	Acceleration a_x, a_y, a_z Angular rate $\omega_x, \omega_y, \omega_z$
Knee bottom	Acceleration a_x, a_y, a_z Angular rate $\omega_x, \omega_y, \omega_z$
Tibia bottom	Acceleration a_x, a_y, a_z
Segments	Acceleration a_y

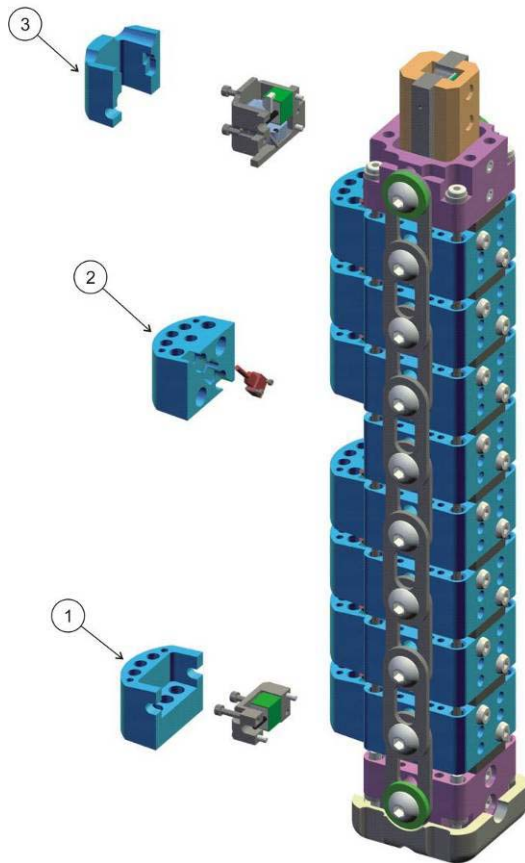


Figure 6: Optional sensors in the tibia

DATA ACQUISITION SYSTEMS (DAS)

Off-board data acquisition

To connect the instrumentation to a static laboratory data acquisition system, two umbilical cables are used, both handling 6 channels of instrumentation. To enable a quick disconnect of the umbilical cable to off-board in case of damage, the Flex-GTR is equipped with two connector blocks installed on either side of the tibia knee. Each connector block handles 6 standard channels and each has additional capacity of 6 channels for optional instrumentation. It is possible to expand the channel count to a total of 24 channels with the use of the standard connector blocks.

The modular system makes it easy to exchange defunct sensors and damaged umbilical cables and also to change between on-board and off-board DAS. The connector block can be seen in the tibia section of the knee in Figure 7. The use of very small nano-D military spec connectors was essential to meet the space constraints.

On-board data acquisition systems

On-board data acquisition is an important addition to the Flex-GTR. Its use helps prevent cable damage particularly on violent rebound with the floor. Off-board umbilical cables could also affect free flight trajectory, therefore on-board DAS would make hitting the intended target more precisely, giving better control and improving repeatability. The use of on-board DAS can reduce operational costs.

The standard 12 channels could be expanded here with the advantage of not affecting free flight stability. The on-board DAS systems use the same connector blocks to interface between the sensors and the DAS.

Two on-board DAS systems were selected for the Flex-GTR prototype to offer customer choice. Both systems had to be very small and light weight to meet the challenging space limitations on the leg. At customer request, alternative DAS systems could be considered, if suitable in terms of mass and size.

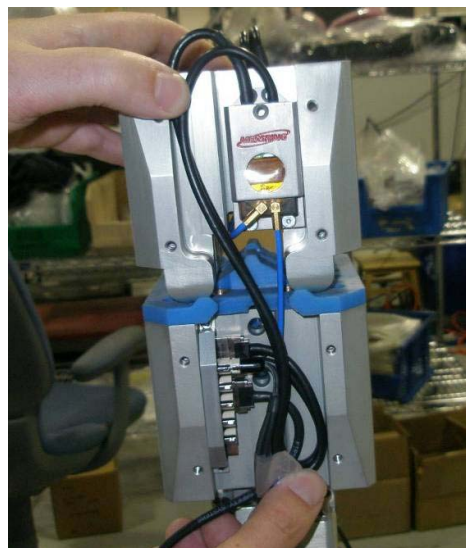


Figure 7: MESSRING M=BUS installation and connector block

MESSRING M=BUS® - The M=BUS® is a data acquisition system based on independent 6 channel data loggers (40x25x14)mm in size (without its aluminium housing). The units can be daisy chained together via a single coax cable ending in a terminator, which checks system integrity and signal quality. Two units were required for the Flex-GTR standard instrumentation and packaged on either side of the femur knee block, see Figure 7. Each logger is equipped with its own battery, allowing gathering data entirely wireless, even without external power supply. The system is equipped with a low friction disconnect fitting, which is located just below the knee. At launch, the disconnect fitting releases and the DAS starts to register data automatically. The units will record for

17 seconds. An external trigger defines t0. After the test, the cable is reconnected and the test data is downloaded to a PC. Time synchronisation of all channels is guaranteed over an integrated master and slave clock concept.

DTS SLICE - The DTS SLICE was under development at the same time as the Flex-GTR. The SLICE data recorder is a modular system built up from functional units by stacking modules of the required functionality. The Base SLICE contains the processor and memory; the Bridge SLICE's are stacked on top providing channel functionality, each Bridge SLICE handles 3 channels. The functional units are interconnected by integrated connectors for easy replacement (see Figure 8). Two super capacitors provide on-board power after disconnect allowing to operate for sufficient time. The super caps could be quickly charged for the next test but had a short record time (the 1 second), a battery will be considered for future use. Like the M=BUS system, there is a disconnect feature, which is reconnected to download test data. The DTS SLICE is triggered on disconnect and a tape switch can also be connected to establish t0.

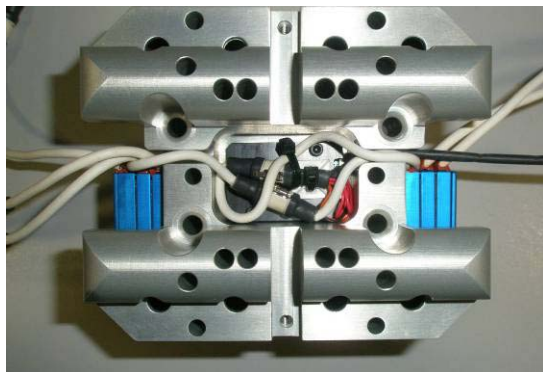


Figure 8: DTS SLICE installation

CALIBRATION

Method

Table 4 provides an overview of the complete Flex-GTR prototype calibration procedures, including the purpose of the test. Five calibration steps and a total of 12 tests are required.

Proposed calibration frequency for all steps:

- At manufacture
- Each year
- [After exceeding injury assessment reference value (IARV)]
- After failure of dynamic test
- After parts exchange

Additionally proposed frequency for step 4 and 5:

- [Each [1-10] tests]

Some of the figures are given between brackets as these are still under discussion and may change.

Table 4: Full calibration test procedure overview

Test	Test Nr	Purpose
Step 1 Bone Core	7	1) Control Bending Characteristic 2) Obtain individual Sensor sensitivity
Step 2 Femur & Tibia Assembly	2	1) Control Bending Characteristics 2) Check ultimate bending moment
Step 3 Knee Assembly	1	1) Control Bending Characteristics 2) Control Ligament Elongation
Step 4 Dynamic stopper block	1	1) Control deceleration pulse dynamic test 2) Evaluate consistency of the stopper block
Step 5 FLEX-PLI Dynamic	1	1) Simple test to control output of sensors 2) Evaluate consistency of the assembly

The Flex-GTR calibration procedures were further developed: single gage calibration to establish gage sensitivity and roller supports under end pivots to rule out elongation and tension-compression loads on bone, femur, tibia and knee assemblies.

The dynamic calibration procedure was enhanced to induce higher loads to the level of loading in actual vehicle tests and closer to the injurious level. Also the fixture was enhanced to improve handling and reproducibility.

Bone calibration

Bone Calibration Fixture Design – To improve the accuracy of the gage response, each gage channel (tension and compression) is certified to establish the sensitivity of each gage in a separate test. To achieve this, a fixture was designed to load centrally over each gage over a pivot distance of 165mm.

Bone/Gage Calibration Procedure – To calibrate the bone, an Instron machine is used with a high definition load cell on the loading ram. The bone is mounted in the bone calibration fixture and is placed over the roller carriages on a hardened steel base. With a support distance of 165mm, the bone is loaded precisely in the middle between the end supports to 10 kN (325 Nm) at a rate of 10mm/min.

Femur and Tibia Calibration

The same fixture parts are used as the Flex-GT tibia and femur assemblies. The only changes made to these fixtures from the Flex-GT specification was the addition of roller cages under the pivots (to prevent linear friction when in bending) and update of the knee-to-leg interface.

Femur and Tibia Calibration Procedure – As with the bones, an Instron machine is used with a high definition load cell. The same base and roller cages are utilised (see Figure 9 and Figure 10). The femur is loaded on the fourth segment from the knee and for the tibia the fifth segment. A piece of Neoprene protects the impact segment from the loading block.

Both assemblies are loaded to 3.76kN. The gage outputs are recorded to check functionality and the moment is calculated from the load multiplied by the known fixture arm.

Femur Moment $M_f = [F(N) / 2] \times 0.165(m)$

Tibia Moment $M_t = [F(N) / 2] \times 0.205(m)$



Figure 9: Tibia calibration fixture



Figure 10: Tibia under load in calibration fixture

Knee Calibration

Similar to the leg assemblies, the same knee fixture design as that of the Flex-GT is used, except the leg interface has been changed and the end pivots sit on roller cages. The Flex-GT procedure had load cells on each support, whereas the Flex-GTR setup just uses one centre load cell on the loading ram.

Knee Calibration Procedure – The same set up is used here as on the femur and tibia assemblies, except the loading is done using a 100 mm diameter profile (see Figure 11). The loading profile is aligned with the edge of the knee centre and loaded to 4 kN. Force and elongation are recorded for the MCL, ACL and PCL. In this test, the LCL is in compression and therefore LCL elongation is not recorded. The knee moment is calculated using the following equation:

Knee Moment $M_k = [F(N) / 2] \times 0.2(m)$



Figure 11: Knee during calibration under load

Dynamic Calibration

The whole leg assembly with flesh is calibrated on a new pendulum calibration fixture (see Figure 12). In order to achieve a similar load level as in a vehicle test, some changes were proposed to the Flex-GT procedure. The leg has been turned upside down so that the tibia is now at the top pivot end; a 5 kg mass was added to the femur end at the bottom. The leg is raised 15 degrees above the horizontal and released via a solenoid latch impacting the upper knee area onto the stopper block buffer. To obtain feedback from the test pulse, an accelerometer was placed in the knee to check repeatability. All 12 standard channels are recorded.

Stopper block calibration

This is a simple fixture (see Figure 13), comprising of a long cylindrical 50 mm diameter 7 kg mass dropped via a solenoid release through a linear bearing onto the stopper block. The impact edges of the mass are radiused to prevent damage to the stopper block. The drop height to the block is 200 mm (2 m/s). An accelerometer is attached to the top of the mass to record deceleration.



Figure 12: Dynamic calibration fixture



Figure 13: Stopper block calibration fixture

Prototype Calibration Results

Bone/Gage Calibration Results

An analysis of the results of three Flex-GTR prototypes from nine gages on three femurs and 12 gages on three tibias is shown in Table 5 and Table 6. The nonlinearity and hysteresis meet SAE J2570

[7] performance specification for transducers, which applies to rigid load cells.

Table 5: Femur bone strain gage calibration summary

Femur	Offset mV/V	Non linearity % Full scale	Hysteresis
Average	0.00007	0.27	0.71
St Dev	0.00036	0.07	0.29

Table 6: Tibia bone strain gage calibration summary

Tibia	Offset mV/V	Non linearity % Full scale	Hysteresis
Average	-0.0029	0.45	0.64
St Dev	0.0061	0.24	0.29

Femur and Tibia Assembly Calibration

Results

Figure 14 shows the femur assembly prototype responses in the corridors that were established with the GT version. The Flex-GTR femur meets the Flex-GT calibration corridors. These corridors will be adopted for the Flex-GTR femur.

Figure 15 shows the tibia assembly prototype responses in the corridors that were established with the GT version. The Flex-GTR tibia meets the Flex-GT calibration corridors and will be adopted for the Flex-GTR tibia assembly.

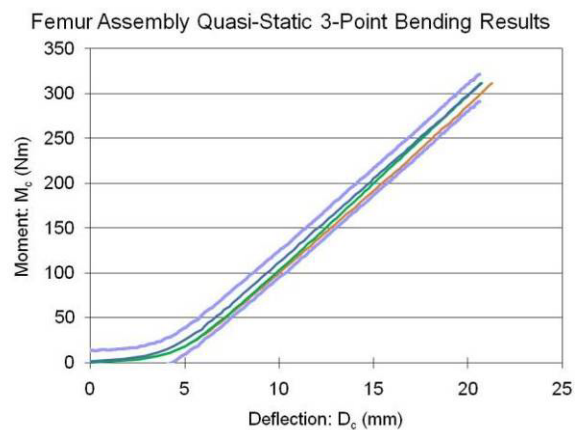


Figure 14: Femur assembly moment/deflection and corridor

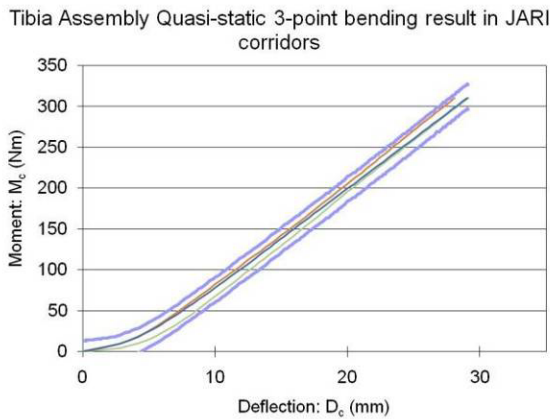


Figure 15: Tibia assembly moment-deflection and corridor

Knee Calibration Results

Figure 16 and Figure 17 show the Flex-GTR knee calibration results in the Flex-GT corridors. The Flex-GTR MCL ligament elongation vs. bending moment is below the lower Flex-GT corridor beyond 18 mm MCL ligament elongation. The reason for this is most likely due to the reduction in friction of the supports by introduction of the roller supports. A possible contributor is the reduction in friction due to the removal of the plastic wire sleeves on the Flex-GT knee and use of bronze bushings in the cruciate ligaments. These hypotheses can be examined by subjecting the GTR version to the Flex-GT calibration procedure without the roller supports. The ACL and PCL ligament elongations were slightly outside the Flex-GT corridors.

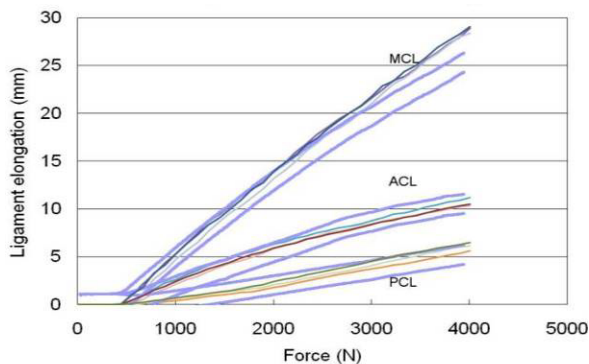


Figure 16: MCL, ACL and PCL elongation to force in the GT corridors

The MCL, ACL and PCL corridors need to be adapted to the new procedure and the Flex-GTR design.

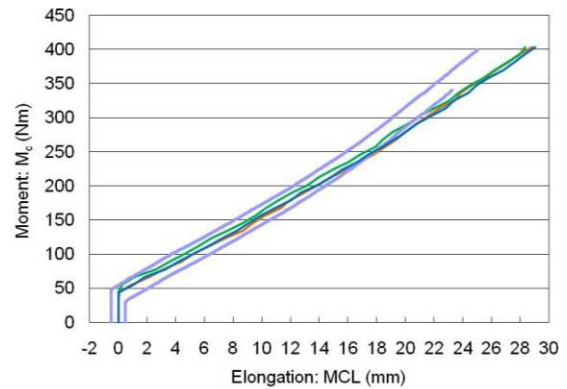


Figure 17: Knee moment to MCL elongation in GT corridor

Proposed Flex-GTR Knee calibration corridors

The responses of the 3 Flex-GTR prototypes were analysed and new corridors were developed. The corridors for the MCL were derived from the average of three prototype MCL responses. A second order polynomial was derived from the average. The upper and lower bounds were determined by addition and subtraction of 15 Nm from the average. The corridors and responses are shown in Figure 18.

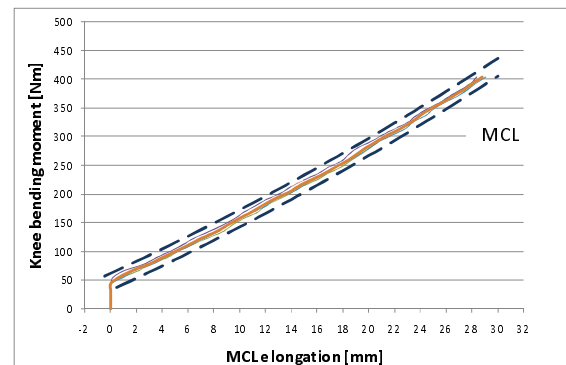


Figure 18: Knee moment to MCL elongation in proposed GTR corridor

The corridors for the ACL and PCL were derived with a similar method. The corridors for the ACL and PCL were derived from the average of three prototype ACL and PCL responses. Second order polynomials were calculated from the average. The upper and lower bounds were determined by addition and subtraction of 1 mm from the average. The corridors and responses are shown in Figure 19. To avoid possible conflicts, no MCL corridor is given for elongation-force (see Figure 16 and Figure 19).

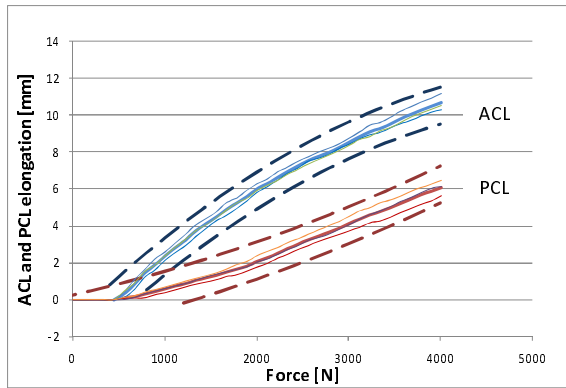


Figure 19: ACL and PCL elongation to force in proposed GTR corridors

Stopper Block Calibration Results

Before the start of the dynamic calibration matrix, the stopper block was tested to establish repeatability and reproducibility. The stopper block calibration was carried out on 3 different assembled stopper blocks to assess its response variation. Tests were repeated twice. Table 7 shows the results including proposed corridors. The reproducibility is good with 2.1% variation.

Table 7: Stopper block drop test results and propose corridor

	Acceln. [G]	Force [kN]
Block #1	56.2	3.859
	55.8	3.832
Block #2	54.5	3.743
	54.2	3.722
Block #3	52.7	3.619
	54.0	3.708
Average	54.6	3.749
St Deviation	1.2	
CV (%)	2.1	
Upper corridor	4.00	
Lower corridor	3.50	

Dynamic calibration

Table 8 shows the dynamic test matrix and the use of two stopper blocks to look at variation. The last 2 tests were known to have an inclination of 15.1° as opposed to 15°.

Table 8: Dynamic test matrix

Test Nr	DAS type	Stopper block
Test 1	Off board	block #1
Test 2	Off board	block #1
Test 3	Off board	block #1
Test 4	Off board	block #2
Test 5	MESSRING	block #2
Test 6	MESSRING	block #1
Test 7	MESSRING	block #2
Test 8	MESSRING	block #1
Test 9	MESSRING	block #1
Test 10	DTS	block #1
Test 11 (15.1°)	DTS	block #1
Test 12 (15.1°)	DTS	block #1

Results

The result of 12 dynamic tests are summarised in Table 9. The table shows the average, standard deviation, coefficient of variation (CV), the draft criteria and standard deviation divided by the criteria. The coefficient of variation is generally well below 3%, which is considered excellent. On tibia gage 3 of leg 3, there was a higher reading than expected. This was due to a fault on the gage, which had a linearity error of 2.5% and was not picked up during gage calibration as a problem. The ACL and PCL were higher than 3% variation; however the variation is larger due the small absolute output. The CV relative to the tentative injury assessment reference values (t-IARV), which are used in Paper Number 09-0145, is closer to 3% for both parameters. The variation of the knee peak acceleration was also higher. This is believed to be due to problems with one of the accelerometers.

Table 9: Summary dynamic calibration

GTR Dynamic calibration results	Peak Acceleration @ Knee	Peak Moment @ Femur Gauge 1	Peak Moment @ Femur Gauge 2	Peak Moment @ Femur Gauge 3	Peak Moment @ Tibia Gauge 1	Peak Moment @ Tibia Gauge 2	Peak Moment @ Tibia Gauge 3	Peak Moment @ Tibia Gauge 4	Peak ACL Elongation	Peak MCL Elongation	Peak LCL Elongation	Peak PCL Elongation
Average	75.3	179	137	91.6	242	201	160	108	8.19	22.4	4.37	4.91
St.Dev	4.2	3.1	1.9	1.7	3.7	3.3	6.8	1.5	0.3	0.1	0.1	0.3
CV	5.6%	1.7%	1.4%	1.9%	1.5%	1.6%	4.3%	1.4%	3.7%	0.4%	2.3%	6.1%
t-IARV	-	-	-	-	318	318	318	318	12.7	20	-	12.7
St.Dev/t-IARV	-	-	-	-	1.2%	1.0%	2.1%	0.5%	2.4%	0.5%	-	2.4%

Preliminary dynamic calibration corridors

The results of the tests with three prototypes were analysed to derive draft dynamic certification corridors. The results of questionable tests were excluded from the database: the faulty accelerometer and one tibia strain gauge. The upper and lower limits are defined according to standard procedures: average measured values plus and minus 10 % or plus and minus two times the standard deviation, whichever gives the broadest corridor.

The final corridors shall be established after there are a minimum number of legs manufactured and delivered (typically at least 10). Also final certification parameters shall be established based

on a large number of tests, conducted at a substantial number of different laboratories to account for lab-to-lab variations. Such process is often referred to as ‘Round Robin Tests’. Typically, establishment of final corridors is part of the process for regulation of a dummy.

Table 10: Draft GTR dynamic certification corridors

GTR Dynamic calibration results	Peak Acceleration at Knee	Peak Moment @ Femur Gauge 1	Peak Moment @ Femur Gauge 2	Peak Moment @ Femur Gauge 3	Peak Moment @ Tibia Gauge 1	Peak Moment @ Tibia Gauge 2	Peak Moment @ Tibia Gauge 3	Peak Moment @ Tibia Gauge 4	Peak ACL Elongation	Peak MCL Elongation	Peak LCL Elongation	Peak PCL Elongation
Average	73.3	179	137	91.6	242	201	160	108	8.19	22.4	4.37	4.91
CV	3.3%	1.7%	1.4%	1.9%	1.5%	1.6%	2.0%	1.4%	3.8%	0.3%	1.8%	7.0%
Upper	80.6	197	150	101	267	221	172	119	9.0	24.6	4.8	5.4
Lower	66.0	161	123	82	218	181	141	97	7.4	20.2	3.9	4.4

The draft dynamic calibration corridors are given in Table 10. The improvement of the CV of the knee acceleration and tibia 3 moment can be observed in this table. All prototype responses, except some of the ones that were excluded, are well within the proposed corridors.

PROTOTYPE MASSES

The segment masses of the three prototypes are shown in Table 11. The Flex-GT segment masses are given for comparison. The three versions of the GTR prototypes were all very close together, however the knee segment mass of the off-board version was about 0.1kg lower. To account for the umbilical cable mass, 0.1 kg was added to the knee segment mass of the off-board DAS version in the table. Table 11 also gives a proposal for segment mass tolerances.

Table 11: Mass comparison of GT and three GTR prototype leg configurations

Part	GT Off board	GTR Off board	GTR On board	Proposed GTR Tolerance
Femur	2.43	2.43	2.44	±0.05
Knee	4.18	4.28*	4.28	±0.1
Tibia	2.61	2.63		±0.05
Flesh	3.72	3.59		±0.2
Total	12.94	12.93	12.94	±0.4

*including 0.1 kg cable to off-board DAS

DISCUSSION AND CONCLUSIONS

Three Flex-GTR prototypes were manufactured in three different versions. The equivalence of the GTR version with previous GT version in terms of mechanical response and mass has been demonstrated. The Flex-GTR test results proved to reproduce the Flex-GT responses closely at the calibration level.

The concerns over the GT version observed during evaluation and the design review were all successfully addressed.

Improvements were made to ligament elongation measurement sensitivity and the twisting moment in the knee was removed. On-board data acquisition was integrated and many additional handling improvements were also made.

The linearity and hysteresis of the gages were established not to exceed 1 % of full scale. This was a design target, but it was uncertain this could be achieved due to the highly flexible nature of the bones.

The Flex-GTR dynamic calibration was updated with respect to the GT version with the target of higher loading closer to vehicle test condition and better reproducibility. This has been achieved and new certification corridors have been proposed.

It may be expected to introduce up to 24 channels for on-board data acquisition. Possibly some modularity of the electrical cables will be lost to keep within the mass tolerances.

It can be concluded that all design targets have been well met and three prototypes are ready for further evaluation by stakeholder groups worldwide.

The difference of the response of the Flex-GTR MCL corridor may be further investigated by subjecting the GTR version to the Flex-GT test condition.

ACKNOWLEDGEMENTS

The authors would like to thank JARI and JAMA for the opportunity to work on this product and the excellent support given throughout the project.

REFERENCES

- [1] European Enhanced Vehicle-safety Committee: EEVC Working Group 17 report, 1998. “Improved test methods to evaluate pedestrian protection afforded by passenger cars”.
- [2] Konosu A. and Tanahashi M. 2003. “Development of a biofidelic pedestrian legform impactor: Introduction of JAMA-JARI legform impactor ver. 2002.”, Proc. 18th International Technical Conference on the Enhanced Safety of Vehicle, Paper No. 378.
- [3] Konosu A. and Tanahashi M. 2005. “Development of a Biofidelic Flexible Pedestrian Leg-form Impactor (Flex-PLI 2004) and Evaluation of its Biofidelity at the Component Level and at the

Assembly Level”, Society of Automotive Engineers
World Congress, SAE paper No. 2005-01-1879.

[4] UN/ECE/WP29/GRSP/INF-GR-PS/Flex-TEG
2008. “First Technology Safety Systems Design
Freeze Status FLEX PLI GTR Development
Mechanical Design”, TEG-054-Rev.1,
[http://www.unece.org/trans/main/wp29/wp29wgs/w
p29grsp/pedestrian_FlexPLI.html](http://www.unece.org/trans/main/wp29/wp29wgs/wp29grsp/pedestrian_FlexPLI.html)

[5] SAE J-211, ‘Instrumentation for Impact Tests,
Sign convention for vehicle crash testing’.

[6] Robbins, D.H. ‘Anthropometry of Motor
Vehicle Occupants, Volume 2’ NHTSA Contract
DTNH22-80-C-07502 Pub. 1985.

[7] SAE J-2570 ‘Performance Specification for
Anthropomorphic Test Device Transducers’, June
2001.

NEW MODULAR ASSESSMENT METHODS FOR PEDESTRIAN PROTECTION IN THE EVENT OF HEAD IMPACTS IN THE WINDSCREEN AREA

Jens Bovenkerk

Christian Sahr

ika - Institut für Kraftfahrzeuge, RWTH Aachen University
Germany

Oliver Zander

Federal Highway Research Institute (BAST), Bergisch Gladbach
Germany

Ingo Kalliske

TAKATA-PETRI AG, Berlin
Germany
Paper Number 09-0159

ABSTRACT

The head impact of pedestrians in the windscreen area shows a high relevance in real-world accidents. Nevertheless, there are neither biomechanical limits nor elaborated testing procedures available. Furthermore, the development of deployable protection systems like pop-up bonnets or external airbags has made faster progress than the corresponding testing methods. New requirements which are currently not considered are taken into account within a research project of BAST and the EC funded APROSYS (Advanced PROtection SYStems) integrated project relating to passive pedestrian protection.

Testing procedures for head impact in the windscreen area should address these new boundary conditions. The presented modular procedure combines the advantages of virtual testing, including full-scale multi-body and finite element simulations, as well as hardware testing containing impactor tests based on the existing procedures of EEVC WG 17. To meet the efforts of harmonization in legislation, it refers to the Global Technical Regulation of UNECE (GTR No. 9).

The basis for this combined hardware and virtual testing procedure is a robust categorization covering all passenger cars and light commercial vehicles and defining the testing zone including the related kinematics. The virtual testing part supports also the choice of the impact points for the hardware test and determines head impact timing for testing deployable systems. The assessment of the neck rotation angle and sharp edge contact in the rear gap of pop-up bonnets is included.

For the demonstration of this procedure, a hardware sedan shaped vehicle was modified by integrating an airbag system. In addition, tests with the Honda Polar-II Dummy were performed for an evaluation of the new testing procedure. Comparing these results, it can be concluded that a combination of simulation and updated subsystem tests forms an important step towards enhanced future pedestrian

safety systems considering the windscreen area and the deployable systems.

INTRODUCTION

Accident statistics show the need for measures relating to the protection of vulnerable road users, especially pedestrians with approximately 15 % of all road fatalities in Europe and 35 % in Japan (OECD Database, 2005). Since the European Directive and the Japanese Regulation on Pedestrian Protection became effective in 2005, new vehicle models have to fulfil the mandatory pedestrian protection requirements. Consumer testing in Euro NCAP and JNCAP already considered pedestrian protection tests before the introduction of legislation. The Global Technical Regulation (GTR) published in January 2009 is the basis for type approval regarding the pedestrian protection requirements for future cars. All these testing protocols prescribe the use of subsystem tests with free-motion impactors representing the human head, as well as the upper and lower leg.

Although the head impact in the windscreen area, i.e. windscreen and windscreen support, shows significant relevance in real-world pedestrian accidents (Bovenkerk et al., 2007), there are neither mandatory limit values to fulfil nor vehicle system technologies in series application available which focus on this impact area. Innovative active safety systems help to prevent accidents and to reduce velocity, e.g. brake assist systems. Nevertheless, passive safety systems are required for the protection of pedestrians to mitigate injuries in the case of an unavoidable accident. Providing a protection zone for the head impact in the windscreen frame region is a demanding target due to significant goal conflicts with the field of view and the occupant protection.

A possible solution for reducing impact severity in this critical area could be a u-shaped airbag system combined with a pop-up bonnet function to increase the deceleration distance. Such an airbag system is

able to offer comprehensive head protection. For the analysis of these protection techniques, both simulation and hardware testing are used in this study. The structure of the new modular testing procedure is presented and applied on the demonstrator. Pre-testing includes the assessment of the timing of deployable systems and a virtual testing part to simulate the vehicle-pedestrian collision to consider the impact kinematics of the entire pedestrian. Besides, virtual impactor tests should extend the number of impact points. For the development of the vehicle prototype, finite element (FE) and multi-body simulations are used.

Hardware testing is performed by the use of linear impactor tests according to the existing procedures. Also dummy tests are performed, in which the pedestrian is represented by the Polar-II Pedestrian Dummy. Furthermore, new advanced subsystem tests are investigated to analyse the head-neck interaction. The evaluation of head impact in pedestrian protection must take more aspects into account than only the current mandatory required HIC criteria. Such aspects are head-neck loading and possible contacts with sharp edges, as well as potential negative influences of deployable systems concerning a rebound effect.

Results of these investigations should contribute to the future development of assessment methods and protection systems for the head impact of pedestrians in the windscreen area. Numerical simulations as well as hardware testing should be considered in an evaluation procedure. The main target is to improve the real-world pedestrian protection in the field of passive safety.

METHODS AND DEMONSTRATORS

Modular Assessment Procedure

Relevant accident cases most likely occur in urban areas with a high variety of impact conditions. For comparable results trying to cover most of this variety, a generic standard configuration has to be defined. Vehicle areas which are not affected by the developed testing procedure (i.e. bumper- or lower bonnet area) are covered in the tests according to the GTR test protocol. All defined boundary conditions in this procedure are derived from a pedestrian impact scenario with a vehicle velocity of 40 km/h.

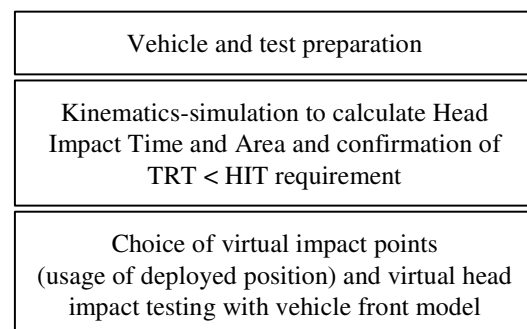
Boundary conditions for the dummy test considered in this study are used from the “Draft Recommended Practice for Pedestrian Dummy” defined in the SAE Pedestrian Dummy Task Group, which aims for the development of worldwide standards for pedestrian dummies. In addition, the “Certification Standard for Type Approval Testing of Active Deployable Systems of the Bonnet Area” which has

been proposed in the context of the UN ECE Global Technical Regulation forms the basis for both simulations and hardware testing. According to these conditions, the configuration contains a lateral walking position of the pedestrian in the vehicle centreline with the leg facing the vehicle in backwards position.

The developed modular testing procedure aims for a combination of the benefits of numerical simulations and hardware testing methods. Furthermore, the testing procedure focuses on the windscreen frame region including the cowl area. Being one of the most obvious possible solutions in this area, the deployable systems, e.g. airbags, play a major role in this testing procedure. Such issues are the main “white spots” in current procedures. The existing procedures form the basis for all the developments. By using numerical simulations of vehicle-pedestrian collisions and of impactor tests for pre-testing, costs for hardware testing can be optimised.

The procedure is divided into two main steps. Step 1 represents the preparation and the pre-testing in virtual tests using simulation methods, while step 2 includes the hardware testing which covers subsystem tests and optionally full-scale dummy testing. In the end, all results are evaluated according to quantitative threshold values or qualitative remarks concerning potential additional injury risks are given. The flow chart of the procedure is shown in Figure 1.

Step 1: Preparation and pre-testing



Step 2: Vehicle testing

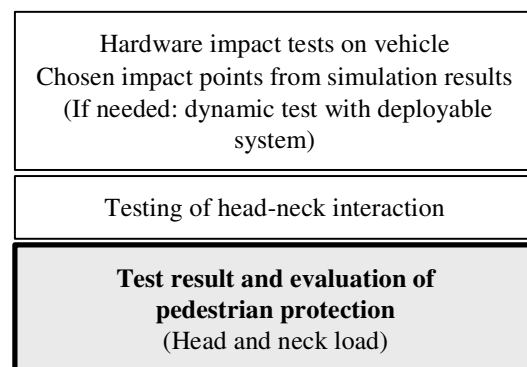


Figure 1. Flow-chart of the procedure.

The preparation and pre-testing begin with the acquisition of the test vehicle and the corresponding simulation model. This forms the basis for the whole testing campaign. If the simulation model is not provided by the manufacturer, methods of re-engineering, such as digitisation methods or simplified models can be alternatively used.

Typical vehicles are classified based on previously conducted simulation studies using generic front shapes (Bovenkerk and Zander, 2008). The classification contains four categories (A: Sedan, B: SUV, C: OneBox, and D: Sports-car) according to different parameters of its front and the resulting impact kinematics, see Figure 2. The method is comparable to the existing IHRA-categorisation with an extension using a Category D with low bumpers and bonnet leading edges (BLEs). These are mainly sports-cars and roadsters. The bonnet leading edge height and the inclination angle of the front (α_B) according to the definitions in the “Blue Book”, 2005 (measured in the vehicle middle, $y = 0$, bonnet front to the rear edge) have been identified as the main parameters which determine the impact kinematics.

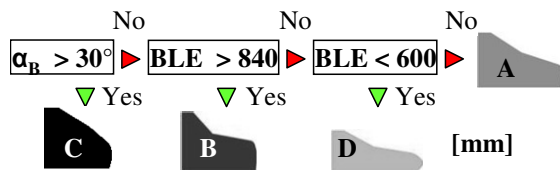


Figure 2. Vehicle categories.

For the subsystem testing part it is proposed to use the ISO-head-impactors in compliance with the GTR protocol and to adjust their impact parameters in each vehicle category by varying the impact angles and the relevant wrap around distances (WADs, Figure 3 and Table 1). The impact area is marked by using references and WADs that are commonly used in the existing procedures.

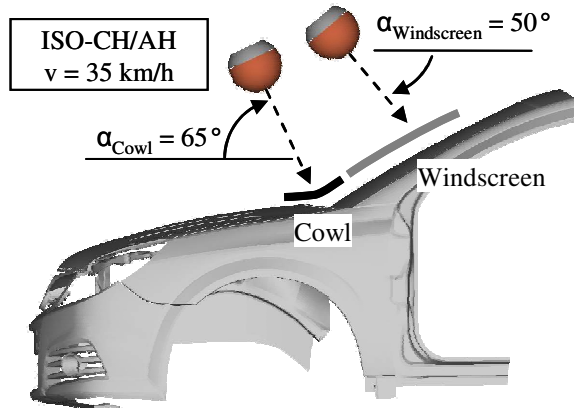


Figure 3. Impactor testing (Category A).

The velocity has a large influence on the structural stiffness and the limitation of deformation space. In

this study, the constant head impact velocity compared to $v = 35$ km/h in the GTR or as an alternative $v = 40$ km/h from Euro NCAP which is much more demanding is proposed. The impact energy is therefore determined by the impactor mass, which is 3.5 kg for the child head (CH) and 4.5 kg for the adult head (AH). The child head impact area contains the 6 year-old child and 5th percentile female, who has almost identical biomechanical parameters compared to the 12 y/o child. The 50th percentile and 95th percentile male are considered for the adult head impact area. The main difference regarding the head impact parameters in the vehicle categorisation can be seen in the relevant wrap around distances and impact angles of the head on the windscreen (Table 1).

Table 1. Head impact parameters for the windscreen area

Category	ISO-Impactor CH: 3.5 kg AH: 4.5 kg	WAD [mm]		Impact angle α [°]	
		from	to	Windscreen	Cowl
A Sedan	CH	1000	1700	50	65
	AH	1700	2300		
B SUV	CH	1000	1500	-	
	AH	1500	2100	*)	
C OneBox	CH	1000	1600	35	
	AH	1600	2100	50	
D Sports-car	CH	1000	1900	65	
	AH	1900	2400		

*) low relevance

For the potentially largest number of Category A “sedan” vehicles, the head impact parameters in the transition of child and adult head impact zone correlate with the GTR. Due to the consideration of the 95th percentile male, the upper boundary is defined as WAD 2300 mm. The WAD-distances are lower with respect to the impact kinematics for SUVs and OneBox-vehicles where the pedestrian is thrown less high onto the front. The contrary effect can be seen for sports-cars and roadsters, where the pedestrian will be thrown higher upwards and the impact angles are steeper at the same time.

For the multi-body or coupled vehicle-pedestrian simulations which analyse the kinematics, the head impact time (HIT) and the corresponding locations for each specific vehicle have to be evaluated. In these simulations, the previously determined boundary conditions should be proven. Adjustments of the parameters listed in Table 1 concerning a possible new vehicle category have to be taken into account. The comparison of the total response time (TRT) of the system to the head impact time confirms its functionality ($TRT < HIT$). Furthermore, the vehicle system has to be in deployed position until the head contacts. That leads, at the same time,

to a sufficient activation time of the system in the case of lower vehicle velocities. If this condition is not fulfilled, a major additional danger occurs due to the opposite directions of the head impact velocity and the bonnet movement.

Step 1 includes the choice of impact points in the marked windscreen area (cowl and windscreen, see Figure 3). The virtual impactor simulations help to identify hard points on the vehicle front (Puppini, 2008). Potentially critical impact points from the previously conducted vehicle-pedestrian simulations can be added. The virtual head impact test forms the transition from step 1 to step 2. Using the specified impact angles, velocities, areas and impactor masses, the numerical head impact simulations supplement the hardware tests on the test points. For the hardware tests, the existing head impactor tests with the modified boundary conditions according to the impact area and the angle are applied.

The second focus in hardware testing apart from the linear head impact is the head and neck load due to the head-neck interaction. Increasing neck loads through large rotations, e.g. caused by the gap at the rear bonnet edge, are an additional risk especially if deployable systems are used. The final step of the modular testing procedure is the evaluation of the pedestrian protection potential by analysing the test results. In general, the scope of the vehicles should consider mainly passenger cars, for which the existing procedures have originally been developed for:

- All M1 vehicles
- All M2 and N1 vehicles up to 3.5 t gross-vehicle mass
- Excluding “Flat Front Vehicles”
(with $D_{(R-Point\ driver\ seat - front\ axis)} < 1000\ mm$)

Due to their front geometry with often short bonnets and higher inclination angles of the windscreen, so-called “Flat Front Vehicles” require system solutions which are often incomparable with the sedan shaped vehicle solutions (Fassbender and Hamacher, 2008).

In the following paragraphs, an overview and breakdown of the proposed steps of the presented procedure will be given.

VEHICLE AND TEST PREPARATION

Experimental Vehicle

For the investigation and demonstration of the developed testing procedure, a reference vehicle is chosen. An average shaped sedan vehicle of the defined Category A (Opel Signum) is upgraded with a pop-up bonnet in combination with an exter-

nal airbag, developed and provided by TAKATA (both numerical and hardware model).

Modifications of the series version related to the hinges in the bonnet rear area, the latch in the front and the integration of the airbag module are the main changes. For the bonnet rear hinge, linear and rotational joints are considered. Due to advantages in kinematics, the rotational hinge solution is chosen. This solution means no risk of self-locking effect, which could be caused by kinematics and friction in the linear guidance. The whole system of hinges and bonnet forms a 4-point hinge kinematics. In a series application, the rear hinges have to be locked in the daily operation position by integrating e.g. shear bolts or pyrotechnical bolts. The necessary clearance for the hinges can be reduced to a space which is comparable to the series hinges. The sheet thickness of the prototype hinges is 5 mm.

The series latch is replaced by two front hinges, which have to be changed into a two latch system in a possible series application. The pivot requires a location which is positioned as far as possible towards the front to avoid collision with the surrounding parts when lifting up the bonnet up to 120 mm. In addition, the front hinges have to be fully covered by the bonnet. Lifting of the bonnet is realised by the lower chamber of the airbag and covering the windscreen area by the upper airbag chamber.

The airbag module is integrated. Fixation points for the module are both suspension towers and the water box. An additional function of the module as a strut bar can also be introduced.

The gas pressure during the deployment of the airbag is measured in a relatively calm area (less gas flow). When fully deployed, the airbag volume is approximately 90 l. A water box cover, which is also fixed laterally and replaces the series plastic cover of this area, is necessary to guide the airbag directly without obstructions towards the windscreen. Sharp edged parts in the airbag deployment area are removed or covered.

The modifications of the vehicle according to the external airbag system require some additional clearance in the water box area. In the series vehicle such a system has not been considered in the early design and the development process. Therefore, the whole wiper system is removed during the following investigations. Changes of the vehicle front are implemented in such a way that the series status of the vehicle can be restored quickly. Necessary cut-outs, especially for placing the airbag module, are an exception. The changes are summarised, and the wrap around distances are marked in Figure 4. The potential impact point for the 50th percentile

male is shown. It is expected that the impact location of the human model in simulations and dummy tests will be nearly identical.

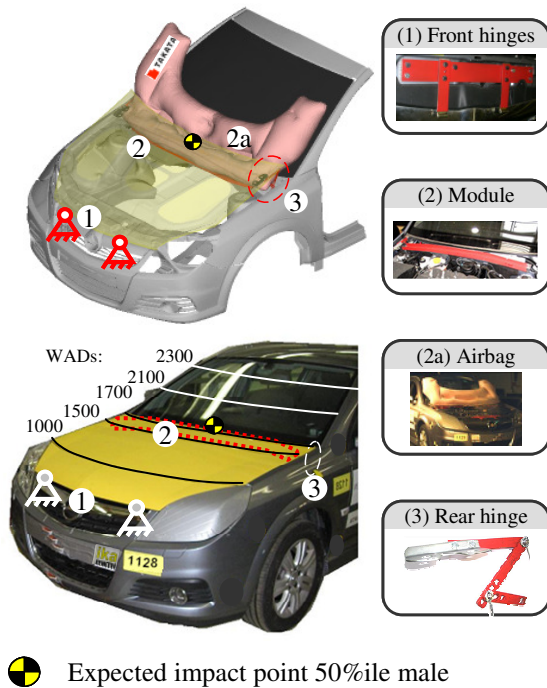


Figure 4. Modifications on the series vehicle and FE-Model (Category A).

Virtual Model

For the pre-tuning and development of the experimental vehicle and the virtual part of the testing procedure, a simulation model of the vehicle front is built up. All relevant components are transferred into a CAD model using the “ATOS I system” for scanning components and CAD for re-engineering the whole front geometry (Figure 5). The vehicle model contains the front-end with bumper, cross member and crash boxes, fender, bonnet and the body with longitudinal beams, suspension towers and A-pillars. The engine package is included as a simplified rigid surface.



Figure 5. Re-engineering of the vehicle front

The numerical airbag model of TAKATA is integrated into the FE simulation. These simulations contain the definition of the lifting mechanism through the airbag deployment and in a second step head impactor simulations using the timing derived from the multi-body simulations as an input. The design changes for the experimental vehicle prototype are implemented in the simulation model (Figure 4).

Multi-body / Coupled Vehicle-Pedestrian Kinematics Simulations

The following comparative analysis always refers to the active deployable airbag system’s performance with a series vehicle without the implementation of pedestrian safety measures. This comparison should help to evaluate the potential of both the new testing procedure and the future pedestrian safety systems.

Multi-body simulations using Madymo or coupled simulations using Madymo and LS-Dyna are performed to investigate the impact kinematics with the main focus on the location and timing of the head impact. The results form an important input for triggering the subsystem impactor in relation to the airbag system in the following hardware testing part. The coupled simulations in Figure 6 show that the head impact of the 50th percentile male takes place at HIT = 128 ms in the transition zone of the bonnet and windscreen of case 1 representing the series version without the deployable system.

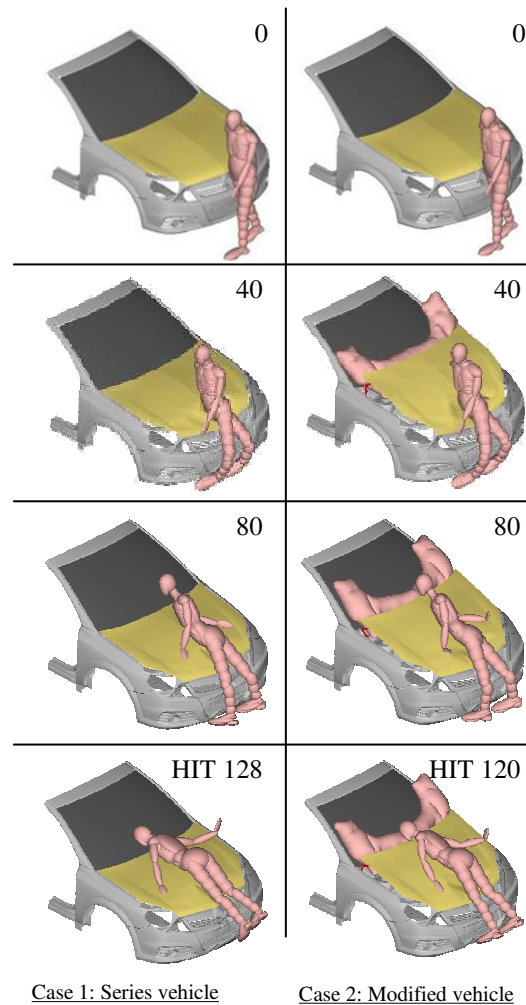


Figure 6. Multi-body simulations with series and modified vehicle, t in [ms].

Comparison of the two cases shows an offset of about 10 ms towards an earlier head impact in case 2 with respect to case 1 due to the deployable system. In that case, the head would impact most likely in the open bonnet rear gap, which is covered by the airbag in the reference vehicle. Simulations with same boundary conditions using the 6 y/o child model indicate that the earliest head impact on the bonnet front is at $t = 60$ ms in activated position. The airbag is fully deployed after 40 ms (TRT).

For the considered impact speed and a sufficient activation time of more than 200 ms of the airbag, which will guarantee the deployed position until the head contacts in the case of lower velocities (i.e. higher head impact time), it can be concluded that the requirement $TRT < HIT$ is fulfilled.

The simulations underline that the upper bonnet and lower windscreen area play an important role for the head impact. This area offers lower protection potential in contrast to the bonnet and windscreen middle, due to the high stiffness and reduced deformation space. Average sedan shaped vehicle fronts in general show this impact scenario.

Choice of Virtual Impact Points / Virtual Head Impact Testing with Vehicle Front Model

FE simulations using LS-Dyna software are carried out to evaluate the function of deployable systems and to identify a particular choice of hard points in the car front. Figure 7 shows such a simulation grid on the vehicle front with regular (marked as a grid structure, white points) and additional points which can be identified from the vehicle-pedestrian simulations (stars) or which are simply identified as additional potentially critical points (red ones).

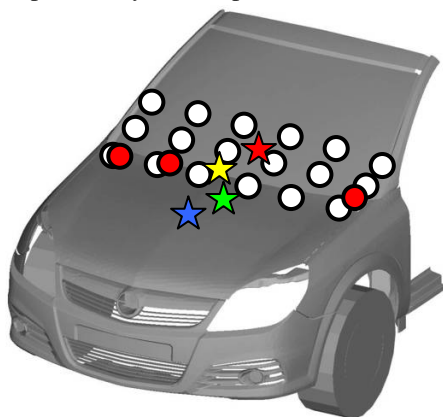


Figure 7. Virtual tests on a grid.

The simulations in Figure 8 show an adequate function of the whole lifting mechanism. The acceleration outputs of the impactor model indicated a good performance. In this sequence, an impact at $t = 0$ ms is shown. This is in the time period, where the airbag model is fully deployed when $t = -100$ ms is the triggering time. In the virtual test series, different

impact points are evaluated. For the comprehensive presentation, the impact point of the 50th percentile male in the middle of the bonnet rear area will be presented with the main emphasis in the following considerations.

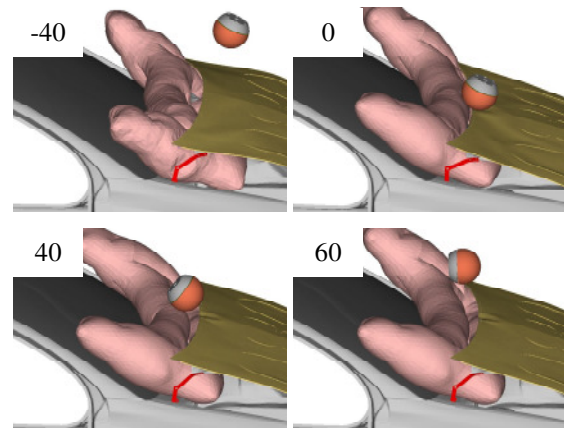


Figure 8. LS-Dyna head impactor simulation, t in [ms].

HARDWARE VEHICLE IMPACT TESTS

Impactor Tests

In the hardware tests, the experimental vehicle is tested according to EEVC WG 17 and GTR testing protocol by extending the impact area to the windscreen region as described in the new testing procedure (Category A, cowl area: WAD 1770 mm, 65° impact angle with adult head). Currently, testing of the bonnet rear area is only included in the Euro-NCAP-procedure. Due to the current availability at ika, the 4.8 kg EEVC WG 17 adult head impactor is used instead of the proposed ISO headform. The velocity of the head impactor is 40 km/h. In the hardware testing, three impact points are chosen in the context of this study. The potentially critical impact points which might be identified in the virtual tests and the chosen impact points for the hardware tests are shown in Figure 9.

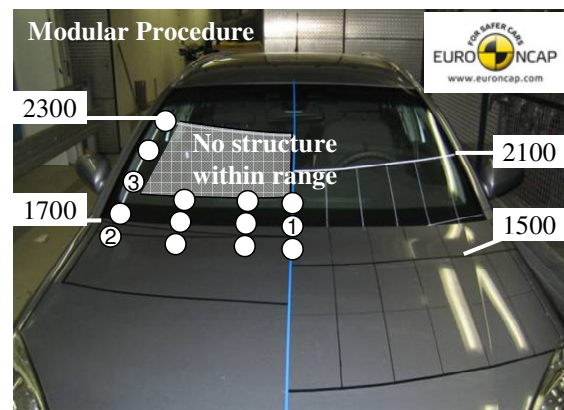


Figure 9. Potential critical impact points and tested points for Category A - Sedan.

Furthermore, the previously defined testing area is compared to the current Euro NCAP zone. The most significant change is the increased wrap around distance of 2300 mm for Category A (Sedan) when considering the 95th percentile male.

Figure 10 shows the subsystem test on the expected impact point of the 50th percentile male (point 1). In general, these conditions correlate with the results of the multi-body model simulations in previous studies (Bovenkerk et al., 2009). Regarding the impact location on the bonnet rear edge, the position of the impact point is one third on the bonnet itself and two thirds on the lower windscreen zone, which is covered by the airbag system.

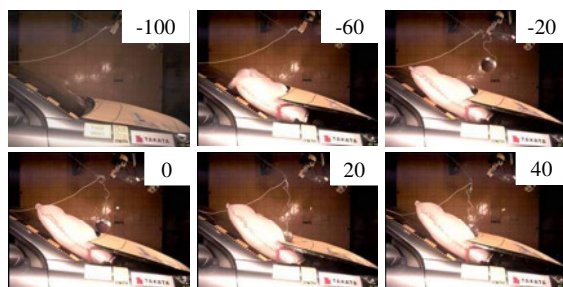


Figure 10. Head impactor test on point (1) of the modified vehicle, t in [ms].

For triggering and timing the impact of the head-form, the previously determined head impact time (HIT) from the numerical simulations is used (about 120 ms). With the first impact of the leg, a pedestrian impact sensing time (ST) of $t = -20$ ms is estimated, so that the impact time of the head impactor is at $t = 0$ ms after triggering the airbag at $t = -100$ ms. After $t = 40$ ms, the airbag is in a fully deployed mode, so that there is a sufficient safety margin with respect to time until the head impacts. During the whole contact phase, the airbag fully covers the rear bonnet area and the A-pillars. The acceleration outputs from the simulations are correlating with these tests. For the determination of the optimum airbag pressure, it has to be considered that too high inner pressure and thus low energy absorption of the airbag itself lead to elastic behaviour with a strong rebound effect that can be reduced by the use of vent holes.

Tests with Polar-II Pedestrian Dummy

In a second (additional) test series, the overall kinematics of the real-world accident are investigated by using the Honda Polar-II Dummy. In addition, these tests form an input for the analysis of the neck loads which cannot be investigated by the common linear impactor testing methods.

The biofidelity of this dummy enables the reconstruction of a realistic pedestrian accident with an average sedan car front. A detailed description of

the Polar-II Dummy can be found in (Takahashi et al., 2007). In addition, the potential of using the external airbag system in the future can be investigated close to reality. Taking into consideration that there are currently only very few vehicles equipped with deployable systems and none with external airbags, the availability of real-world accident data from such vehicles will be far in the future. Confirmation of benefit in real-world accidents is therefore not possible.

Results of the dummy tests are compared to the performed vehicle-pedestrian simulations. Furthermore, a comparison of the series vehicle and the modified version using the airbag system is included. Merging all these results, it becomes more clear that using a combination of subsystem tests and simplified simulations and with the dummy test as an option for complex systems is an adequate method to evaluate the protection potential of a car.

The dummy is positioned according to the defined boundary conditions, i.e. vehicle faced leg backwards and the position of the dummy in the vehicle centreline. The release mechanism of the dummy is triggered approximately 50 ms prior to impact and braking takes place 100 ms after impact. Figure 11 gives an overview of the test set up and the distances at the ika crash test facility.

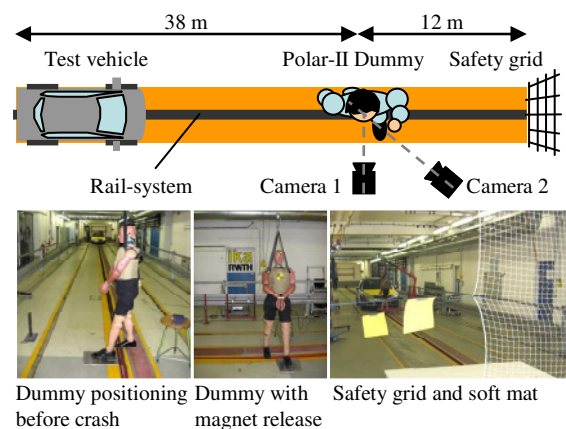
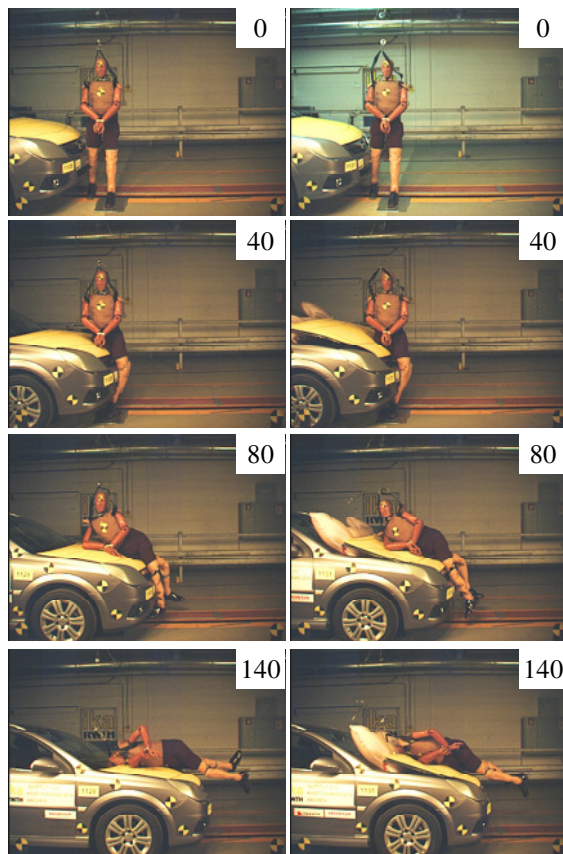


Figure 11. Test set-up for the pedestrian dummy test with Polar-II Dummy.

Figure 12 shows the comparison of high speed sequences of the dummy tests with the series vehicle and the modified vehicle using the airbag system. In both cases, the vehicle velocity is 40 km/h. Triggering of the airbag system is realised by contact sensors on the bumper. The first impact of the leg corresponds to $t = 0$ ms. After the leg impact, the hip impact for both cases takes place at $t = 40$ ms; following this, the full body wraps around the vehicle front and has flat contact on the bonnet. After the shoulder impact between 100 ms and 120 ms, the first contact of the head takes place at 131 ms in the first case and at 121 ms in the second case with

the deployed bonnet and the activated airbag. In this case, an offset of approximately 10 ms to an earlier time occurs for all body regions after the upper leg impact due to the lifted bonnet.

The timing of airbag deployment complies with the results of the head impactor tests. Wrap around distances to the head impact point are 1830 mm in the first case and 1860 mm in the second case proving the expected impact point on the bonnet rear (point 1). After 200 ms the dummy flight phase starts, and the dummy separates from the vehicle (not shown).



Case 1: Series vehicle Case 2: Modified vehicle

Figure 12. Polar-II Dummy test with series (Case 1) and modified vehicle (Case 2), t in [ms].

The contact location of the upper leg is on the first third of the bonnet. Further bonnet deformation results from the whole body contact. Figure 13 shows the post-crash scenario of both tests regarding the head impact. The deformations of the rear edge of the bonnet and the locally cracked lower windscreen for case 1 without airbag indicate the locations of the head contacts. The damage of the windscreen centre results from the release device after the head impact and has no influence on the test results. In comparison to the series version, there is nearly no deformation of the lower windscreen area in the modified version.

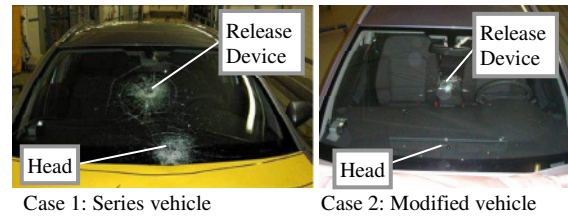


Figure 13. Post-crash scenario.

The impact location meets exactly the expectations from the multi-body and coupled simulations. The behaviour of the dummy in the secondary impact on the ground is not the main focus of this study.

HEAD-NECK TESTING

There are different possibilities to include the evaluation of the head-neck interaction. On the one hand, the dummy test results regarding the interaction forces, moments and angles can be used. On the other hand, in the case of lacking availability of a dummy test, trends of these values can be derived from the previously conducted numerical vehicle-pedestrian simulations. Additional subsystems can be applied which are proposed by Kalliske and Bovenkerk (2009), see Figure 14.

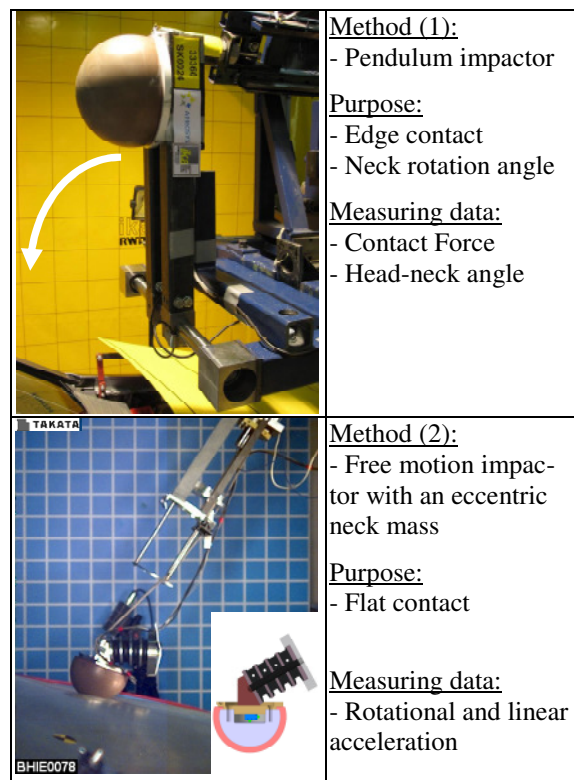


Figure 14. Subsystem tests for head neck interaction.

The first head-neck subsystem testing method (1) uses a pendulum impactor which is fixed to the head impact test bench. The main purpose of this

method is to record contact forces in the case of an edge impact. The contact area has to be evaluated additionally by pressure foils and included in the calculations for the determination of the contact pressure acting on the head. Furthermore, the neck rotation angle can be statically measured. This angle can be very high in the case that the head rotates into a deployed bonnet rear gap.

The free motion impactor in method (2) uses an eccentric neck mass leading to a more biofidelic representation of the influence of the body, which introduces a head rotation through the neck. Subsequently, the linear and the rotational acceleration responses are recorded. This enables to evaluate the head rotation, in addition to the HIC-values. The dimensions of the impactor spheres are based on the existing adult headforms.

In this paper, these methods will be used to include a qualitative assessment of additional risks regarding the head-neck interaction.

TEST RESULTS AND EVALUATION OF PEDESTRIAN PROTECTION

Subsystem Testing

The outputs of the linear impactor tests concerning the head accelerations and the resulting HIC-values are presented in Figure 15. The virtual and hardware impactor tests do not lead to different evaluation results. Tests and simulations are in good correlation. In all three cases it can be shown that the requirement of the HIC-value below 1000 of the modified vehicle can be met with a significant safety margin. Compared to these results, the testing of the series vehicle leads to a higher acceleration level and therefore all the HIC-values are above 1000. The A-pillars are completely covered by the airbag in the modified version. Testing the region without an airbag was left out due to the clearly lowest available deformation space and highest structural stiffness, which would result in an extremely high HIC-level.

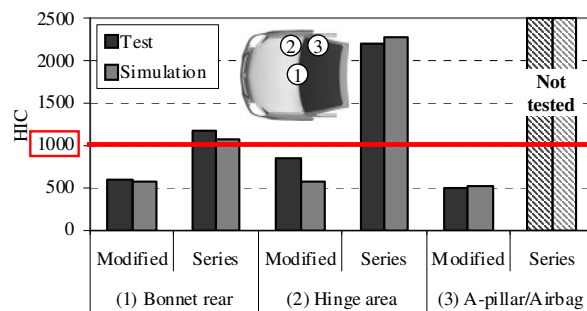


Figure 15. HIC-values of the chosen impact locations.

Table 2 shows an evaluation matrix for the modified vehicle including the possible additional injury risks of the analysed impact points. Some of them are conflictive.

Table 2. Evaluation matrix of the modular procedure for the modified vehicle

Point No.	1	2	3
Location	Bonnet rear	Hinge area	Airbag
HIC	Low (591)	Medium (840)	Low (500)
Rebound	Medium	Low	High
Risk of edge Contact	High	Medium	Low
Head rotation	Medium	Low	Medium

On the one hand, the HIC on the airbag is at the lowest level and there is no significant risk of head contact with sharp edges. On the other hand, the rebound of the head is at a high level due to the low energy absorption of the airbag itself. The combination of the energy absorption through the bonnet with an underlying airbag on point (1) seems to be a good compromise. Furthermore, sharp edges of the deployed bonnet rear gap have to be avoided by solutions which cover this area. Such an exposed bonnet rear may also result in a higher neck rotation angle as well as in higher angular acceleration due to the possible pendulum movement of the head. Kalliske and Bovenkerk (2009) listed these effects as potential new injury risks.

Dummy Testing

For the evaluation of the test results, the head and neck outputs of the dummy are exemplarily shown. The diagrams in Figure 16 to Figure 18 show the head and neck loading for the two cases. These curves illustrate the result of the series vehicle in red colour and the modified vehicle with the airbag system in grey colour. Further on, the first head contact is marked.

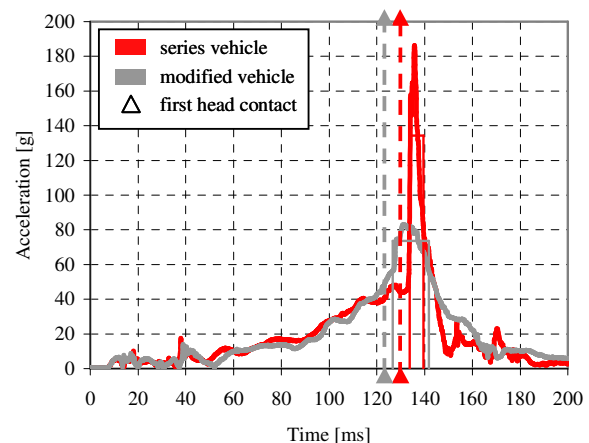


Figure 16. Head CG acceleration.

Head CG acceleration curves show a decrease of the maximum acceleration from the series vehicle $a_{\max, \text{series}} = 186 \text{ g}$ to $a_{\max, \text{mod}} = 83 \text{ g}$, which results in a decrease from $\text{HIC}_{15, \text{series}} = 1212$ to a value of $\text{HIC}_{15, \text{mod}} = 705$. Reducing the HIC-value by 42 % with regard to the series vehicle and going at the same time significantly below the limit of $\text{HIC} = 1000$, defined by EEVC WG 17, indicate the protection potential of an airbag system in the windscreen area. Due to the influence of the airbag and increasing of available deceleration space, the shape of the acceleration peak is transformed from a straight high peak into a broader peak on a lower level. The influence of the changed vehicle shape, caused by the lifting of the bonnet by the airbag, on the acceleration of the head CG is starting from 120 ms with an earlier increase until 160 ms with a later decrease of acceleration.

Neck forces and moments in the lower and upper neck load cells are shown in the following diagrams. Shear forces in x- and y-direction do not play the most significant role; they neither show any tendencies of differences nor exceed any defined threshold value. The force component in vertical z-direction is of dominating influence. Tension forces at a maximum level of 2000 N change into a higher level of compression forces for the series vehicle with a magnitude of over 5000 N which exceeds the FMVSS 208 limit of 4000 N (red area). The two cases differ significantly after 135 ms. The modified vehicle shows a maximum compression force of 2000 N, which is below this limit value (grey area).

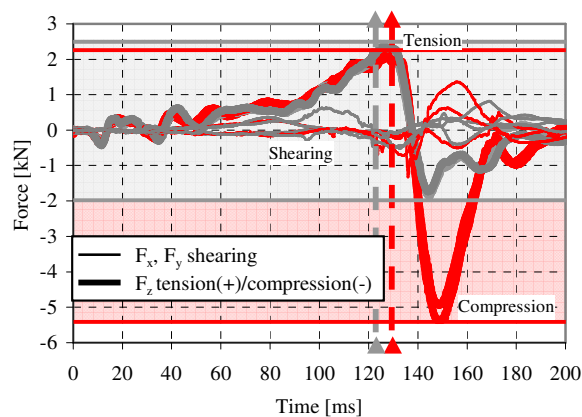


Figure 17. Neck forces.

For the neck, it can be stated that the moments (M_x , M_y) can be reduced by 30 % or more compared to the series vehicle, in case it is equipped with an airbag. As mentioned above, a too high airbag pressure might result in higher neck load values due to the rebound effect.

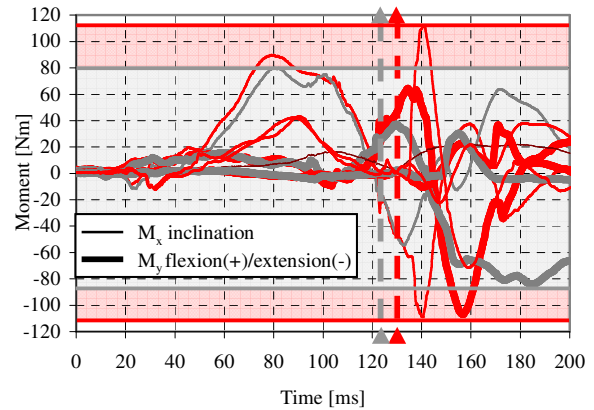


Figure 18. Neck moments.

A comparison of the head trajectories in testing and simulation is shown in Figure 19. A correlation between the head kinematics in the flight phase can be seen. The upper leg movement does not correlate due to the contact stiffness definition of the simplified multi-body model. In general, the results regarding the impact timing and location of the head, which are the main focus of this paper, are comparable. It has to be considered that in this version of the model, the airbag is not included in the simulation model, and therefore the impact angle is significantly higher due to the exposed rear gap.

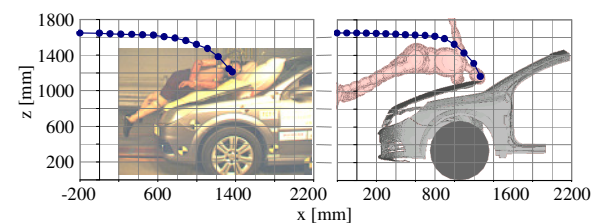


Figure 19. Head trajectories in testing and simulation.

CONCLUSIONS

In this paper, a modular structured procedure for pedestrian impact testing was proposed according to a combination of hardware and virtual tests. Two main steps concerning preparation and pre-testing with vehicle-pedestrian and impactor simulations as well as a hardware testing phase are included. First, the boundary conditions for the linear impactor tests were pre-defined within four vehicle categories including Sedan, SUV, OneBox and Sports-car front shape. These categories were based on the bonnet leading edge height and the inclination angle of the front. The second step includes impactor tests and optionally dummy tests. As an extension of the existing linear head impactor tests, new impactors developed in the APROSYS project were presented. These tests enable a better evaluation of the head-neck interaction.

A sedan shaped car was used as the virtual and physical test environment. By using a human model in multi-body and coupled simulations, test conditions regarding the impact point and the timing were defined. The simulations would also be able to create further test input data such as tendencies for head-neck loading output.

To confirm the simulation results obtained with the whole pedestrian model, Polar-II Pedestrian Dummy tests were performed. A good correlation between the human model simulation and the Polar dummy test could be reached with respect to impact point and timing. Furthermore, it could be shown that such an approach of combining simulation and testing is able to cover also particularities of deployable passive safety systems such as an airbag, e.g. with respect to triggering.

In the evaluation part of this modular procedure, the pedestrian protection potential of passive safety systems referring to an airbag in comparison to current non-activated vehicle front structures were presented. Even hardware testing could show that advanced safety systems involving airbags will have a big potential to protect pedestrians well in real-world accidents. As an example, the head and neck loading was considered. In this study, the outcome of using an airbag was a HIC reduction of 42 % and a reduction of the neck compression forces of about 60 %, as well as a neck moment reduction of about 30 %. However, the focus was not on the sensing system, which is necessary for the series application of such a deployable airbag system.

It could be shown within this paper that new testing methods consisting of a combination of simulation and subsystem testing lead to an improved evaluation of pedestrian protection and complement each other. Vehicle-pedestrian collision simulations are concluded to be an efficient way to estimate the influence of the vehicle front shape on the impact parameters. Impactor simulations offer the multiplication of analysed impact points and the identification of most critical points. The hardware tests allow the verification of simulation results. The final evaluation includes additional aspects for complementing the HIC-value with the consideration of impact forces and the head-neck interaction. Further research is needed in the development and application of these new testing methods including subsystems for the head-neck interaction. For a more biofidelic representation of the real-world accident, it is recommended to continue research on improved impact evaluation.

ACKNOWLEDGEMENT

Ika - Institut für Kraftfahrzeuge of RWTH Aachen University would like to thank all the involved partners of Honda, Opel, TAKATA, BASt and the European project APROSYS for their kind contributions and support.

REFERENCES

Automobile Type Approval Handbook for Japanese Certification (“Blue Book”), Test procedure for head protection of pedestrian; Article 18 of Section 11, as completed by TRIAS 63 – 2004 of Sec. 12 and attachment 99 of Sec. 11, 2005.

Bovenkerk J., Lorenz B., Zander O., Research Projects FE82.229/2002 and FE82.308/2006, “Protection of Pedestrians in a Windscreen Impact”, Federal Highway Research Institute (BASt), 2006 and 2009.

Bovenkerk J., Lorenz B., Zander O., Guerra L., C E Neal-Sturgess, 'Pedestrian Protection in Case of Windscreen Impact', crash.tech, Leipzig, 2007.

EEVC Working Group 17 Report, Improved Test Methods to Evaluate Pedestrian Protection Afforded by Passenger Cars, www.eevc.org, 1998 incl. update 2002.

European Parliament, Directive 2003/102/EC: the protection of pedestrians and other vulnerable road users before and in the event of a collision with a motor vehicle, 2003.

GTR - INF GR/PS/141 Rev. 1, Certification Standard for Type Approval Testing of Active Deployable Systems of the Bonnet Area, www.unece.org, 2005.

United Nations Economic Commission for Europe. (UNECE) Global Registry: Agreement concerning the establishing of global technical regulations for wheeled vehicles, equipment and parts which can be fitted and/or be used on wheeled vehicles (ECE/TRANS/132 and Corr.1) – Addendum: Global technical regulation No. 9 Pedestrian Safety ECE/TRANS/180/Add.9 and /Add./Appendix 1, 26 January 2009.

Fassbender S., Hamacher, M., “Development of a Run Over Test Procedure for Heavy Goods Vehicles”, APROSYS SP2 Final Workshop Neumuenster, May 2008.

Honda R&D Americas Inc., Polar-II Testing Protocol, 2004.

Kalliske I., Bovenkerk J., “New and improved test methods to address head impacts”, Deliverable D333C (Report-No. AP-SP33-021R) of the European FP6 research project on Advanced Protection Systems (APROSYS), 2009.

OECD - International Road Traffic and Accident Database, 2005.

Puppini, R., “Integration of virtual testing in regulatory procedures”, APROSYS 2nd Virtual Testing Workshop, Helmond, January 2008.

SAE International, Dummy Task Group, Draft Recommended Practice, Performance Specifications for a 50th Percentile Male Pedestrian Research Dummy, 2007.

Takahashi Y., Akiyama A., Okamoto M., “Polar-II Pedestrian Dummy”, VKU Pedestrian Protection Conference, Aachen, 2007.

PREDICTIVE PEDESTRIAN PROTECTION – SENSOR REQUIREMENTS AND RISK ASSESSMENT

Nils Tiemann,

Dr. Wolfgang Branz,

Robert Bosch GmbH, Corporate Research and Advance Engineering,
Vehicle Safety and Assistance Systems, Postfach 30 02 40, 70442 Stuttgart
Germany

Prof. Dr. Dieter Schramm,

University of Duisburg – Essen, Department of Mechanical Engineering, 47048 Duisburg
Germany

Paper Number 09-0226

ABSTRACT

In this paper an approach to predictive pedestrian protection is being proposed. The main issues regarding the identification of high benefit scenarios, the requirements for an appropriate risk assessment algorithm as well as the requirements for the environmental sensor system are discussed.

A general survey of the topic is given first, including accident statistics regarding vulnerable road users.

Based on more detailed accident data the requirements for a video-based pedestrian recognition system are derived. As a result the best suited aperture angle for early detection of pedestrians was determined.

A possible approach for predictive pedestrian protection is to issue an adequate driver warning in case of an impending vehicle-pedestrian collision. In order to justify driver warnings it is necessary to calculate the collision risk with a relatively large time-foresight. To cope with this task a pedestrian motion model based on likely and possible accelerations has been developed.

1. INTRODUCTION

In the context of today's vehicle safety systems pedestrian protection is an important issue. Most vehicle safety systems are designed to protect occupants from the consequences of an accident (passive systems). In recent years active systems emerged with the goal to avoid accidents with other vehicles or reduce collision velocity.

In the field of pedestrian protection passive systems (mostly special vehicle-front structures) are very common. Active systems are still very rare, especially systems which aim to avoid the accident completely. The importance of both passive and active systems can be deduced from international accident statistics. In South Korea for example pedestrians account for 39% (2,468 people) of the overall number of fatalities in road traffic (2006) [1]. In Europe the percentage is lower (combined 18%) but still over 10% in almost every country. Combined with bicyclists every fourth person killed

in road traffic in Europe 2006 was a vulnerable road user, i.e. pedestrian or bicyclist [2] (see Figure 1).

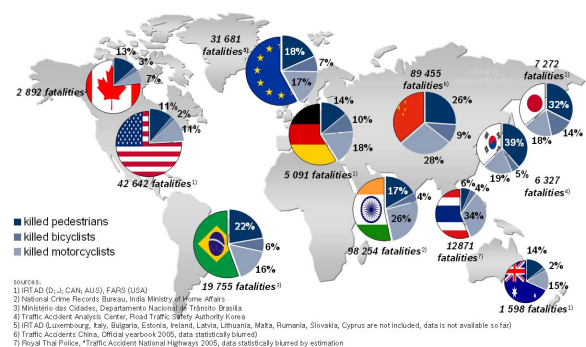


Figure 1. Fatalities in road traffic 2006 – share of vulnerable road users [3].

Because of these high accident rates the EU will tighten the guideline for pedestrian protection in 2009. The guideline includes considering brake assist systems (BAS) and, as an alternative to the crash-test requirements, active collision avoidance systems [4]. From 2009 on, pedestrian protection will also play a bigger role in the Euro-NCAP scoring [5]. In chapter 3 an active system for pedestrian protection is being proposed, which aims to avoid or at least mitigate accidents involving pedestrians by issuing a driver warning. Because the driver still needs time to react after the warning, not only a precise recognition of the pedestrian but also a very good estimate of the collision risk is essential. Prior to that, results of an accident study will be presented in chapter 2. These results contribute to the system layout in order to maximize the field accidents addressed by the system.

2. ACCIDENT STUDY

In order to consider as many accident situations as possible a detailed accident study has been carried out. The database for the study consisted of 217 accidents involving pedestrians which were hit frontally by a passenger car. The data was provided by the GIDAS – database [6]. This analysis showed

that about 95% of all accidents occurred in urban areas and 74% can be characterized as "crossing-accidents", i.e. the pedestrian wanted to cross the road from the left (41.5%) or from the right (58.5%) and was then hit by the passenger car. In 47% of these accidents there has been an occlusion in the driver's line of sight (see Figure 2).

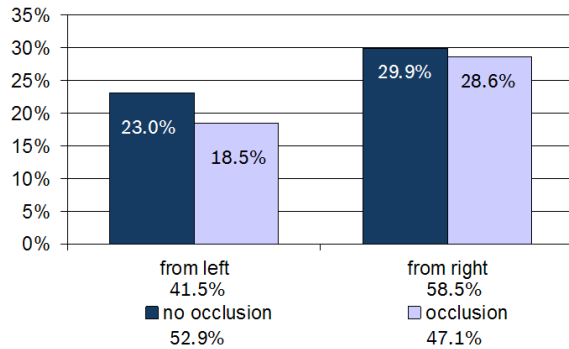


Figure 2. Distribution of "crossing - accidents".

Further accident types and frequencies are e. g. "turning-accidents" (15%) and "accidents with pedestrians walking along the road" (4%). The recognition and classification of pedestrians is typically realized with a video system. Therefore the time before the collision was determined considering a theoretically mounted, pedestrian detecting video system. This time depends on the accident details as well as optical parameters of the video system. For the considered accidents the GIDAS database provided detailed reconstruction data like velocities of the passenger car and the pedestrian, as well as the approaching direction of the pedestrian. From this data the relative direction of approach (RDA) of the pedestrian towards the car was derived (see Figure 3).

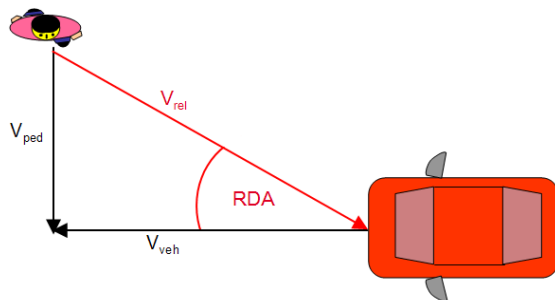


Figure 3. RDA - Relative direction of approach.

In Table 1 the distribution of accidents with certain RDAs is presented.

The table shows that in 83% of all accidents the RDA lies between $\pm 20^\circ$.

In a next step the exact time of the theoretical detection was calculated. In those cases where no occlusion for the driver was present, the Sight Time to Collision (STTC) was determined by calculating back from the collision.

Table 1.
Relative Direction of Approach

RDA between	Percentage
$\pm 10^\circ$	53.8%
$\pm 20^\circ$	82.8%
$\pm 30^\circ$	92.4%
$\pm 40^\circ$	94.8%
$\pm 50^\circ$	97.0%
$\pm 60^\circ$	97.5%

The STTC is the time at which the video system could possibly have detected the pedestrian, considering aperture angle and other parameters. In cases with an occlusion for the driver the position and dimensions of this occlusion was reproduced from an accident diagram. With this information the STTC could be calculated. Due to the fact that not every accident diagram held information about the occlusion and not all of the reconstructed data was complete, the STTC could be determined for 131 of 217 cases (60.4%). It was calculated for three different video aperture angles $\pm 10^\circ$, $\pm 20^\circ$ and $\pm 60^\circ$. A greater aperture angle leads to less range, because the resolution of the video system is assumed to be constant at 1024pel (horizontal). It was also assumed, that a video recognition algorithm needs at least 20pel/m to recognize a pedestrian. Figure 4 shows the percentage (vertical) of the cases in which at least a certain STTC (horizontal) was calculated.

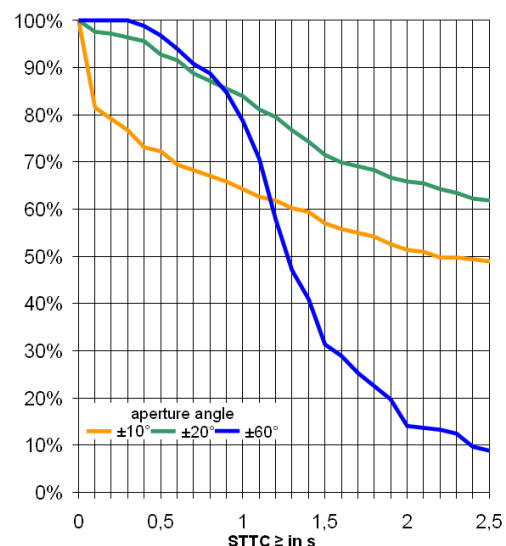


Figure 4. STTC with different aperture angle.

The figure yields that the best-suited aperture angle for a STTC $> 1s$ is $\pm 20^\circ$ rather than $\pm 10^\circ$ or $\pm 60^\circ$. With this angle almost 85% of the considered cases meet the requirement of STTC $> 1s$ which is the minimal requirement for the warning function as will be discussed in chapter 3. Increasing the STTC leads to decreasing this percentage to 71% (STTC $> 1.5s$) or 67% (STTC $> 2s$) respectively.

Another investigated topic was the question of how much time could be gained, if the pedestrian could be detected while standing in front of a passenger car parked at the roadside. In such a case the upper body of the pedestrian could be visible for the video system and so detection could succeed before the pedestrian enters the road.

First it is necessary to know in how many cases the occlusion actually was a passenger car. This amount is at least 45% according to the present data (20% of the occlusions are unknown). Here it can be assumed, that the upper body of the pedestrian would have been visible a little sooner and that the video system therefore could have detected the pedestrian earlier. The temporal advantage of an earlier detection was calculated on the assumption of three different lengths of the passenger cars hood and can be seen in Table 2.

Table 2.
Timely gain in ms from upper body recognition of partially occluded pedestrians

aperture angle	length hood		
	0.5m	1m	1.5m
±10°	22	45	68
±20°	41	81	120
±60°	26	52	77

The effect is small; even under the best circumstances only about 100ms can be gained. However, in best case this could result in additional collision velocity reduction of 3-4 km/h regarding a full braking maneuver.

3. PREDICTIVE PEDESTRIAN PROTECTION

The Robert Bosch GmbH develops a driver assistance system in order to protect pedestrians by avoiding or mitigating vehicle - pedestrian collisions. The system aims at issuing a driver warning in order to draw the driver's attention to the pedestrian.

3.1. Environment Sensing Technology

The pedestrian detection and recognition system is based on stereo video. The system has an aperture angle of ±20° and is therefore conform to the condition presented in chapter 2.

3.2. System Layout

The important factors for a successful driver warning are the design of the warning itself (Human Machine Interface) and the time at which the warning is issued. In order to find the appropriate moment for a warning the reaction time of the driver has to be

considered first. In literature the reaction time is described to be fairly volatile, nevertheless we assume the reaction-time to be $T_{\text{reac}} = 0.8\text{s}$ (see also [7]). Additionally the time needed by the driver to take action has to be considered; we assume $T_{\text{act}} = 0.2\text{s}$. We neglect the time it takes to build up the brake pressure because we assume the passenger car to be equipped with an extended brake assist system and pre-fill of the brake system prior to the warning. As a result we get as a minimal warning time

$$T_{\text{warn}} > T_{\text{reac}} + T_{\text{act}} = 1\text{s}. \quad (1)$$

Only if this condition is fulfilled the driver will be able to reduce the collision velocity and therefore mitigate the consequences for the pedestrian. Of course avoiding the accident takes more time, depending on the velocity of the vehicle. On the assumption, that a brake assist provides full brake pressure from the start, a deceleration of 1g can be assumed. This leads to a decrease in the collision speed of the vehicle of about 30km/h (18mph) in 0.8s. Thus with a braking-time of 0.8s about 65% of the considered vehicle-pedestrian collisions could possibly be avoided (result of the accident study of chapter 2). An even earlier warning may be preferable in certain situations but could also lead to an irritation of the driver and therefore become useless. This circumstance is described by the "warning dilemma".

Definition "Warning Dilemma":

An appropriate warning for an inattentive driver has to be issued earlier than a warning for an attentive driver. The dilemma lies in the fact that the driver's state of attention is unknown.

Nevertheless we believe the following Time to Collision (TTC) values can be assumed reasonable as parameters for an intervention scheme:

TTC 2 – 2,5s	early warning
TTC 1 – 2s	acute warning
TTC < 1	[autonomous braking (partially)]

The TTC values here are not strict, because the situation analysis does not rely solely on the TTC in order to measure the risk of an impending collision (see chapter 4).

The early warning will be designed to be optical and directional, so it will attract driver awareness to the direction (left / right) of the pedestrian's approach. At the acute warning an acoustic signal will be generated additionally. It is also envisaged to generate a haptic warning by means of a brake jerk that will not significantly decrease the vehicle speed but clearly signal the driver to take action.

4. SITUATION ANALYSIS AND RISK ASSESSMENT

Essential for the proper performance and therefore for the acceptance of the system is the quality of the situation analysis and the risk assessment. The warning dilemma as described in chapter 3 has to be solved with an appropriate situation analysis which has to cope with the following tasks:

- sensor data processing (recognition of the situation)
- prediction of the pedestrian's movement
- determination of the collision relevance of the pedestrian
- risk assessment
- initiating the warning strategy

As an overview we will briefly present two different approaches for a situation analysis.

TTC Approaches

Time to Collision (TTC) approaches primary assess the time which is left before the collision, given the current prediction of movement for the vehicle and the pedestrian. The prediction of the pedestrian movement can vary; the easiest way is to extrapolate the position linear using the current velocity data. If the pedestrian is heading for a collision with the vehicle, the TTC can be determined. When the TTC decreases under a certain threshold, a warning is issued or another action strategy can be initiated. The obvious advantage of this approach lies in its simplicity. This approach is also very robust, predictable and easy to parameterize. However the performance largely depends on the quality of the movement-prediction of the pedestrian and because of its simplicity the approach is prone to generating false alerts in situations where a warning must not occur. Here a combination with the Pedestrian Motion Model (as proposed in chapter 4.2) could lead to improvements.

Acceleration Approaches

Acceleration approaches are based on the physical motion abilities of the pedestrian and the vehicle. Based on the assumption that both vehicle and pedestrian can achieve only a certain maximum acceleration (lateral and longitudinal) it can be determined if a collision is physically unavoidable (CU, i.e. Collision Unavoidable). Such an approach is proposed in [8], where the maximum accelerations for both pedestrian and vehicle are assumed to be 1g (not depending on the direction). Based hereupon the CU criterion is fulfilled first at TTC's of a few hundred milliseconds. Enough time to trigger for example a deployable hood [8]. However, this time interval is obviously too short for a suitable driver warning. Thus, to make this kind of algorithm usable for a warning system more realistic values for

pedestrian accelerations have to be modelled. Indeed thereby the above mentioned acceleration of 1g for a pedestrian can be considered as an overestimating envelope. It is based on a series of tests with 10 persons who had to cover a distance of 80cm from a standing position as fast as possible [8].

Summarizing it can be stated that a simple TTC-based approach is too susceptible to false warnings while the existing acceleration-based approach does not provide enough time for a warning. As further development in the course of this work we propose an advanced acceleration-based approach that considers the possible movements of pedestrians and allows a risk assessment with more levels than just CU. In this context it is therefore appropriate to further investigate the movement abilities of pedestrians and design a new Pedestrian-Motion-Model (PMM) which can limit the theoretically assumed mobility (see 4.2). Only a few studies on the topic of pedestrian speeds and accelerations can be found in relevant literature like [9], [10], [11] and [12]. Except the latter, neither of these studies has been conducted in the context of pedestrian protection. In the following (chapter 4.2) the data found in [9] and [10] will be used for the investigations concerning a suitable PMM.

4.1. Situation Analysis

The situation analysis processes the sensor data and determines if a pedestrian is relevant in terms of an impending collision. If a pedestrian is recognized it will be determined how he has to alter his trajectory in order to avoid the collision on his own account. The underlying idea is that a situation is relatively uncritical, when the efforts for the pedestrian to leave the dangerous area are comparatively small. For example, situations where pedestrians initially are on collision course and then stop in good time prior to reaching the roadside occur frequently in dense inner-city traffic. A system reaction in each case would result in too many false alerts. Therefore the minimal acceleration is determined which allows the pedestrian to maintain a safe distance to the vehicle. In case of a lateral crossing pedestrian (main cause of vehicle-pedestrian accidents, see chapter 2) the pedestrian can either stop prior to reaching the vehicle path; accelerate to have left the vehicle path in due time or step into the path and turn around. For each possibility the required acceleration is calculated based upon the following equation:

$$s_{l/r} = pos_{ped} + t \cdot v_{ped} + \frac{1}{2} t^2 a_{ped} \quad (2)$$

Where $s_{l/r}$ is the safe position the pedestrian needs to reach either on the left or the right side of the vehicle. Note that this position is not necessarily the edge of the vehicle path but can include an adaptive safety

gap. Solving (2) with respect to a_{ped} yields a set of acceleration values which can be assessed by the PMM. Besides this assessment of the pedestrian's efforts to avoid the collision, it also considered how comfortably the driver can avoid the collision. That means the deceleration needed to stop the vehicle before reaching the pedestrian is derived from the current velocity of the vehicle, the distance to the pedestrian and the assumed reaction-time of the driver. This information additionally contributes to the risk assessment of the situation. The risk will be estimated higher if the needed deceleration for the vehicle increases. Only if this deceleration exceeds a comfort – value, e.g. the maximum deceleration of adaptive cruise control systems, the risk will be estimated high enough to initiate the warning strategy.

Figure 5 shows a typical scene with a pedestrian crossing from the right. The results of the situation analysis are shown graphically as coloured areas in front of the vehicle. Every area corresponds to a different level of risk. Is the pedestrian located outside these areas the estimated effort for him to alter his trajectory is too low; therefore he is not (yet) at risk. The risk level increases the closer the pedestrian gets to the vehicle until the collision is unavoidable even with full cooperative behaviour of vehicle and pedestrian (red area). As can be seen, the actual motion direction of the pedestrian leads to the asymmetric shape of the risk areas. The different shades of each colour (see red arrows) divide each area into two sub-areas. These represent the preferable alterations of the pedestrian's trajectory, i.e. an acceleration or deceleration.

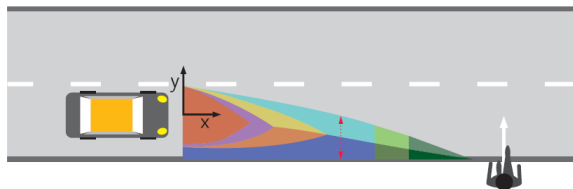


Figure 5. Typical scene with crossing pedestrian, results of situation analysis as different areas of risk.

4.2. Pedestrian-Motion-Model

The feasibility of possible trajectory alterations is assessed within the PMM. Primarily it will estimate to what extent a pedestrian can accelerate and how comfortably this acceleration can be accomplished. At first we characterize the different aspects which shall be considered for the estimation.

Direction of acceleration - As stated in [12] the acceleration abilities of pedestrians are not isotropic, but depend on the direction at which it is aimed.

Current Movement - Previous studies like [9]-[11] only refer to velocities and accelerations of pedestrians starting from standing still. However, accident scenarios where pedestrians are already in

motion are statistically much more relevant. It can be assumed that a pedestrian who is already moving forward will not be able to accelerate as fast as a pedestrian starting from standing still.

Duration - Pedestrians are not able to accelerate uniformly over a given period of time (see for example [10]). The acceleration process can more likely be characterized by an "acceleration jerk" followed by a declining phase (Figure 6).

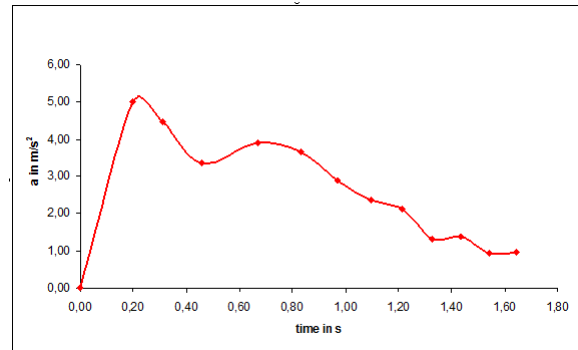


Figure 6. Acceleration process from standing position to running [10].

An example for different levels of comfort while accelerating can be seen in the different acceleration processes from the start to walking, jogging or running.

The necessary inputs for the model are the position, and velocity of the pedestrian, the "target-acceleration" and the duration in which this acceleration should be sustained.

4.2.1. Pedestrian – Motion – Model in 1D

As already shown in Figure 6, a typical acceleration process is not uniform but characterized by a jerk with a following declining phase. Such shapes can be derived from data in [9] and [10]. Starting from such a process the following mapping can be defined:

$A(t) :=$ Mean uniform acceleration which can be sustained in time $t > 0$

Here, mean uniform acceleration (MUA) means the average rate at which the pedestrian can accelerate uniformly.

Given a time dependant acceleration curve $a(s)$, $A(t)$ can be calculated as:

$$A(t) = t^{-1} \int_0^t a(s) ds \quad (3)$$

Applying (3) to the process shown in Figure 6 we get the MUA as shown in Figure 7.

We see that these values are significantly lower than those from typical acceleration based approaches. This can limit the theoretical mobility of a pedestrian considerably. Of course this data represents only one test sequence with 5-10 persons (see [10]), but it is

obvious that there seems to be a great potential for a better understanding and assessment of the pedestrian's mobility. This is underlined even more by the fact, that the values in Figure 6 and 7 were derived from a test sequence in which the persons were asked to run as fast as possible from standing start. This supports the conclusion that the comfort of this acceleration has been rather low, thus most pedestrians may not even reach these values.

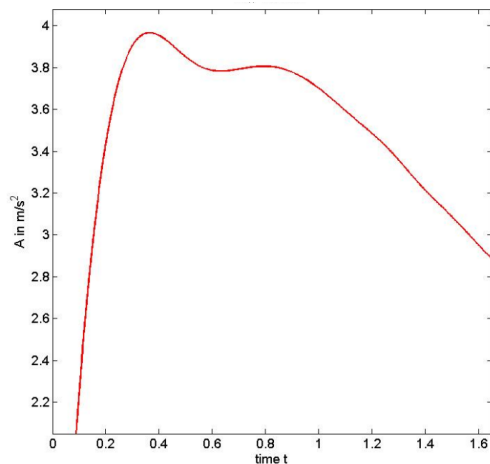


Figure 7. Mean uniform acceleration process from start to running.

A possible rating for the acceleration comfort (implying a risk assessment) can be defined by the comfort of the different states of movement "walking" (~1-2m/s), "jogging" (~3-4m/s) and "running" (5-6m/s). Curves representing acceleration processes for these states (similar to Figure 6) were derived for the start from standing still. For these states a level of comfort can be defined. Values between the 3 curves can be mapped to an interpolated comfort value.

4.2.2. 2D – Model development and test sequences

The above mentioned model does neither consider the current movement of a pedestrian nor altering direction in 2d yet. Therefore further test sequences are planned which shall generate data to derive curves similar to Figure 6 for such motion patterns. In particular test sequences are planned where test persons are asked to accelerate while already walking with and without change of direction. Furthermore tests regarding the deceleration abilities of pedestrians will be conducted. With this new data it will be possible to further enhance the model.

5. CONCLUSIONS

Detailed results of an accident study were presented. These results show that the proposed pedestrian protection system covers up to 85% of all vehicle – pedestrian "crossing – accidents". A decisive factor for this percentage was the system's aperture angle

which has been investigated further. It has been shown, that based on given assumptions an aperture angle of about $\pm 20^\circ$ is best suited for the system. Then the layout of the proposed pedestrian protections system has been presented and the warning dilemma discussed. To solve this dilemma an acceleration-based situation analysis approach has been proposed in chapter 4. It is based on a new pedestrian motion model which considers the acceleration abilities of pedestrians. The risk assessment of an impending collision is accomplished by estimating the effort for the pedestrian caused by altering his trajectory in order to avoid the accident. Thus it is possible to prevent false alerts which would otherwise occur because of the large time scale which is needed for a driver warning.

This work is partly funded by the German Federal Ministry of Economics and Technology (BMWi) in the context of the research project AKTIV.

REFERENCES

- [1] Traffic Accident Analysis Center, Road Traffic Safety Authority Korea
- [2] International Road Traffic and Accident Database
- [3] Robert Bosch GmbH, Accident Research
- [4] Regulation (EC) No 78/2009 of the European Parliament and of the Council of 14 January 2009
- [5] Euro NCAP, www.euroncap.com
- [6] Georgi A., Brunner H., Scheunert D. 2004. "GIDAS German In-Depth Accident Study." Proceedings of FISITA Congress 2004.
- [7] Bäumlner H. 2007. "Reaktionszeiten im Strassenverkehr." Verkehrsunfall u. Fahrzeugtech., No. 45: 334-340
- [8] Fuerstenberg K. 2005. "Pedestrian protection using laserscanners." Proceedings of the 8th International IEEE Conference on Intelligent Transportation Systems Vienna, Austria, September: 13-16
- [9] Hein H. 1994. "Messungen von Fußgängergeschwindigkeiten und – Beschleunigungen." Diplomarbeit FH München
- [10] Eberhardt W., Himbert G. 1977. "Bewegungsgeschwindigkeiten- Ergebnisse nichtmotorisierter Verkehrsteilnehmer." Eigenverlag
- [11] Vaughan R., Bain J. 2001. "Speeds and accelerations of school children." Road & Transport Research, No. 107/3: 28-36
- [12] Scherf O. et.al. 2008. "Optimaler Fußgängerschutz durch situationsgerechte Einschätzung der Fußgängerbewegung." Berichte der 24. VDI/VW Gemeinschaftstagung "Integrierte Sicherheit und Fahrerassistenz" (Okt. 29 -30).

PEDESTRIAN COLLISIONS WITH FLAT-FRONTED VEHICLES: INJURY PATTERNS AND IMPORTANCE OF ROTATIONAL ACCELERATIONS AS A PREDICTOR FOR TRAUMATIC BRAIN INJURY (TBI)

Feist, Florian

Gugler, Jürgen

Vehicle Safety Institute, Graz University of Technology
Austria

Arregui-Dalmases, Carlos

del Pozo de Dios, Eduardo

López-Valdés, Francisco

European Center for Injury Prevention, Universidad de Navarra
Spain

Deck, Caroline

Willinger, Rémy

University of Strasbourg, IMFS-CNRS
France

Paper Number 09-0264

ABSTRACT

Research on pedestrian protection currently is focusing mainly on passenger cars. However, impacts with heavy goods vehicles (HGV) and buses are also important, especially in urban areas and in developing countries. This study is an attempt to show the distribution of injury patterns focused on the head injury mechanism. In the European project APOLLO WPII database with a number of 104 pedestrians injured by a HGV or bus were identified. The head was found the most severely injured anatomic region, with an average AIS of 3.1, followed by the abdomen/pelvis (AIS 2.9), and the thorax (AIS 2.1). Using the Dr. Martin transformation matrix, head injury mechanisms were assigned to codified head injuries. Around 69% of the sustained head injuries had a rotational injury mechanism, 21% translational, and 10% either. Three multi-body vehicle models, representing two HGV and one bus, were used in a large parameter analysis. The simulations showed that the angular velocity change is exceeding 30rad/s and the angular acceleration is exceeding 10.000rad/s² in simulations where the HIC value was below 1000. Additionally the head injury risk was assessed by prescribing the accelerations of the human pedestrian model's head to a finite element head and brain model. It can be concluded that head injuries are the most frequent injuries sustained by pedestrians involved in a collision with a flat-fronted vehicle and rotational accelerations are responsible for around 70% of head injuries. Impactors currently used in pedestrian protection regulations do not assess rotation-induced injuries.

Keywords: Vulnerable Road Users, Pedestrian, Bicyclist, Heavy Goods Vehicles, Trucks, Head Injuries, Rotational accelerations, FE head/brain model

MOTIVATION

In numerical studies conducted in the project APROSYS [1], [2], [3] the interaction between vulnerable road user and heavy goods vehicle were studied by means of finite element vehicle models (IVECO Stralis and generic short-haul goods vehicle) and finite element and multi-body pedestrian models (pedestrian accident compliant (PAC) model and Madymo human pedestrian models). The numerical studies highlighted threatened and highly loaded body regions [1].

In parallel the HV-CIS injury and accident database was analysed by Smith [4]. The accidentology pointed out, that the head is the most frequently (seriously) injured body region. Other studies proof the same [5].

The numerical studies, however, did not show the relevance of head injuries to that extent. It was therefore assumed, that the secondary contact with the ground leads to the large number of head injuries. The secondary impact (with the ground) was not investigated in the previously mentioned studies.

In 2008 a workshop organised by APROSYS SP2 was held in Neumünster, Germany. There, Arregui [6] pointed out that head injuries in accidents between pedestrians and flat front vehicles are more frequently due to rotation (rotational acceleration/velocity) than due to translation.

It therefore seemed worthwhile to rerun the numerical simulations and pay attention to the head rotation and the secondary impact (with the ground). In collaboration with APROSYS SP5 (biomechanics) the head injury risk was re-evaluated using a finite element head/brain model.

Eventually, the findings of the numerical studies were compared with the field data of the injury database APOLLO.

INTRODUCTION

Very little research has been carried out so far in the field of pedestrian collisions involving HGV. Most studies performed are focusing on passenger cars, and LTV (light truck vehicle).

Graz University of Technology and the University of Strasbourg were involved in the EC funded project APROSYS. Sub-project 2 initiated research in the field of HGV-VRU accidents, investigated the interaction of vulnerable road users (VRU) with heavy goods vehicles (HGV) in experiment and in a numerical environment and came up with a so-called aggressivity index (HVAI) assessing the risk imposed by a HGV on vulnerable road users. Sub-project 5, Biomechanics, developed improved head injury criteria based on a finite element head-brain model by reconstructing 68 accident case results (6 motorsport, 22 football player, 29 pedestrian and 11 motorcycle accidents) [7]. This model is capable of assessing the potential head injury risk in road safety and distinguishing between contusion, sub-dural haematoma (SDH), skull-fracture, and diffuse axonal injuries (DAI).

The European Center for Injury Prevention was involved in the European Project APOLLO, in the Work Package II, investigating the injuries associated to the hospital discharges in Europe. Work-package II, "The burden of injuries in the EU: indicators and recommendations for prevention and control", is coordinated by the University of Navarra [8]. The "core" project consists on the development of report on the burden of (non-fatal) injuries in the European Union. The APOLLO database stores the information of 1.085.673 cases from the hospital discharges, of which some 74.660 cases are traffic-related injuries.

HEAD INJURY MECHANISMS

Many experiments and studies on head impact have been carried out to investigate the head's mechanical response properties. In general, the impact response was described in terms of head acceleration, impact force and intracranial pressure.

Translational accelerations

The pioneer of the experimental studies in this field was Holburn (1943) [9]. He worked on tangential stresses in a gel model, observing that the rotation between skull and brain could explain most of the traumatic brain injuries. It was noted that translations were not as harmful as rotations; an amazing conclusion that is still valid nowadays.

Profound research has been carried out on impact tolerance of human head sponsored by the automotive industry. The first approach to human tolerance limits was introduced by Gurdjian in 1953 [10] and Lissner et al in 1960 [11], and it is widely known as the Wayne State Tolerance Curve (WSTC). Figure 1 reproduces that curve.

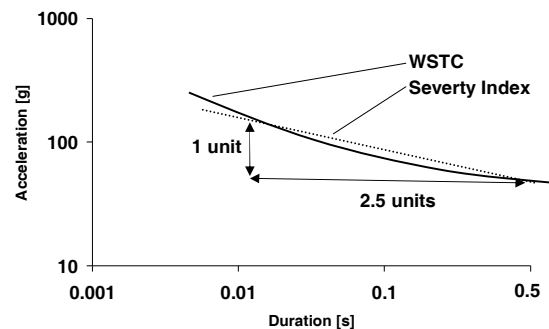


Figure 1: Severity Index, based on [12]

The WSTC indicates a relationship between average translational anterior-posterior acceleration level and duration of the acceleration pulse that accounts for similar head injury severity in head contact impacts. Gurdjian and colleagues assumed that measuring the tolerance of the skull to a fracture was equivalent to measuring the tolerance to a brain injury.

Combinations of acceleration level and pulse duration that lie above the curve are assumed to exceed human tolerance, and will cause severe irreversible brain injury. Combinations below the curve do not exceed human tolerance.

In 1966 Gadd [12] introduced the SI (Severity Index) based on WSTC studies. It was calculated by integrating the linear acceleration and raised to the power of 2.5 (the slope of curve expressing the WSTC in log t– see Figure 1). Gadd indicated an acceptable maximum value of 1000.

Using the WSTC and the criteria developed thereafter, restrictions that arise from the test conditions have to be considered. The major limitations are the shortage of data of initial curve points, the accelerometer position located in the back of the head (far from the centre of gravity) and techniques for scaling the animal data and the supposed correspondence of skull fracture and brain injury. Bearing in mind that WSTC is based on direct

frontal impact tests, the result should not be applied to other impact directions.

In 1971, Versace ^[13] proposed an alternative formulation of the Severity Index, subsequently proposed by the US National Highway Traffic Safety Administration (NHTSA) and included in the FMVSS 208. This injury criterion is called HIC (Head Injury Criterion) – see (1):

$$HIC = (t_2 - t_1) \left[\frac{\int_{t_1}^{t_2} a_r dt}{t_2 - t_1} \right]^{2.5} \quad (1)$$

Where a_r is the resultant linear acceleration measured at head centre of gravity (in G's) and t_1 and t_2 are two arbitrary times (in s).

To determine the relationship between HIC and injuries to the skull and brain, available test data were analysed statistically by fitting normal, log normal, and two parameter Weibull cumulative distributions to the data set, using the maximum likelihood method to achieve the best fit for each function ^[14]. The best fit of the data was achieved with the log normal curve.

A major limitation of the HIC - not taking into account rotational acceleration - is often criticized. Another common limitation is the lack of a relationship between human head injury and the acceleration response measured with anthropomorphic test devices that is the transformation function between the dummy and the cadaver.

Nevertheless, the HIC is the index of cerebral damage most commonly accepted by the scientific community and the only value that the automotive industry uses to develop new vehicles or to fulfil regulations.

The a3ms (or cum3ms) criterion is also based on the WSTC, and it is defined as the maximum acceleration level obtained for an impact-duration of 3 ms, where any three milliseconds window should not exceed 80 g in the resultant acceleration curve. This requirement has also been incorporated in European and American regulations.

Rotational accelerations

In experimental studies using animals by Unterharnscheidt and Higgins ^[15], angular accelerations were applied to primates' heads. They could reproduce subdural haematoma, bridge veins ruptures between skull and brain, as well as brain injuries and spinal cord injuries.

Ommaya ^[16] carried out a study with 25 monkey squirrels, in which they induced and compared pure translational motions with combinations of rotational and translational accelerations, determining the reduction of the resistance in case of combined

motion - despite being smaller in intensity. It was also found that the angular acceleration and the according injury thresholds are related to the mass of the brain. The tolerance limit for human beings was obtained by scaling the results from the primate test.

In 1993, working on rotational acceleration as an injury mechanism, Melvin ^[17] determined human being's tolerance to angular acceleration in 7500 rad/s² with a concussion probability of 99%. In 1974 Löwenhielm suggested that the bridging veins between skull and brain started to tear from 400 rad/s² angular acceleration or a change of angular speed from 70 rad/s ^[18].

Margulies and Thibault ^[19] proposed a criterion to produce a Diffuse Axonal Injury (DAI) according to the Angular Acceleration and the Delta Angular Speed, which is reproduced in Figure 2.

The area below the curve indicates the head acceptable limit for two different brain weights (500g, 1400g). The solid black curve indicates the tolerance for the human brain.

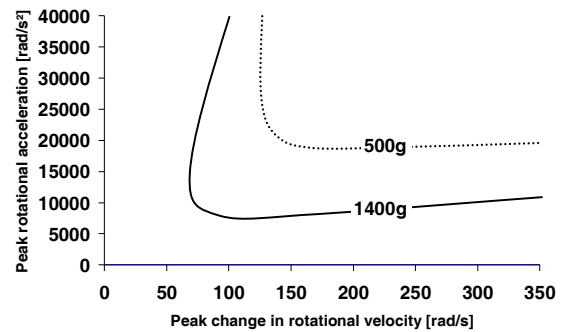


Figure 2: Rotational acceleration and rotational velocity as injury mechanism, based on ^[19]

Table 1 shows tolerance values commonly used. However, additional studies on volunteers suggest that much higher tolerance values may be possible for short durations.

Table 1.
Tolerance thresholds for rotational acceleration and angular velocity. [20]

Tolerance threshold, 50% probability	Type of brain injury	Reference
$\alpha = 1800 \text{ rad/s}^2, \Delta t < 20 \text{ ms}$	Cerebral concussion	Ommaya et al., 1967
$\omega = 30 \text{ rad/s}, \Delta t > 20 \text{ ms}$	Rupture of bridging veins	Löwenhielm et al., 1975
$\alpha < 4500 \text{ rad/s}^2, \Delta t < 20 \text{ ms}$	Brain surface shearing	Advani et al., 1982
$\alpha < 3000 \text{ rad/s}^2$		
For $\omega < 30 \text{ rad/s}$:		
AIS 5; $\alpha > 4500 \text{ rad/s}^2$		
For $\omega > 30 \text{ rad/s}$:		
AIS 2; $\alpha > 1700 \text{ rad/s}^2$	General injury	Ommaya et al., 1984
AIS 3; $\alpha > 3000 \text{ rad/s}^2$		
AIS 4; $\alpha > 3900 \text{ rad/s}^2$		
AIS 5; $\alpha > 4500 \text{ rad/s}^2$		

In an attempt to combine translational and rotational acceleration, Newman in 1986 [21], in contact with Transport Canada, introduced the concept of generalized GAMBIT (Generalized Acceleration Model for Brain Injury Tolerance). The model attempts to weight, in an analogous manner to the principal shear stress theory, the effects of the two forms of motion. The GAMBIT equation is as follows:

$$G(t) = \left[\left(\frac{\alpha(t)}{a_c} \right)^m + \left(\frac{\alpha(t)}{a_c} \right)^n \right]^{\frac{1}{s}} \quad (2)$$

Where $a(t)$ and $\alpha(t)$ are the instantaneous values of translational and rotational acceleration respectively. a_c and a_c are limiting critical values and n , m and s are empirical constants selected to fit the available data from Kramer and Appel field accident database [22]. ($n = m = s = 2.5$, $a_c = 250g$, $\alpha_c = 25.000 \text{ rad/s}^2$). These values were more or less confirmed in a more recent publication [23]. $G=1$ is set to correspond to a 50% probability of MAIS 3.

Using simulations of the injuries sustained by passengers in documented automobile accidents, the severity / probability relationship shown in Figure 3 was generated [21] These have not been fully validated but may serve as basis for future development.

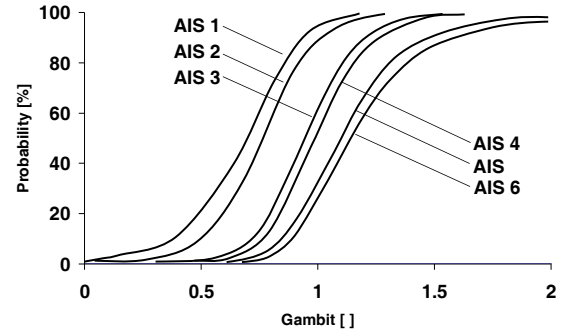


Figure 3: Head injury severity probability as a function of GAMBIT criterion [21]

The GAMBIT has been criticized on the grounds that it does not take into account any time related aspect of head injury process. That is, it only depends on maximum values and does not invoke any particular limit of velocity change or time duration of acceleration exposure. Another weak point of this criterion is its inadequate validation.

The HIP (head impact power) is a more global approach to a head protection criterion [24]. The formula is the sum of power terms for all rotational and translational degrees of freedom – see (3) -and is based on the hypothesis that head injuries do occur if a certain rate of kinetic energy change is exceeded. A threshold value of 12.79 kW (kNm/s) is proposed for 50% of concussion, a mild traumatic brain injury where unconsciousness [25] may occur (see Table 2).

$$HIP = \sum_{i=1}^3 m a_i \int a_i dt + \sum_{i=1}^3 I_{ii} \alpha_i \int \alpha_i dt \quad (3)$$

Table 2.
Relationship between HIP and probability for concussion [25]

Probability for concussion	HIP [kW]
5%	4.7
50%	12.79
95%	20.88

Gennarelli et al. [26] presented a set of interrelationships between biomechanical metrics and the entire spectrum of DBI (Diffuse Brain Injury), and the first hypothesis of the potential influence of a generic factor on human tolerance to trauma. The main limitation of this study is the simplification used in presenting the tolerance hypothesis, assuming that just the angular acceleration is responsible for the DBI (when it is commonly accepted that duration of acceleration and angular velocity are also required).

Table 3 represents the connection between rotational acceleration and Diffuse Brain Tolerance related to

the Abbreviated Injury Scale (AIS) – as found by Gennarelli et al. [26].

Table 3.
Relationship between rotational acceleration and AIS, based on [26]

AIS	Rotational Acceleration [rad/s ²]
1	2878
2	5756
3	8633
4	11511
5	14389

At this time, no rotational criteria have been approved by the scientific community or adopted by the automotive industry.

Currently, the FE models are gradually becoming more sophisticated and they have the potential for understanding the complex injury mechanism of head impact. And the scientific community aggress in exploring this new tool to increase the knowledge the head injury field.

METHOD

Earlier numerical studies showed that the injury risk of a certain body region depends largely on the vehicle size and initial position of the VRU with respect the HGV [27]. In these studies, however, different codes and numerical pedestrian models were used. Therefore, it was difficult to draw consistent conclusions.

Instead of using different numerical models of vehicle and pedestrian, one parameterisable multi-body vehicle model was developed. Three front shape geometries (short-haul HGV: MAN L2000, long-haul HGV: IVECO Stralis and one bus: MAN Lion) were used for the analysis of head-injuries and later for the front-shape optimization based on a generic-algorithm. The bus geometry was included in order to be consistent with the analysis of the APOLLO injury database, which does not allow for a discrimination of bus and truck.

The numerical study is conducted in three steps:

1. The three breed models were used to analyse the head acceleration (rotation/translation) and head rotation velocity. Additionally a number of parameters were varied to find the maxima and minima of the simulation outputs. Parameter that have been varied:
 - Friction between HGV and VRU: 0.2 ... 0.4
 - Friction between Shoes and Ground: 0.5 ... 0.7
 - Friction between VRU and Ground: 0.4 ... 0.75
 - Facing direction of pedestrian: +60° ... -60°

- Start of braking: -1s ... 0.2s
 - Initial velocity: 30 ... 40 km/h
 - Pedestrian gait: 10 postures
 - Ground-Clearance of the vehicle: depending on vehicle model
2. In a further step, the secondary impact (with the ground) was studied. Finally head accelerations in primary and secondary impact are compared.
 3. The three breed models were used in a generic algorithm aiming to reduce the objective function. The objective function is a combination of head injury risk evaluation (rotation and translation) and thorax injury risk evaluation. Weighting factors are based on the findings of the accidentology. (To be described in another publication to come).
 4. Accelerations measured in the COG of the pedestrian's head were prescribed to a finite element head/brain model. That model was used to assess the risk for brain injuries. The evaluation is compared to the results obtained by applying "conventional" injury criterions
 5. The APOLLO database was analysed. Head injuries related to an accident with a heavy goods vehicle or bus were distinguished in rotational acceleration induced injuries and translational acceleration induced injuries.

Numerical Vehicle Model

Multi-body framework of vehicle - The vehicle consists of four major rigid bodies (see Figure 4):

1. Two rigid bodies representing the unsuspended mass of the rear and front axle. The front axle is connected to the reference body (the ground) by a translational joint (front axle) and a restraint (rear axle). The front and rear axle are supporting the chassis. Spring-damper elements account for the suspension of the vehicle.
2. The chassis is bearing the bumper and the front underrun protection (the lower bumper).
3. The cabin is bearing the remaining front (grill, hood, windshield frame and windshield). The cabin is suspended by a planar joint (and restraints in x- and z-direction) and a free joint (and a restraint in z-direction).
4. Other rigid bodies are supporting the contact surfaces (ellipsoids or facet surface) of the vehicle front. A marginal mass and inertia is assigned to these rigid bodies.

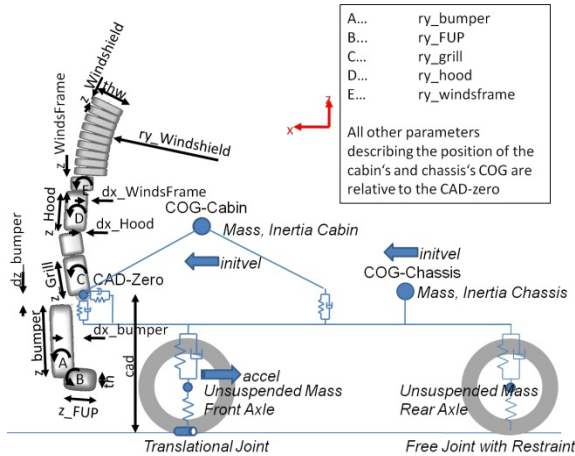


Figure 4: Multi-body framework of the HGV model

Geometry

The geometry of the vehicle (the phenotype) can be defined by a number of parameters (the genotype) [28]. Generally the front shape is defined by the following parameters:

- Height of facet surface and ellipsoid (z_name)
- Rotation of facet surface and ellipsoid in relation to parent ellipsoid (ry_name)
- Offset of facet surface and ellipsoid in relation to parent surface (dx_name)

In total a string of 18 numerical parameters defines the geometry.

Using initial scaling, the facet surfaces (e.g. the facet surface for the bumper) are scaled accordingly to the parameter z_name . As a result the mesh size changes from one vehicle to the other. The initial element size was chosen such that the maximal effective element-size is not exceeding $5 \times 10 \text{ mm}$ (as long as the value of z_name is not exceeding a predefined value).

Three reference models were created, to fit the front shape of a short-haul truck, a long-haul truck and a bus (see Figure 5).

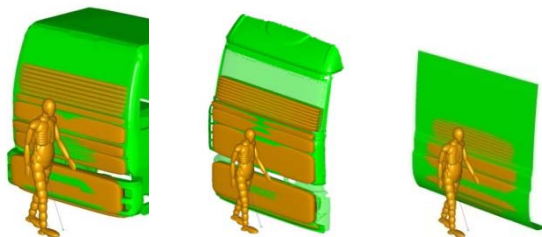


Figure 5: The three breed models

Contact Pedestrian – Vehicle

The initial truck model was built up by ellipsoids. Initial simulations showed up the deficiencies of the

ellipsoid contact for the analysis of the primary contact with the truck: The MB-MB contact does not take into account the shape of the contact partners and gaps between the ellipsoids might cause body parts to be braced. Generally the contact involving at least one ellipsoid (the human body) has a major drawback: As soon as the penetration is exceeding the semi-axis, contact forces are inverted.

The stress-based FE-MB contact shows drawbacks as well. Failure of materials (e.g. windshield) can not be modelled directly, but by a work-around. Facet models are less CPU time efficient. Hysteresis model 3, where “[...]the unloading curve is shifted and scaled without using a hysteresis slope [...]” [29] is not available and again: as soon as the penetration is exceeding the ellipsoid’s semi-axis, the contact-force is inverted.

Still, the advantages of FE-MB contact with a stress-based contact model prevail for the analysis of the primary contact (which is the contact with the truck front). For the analysis of the secondary contact (which is the contact with the ground), the ellipsoid HGV model was used, since less CPU time is needed for rather long simulation durations. The sub-chapters below describe briefly the particular issues considered with the contact interaction of the ellipsoid HGV model and the facet HGV model.

Multi-body-Multi-body (MB-MB) contact

The ellipsoid HGV model and consequently the MB-MB contact were used in the study of the secondary impact (pedestrian to ground contact). No contact characteristics were assigned to the HGV ellipsoids. The contact type was referring to the characteristics of the pedestrian model. The vehicle was assumed to be non-compliant. This assumption is fair for the analysis of the secondary contact.

For the contact with the ground the contact type “combined” was used.

Multi-body-Finite Element (FE-MB) contact-

By a switch in the input file, the user can select between the ellipsoid HGV model and the facet surface HGV model. The FE-MB stress based contact requires the force-penetration functions (as they are normally used in MB-MB contacts) to be transformed into stress-strain functions (or in fact a stress-penetration functions, when the thickness of the null-shells is selected to be 1m).

A force-penetration $F(e)$ curve is given from quasi-static or dynamic testing. The shape of the penetrating body is given and can be approximated by an ellipsoid. That ellipsoid (master surface) is impacting a flat facet surface (slave surface). The stress as a function of the penetration (contact thickness = 1m) can be calculated in the following

manner: The nominal penetration is $e_j = \Delta e \cdot j$, where Δe is the step-width of the numerical solution and j the number of the step. The penetration of node i at timestep j is p_{ij} . The area associated to each step is A_j . For a sphere with a radius r the area associated to a newly penetrating node i^* is $A_{i^*j} = \pi [(2r e_j - e_j^2) - (2r e_{j-1} - e_{j-1}^2)] / \cos(\alpha_{i^*j})$ where α_{i^*j} is the angle between the vector from node i to the centre of the ellipsoid and the vertical at time j (see Figure 6).

For node 1, which always has the largest penetration (p_{1j}) of all penetrating nodes, the stress σ_{1j} is calculated such that the formula $F(e) = \sum \sigma_{ij}(p_{ij}) A_i$ is met. For all other nodes the stress σ_{ij} is interpolated from previous steps j . A simple visual basic macro implemented in MS Excel is solving that problem numerically with a step-width $\Delta e = r/100$.

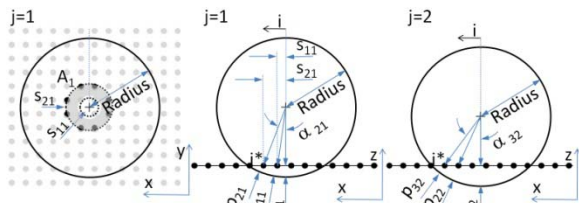


Figure 6: Approach for converting the force-deflection curves to stress-strain curves for slave nodes intruding into a master surface

Some body parts of the vulnerable road user are penetrating deeply into the truck front, such as into the grill area or into the windshield when this is failing. Two approaches were chosen as work-around:

- The struck-side arm, hand and shoulder ellipsoid were converted into a facet surface
- A multi-layered surface was chosen to model the windshield and the grill

The windshield is modelled by up to three layers of facet surfaces (there are only two layers required for the windshield close to the windshield frame, three layers are required more to the centre of the windshield, see Figure 7). The first layer is for simulating the glass itself, while the second and third layer is for simulating the laminate (the polyvinyl butyral film). The second layer has an offset of 7mm. As soon as the contact force between the intruding surface and second windshield layer exceeds a certain threshold value, the contact with the first windshield layer is turned off. By doing so, the failure (the cracking) of the windshield can be simulated. The third layer has an offset of about 60mm to the second layer, which is a little less than the half-diameter of the adult pedestrian's head. This is to prevent contact force inversion, when an ellipsoid is intruding by more than its semi-axis. The third layer is inactive for facet-facet contacts (with the shoulder and the arm).

It was assumed, that the failure of the windshield affects any following contacts with the windshield. Example: Is the pedestrian's shoulder contacting the second layer of the windshield (which can be the case, when the pedestrian is hit by a flat front vehicle with a low windshield, e.g. a bus) and the contact force is exceeding a predefined force level (about 200-700N), the first layer's contact is turned off. That in turn means that any body part (e.g. the head) impacting the windshield later than the shoulder is never intercepted by the first layer. This was found a reasonable assumption, when looking to impactor tests of the windshield, where the circumferential and in particular the "spider-web" cracks propagated well beyond the outer dimensions of the intruding body.

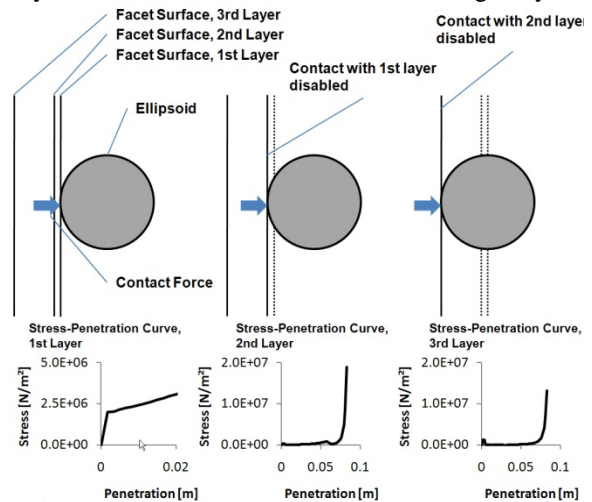


Figure 7: Three layered windshield model

This approach was found to be very effective for simulating the failure of the windshield or generally non-monotonously increasing force-deflection characteristics. Figure 7 shows the modelling of the windshield. Figure 8 shows a comparison between the given force-deflection curve of a dynamic impactor test and the model response of the three layered windshield model.

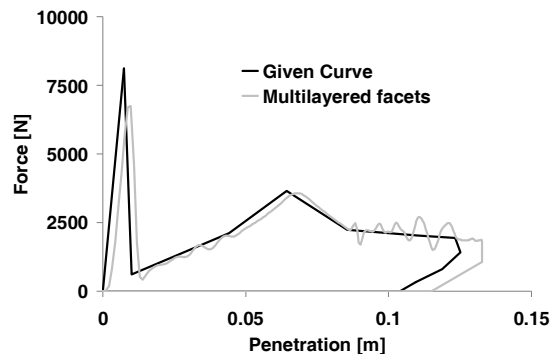


Figure 8: Three layered windshield model

The grill area is modelled by two layers. The second layer is to model the more rigid parts behind the grill-like the radiator.

Stress-Penetration Characteristics

It was assumed that the windshield of a HGV is comparable in terms of force-deflection to a windshield of a passenger car. Hence, the force-deflection characteristics as obtained by Mizuno [30] and used in other publications on pedestrian accident simulation [31] were applied to the HGV windshield. Two experimental tests of the windshield impacted by an EEVC WG17 adult hemisphere were available. A comparison with the response of the numerical model showed a fair correlation. The first experimental test was performed at 20kph, leading to a HIC of 286. A similar point selected on the windshield of the numerical model led to a HIC of 362. A second test, performed at 25kph showed a HIC of 756 in the experiment and 848 in the numerical simulation.

Most of the contact characteristics of the generic multi-body trucks are based on the quasi-static measurements of the IVECO Stralis front [32]. These characteristics have been assigned to the front of the three reference models. Dynamic impact tests of the MAN L2000 and IVECO Stralis front with adult and child EEVC WG 17 head impactors were available [33], too. Finally, the performances of the generic multi-body models have been compared with the results of these dynamic tests – see Figure 9 and Figure 10.

Impact Speed	Size	HIC Range Experiment	HIC Generic Madymo Model
30kph	Adult	179 ... 417	799
30kph	Adult	270 ... 461	574
30kph	Adult	1302 ... 2777	2007
30kph	Adult	2037 ... 4116	2070
30kph	Adult	755 ... 976	745

Figure 9: Performance of generic Madymo model, long-haul HGV [32]

Impact Speed	Size	HIC Range Experiment	HIC Generic Madymo Model
20kph	Adult	286	362
25kph	Adult	1948	1946
25kph	Adult	921	854
25kph	Child	1134 ... 1256	934
20kph	Child	757 ... 1115	1005

Figure 10: Performance of generic Madymo model, short-haul HGV [33]

Friction Characteristics

In pedestrian accident reconstructions, Ziegenhain [34] found a friction-coefficient of 0.2 between pedestrian and vehicle appropriate in almost all accidents. Deviations are marginal. However, the values may get larger in form-locking cases (e.g. where the pedestrian’s clothes are caught by the wiper or other protruding parts).

Same value was used by Wood et al. [35], [36]. A slightly higher value (0.25) was used by Yoshida [37]. IHRA used a value of 0.3 [38].

In a recent study by Untaroiu [39] a value of 0.4 was used. In the present study a friction between 0.2 and 0.4 was used.

Contact Pedestrian - Ground

Force-Deflection Characteristics

Stevenson [40] referred to values given by Chadbourn et al. [41] and used these values in a sensitivity analysis of the HIC response to the ground stiffness, Stevenson used values from 2.6 kN/mm (lowest value from Chadbourn et al.), over 40 kN/mm (mid-range value from Chadbourn) up to 10.000 kN/mm (extremely stiff-approximately equivalent to a solid steel road). Finally an infinitely stiff road was assumed, where only the head’s force-deflection characteristics were used for the calculation of the head accelerations. Stevenson concluded, that the “[...] ground stiffness values only need to be of the correct order of magnitude to ensure reasonable results [...]”.

Davich et al. [42] examined the mechanical properties of 36 soil specimens from six subgrade soil samples. The specimens were different with respect to confinement and moisture content. The young’s modulus reached from 129 MPa (having a poisson’s ratio of 0.4) up to 958 MPa (with a poisson’s ratio of 0.36). The poisson’s ratio in all soil specimens ranged from 0.18 up to 0.40.

Salem et al. [43] studied the asphalt concrete modulus of 11 freeze and non-freezing sites in the US. At a mid-depth temperature of 20°Celsius, the young's modulus reached from 8800 to 14000 MPa in the samples from non-freezing sites, and from 3800 to 7000 MPa in those from freezing sites. Overall the values reached from 1600 up to 22500 MPa.

In another publication, Nessnas [44] set up a numerical model of a pavement, where a young's modulus of 3745 MPa, 7490 MPa and 14980 MPa and a Poisson ratio of 0.35 for the wearing course were assumed.

Using Hertz's Formulas [45] for spheres impacting a flat plate, the force deflection curves were calculated. The following values were used:

- The head was assumed to be a sphere with a diameter of 165mm.
- For soil-grounds, a young's modulus of 129 and 958 MPa (according to Davich [42]) was assumed
- For roads with an asphalt wearing course, a stiffness of 1600, 3750, 7490, 14980 and 22500 MPa (according to Nessnas and Salem [44], [43]) was assumed.
- Additionally three Poisson's ratios were used 0.18, 0.35 and 0.4 (according to Davich and Nessnas [42], [44]).

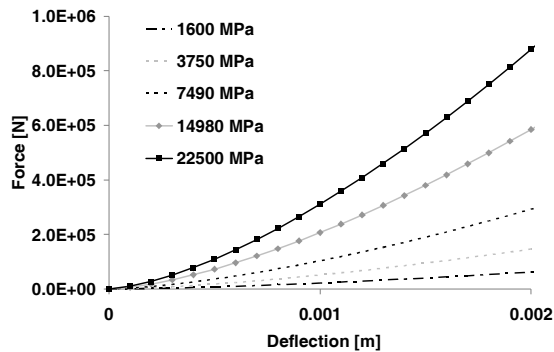


Figure 11: Force-deflection curve for roads with asphalt course (poisson's ratio = 0.35)

For a penetration of 2mm (see Figure 11), the linear stiffness of the road is in between 2.5kN/mm (soil) and 30 to 440 kN/mm (asphalt). These values are correlating very well with the linear stiffness used by Stevenson [40].

Friction Characteristics

Two coefficients of friction are needed for the contact between pedestrian and ground: one for the contact between the shoe sole and the ground and another one for the contact between the pedestrian's body and the ground.

For the contact between shoes and ground, Simms and Wood [46], [36] used a value of 0.58. Sacher [47] reported a coefficient of friction of 0.5 (for turf). Stevenson [40] used a value of 0.7 in the numerical study.

Table 4 summarizes the values reported in various studies on the coefficient of friction, showing a range from 0.37 to 0.75. These values do not apply for the friction with the shoe sole.

In previous numerical studies the upper range of these values was applied: Yoshida [37] used a friction-coefficient of 0.67. The same value was used by IHRA [38]. In a recent study by Untaroiu [39] a friction coefficient of 0.6 was applied.

Table 4. Coefficient of Friction Pedestrian-Ground [46], [40]

Source	Surface	n	Range	Mean
Becke, Golder	Asphalt, wet	15	0.43-0.53	0.47
Becke, Golder	Asphalt	30	0.50-0.72	0.63
Kuhnel	Asphalt	4	0.52-0.67	0.54
Sturtz	Asphalt	8	0.40-0.74	0.57
Lucchini	Asphalt	16	0.37-0.51	0.43
Severy	Asphalt	15	0.40-0.75	0.66
Searle (1983)	Asphalt			0.66
Severy (1966)	Asphalt		0.45-0.60	
Fricke (1990)	Concrete		0.40-0.65	
Wood (1988)	Asphalt		0.57-0.58	
Searle (1983)	Grass			0.79
Fricke (1990)	Grass		0.45-0.70	

Numerical Human Model

Posture

Earlier studies by Anderson et al [48] showed that the walking posture of the pedestrian influences kinematics and injury outcomes.

IHRA [38] conducted a parameter study with multi-body pedestrian models in three walking positions (corresponding to a six stance sequence). A more recent study by Untaroiu [39] describes an accident reconstruction based on optimisation techniques and taking into consideration a number of initial postures. Based on 10 stances of the gait cycle, functions for H-point height and joint-angles were approximated, allowing for a continuous stance sequence.

Based on curves published in the study by Untaroiu [39], a sequence of ten gait cycles for the 50th percentile human pedestrian model was developed. The hip-angle (the curve published by Untaroiu [39] for the hip seems to be corrupted) was changed properly, to fit the pictures of the gait cycle (and the angles of the ankle) published in the same.

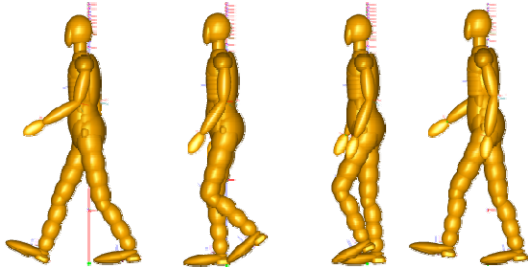


Figure 12: Gait Cycle

Table 5 summarizes initial joint positions as set in the numerical simulations. In pre-simulations (where all major joints except for the human joint were locked) the H-Point was altered such that the contact force between floor and shoes (contact characteristics of the shoes were used) amounted for about 730-740N. The human body's joints were locked at simulation start. A logic switch (connected to a contact sensor) is unlocking all joints as soon as there is a contact force between HGV and the pedestrian. The free joints between shoes and feet were kept locked throughout the simulations.

Table 5.
Initial Joint Positions for a continuous sequence of gait

Stride	0%	10%	20%	30%	40%
H-Point	0.872	0.901	0.915	0.919	0.911
Hip left	0.201	0.178	-0.279	-0.454	-0.470
Hip right	-0.413	-0.282	-0.200	0.018	0.175
Knee left	0.342	0.840	1.120	0.871	0.255
Knee right	0.093	0.093	0.327	0.120	0.156
Ankle left	-0.349	-0.205	-0.082	0.090	0.115
Ankle right	0.049	0.041	0.041	0.000	-0.100
Shoulder left	-0.171	-0.112	0.034	0.190	0.295
Shoulder right	0.329	0.261	0.138	0.011	-0.125
Elbow left	-0.817	-0.727	-0.545	-0.443	-0.386
Elbow right	-0.352	-0.352	-0.352	-0.611	-0.733
Neck low	-0.400	-0.400	-0.400	-0.400	-0.400

Design of Experiments

Three breed models (a long-haul and a short-haul traffic truck front and a bus) have been used in the numerical simulations. Beside of the front geometry the following parameters have been varied:

- Friction: HGV and VRU: 0.2 ... 0.4
- Friction: Shoes and Ground: 0.5 ... 0.7
- Friction: VRU and Ground: 0.4 ... 0.75
- Facing direction of pedestrian: +60° ... -60°
- Start of braking: -1s ... 0.2s
- Initial velocity: 30 ... 40 km/h
- Pedestrian gait: 10 postures
- Ground-Clearance of the vehicle: depending on vehicle model

The software ModeFrontier Version 4.1.0 by Esteco was used for the design of experiments (DOE). The

experiments are based on a random sequence. The software fills the design space (bounded by the values mentioned above) randomly, with a uniform distribution. The randomly generated simulations are used to analyse the head accelerations (rotation/translation) and associated injury criteria.

Finite Element Head Model

Model

Conventional head injury predictors such as HIC cannot predict the risk for injuries due to rotational accelerations. Also, they fail in distinguishing the types of injuries to the head, as there are:

- Skull-fractures: Fractures of the skull can be comminuted, depressed – due to local forces, leading to inward displaced bones - or linear – due to widely distributed forces.
- Subdural (SDH) or subarachnoid haematoma (SAH): Injuries to the vasculature, leading to bleeding between brain and skull (subdural) or under the arachnoid membrane, which covers the brain and spinal cord (subarachnoid).
- Diffuse axonal injuries (DAI): Extensive lesions in white matter tracts, leading in most cases to unconsciousness and persistent vegetative state. 90% of all patients suffering a severe DAI never regain consciousness [49].

Furthermore, conventional head injury predictors are insensitive to the direction of force/acceleration imposed to the head.

A finite element skull-brain model overcomes these deficiencies. Currently there are a number of such finite-element models available. These models differ from each other with respect to the number of elements, ranging from the 10 to the 300 thousands, and the anatomic details modelled.

- WSUBIM: The Wayne State University brain model consists of approx. 320.000 elements and represents a 50th percentile male human head with a mass of 4.3 kg. It was used extensively for the reconstruction of sports accidents, resulting in concussions.
- SIMon: The simulated injury monitor FEM head model was initially developed by DiMasi et al. [50] and extended by Eppinger, Takhounts and Bandak [51], [52]. It represents a 50th percentile male human head with a mass of 4.7 kg. The model has less than 10.000 elements.
- KTH: A head-neck model developed by Kleiven and Hardy [53].
- UCDBTM: The University College Dublin Brain Trauma Model was created by Horgan and Gilchrist [54]. The influence of number of elements on the model response was investigated,

by varying the element density from 9000 to 50000 elements. Also, the model is scalable with respect to size, weight and thickness of the CSF.

In the present study, the Strasbourg University Finite Element Head Model (SUFEHM) head model was used. The model was initially developed by Kang et al. [55] in 1997. The SUFEHM head model has approx. 13.000 elements. It represents a 50th percentile male human head with a mass of 4.7 kg. First tolerance limits for that head model were identified by Willinger and Baumgartner [56]. Further improvements to the model's geometry were initiated by Deck et al. [57]. More tolerance limits were identified by the reconstruction of 68 accidents [7].

By contrast to other models, e.g. SIMon, the skull is non-rigid, made of a three-layered composite shell. In order to reproduce the overall compliance of cranial bone, a thickness in combination with an elastic brittle law were selected for each layer with a Tsai-Wu criterion. The cerebral spinal fluid filling the space between the brain and the skull is made of brick elements using an elastic material. The brain is modelled by brick elements using a visco-elastic material model [58] (see Figure 13).

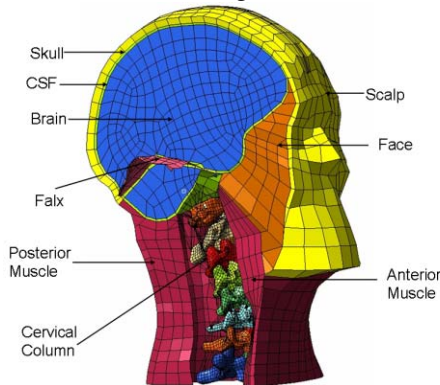


Figure 13: Section of SUFEHM

The SUFEHM injury predictors

Based on the simulation of 68 well documented accidents with occurrence of head trauma, tolerance limits for the SUFEHM head model have been identified within APROSYS SP5 [7], [59]. Using logical regression techniques, tolerance limits have been identified by comparing the FE model response and the reported injuries.

Diffuse axonal injuries were further distinguished by severity: Mild (or moderate) diffuse axonal injuries (DAI) assigned to AIS 2 or 3 and severe DAI assigned to AIS 4+.

With the help of the regression, tolerance limits for three types of injuries (fracture, SDH, DAI) were established. The mechanical parameters constituting

the tolerance limits refer to a risk of 50% (see Table 6) for the respective injury [7].

Table 6.
Tolerance limits for 50% risk of injury used in FE simulation [7]

Injury	Mechanical Parameter	Tolerance limits
Skull fracture	Strain Energy, Skull	865 mJ
Subdural or subarachnoid haematoma	Min. Pressure Spinal Fluid	-135 kPa
	Strain Energy, Spinal Fluid	4211 mJ
Mild diffuse axonal injury	Von Mises Stress, Brain	26 kPa
	Von Mises Strain, Brain	0.25
	First Principle Strain, Brain	0.31
Severe diffuse axonal injury	Von Mises Stress, Brain	33 kPa
	Von Mises Strain, Brain	0.35
	First Principle Strain, Brain	0.40

Analysis of Apollo Database

One of the biggest challenges in head injury is to identify the injury mechanisms leading to a certain injury type. One of the main hypotheses of this study is to assume that rotational accelerations have a great influence in the case of pedestrians involved in an accident with a flat front vehicle.

Martin et al [60] analysed the different AIS codes for head injury, and classified these codes by injury mechanisms: Injuries induced by rotational acceleration, translational acceleration and either (when the injury could be produced by rotational and/or translational acceleration). Table 16 (in the Annex) shows an excerpt of the matrix by Martin which classifies the head injury codes by their injury mechanism.

To evaluate the influence of the rotational acceleration in the APOLLO database a new variable has been included. The Martin transformation matrix has been implemented in the database to evaluate the presence of the different injury mechanisms.

RESULTS

Multi-body Simulations

Results are separated by primary impact (the impact of the pedestrian with the front of the vehicle) and secondary impact (the impact of the pedestrian with the ground). For the calculation of the HIP (head impact power), the following values were applied: Mass = 4.69kg, $I_{xx}=0.02\text{kgm}^2$, $I_{yy}=0.0222\text{kgm}^2$, $I_{zz}=0.0145\text{kgm}^2$. These values are consistent with the values applied in the human pedestrian model supplied with Madymo. When referring to HIC, the HIC 36ms is meant.

Primary Impact

Statistical parameters of the 300 numerical simulations are summarized in Table 7. The table shows the mean value and the quartiles (25th, 50th and 75th percentile) for the peak rotational/translational acceleration, head injury criterion (HIC), cumulative 3ms criterion (cum3ms), Gambit (G) and head impact power (HIP).

The median value of the HIC is only slightly above the widely applied threshold value of 1000. The median Gambit suggests a rather low risk for head injuries. The HIP, which is used to assess the risk for concussion, is exceeding the 50% probability value for concussion (12.8kW). The median cum3ms value is clearly above 80g.

Table 7.
Mean and statistical dispersion of the numerical simulation – Primary Impact

	Peak head acceleration		HIC	3ms	G	HIP
	[rad/s ²]	[g]				
Mean	9605	195	2999	136	0.82	90
25 th p.	5329	93	477	87	0.40	30
50 th p.	7848	156	1022	114	0.64	55
75 th p.	11616	225	2041	160	0.95	83

Table 8 distinguishes the results by vehicle type. Clearly the short-haul truck is leading to the worst results. That is also in line with the findings of previous studies, where full finite element models were used to study the interaction between vulnerable road users and HGV [27].

Table 8.
Median by vehicle type – Primary Impact

	Peak head acceleration		HIC	3ms	G	HIP
	[rad/s ²]	[g]				
All	7848	156	1022	114	0.64	55
s. HGV	11919	216	1756	159	0.89	79
l. HGV	6642	117	835	108	0.59	40
Bus	6452	92	577	87	0.40	31

s. HGV = short-haul HGV, l. HGV = long-haul HGV

Secondary Impact

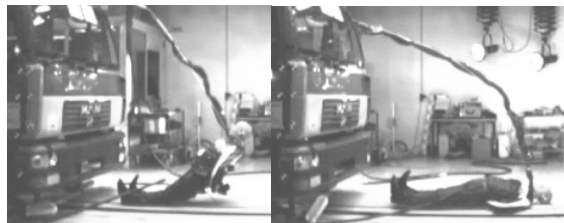


Figure 14: Hybrid III impacting the floor

Previous experimental tests with a standing Hybrid III [2] dummy have shown that the secondary contact is extremely critical with respect to loading of the

head. A HIC of 17600 to 33900 was found in four tests (see Figure 14). Peak head accelerations reached up to 1170g.

The numerical simulations show similar results. Statistical parameters of 300 numerical simulations are summarized in Table 11. A median (50th percentile) head rotation acceleration (peak) of 66 krad/s² and a translational acceleration of 870g was found. These high accelerations come along with extremely high criterions: a HIC of 20500, a cum3ms of 430g and a Gambit of 4.

Table 9.
Mean and statistical dispersion of the numerical simulation – Secondary Impact

	Peak head acceleration		HIC	3ms	G	HIP
	[rad/s ²]	[g]				
Mean	69285	809	21013	398	3.82	444
25 th p.	44552	553	6850	284	2.75	240
50 th p.	66292	866	20527	434	4.10	406
75 th p.	91976	1026	29122	499	4.74	605

Still, cases were found with very low criterions: About 5% of simulations show uncritical HIC, 3ms, Gambit and HIP criterion values.

A very severe case was selected for a sensitivity analysis of the ground stiffness. A linear force-deflection curve was assumed. Results are shown in Table 13. Starting from 40kN/mm, there was a relatively limited influence of different orders of magnitude of ground contact stiffness on the resulting injury criteria. Soil grounds (2.6kN/mm), however, led to completely different results with respect to injury criteria.

Table 10.
Sensitivity to stiffness of ground

Stiffness [kN/mm]	Peak head acceleration [krad/s ²]	HIC [10 ³ g]	G	HIP [kW]
2.6	36.9	5.1	13641	2.1
40	59.4	11.8	46503	4.8
60	61.2	12.4	49930	5.1
100	62.6	12.8	51591	5.3
10.000	67.9	13.9	56827	5.7

Finite Element Simulation

Nine out of 300 numerical simulations have been selected for a more detailed analysis with a FEM head model. Angular and translational accelerations measured in the multi-body simulations of the primary impact were prescribed to the SUFEHM head model. The acceleration curves were pre-filtered with CFC-1000.

Besides assessing these nine cases with the SUFEHM head model, conventional injury predictors, such as the HIC (head injury criterion), the GAMBIT (Generalised Acceleration Model for Brain Injury

Threshold), the cum3ms (the accumulative 3 milliseconds acceleration) and the HPC (Head power criterion) – see Table 11 – were applied, too.

The simulations are:

- (1) A 50th percentile, ellipsoid male human pedestrian model in walking posture is hit on the left side by the generic facet heavy goods vehicle model having the geometry and the characteristics of an IVECO Stralis. The cabin pivot is 950mm above ground. The vehicle is travelling at 40kph.
 - (2) A 50th percentile, ellipsoid male human pedestrian model in walking posture is hit on the left side by the generic facet heavy goods vehicle model having the geometry of a MAN L2000. The cabin pivot is 870mm above ground. The vehicle is travelling at 40kph.
 - (3) Like ID 2, however, cabin pivot 930mm above ground
 - (4) Like ID 2, however, cabin pivot 800mm above ground
 - (5) Like ID 2, however, cabin pivot 1080mm above ground
 - (6) Like ID 2, pedestrian turned about the z-axis such that the pedestrian is approaching the truck front at 45°.
 - (7) Like ID 6, however, cabin pivot: 800mm above ground
- Finally two simulations were performed with a 50th percentile facet male occupant model in standing posture
- (8) hit on the rear by a finite element heavy goods vehicle model having the geometry and the characteristics of a MAN L2000. The cabin pivot is 930mm above ground. The vehicle is travelling at 40kph.
 - (9) Like ID 8, however, hit on the left shoulder. Cabin pivot 830mm above ground. The vehicle is travelling at 30kph.

Table 11 summarizes the characteristics of the selected cases.

Table 11.
Characteristics of selected cases

ID	Peak head acceleration [rad/s ²]	HIC [g]	G []	cum3ms [g]	HIP [kW]	
1	6327	108	817	0.47	102.3	41.9
2	4520	88	366	0.38	66.1	33.7
3	8562	146	700	0.64	100.3	67.1
4	11423	269	1958	1.11	86.3	103.9
5	7416	135	1090	0.58	132	51.9
6	22841	410	4915	1.65	197.6	122.8
7	6428	191	1864	0.76	160.8	70.8
8	2730	151	1613	0.6	138.1	68.2
9	2672	74	359	0.3	70	22.1

By applying the expanded Prasad-Mertz ^[61] curves and it's counterpart for the Gambit (see Figure 3), the

risk of head injuries associated to the HIC and Gambit were summarized in Table 12.

Table 12.
Conventional injury predictors and the associated risk for injury

ID	Risk of Head injury related to the HIC [%]		Risk of Head injury related to the Gambit [%]	
	Moderate	Severe	Moderate	Severe
1	77	9	9	0
2	22	2	4	0
3	64	6	31	<3
4	100	87	91	71
5	93	22	<3	<3
6	100	100	100	1
7	100	82	0.74	8
8	99	65	22	<3
9	21	2	<3	0

Table 13 and Table 14 summarize the risk for specific head injuries as predicted by the SUFEHM head model. In six out of nine cases under study a risk greater than 50% for severe DAI and SDH is predicted.

Table 13.
Injury predictors calculated by SUFEHM head and the associated risk for injury – Part A

ID	Von Misses stress Brain [kPa]	Risk of diffuse axonal injury [%]	
		Moderate	Severe
1	39.5	100	88
2	39.5	100	88
3	51	100	99.9
4	74	100	99.9
5	44.6	100	98
6	52	100	99.9
7	31.4	100	38
8	16.1	<1	0
9	12	<1	0

Table 14.
Injury predictors calculated by SUFEHM head and the associated risk for injury – Part B

ID	Minimum pressure Spinal Fluid [kPa]	Risk of subdural haematoma [%]
	1	-126
2	-126	34
3	-145	66
4	-166	90
5	-151	75
6	-177	98
7	-159	84
8	-114	18
9	-68	<1

Analysis of Apollo Database

The APOLLO database contains 1.085.673 cases from the hospital discharges, of which 74.660 are traffic related injuries (8 European countries codify including the injury mechanism). This subgroup

comprises 10.341 pedestrians. Taking into account only cases that were codified according to the International Classification of Diseases (ICD 10) [62] 3.786 pedestrians remain, of which 104 are pedestrians involved in an accident with Heavy Good Vehicles.

HGV or bus versus pedestrian

Table 15 was obtained by analyzing the APOLLO database and classifying the injuries by body region and nature (Barell injury matrix) [63]. Remark: Table 15 shows only an excerpt of the results (the original table contains a total of 252 injuries).

Table 15.
Barell injury matrix for pedestrian involved in HGV collision (excerpt)

Type of Injury	Fracture	Internal	Open wound	Contusion/superficial	Crush	%	AIS
Traumatic brain injury	17	58	4	0	6	37%	3.14
Thorax	14	12	0	4	0	12%	2.14
Abdomen, pelvis, trunk	17	4	0	2	6	12%	2.91
Lower extremity	24	0	18	4	0	21%	1.87
TOTAL	102	74	25	12	12	100%	

It can be observed that the most frequently injured area is the head with 37% of all injuries, followed by lower extremities 21%, thorax 12%, and the abdominal/pelvic area 12%.

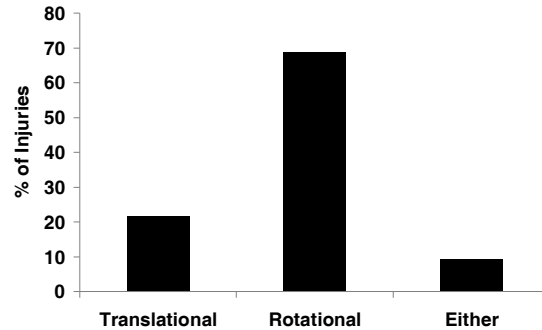
Compared with the injuries sustained for pedestrians involved in passenger car collisions in case of survival, the results are different: According to Yang et al [64] the most frequently injured area was found the lower extremities with 32.4% of all injuries, followed by the head (26%), the abdominal/pelvic area (12%), and the thorax (5.5%).

To evaluate the influence of the rotational acceleration in the APOLLO database a new variable has been included. The Martin transformation matrix [60] has been implemented in the database (see excerpt in Table 16) to evaluate the presence of the different injury mechanisms.

From the 93 head injuries only 74 could be matched with the AIS code or matrix to be included in the study. All of the not classifiable were categorised as minor injuries (AIS 1), so there is no loss of information for moderate or more severe injuries (AIS 2+).

Figure 15 shows that just 21% of all head injuries analyzed have the translation acceleration as a single

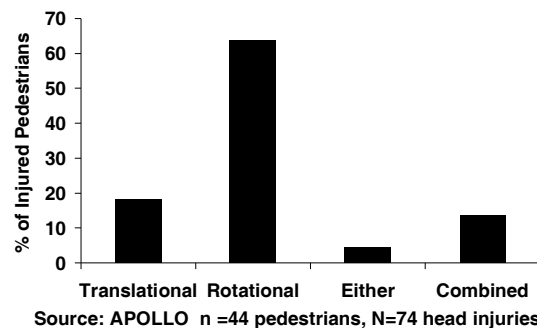
injury mechanism, in 69% of all cases rotational acceleration is the only injury mechanism, and in 10% of the cases rotational or translational acceleration can be responsible for the head injury.



Source: APOLLO n =104 pedestrians, N=74 head injuries

Figure 15: Head injuries by injury mechanism (HGV or bus versus pedestrian)

Following the methodology developed by Martin et al. examining all 104 pedestrian cases individually, all the head injuries have been re-processed with the transformation matrix, analyzing all the different combinations of Translational, Rotational or Either. Some of the codes show up several times while others never appear at all. Cases where a single pedestrian sustains two or more types of head injuries, a “combination” is assigned – see Figure 16. From initial 104 injured pedestrians only 44 sustained head injuries that can be processed with the Martin matrix. From these pedestrians only 8 had sustained head injuries solely due to translational acceleration, 28 due to rotational acceleration, 2 pedestrian had head injuries due to rotational or translational acceleration and 6 due to a combination of injury mechanisms.



Source: APOLLO n =44 pedestrians, N=74 head injuries

Figure 16: Injured pedestrians and injury mechanism (HGV or bus versus pedestrian)

Rotational acceleration is clearly more frequent as the translational acceleration in the case of pedestrian accident. The large presence of “combined” as an

injury mechanism is due to the immense number of injuries sustained by some pedestrians, making it very unlikely that all injuries are assigned to one single injury mechanism.

Passenger car versus pedestrian

The results are considerably different from the figures reported in the literature: Pedestrians involved in a crash with a passenger car ^[65] (see Figure 17) only 17% sustain head injuries due to rotational accelerations. Another 17% sustain injuries solely induced by translational accelerations, 38% either and 28% due to combined mechanisms (data from the Pedestrian Crash Data Study PCDS). The percentage in motorbike accidents is quite similar: 5% for translational, 13% for rotational, 34% for either and 48% in case of combined [60].

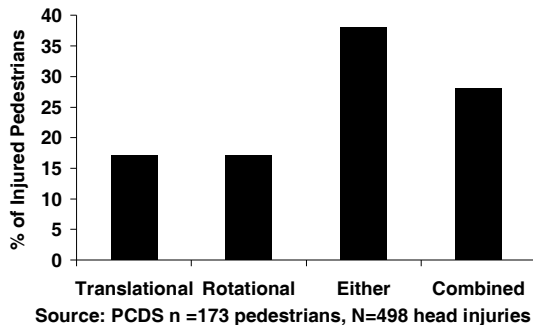


Figure 17: Injured pedestrians and injury mechanism (Passenger car versus pedestrian)

DISCUSSION

Multi-body Simulations

Considering the median values found in the study of the primary impact, the findings of previous studies were confirmed: The HIC is rather uncritical. The peak head rotational accelerations (median value for all flat front vehicles: 7848 rad/s²) can be assessed more critical, when applying the values found by Genarelli [26] or Ommaya ^[66]. The same applies to the median value of the cum3ms, which is clearly above 80g. Also the HIP is clearly exceeding the level of 12.8 kW (50% probability of concussion). A median Gambit, of 0.64 was found for all vehicles under study, which is equivalent to 25% probability of AIS 2 head injuries.

The study showed that the short-haul truck is leading to the worst results with respect to head injury criteria. This is in correlation with the findings of previous studies. While the adult's head is impacting the unforgiving lowermost edge of the windshield of the short-haul truck, the head is intercepted rather

softly by the grill of the long-haul truck. The vehicles, that were inspiring the generic models, are not only different with respect to size. Also, different materials are applied in the design of the front structure. While sheet metal is covering the front of the short-haul truck, almost the complete grill of the long-haul truck is made of fibre reinforced plastics.

For the short-haul truck a Gambit median value of 0.89 was observed, which is equivalent to a 40% probability of AIS 3 injuries. Best results were achieved by the bus.

Secondary Impact

Experimental tests with a standing Hybrid III dummy hit by a MAN L 2000 truck travelling at 30kph showed clearly the severity of the secondary impact. In the four experimental tests the resultant peak head acceleration ranged from 1020g to 1170g, leading to a HIC between 17.600 and 33.900. The Hybrid III pedestrian dummy was facing towards the front of the HG. The situation does not reflect what really happens on the road: In most real-world accidents the pedestrian is hit laterally. The Hybrid III, however, was designed for frontal impact: Hitting the Hybrid III pedestrian dummy laterally will have likely led to damage of thorax and legs and knee joints respectively.

As a result of the initial orientation of the pedestrian, the dummy's back of the head was fiercely hit, when falling to the ground (see Figure 14).

It was expected, that the numerical simulations show less severe head to ground impacts, since the pedestrian model is mostly hit laterally in the numerical simulations. Consequently it was assumed, that the human model hits the ground with its side first. However, in most cases the walking posture of the human model led to a rotation about the pedestrian's vertical axis. Eventually, the pedestrian was hitting the ground with the face or the back of the head. The shoulder did not mitigate the severity of the impacts. As a result injury criteria for the head were extremely high and so is the risk for fatal injuries.

The present study shows clearly that the secondary impact is by far more severe than the primary impact. Pedestrian protection afforded by HG and flat front vehicles need to address the pedestrian post-impact kinematics. Studies by Faßbender [32] indicate that a sort of an aerodynamic front (referred as "nose-cone") is capable of reducing the severity of the secondary impact – beside of reducing the risk for run-over.

Clearly, the problem of the secondary impact exists also with passenger cars. Yang et al. ^[67] noted that if the pedestrian strikes the ground head-first, following a collision with a passenger car, head injuries from

the secondary impact will generally be more severe than injuries related to the primary impact. Otte and Pohlmann^[68] concluded that 56% of all injuries are due to the secondary impact.

The forward projection kinematics of pedestrians hit by a flat fronted vehicle seems to facilitate the severity of the secondary impact. Same was noted by Tanno et al.^[69] and^[70].

In two multibody simulations a facet human occupant model was used, instead of the ellipsoid human pedestrian model. Previous studies showed [27] that the facet model can be used for the very initial phase of the impact. The head-neck kinematics differed significantly: While in the facet model the head showed a distinct translational movement in the very initial phase of the impact (followed by a rotation), the ellipsoid model showed a rotational movement right from the beginning.

Finite Element Simulations

For the simulations with the finite element head model, cases have been selected, where at least one criterion (peak acceleration, HIC, cum3ms or Gambit) was exceeding the given threshold value.

The comparison of injury predictors calculated with the SUFEHM head and “conventional” injury criteria showed that one criterion is not enough for predicting head injuries. According to a regression analysis by Deck^[7], the HIC shows a high correlation to severe DAI and skull fracture. To other injuries (SDH, mild DAI), there is little regression.

The analysis with the FEM head predicts for 6 out of 9 cases under study a very high risk (greater than 50%) for DAI, even in cases where the HIC was well below 1000 (e.g. case ID 2). For six out of nine cases under study a high risk (greater than 50%) for SDH is predicted by the finite element head model.

Analysis of Apollo Database

Clearly the analysis of the Apollo database shows the high relevance of head injuries sustained by pedestrians following a collision with a flat front vehicle. The database also shows the high relevance of head injuries due to rotational accelerations. While in passenger cars hitting a pedestrian the occurrence of head injuries induced by rotational and translational accelerations is almost equivalent, rotation-induced head injuries to pedestrians in HGV and busses are three times more frequent than translation-induced injuries.

A possible explanation for the difference could be the different kinematics in these pedestrian accidents, and also the small sample size used in the present study.

Connecting the findings of the field data with the numerical simulations is not straight-forward, but it can be assumed that head injuries are more likely caused by the secondary contact, as it is the more severe contact, showing extremely high translational and rotational accelerations.

CONCLUSIONS

In a multi-disciplinary approach (using generic multi-body vehicle models, a detailed finite element head/brain model as well as field data from an injury database) it was tried to investigate the relevance of rotation-induced head injuries to pedestrians hit by a large flat front vehicle (a heavy goods vehicle or bus).

The primary and the secondary impact of the pedestrian were investigated by using a parameterisable multi-body vehicle model and a numerical human pedestrian model.

Using DOE software a number of boundary conditions were varied, such as vehicle geometry, gait, orientation of the pedestrian, vehicle speed and friction coefficients. For the study in total 600 numerical simulations were analysed.

Measured head accelerations were evaluated by using HIC, HIP, Gambit and cum3ms. Nine simulations of the primary impact were selected and the measured head accelerations were prescribed to a FEM head model and evaluated by applying the tolerance limits developed for the SUFEHM.

Additionally field data from a European database on hospital discharges was included in the analysis to highlight the relevance of rotation-induced head injuries.

Following conclusions can be drawn

- There is no single injury predictor (like HIC, Gambit, HIP), that can assess the risk for injuries to the head or brain alone. The present study suggests that FEM head models can predict head injuries more reliably and more differentiated, than conventional injury predictors or criteria.
- The secondary impact (with the ground) is a big issue for all vulnerable road-users hit by a vehicle. In particular for flat fronted vehicles, like busses or trucks. Providing a better protection in the primary impact only is not enough. Additionally the post-impact kinematics needs to be considered. These could mitigate the consequences of the ground impact significantly (e.g. by causing a sliding impact of the pedestrian to the ground).
- Future human pedestrian models need a good validation of head rotation kinematics. The use of different numerical models revealed in-consistent

head and neck kinematics, resulting in deviations with respect to rotational accelerations.

- The HIC (Head injury Criterion) is a good indicator for head injuries like severe DAIs or skull fractures in frontal impacts and is a good initial tool to improve pedestrian protection. However this criterion cannot predict all the injuries sustained by a pedestrian. Rotational velocity and rotational acceleration should also be included in the pedestrian criteria in the future; otherwise injuries could be sustained by pedestrians despite a low HIC. The use of FE models to predict brain injuries needs to be the first source of knowledge in the near future. Such models are required to be applicable for any direction of impact.

LIMITATIONS

Multi-body Simulation

For the analysis of the secondary impact (when the pedestrian is hitting the ground) a rigid vehicle was assumed. In the primary impact some of the impact energy will be dissipated by the vehicle. This might slightly change the post-impact kinematics.

Also, the impact speed was assumed to be between 30 to 40kph and only frontal impacts were considered. The data in the Apollo database, however, contain all sorts of HGV-pedestrian accidents including those at lower impact speeds and to the side of the vehicle.

Finite Element Simulation

In this study the SUFEHM is driven by accelerations fields applied at the centre of gravity of the head which skull is supposed to be rigid. In this context no bone fractures can be predicted but similar analysis can be done with a deformable skull by simulating direct impacts. In this case the SUFEHM (deformable skull) is launched - just before impact - with an initial velocity on deformable structures and head injuries can be estimated.

Injury Database

The small number of pedestrian injured by a HGV is the main limitation of this epidemiologic study. The Transformation Matrix have been developed by well know researchers, but some AIS codes could be classified by other researches in a different group.

ANNEX

Table 16.
Excerpt of transformation Matrix [60]

Code	Severity	Type	Code	Severity	Type
113000	6	T	120602	4	R
115099	9	B	121002	5	R
115299	9	B	121004	4	R
115999	7	B	121099	3	B
120202	5	R	121202	4	R
120402	5	R	121299	3	B
120499	5	B	121402	5	R

R – rotation induced, T- translation induced; B- induced by either translation or rotation

REFERENCES

- [1] F. Feist, C. Ciglaric, E. Mayrhofer and H. Steffan. An Interaction Study between Vulnerable Road Users and Heavy Truck Front Structures. 1-14. 22-7-2006. Athens, Greece, Bolton University. ICrash Conference Proceedings 2006.
- [2] F. Feist, R. Puppini, A. Giorda, M. Avalle and J. Gugler. Improvements to the protection of vulnerable road users: retrofittable, energy absorbing front-end for heavy goods vehicles. 1-18. 22-7-2008. Kyoto, Japan, Bolton University. ICrash Conference Proceedings 2008.
- [3] R. Puppini, P. Smeriglio, L. Consano and E. Mayrhofer. Heavy Vehicle Accidents Involving Pedestrians & Cyclists. 2006. Göteborg, Transport Research Arena Europe.
- [4] T. Smith and I. Knight. Summary of UK accident data. AP-SP21-0038. 2005. London, Crowthorne, Transport Research Laboratory (TRL). Unpublished report for the EC-project APROSYS.
- [5] D. Otte and J. Nehmzow. German In-Depth Accident Study (GIDAS): Accidents of commercial vehicles with pedestrian and bicycles. Feist, F. AP-SP21-0074 VRU Workshop Proceedings Praha, 43-54. 23-3-2005. Graz, Austria, Graz University of Technology, Graz. Deliverable report. Published report for EC-project APROSYS.
- [6] C. Arregui. What can be learnt from the introduction of pedestrian protection in passenger cars. AP-SP21-0088, 1-26. 7-5-2008. Navarra, Spain, European Centre for Injury Prevention, University Navarra. Presentation at the APROSYS Workshop held in Neumünster, Germany.
- [7] C. Deck and R. Willinger. Improved head injury criteria based on head FE model. International Journal of Crashworthiness 13 (6), 667-678. 6-12-2008. Oxon, UK, Taylor&Francis.
- [8] APOLLO. Burden of Injuries in the EU: Indicators and recommendations for prevention and control. <http://www.euroipn.org/apollo/WP2.htm> . 10-3-2009. 15-3-2009.
- [9] A. H. S. Holburn. Mechanics of head injuries. The Lancet - Neurology 2, 438-441. 1943.
- [10] E. Gurdjian, H. Lissner, R. Latimer, B. Haddad and J. Webster. Quantitative determination of acceleration and

- intercranial pressure in experimental head injury. *Neurology* 3, 417-423. 1953.
- [11] H.R.Lissner, M.Lebow and F.G.Evans. Experimental studies on the relation between acceleration and intracranial pressure changes in man. 329-338. 1960. surgery, gynecology and obstetrics 111.
- [12] C.Gadd. Use of a weighted - impulse criterion for estimating injury hazard. SAE Paper 660793 . 1966.
- [13] J.Versace. Review of the Severity index. 1971. 15th Stapp Car Crash Conference, SAE.
- [14] E. Hertz. A note on the head injury criterion (HIC) as a predictor of the risk of skull fracture. 37th Annual Proceedings of the AAAM . 1993.
- [15] F. Unterharscheidt and L. S. Higgins. Traumatic Lesions of Brain and Spinal Cord due to Nondeforming Angular acceleration of the Head. *Texas Reports on Biology and Medicine* 27(1), 127-166. 1969.
- [16] A. Ommaya, P. Yarnell, A. Hirsch and Z. Harris. Scaling of experimental data on cerebral concussion on sub-human primates to concussion threshold for men. SAE 670906. 11th Stapp Car Crash Conference , 47-52. 1967.
- [17] J. W. Melvin and W. Lighthall, *Brain-Injury Biomechanics*. In *Accidental Injury*. (Ed. A. M. Nahum and J. W. Melvin) pp. 277-302, 1993.
- [18] P. Löwenhielm. Strain tolerance of the Vv cerebri sup (bridging veins) calculated from head-on collision tests with cadavers. *Z.Rechtsmedizin* 75, 131-144. 1974.
- [19] S. Margulies and L. Thibault. A proposed tolerance criterion for diffuse axonal injury in man. *J.Biomechanics* 25, 917-923. 1992.
- [20] K.-U. Schmitt, P. Niederer and F. Walz, *Trauma Biomechanics: Introduction to Accidental Injury*, pp. 1-174, Swiss Federal Institute of Technology (ETH) and University of Zurich, Zurich 2004.
- [21] J. Newman. A generalized acceleration model for brain injury threshold (GAMBIT). Proceedings of IRCOBI Conference , 121-131. 1986.
- [22] F. Kramer and H. Appel. Evaluation of protection criteria on the basis of statistical biomechanics. Proceedings of IRCOBI Conference , 45-57. 1990.
- [23] J. Newman. Criteria for Head Injury and Helmet Standards. Snell Memorial Foundation Seminar , 1-23. 6-5-2005. Medical College of Wisconsin.
- [24] J. Newman, N. Shewchenko and E. Welbourne. A Proposed New Biomechanical Head Injury Assessment Function - The Maximum Power Index. 44th Stapp Car Crash Conference . 2000. Atlanta, Georgia, SAE.
- [25] J. Newman, C. Barr, M. Beusenbergh, E. Fournier, N. Shewchenko, E. Welbourne and C. Withnall. A New Biomechanical Assessment of Mild Traumatic Brain Injury - Part 1 - Methodology. Proceedings of IRCOBI Conference . 1999. Barcelona, Spain.
- [26] T.Gennarelli, F.Pintar and N.Yoganandan. Biomechanical tolerances for diffuse brain injury and a hypothesis for genotypic variability in response to trauma. 2003. Annual proceeding AAAM.
- [27] F. Feist, S. Faßbender, R. Puppini, E. Mayrhofer, T. Smith and J. Gugler. Impact situations and pedestrian/cyclist kinematics based on real world accident scenarios. Deliverable report for APROSYS WP2.1 AP-SP21-0069 D211B, 1-135. 18-4-2006. European Commission.
- [28] Emma Carter, Steve Ebdon and Clive Neal-Sturgess. Optimization of Passenger Car Design for the Mitigation of Pedestrian Head Injury Using a Genetic Algorithm. 2005. Genetic And Evolutionary Computation Conference, Association for Computing Machinery.
- [29] Madymo Theory Manual - Release 6.4.1, pp. 1-400, 2007.
- [30] Koji Mizuno and Janusz Kajzer. Head Injury in Vehicle-Pedestrian Impact. SAE Paper 2000-01-0157 . 2000. SAE 2000 World Congress.
- [31] Lex van Rooij, Kavi Bhalla, Mark U.Meissner, Johann Ivarsson, Jeff Crandall, Douglas Longhitano, Yukou Takahashi, Yasuhiro Dokko and Yuji Kikuchi. Pedestrian Crash Reconstruction using Multi-Body Modeling with Geometrically detailed, validated Vehicle Models and Advanced Pedestrian Injury Criteria. Proceedings of the 18th International Technical Conference on the Enhanced Safety of Vehicles (ESV) , 1-19. 2003.
- [32] S. Faßbender, M. Hamacher, R. Puppini, F. Feist and J. Gugler. AP-SP21-0077 D2.1.3 Demonstrator Module for New Design Concepts. 2007. Aachen, Deutschland, Institut für Kraftfahrzeugwesen (IKA), RWTH Aachen.
- [33] APROSYS WP 2.1. Hemisphere testing of MAN L-2000 cabin. Feist, F., Kassegger, H., and Mayrhofer, E. AP SP21 0056, 1-76. 15-4-2005. Graz, Austria, Vehicle Safety Institute, TU Graz.
- [34] T. Ziegenhain. Rechnergestützte Untersuchung mittels Mehrkörpermodell in PC-Crash 8.1 zum Zusammenhang zwischen Aufwurf- und Wurfweite eines Fußgängers. 1-119. 28-5-2008. Vehicle Safety Institute, Graz University of Technology.
- [35] Denis Wood and Ciaran Simms. Coefficient of Friction in Pedestrian throw. 12-14. 2000. Impact - Journal of ITAI, vol. 9 no 1.
- [36] C. K. Simms and D. P. Wood. The Effect of Pedestrian Motion on Head Contact Forces with Vehicle and Ground. Proceedings of IRCOBI Conference . 2005. Prague, Czech Republic.
- [37] S. Yoshida. Computer Simulation System for Car-Pedestrian Accident. Proceedings of the 16th International Technical Conference on the Enhanced Safety of Vehicles . 1998. Windsor, Canada.
- [38] Y.Mizuno. Summary of IHRA Pedestrian safety WG activities - Proposed test methods to evaluate pedestrian protection afforded by passenger cars. 2003. Japan Automobile Standards Internationalization Center.
- [39] Costin D.Untaroiu, Mark U.Meissner, J.Crandall, Yukou Takahashi, Masayoshi Okamoto and Osamu Ito. Crash reconstruction of pedestrian accidents using optimization techniques. 2008. International Journal of Impact Engineering.
- [40] T. J. Stevenson. Simulation of Vehicle-Pedestrian Interaction. 1-342. 2006. Canterbury, United Kingdom, University of Canterbury.
- [41] B. Chadbourn, D. Newcomb and D. Timm. Measured and Theoretical Comparisons of Traffic Loads and Pavement Response Distributions. Proceedings, 8th International Conference on Asphalt Pavements , 229-238. 1997. Seattle, Washington, USA.

- [42] P. Davich, J. Labuz, B. Guzina and A. Drescher. Small Strain and resilient modulus testing of granular soils. 2004-39, 1-117. 2004. Minneapolis, Minnesota, USA, University of Minnesota, Department of Civil engineering.
- [43] H. Salem and F. Bayomy. Predictopm of Seasonal Variation of the Asphalt Concrete Modulus using LTPP Data. 1-33. 2005. Moscow, Idaho, USA, University of Idaho.
- [44] K. Nesnas and B. Ferne. A theoretical evaluation of the use of the Falling Weight Deflectometer to predict stiffness. UPR/IE/212/06, 1-52. 2006. Crowthorne, UK, TRL Limited.
- [45] W. C. Young and R. G. Budynas, Roark's Formulas for Stress and Strain, pp. 1-854, McGraw-Hill, 2002.
- [46] D. P. Wood and C. K. Simms. Coefficient of friction in pedestrian throw. *Impact* 9 (1), 12-15. 2000.
- [47] A. Sacher. Slip Resistance and the James Machine 0.5 Static Coefficient of Friction-Sine Qua Non. *ASTM Standardization News* , 52-59. 1993.
- [48] R.W.G.Anderson, A.D.Long, T.Serre and C.Masson. Determination of boundary conditions for pedestrian collision reconstructions. *Proceedings of the ICrash Conference 2008* . 2008. Kyoto.
- [49] J. R. Wassermann and R. A. Koenigsberg. Diffuse Axonal Injury. *eMedicine - Medscape's Continually Updated Clinical Reference* . 26-7-2007.
- [50] F. Dimasi, R. Eppinger and F. Bandak. Computational analysis of head impact response under car crash loadings. *Proceedings 39th Stapp Car Crash Conference* , 425-438. 1995. SAE.
- [51] E. Takhounts and R. Eppinger. On the development of the SIMon finite element head model. *Proceedings 47th Stapp Car Crash Conference* , 107-133. 2003. SAE.
- [52] F. Bandak, A. X. Zhang, R. E. Tannous, F. Dimasi, P. Masielle and R. Eppinger. Simon: a simulated injury monitro; application to head injury assessment. *Proceedings of the 17th International Technical Conference on the Enhanced Safety of Vehicles (ESV)* . 2001. Washington, D.C., National Highway Traffic Safety Administraion.
- [53] S. Kleiven and W. Hardy. Correlation of an FE model of the human head with loacl brain motion - Consequence for injury prediction. *Proceedings 46th Stapp Car Crash Conference* , 123-144. 2002. SAE.
- [54] M. Gilchrist and T. J. Horgan. Influence of FE model variability in predicting brain motion and intercranial pressure changes in head impact simulations. *International Journal of Crashworthiness* 9, 401-418. 2004.
- [55] H. S. Kang, R. Willinger, B. Diaw and B. Chinn. Validation of a 3D anatomic huamn head model and replication of head impact in motorcycle accident by finiet element modelling. *Proceedings 41th Stapp Car Crash Conference* , 329-338. 1997. SAE.
- [56] R. Willinger and D. Baumgartner. Human head tolerance limits to specific injury mechanisms. *International Journal of Crashworthiness* 8, 605-617. 2003.
- [57] C. Deck, S. Nicolle and R. Willinger. Human head FE modelling: improvement of skull geometry and brain constitutive laws. *Proceedings of IRCOBI Conference (International Conference on the Biomechanics of Impact)* , 79-92. 2004. Graz, Austria.
- [58] R. Willinger, H. S. Kang and B. Diaw. 3D human head finite element model validation against two experimental impacts. *Annals of Biomed.Eng.* 27(3), 403-410. 1999.
- [59] T. Dziejowski, S. Bidal, P. J. Arnoux, C. Deck, R. Willinger, I. Ciglaric, F. Feist, M. Beaugonin and R. Meijer. Usage of human model in virtual testing of pedestrian impact - A virtual testing demonstrator and discussion. AP-SP53-0026, D5324, 1-68. 18-2-2008. European Commission. Aprosys Deliverable Reports.
- [60] P. Martin and R. Eppinger. Incidence of Head Injuries Attributable to rotation. *Proceedings of the 31st International Workshop on Injury Biomechanics* . 2002.
- [61] P. Prasad and H. J. Mertz. The position of the United States Delegation to the ISO Working Group 6 on the use of HIC in the automotive environment. *SAE Transactions*, Vol.94 . 1984. SAE International, Warrendale, Pennsylvania, USA.
- [62] World Health Organisation and German Insitute of Medical Documentation. *International Statistical Classification of Diseases and Related Health Problems, 10th Revision, Version for 2007*. <http://www.who.int/classifications/apps/icd/icd10online/> . 2007. 13-3-2009.
- [63] V. Barell and E. MacKenzie. The Barell Injury Diagnosis Matrix - Classification by Body Region and Nature of the Injury. http://www.cdc.gov/nchs/data/ice/final_matrix_post_ice.pdf . 1-11-2005. 1-3-2009.
- [64] J. Yang, *Review of injury biomechanics in car-pedestrian collisions*. *Int J Vehicle Safety I, Nos.1/2/3*, 100-117 (2005).
- [65] C.Arregui. Rotational acceleration as a traumatic brain injury mechanism in pedestrian-vehicle collisions. Doctoral dissertation . 2005. Polytechnic University of Cataluna.
- [66] A. Ommaya, *Biomechanics of head injury*. In *Biomechanics of Trauma*. (Ed. A. M. Nahum and J. W. Melvin) Appleton-Century-Crofts, Norwalk 1984.
- [67] J. Yang, J. Yao and D. Otte. Correlation of Different Impact Conditions to the Injury Severity of Pedestrians in Real World Accidents. *Proceedings of the 19th International Technical Conference on the Enhanced Safety of Vehicles (ESV)* . 6-6-2005. Washington DC, USA.
- [68] D. Otte and T. Pohlemann. Analysis and Load Assessment of Secondary Impact to Adult Pedestrians After Car Collisions on Roads. *Proceedings of IRCOBI Conference (International Conference on the Biomechanics of Impact)* . 2001. Isle of Man, UK.
- [69] K. Tanno, M. Kohno, N. Ohashi, K. Ono, K. Aita, H. Oikawa, M. T. Oo, K. Honda and S. Misawa. Patterns and Mechanisms of Pedestrian Injuries Induced by Vehicles with Flat-Front Shape. *Legal Medicine* 2(2), 68-74. 2000.
- [70] J. W. Garrett. An analysis of fatal pedestrian accidents. *SAE International Congress and Exposition* . 23-2-1981. Detroit, Michigan, USA, SAE International, Warrendale, Pennsylvania, USA.

STATIONARY VIDEO-BASED PEDESTRIAN RECOGNITION FOR DRIVER ASSISTANCE SYSTEMS

Steffen Schaack

Alois Mauthofer

carhs.communication GmbH

Germany

Ulrich Brunsmann

Labor für Mustererkennung und Computational Intelligence,

Hochschule Aschaffenburg – University of Applied Sciences

Germany

Paper Number 09-0276

ABSTRACT

As statistics have shown, forty-two percent of all injury accidents in Germany's road traffic happen at intersections. Infrastructure-mounted cameras for traffic analysis have been proposed to reduce this number as well as simulation tools, which assist in developing Car-to-Infrastructure (C2I) communication applications in the field of driver assistance, pedestrian, vehicle and traffic safety by a combination of a real application and virtual scenarios.

This paper describes an infrastructure-based vision system for pedestrian and vehicle detection, its integration in the C2X-communication software development framework viilab and the visualisation to display the acquired data in a C2X-vehicle. Two cameras are used to monitor an intersection in the visible spectral range out of different views. With methods of computer vision and machine learning road users are detected and analysed as pedestrians or vehicles for both views. The merged objects' positions are transformed into world coordinates and tracks within the traffic trace are generated. The data can be used in a simulation or can be requested in real time from C2X enabled cars via a roadside unit (RSU) as an environment radar. The performance of the system is discussed.

INTRODUCTION

In the future vehicles will be equipped with technology for car-to-car- and car-to-infrastructure-communication (C2X-communication). Examples for car-to-infrastructure-communication to avoid dangerous situations or an accident might be the broadcast of the traffic light status to cars near a crossing or a warning if a pedestrian crosses the road behind a bend. With forty-two percent of all road traffic accidents intersections are hotspots for accidents involving injury in Germany's road traffic [1]. This project focuses on infrastructure-based image processing at intersections.

Infrastructure-based image processing is already widely used for surveillance applications of road traffic. Examples are traffic control systems that recognise cars moving reverse to the driving direction on motorways or that detect smoke in

video images to avoid a fire in a tunnel, frequently assisting security personnel who monitor many video cameras in a coordinating office [2]. Other concepts of infrastructure based image processing are topic of research projects. For instance the project OIS ("Optische Informationssysteme") [3] evaluated a system for adaptive control of traffic lights at a crossing depending on the volume of traffic. The detection mechanism rests upon several stationary mounted cameras monitoring the intersection from different angular fields. Another concept similar to the system introduced in this paper is discussed in the project PUVAME ([4] and [5]), where a detection of pedestrians with a multi camera setup on a park deck is executed. The evaluated system communicates the results of the road based image processing to an omnibus. The aim is to avoid collisions between pedestrian and omnibus in urban road traffic. The focus for this monitoring system is set on intersection and bus stop.

The development of intelligent co-operative systems requires a new generation of development tools which assist the automotive manufacturers and suppliers in developing Car2X communication applications. The software development framework viilab (vehicle infrastructure integration laboratory) ([6] and [7]) is especially designed for Car2X communication application developments. It can be installed as On Board Unit (OBU), Road Side Unit (RSU) or Monitoring Device (MON). Typical vehicle related interfaces (navigation, positioning, Display/HMI or bus systems) as well as infrastructure related interfaces (camera, traffic light) can be included. viilab is used in this project for the demonstration of the integration of infrastructure based data in a C2X environment.

This paper describes the architecture and the integration of a two-camera-based vision system for pedestrian-vehicle detection and tracking and the visualisation to display the acquired data in a C2X-vehicle. The performance of the subsystem is discussed.

REALISATION

For visualisation of pedestrians and vehicles within the simulation tool the following tasks have been solved:

1. Background/foreground separation and segmentation of objects in a region of interest
2. First classification of the segmented objects
3. Transformation of the position of the segmented objects into an ortho picture
4. Datafusion in the ortho picture
5. Tracking of the objects and second classification step
6. Transformation of the objects' positions in the ortho picture into WGS84 coordinates
7. Visualisation inside the simulation tool

Experimental

Figure 1 shows the positions of the two cameras and the corresponding fields of view. The cameras have resolutions of 720x576 pixels and 640x480 pixels, respectively. They are installed on the fourth floor of the university building, the baseline of approximately 20 m corresponds to the width of the building. For the implementation of image processing and machine learning methods the Open Computer Vision Library (OpenCV) and MVTec Halcon 8.0 were used on a 3 GHz dual-core CPU under Windows XP. The video data have been read out serially via Halcon addressing two frame grabbers. The time-lag due to synchronisation was about 52ms, resulting in a maximum positioning error of about 1m, if a maximum speed of 70 km/h is assumed. An overall repetition rate of processed data of 10 Hz was achieved with this system.

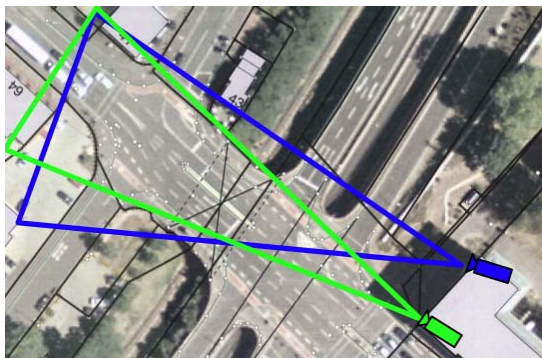


Figure 1. Setup of the cameras to monitor the intersection and field of view.

To implement the communication of the infrastructure based data to a C2X-vehicle the C2X software development framework viilab was used. In the C2X-vehicle both the CAN bus and GPS data can be accessed with the help of viilab to evaluate

possible applications of C2X communication. Another part of viilab is the data-visualisation inside the C2X-vehicle, the so called viilab user interface (vui). Based on Mozilla's XUL technology visualisation pages for received data were programmed using JavaScript and scalable vector graphics (SVG) and displayed on the cars' monitor.

Video based pattern recognition

Differencing which means subtracting two images in succession (movement detector) has been implemented for background/foreground separation. In each of the two images a region of interest is used to confine the necessary operations on the observed intersection. The region of interest is visualised in figure 2 and 3 by the outer white polygon surrounding the monitored area. Due to the requirement that the region of interest should cover an identical area of the crossing in both camera pictures, prominent points serve as vertices of the polygons to limit this region.

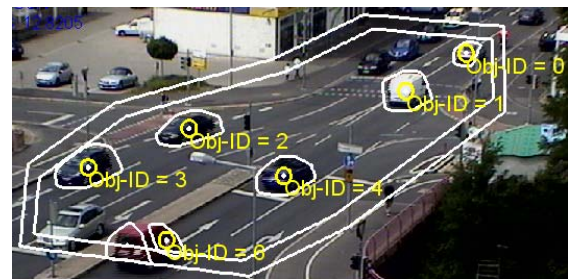


Figure 2. Results of the fusion algorithm for moving objects (Camera picture 1).

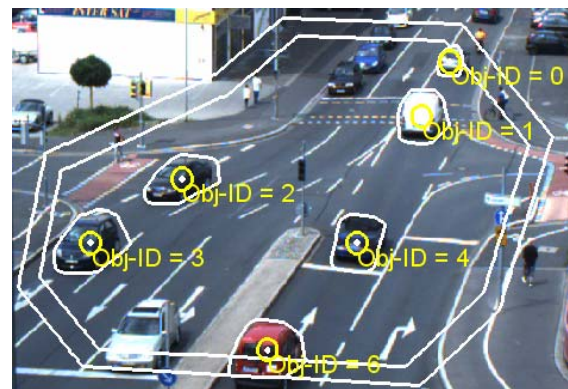


Figure 3. Results of the fusion algorithm for moving objects (Camera picture 2).

To discriminate between pedestrians and vehicles, a two step approach was implemented. In the first classification step features based on the normalised centered moments of second and third order were used. The second classification step is based on tracking statistics and will be described later on. The normalised centered moments of second order (M02, M20, M11) describe the variance of the

object regions from translation and scaling independently. The moments of third order (M30, M03, M21, M12) specify the asymmetry of the region also independently from translation and scaling. A Support Vector Machine (SVM) was trained with these features. For training a feature array was manually generated from a set of objects observed at an image sequence recorded from this crossing. Table 1 shows the confusion matrices of this first classification step for both cameras. The sensitivities for pedestrians and vehicles are in the order of 0.8.

Table 1.
Confusion matrices for the two implemented Support Vector Machines

Confusionmatrix Camera 1		Real Class	
		Pedestrian'	Vehicle'
Determined Class	Pedestrian'	108	76
	Vehicle'	19	769

Confusionmatrix Camera 2		Real Class	
		Pedestrian'	Vehicle'
Determined Class	Pedestrian'	67	119
	Vehicle'	26	711

Coordinate transformation and data fusion

The approach for datafusion was to transform the center of mass of all classified objects into an ortho picture of the intersection and to use the pixel coordinates of the ortho picture as reference coordinate system. The ortho picture was a survey map with reference points given in Gauss-Krüger coordinates.

If an identical object is detected by the two sensors within this approach it is assumed that a transformation of its centers of mass should result in two points that are located next to each other in the ortho coordinate system. So the minimum Euclidean distance within the ortho system was used to join objects.

The task of transformation from the two camera coordinate systems into the ortho coordinate system is achieved by artificial neural networks (ANN). For each camera a separate ANN is created to transform an x-/y-coordinate from the camera picture into an x-/y-coordinate in the ortho picture of the crossing. The training vectors were created from pixel coordinate pairs within the ROI of the ortho picture. The backpropagation algorithm was used to train two multilayer perceptrons. Figures 2 to 4 show the results of the implemented fusion algorithm for objects that were detected by the movement detector. Regions that belong to an identical road user obtain an identical ID in the two images as well as in the ortho picture of the scene. Furthermore the outlines of the detected objects are transformed into the ortho picture of the crossing.

With respect to real time processing contour data was approximated by means of the Douglas-Peucker algorithm [8] before this transformation was applied.

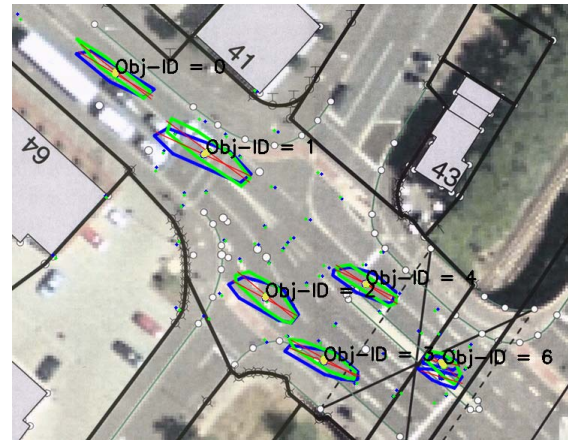


Figure 4. Results of the fusion algorithm for moving objects (ortho picture). The white circles mark the reference points, for which Gauss Krüger coordinates are available.

To use the results of image processing in the C2X-vehicle a final transformation from the ortho coordinate system to the WGS84 (World Geodetic System 1984) coordinate system was applied, because the coordinates which are determined by a GPS receiver are based on WGS84. This second transformation is based on artificial neural networks as described above. An equidistant grid with a point distance of three meters was placed over the ortho picture of the crossing and the correspondent WGS84 coordinates were calculated from the known Gauss-Krüger coordinates. With these pairs of coordinates an additional multilayer perceptron was trained. A mean displacement error and a standard deviation both of about 0.2m were achieved by this method.

Tracking

In order to track the detected objects the following Euclidean distances are calculated:

- The distance of a tracked object's center of mass in the old and in the new picture
- The distance between a coordinate that results from the old center of mass plus its mean measured displacement vector and the object's center of mass in the new picture
- The distance between the new position estimated by a Kalman filter and the position of the center of mass in the new picture

These three distances are summed up to an overall distance giving the last two distances double weight

to adapt their influence. The overall distance is used to assign the newly detected objects to already tracked objects. Newly detected objects that haven't been assigned to an already tracked object yet get added to the list of tracked objects as a new track. To avoid that a quick change of illumination or a reflection can create foreground objects that will get tracked, objects have been detected and assigned to tracked objects several times consecutively before they are valid for communication with the car. Results of the tracking algorithm are classification statistics, object IDs and displacement vectors for the tracked objects. In later steps the displacement vector is used to determine the object heading in the display of the C2X-vehicle. Figure 5 illustrates the tracking result for a pedestrian, figures 6 to 8 show the tracking of vehicles in both camera pictures and in the orthoimage of the crossing.

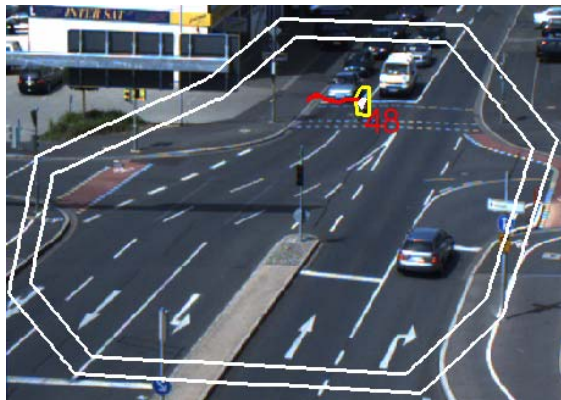


Figure 5. Tracking of a pedestrian visualised in the picture of the second camera.

Objects that are tracked obtain an object ID. Additionally the displacement vector of each tracked road user is displayed in the colour white, the trajectory is displayed in red. When the tracking algorithm is activated the final classification results from the fusion of both acquired images and the classification history collected in the previous tracking steps. In each cycle the tracking algorithm counts how often the road users were assigned to the class pedestrian and to the class vehicle. The class label the object received at most will be the resulting class label of the tracking algorithm. Table 2 shows the confusion matrices of this second classification step for both cameras. The historical tracking data improves the classification results. With enabled tracking sensitivities for pedestrians and vehicles are increased to 0.95. In addition the results of classification are visualised by the colour of the outline of the tracked objects. Pedestrians obtain a yellow (Figure 5), vehicles a green contour (Figure 6 and 7).

Table 2. Confusion matrices for the two cameras with enabled tracking

Confusionmatrix Camera 1		Real Class	
		Pedestrian	Vehicle
Determined Class	Pedestrian'	55	29
	Vehicle'	0	606

Confusionmatrix Camera 2		Real Class	
		Pedestrian	Vehicle
Determined Class	Pedestrian'	41	16
	Vehicle'	0	663

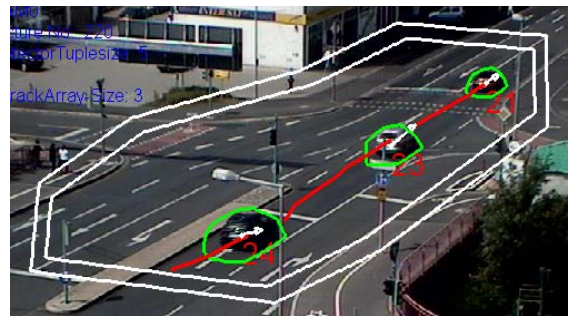


Figure 6. Tracking results displayed in the image of camera 1.

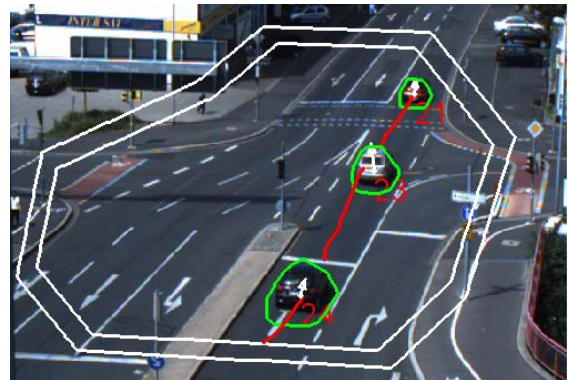


Figure 7. Tracking results displayed in the image of camera 2.

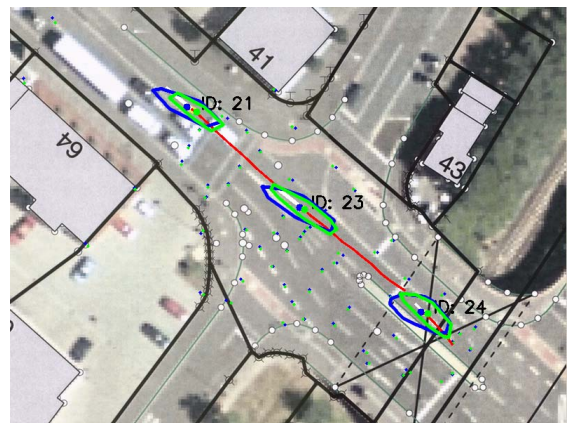


Figure 8. Tracking results displayed in the ortho image.

Communication and visualisation

To transfer the data from the infrastructure to the C2X-vehicle the viilab communication technology based on standard wireless 802.11g technology is used. To exchange the acquired information a SOAP-Server (Simple Object Access Protocol) is implemented in the infrastructure image processing software. From this infrastructure server viilab, which may be used as a simulation environment or an onboard unit, can request information about the objects on the crossing. The SOAP-Server replies to such a request with the WGS84 coordinate and heading, the class and the object ID of all detected objects. If any objects were received from the image processing environment, these objects are visualised in the viilab user interface. To display the received information an environment radar page was created for the vui. Depending on the simulated or real time position and heading of the C2X-vehicle determined by an onboard GPS receiver all detected objects in the surrounding are shown in this environment radar. Figure 10 shows the visualisation page implemented in the viilab user interface.

The communication to viilab was tested with a virtual C2X-vehicle. Figure 9 shows position and heading of such a virtual C2X-vehicle at the observed crossing. Figures 6 to 8 visualise the detection and tracking results in the two camera pictures and the ortho picture of the crossing. Figure 10 finally shows this traffic situation at the crossing in the environment radar of vui with respect to the position of the virtual C2X-vehicle in figure 9.

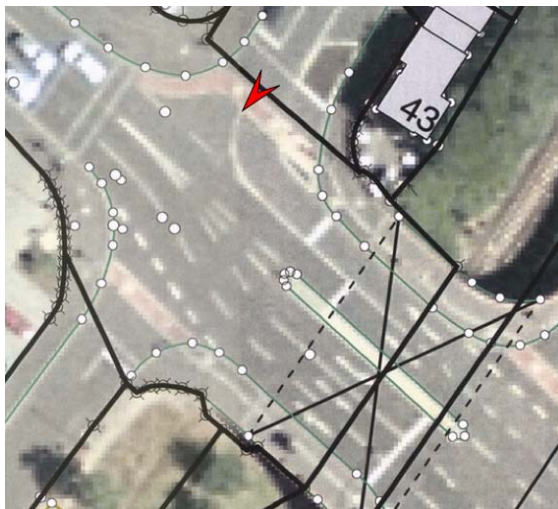


Figure 9. Position and heading of the virtual C2X-vehicle at the crossing.

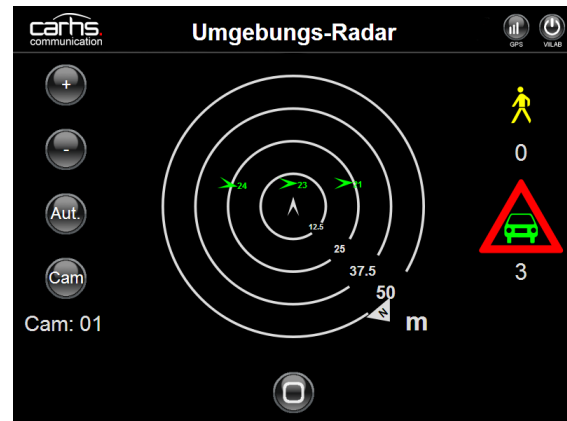


Figure 10. The environment radar visualises the actual traffic at the crossing in front of the virtual car.

CONCLUSIONS

The integration of an infrastructure-based vision system for pedestrian and vehicle detection in viilab, which may be used as simulation tool or as on board unit, and the visualisation to display the acquired data in a C2X-vehicle is described. A two camera approach, a neural net-based camera calibration, a two step classification and a data fusion based on Euclidean metric allow a tracking of road users within a trace of the road in real time even when occlusions occur in a single camera view.

The approach may be adapted to a multi-camera view. To increase the reliability and quality of recognition, classification and positioning the fusion of onboard and offboard sensor data may be considered as a future development target. Due to the fact that cameras for the visible spectral range are used, the current system's time of operation is limited, because good lighting conditions are needed to obtain evaluable images. So in further steps infrared cameras may be added to the system to allow a 24-hour service. Extended training of the first classifier using databases of pedestrians and vehicles as well as integrating additional features, e.g. histograms of oriented gradients, will increase its performance. Another development aim might be the implementation of intelligent assistance into the software of the on board unit. By coupling this infrastructure based technology with C2X-technology benefits for C2X-vehicles in the introduction phase of the new C2X-technology on the market can be expected. Vehicles and pedestrians without communication technology can be detected, localised and tracked on intersections, vehicles with communication technology can receive their positions and use it for intersection assistance.

REFERENCES

- [1] Fuerstenberg, K., Hopstock, M., Obojski, A., Rössler, B., Chen, J., Deutsche, S., Benson, Ch., Weingart, J. and de Lara, A. 2007. INTERSAFE a PReVENT Project, 40.75 Final Report (Project Evaluation and Effectiveness of the Intersection Safety System)
- [2] Schaufelberger, W., Gadiant, F., Lingwood, S. and Rütthemann, D. 2006. Systeme für die automatische Verkehrsüberwachung (Monitoring) mit digitaler Bildverarbeitung, Forschungsauftrag VSS 1999/265 auf Antrag des Schweizerischen Verbandes der Strassen- und Verkehrsfachleute (VSS)
- [3] Dalaff, C., Reulke, R., Ruhé, M., Schischmanow, A. and Schlotzhauer, G. 2003. OIS - An optical information system for road traffic measurement and management, Proc. of the ISPRS Commission IV Joint Workshop "Challenges in Geospatial Analysis, Integration and Visualization II", pp. 209 – 213
- [4] Aycard, O., Spalanzani, A., Yguel, M., Burlet, J., Du Lac, N., De La Fortelle, A., Fraichard, T., Ghorayeb, H., Kais, M., Laugier, C., Laugeau, C., Michel, G., Raulo, D. and Steux, B. 2006. PUVAME - New French Approach for Vulnerable Road Users Safety, Proc. of the IEEE Intelligent Vehicle Symp
- [5] Aycard, O., Spalanzani, A., Burlet, J., Fulgenzi, Ch., Dung Vu, T., Raulo, D. and Yguel, M. 2006. Pedestrians Tracking Using Offboard Cameras Proc. of the IEEE-RSJ Int. Conf. on Intelligent Robots and Systems
- [6] Mauthofer, A. and Glaab, M. 2008. A new Simulation Method for the Rapid Development of Car-to-X Communication Applications, Internet of Things 2008, 1st International Workshop on Interoperable Vehicles (IOV2008), Zurich, Switzerland
- [7] Mauthofer, A., Zang, M. and Glaab, M. 2008. Extended Reality – A new simulation method for the rapid development of car2x communication applications, 15th World Congress on Intelligent Transport Systems ITS, New York, USA
- [8] Douglas, D. H. and Peuker, T. K. 1973. Algorithms for the reduction of the number of points required to represent a digitized line or its caricature, The Canadian Cartographer, Vol 10, No. 2, pp. 112 – 122

THE HEAVY GOODS VEHICLE AGGRESSIVITY INDEX

Feist, Florian

Gugler, Jürgen

Vehicle Safety Institute, Graz University of Technology
Austria

Robinson (nee Smith), Tanya

TRL

United Kingdom

Faßbender, Sven

Institut für Kraftfahrwesen, Body Department, RWTH Aachen University
Germany

Niewöhner, Walter

DEKRA Technology Center Stuttgart, AG73 Accident Research
Germany

Barrios, José Manuel

Aparicio, Andrés

Applus+IDIADA,
Spain

On behalf of the APROSYS WP 2.1 consortium
Paper Number 09-0323

ABSTRACT

The provision of protection for vulnerable road users (pedestrians and pedal cyclists) is not a new concept for vehicle design. Directives 2003/102/EC [1] and 2005/66/EC [2] assess the “structural aggressivity” of passenger cars and front protection systems (“bullbars”) with respect to the protection of pedestrians. Adopting these directives for assessing heavy goods vehicles (HGVs) would be straightforward. However, assessing the “structural aggressivity” only, will fail to address a relatively large number of fatalities, particularly those that occur at low-speeds.

This manuscript describes the development of the test procedures and assessment criteria for the Heavy Vehicle Aggressivity Index (HVAI). The procedure and criteria are derived based on the study of real world accidents. The proposed procedure integrates numerical simulation and physical testing methods.

The HVAI aims to reduce the number or severity of vulnerable road user (pedestrian and pedal cyclist) casualties from accidents involving HGVs by providing guidance to manufacturers/designers of such vehicles.

The HVAI consists of three parts, assessing the field of view of the driver (active HVAI), the direct contact between the casualty and the vehicle structure

(structural HVAI) and the risk of the casualty being over run by the HGV (run-over HVAI). Each of these sub-indexes returns a value between 0 and 10. The three parts ensure that a wide range of accident scenarios are addressed.

Keywords: Vulnerable Road Users, Pedestrian, Bicyclist, Heavy Goods Vehicles, Trucks

INTRODUCTION

The Heavy Vehicle Aggressivity Index (HVAI) aims to improve the protection offered to pedestrians and pedal cyclists – often referred as vulnerable road users in impacts with HGVs. The HVAI is a set of test procedures for the assessment of the protection afforded to vulnerable road users (VRU) by heavy goods vehicles (HGV). The HVAI aims to encourage HGV manufacturers and designers to develop more pedestrian and cyclist friendly vehicles in order to reduce the number or severity of VRU casualties from accidents involving HGVs.

METHOD

The HVAI consists of three parts assessing the performance of the design in relation to the following areas (see Figure 1):

- Active Index: The ability for the accident to be avoided though good visibility and/or active safety systems.

- Structural Index: Direct contact between the casualty and the vehicle structure,
- Run-over Index: Risk of the casualty being run over by the HGv.

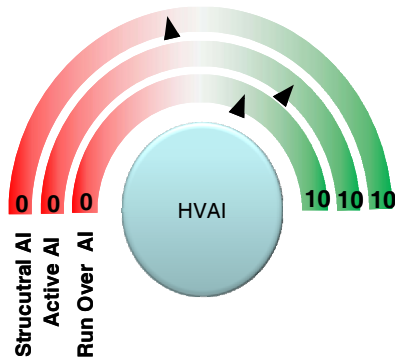


Figure 1. Presentation of the HVAI.

Each individual part of the HVAI is assessed on a scale from 0 to 10 with the score increasing with improved protection of the VRU.

Active Index

The accident analysis revealed numerous accidents at low impact speeds [3]. Passive safety measures will have limited effect on very low speed accidents because of the kinematics involved. These accidents are addressed by the active AI. The index evaluates the field of view of a 50th percentile driver, separated into a primary area of interest (in the close surroundings of the vehicle) and a secondary area of interest (>5m away from the right front edge of the HGv).

The active part of the HVAI is a methodology for comparison of cab designs of HGvs over 7.5t with respect to the driver's field of view. It is a proposal for comparing the driver's field of view by considering four basic components:

- areas only seen directly;
- areas only seen through the various mandatory mirrors;
- areas which can be seen directly and at least through one mirror;
- blind spots /areas not visible at any time.

The development of this assessment procedure is based on geometrical relations in 2D blueprints of the commercial vehicles and cabs. In addition, the mandatory mirror view areas around the vehicle were used. The assessment could be carried out using 3D-CAD and/or ergonomics software packages.

The current proposal is restricted to the assessment of cab-over-engine HGvs and includes only the primary structures affecting the visible area (edge of glazing and mirrors). Obstructions due to the dashboard or the steering wheel were not considered.

The test procedure defines two areas of interest in which measurements will be taken. These are the primary area of interest (PAI) and the secondary area of interest (SAI) as shown in Figure 2.

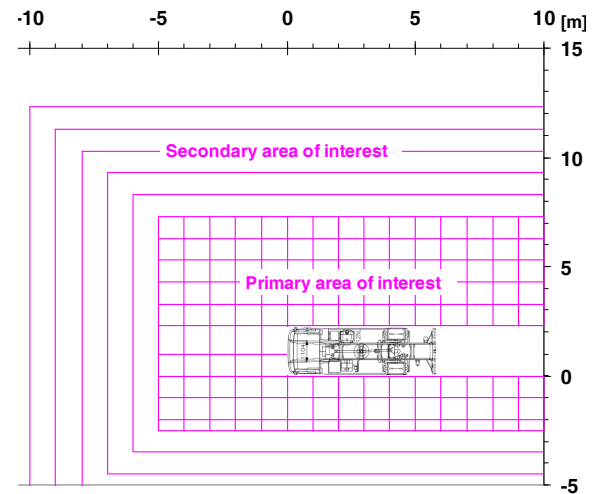


Figure 2. Definition of primary and secondary areas of interest.

Direct field of view

The direct field of view is that which can be seen by the driver without the use of visual aids such as mirrors or cameras. The direct field of view is often measured by marking the boundary of the visible area on the ground plane either physically or numerically by the use of CAD/ergonomics software. For the purpose of this proposed assessment protocol, the direct field of view is measured at a height of 1.6m from the ground. 1.6m is an estimate of the vertical position of the centre of the head of a walking 50th percentile person and will ensure that a pedestrian of this stature will be seen when standing in the visible area. However there are also other statures of VRU that could be considered for future development of this procedure, for example 5th percentile females, cyclists or child pedestrians.

Figure 3 shows an example of the direct field of view. Blind spots that result from the main structure of the cab are shown in red, whilst blind spots associated with other structures such as the mirrors are shown in blue. The assessment is based upon the monocular vision of a 50th percentile male driver sitting in a normal driving position.

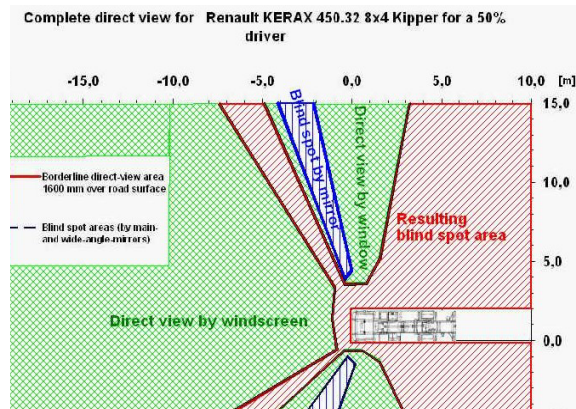


Figure 3. Direct field of view.

Indirect field of view

The indirect field of view is that which can be seen by the driver through the mirrors (or other features such as video cameras). Current legislation requires that the indirect field of view is measured on the ground plane. This can allow small objects within the prescribed area to be seen, however, it may not necessarily be possible to identify what the object is. To allow the driver to correctly identify a VRU, it is proposed that the indirect field of view is assessed at a distance of 0.5m from the ground plane. This should allow at least the lower half of a pedestrian's leg or half a bicycle wheel to be identified in the mirrors. The proposed assessment of indirect view does not include the Class II (main exterior mirrors) because they are not considered influential for current VRU accident scenarios. However, they are included for the purpose of assessing the direct field of view because they form an obstruction to the direct field of view. Figure 4 shows an example of the indirect field of view. The proposed index promotes an indirect field of view that exceeds existing regulations.

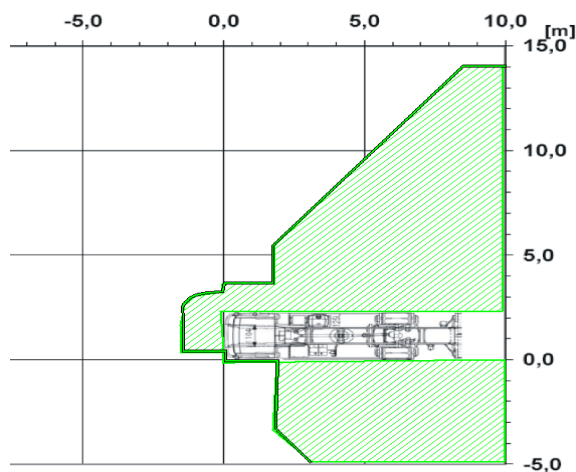


Figure 4. Indirect field of view.

Valuation of visible areas and blind spots

The areas defined above are combined as shown in Figure 5 and the following areas are calculated for both the PAI and SAI:

- Blind spots;
- Mirror view only;
- Direct view only; and
- Combined mirror and direct view.

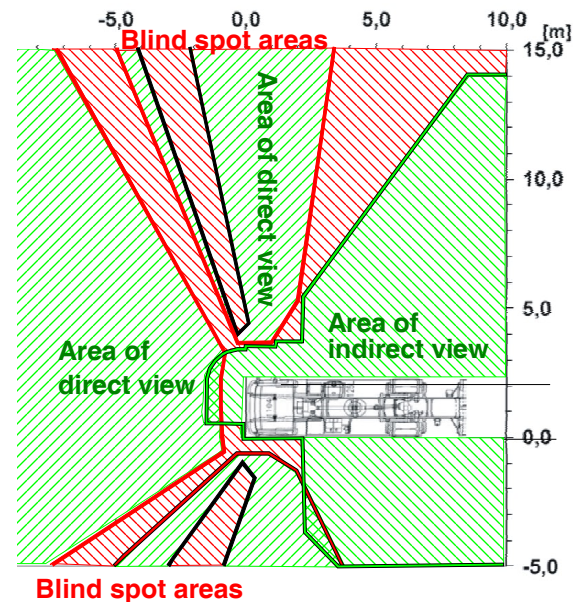


Figure 5. Diagram combining direct and indirect fields of view and blind spots.

To allow for the relative importance of the different view areas with respect to the safety of VRU, weighting factors were applied:

- Blind spots in the PAI were considered more relevant than those in the SAI because of the close proximity to the vehicle. These were therefore upgraded by 20% by applying a weighting factor;
- It is often more difficult to correctly identify an object in a mirror than through the windshield (direct view). Therefore areas that were only visible in mirrors were downgraded by 20%;
 - Mirror views in the SAI were downgraded a further 20% because the mirror views at that distance are even more difficult to interpret.
- Where the direct and indirect views overlap there is an increased probability that the driver will be able to correctly identify the VRU, for example if part of the head is visible through the window and part of the leg is in the view given by a mirror. However, because this area is also

part of the direct view, a neutral weighting is applied.

PAI Example

As example, the PAI around the truck has a total visible area of 123m² (see Table 1). The visible area of the PAI is divided in the areas of direct view (49m²) and in areas of mirror view (55m²). An area of 14m² can be seen both directly and in-directly (in the mirrors). The blind spot areas have a value of 5m². The value of direct view and overlapped view are un-weighted and will not be changed, remaining at 49m² + 14m² respectively. The value for the mirror view will decrease 20% from 55m² to 44m² and the value of the blind spot areas will increase 20% from 5m² to 6m². Consequently, the sum of the weighted areas of the PAI will decrease from 123m² to 113m². The direct view and overlap view areas will account for 43% and 12% of the total weighted area. The mirror view area is 39% (and 12% overlap) and the blind spot areas account for 5% in the PAI.

Table 1.
Example of calculated and weighted areas, PAI.

	Primary Area of Interest		
	Weightin g Factor	Area ([m ²)] [%]	Weighted Area ([m ²)] [%]
Blind spots	1.2	(5) 4	(6) 5
Mirror view	0.8	(55) 45	(44) 39
Overlap direct -mirror	1.0	(14) 11	(14) 12
Direct view area	1.0	(49) 40	(49) 43
Total		(123) 100	(113) 100

SAI Example

The SAI around the truck is usually about 60% larger than the PAI and has in our example a total amount of 195m² (see Table 2). The weighted value of direct view will not be changed and remains at 131m². The value of mirror view will decrease from 45m² by 20% to account for it being the indirect view and by a further 20% because it is the SAI (as described earlier) to 35m² (including 16m² overlap). The value of the blind spot areas on the other hand remain at 19m². Hence the sum of the areas of the SAI will decrease to 184m². The direct view area and overlap area will account for 71% and 9% of the weighted area. The mirror view area is 19% (incl. 9% overlap) and the blind spot areas 10% in the SAI.

Table 2.

Example of calculated and weighted areas, SAI.

	Secondary Area of Interest		
	Weightin g Factor	Area ([m ²)] [%]	Weighted Area ([m ²)] [%]
Blind spots	1.0	(19) 10	(19) 10
Mirror view	0.64	(29) 15	(19) 10
Overlap direct- mirror	1.0	(16) 8	(16) 9
Direct view area	1.0	(131) 67	(131) 71
Total		(195) 100	(185) 100

Modifiers

Even when the design of HGV enables the driver to see almost every detail around the vehicle, there will remain some specific situations when the VRU is not visible, particularly when in very close proximity to the HGV:

- VRU is standing just in front of the HGV;
- VRU is just to the nearside of the HGV; or
- VRU is walking towards the HGV roughly behind the B-pillar.

Modifier points are awarded to vehicles where the following criteria apply:

1. Step one is to evaluate if there is an overlap area of direct view and indirect view by one of the mirrors in the PAI around the vehicle. For example, this overlap could be found between the area covered by the direct view and the area covered by the wide-angle-mirror on the nearside. This criterion is fulfilled, if there is an overlap of at least 100mm, in which case a modifier of 3 will be awarded;
2. The second criterion is applied if the first criterion is fulfilled. This criterion focuses on the overlap of the direct view out of the nearside window and the proximity mirror area. The criterion is fulfilled, if there is an overlap of at least 100mm between the interior borderline of the direct view through the nearside window and the exterior borderline of the proximity mirror view. In this case the modifier number increases to a maximum of 6.
3. This criterion focuses on the overlap of the direct view out of the side window and the wide angle mirror area in the PAI on the nearside of the vehicle. The criterion is fulfilled, if there is a point where the overlap of the rear borderline of the direct view through the right window and the frontal borderline of the right wide angle-mirror-

view. If this is the case, the modifier number increases to a value of up to 10.

Overall score for Active HVAI

Figure 6 shows an example of the presentation of the results of the assessment. The outer circle shows results for the SAI, the inner circle is the PAI and the number in the centre refers to the modifier score.

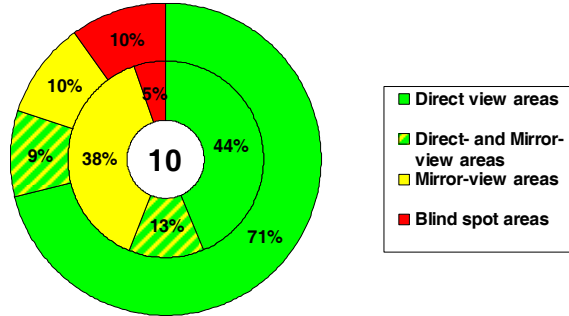


Figure 6. Example presentation of assessment results.

There are three important values required to assess the overall field of view (direct view, mirror view and blind spots). For each area of interest, the direct view and blind spots were benchmarked against 10 existing HGV designs. Benchmarking two of the three values was considered sufficient since the mirror view would be the remainder of the total (i.e. mirror view = 100% - direct view – blind spots). The results of the benchmarking are shown in Table 3.

Table 3. Benchmarking of direct view and blind spots.

PAI	Direct View	Blind Spot	SAI	Direct View	Blind Spot
10	58%	4,0%	10	80,0%	9,0%
9	55,5%	5,5%	9	77,5%	10,5%
8	53,0%	7,0%	8	75,0%	12,0%
7	50,5%	8,5%	7	72,5%	13,5%
6	48,0%	10,0%	6	70,0%	15,0%
5	45,5%	11,5%	5	67,5%	16,5%
4	43,0%	13,0%	4	65,0%	18,0%
3	40,5%	14,5%	3	62,5%	19,5%
2	38,0%	16,0%	2	60,0%	21,0%
1	35,5%	17,5%	1	57,5%	22,5%

This allowed a score from 0 to 10 to be applied to each of the four parts (direct view PAI, blind spot PAI, direct view SAI and blind spot PAI). These four values are then combined with the modifier score and averaged to give the Active HVAI score out of 10 as shown by the example in Table 4.

Table 4. Example of overall Active AI score.

	Single Rating	Overall Rating
Modifier	10	
Direct view PAI	9	
Blind spot PAI	9	8.8
Direct view SAI	8	
Blind spot SAI	8	

Structural Index

Test procedures for the assessment of the structural interaction between passenger cars and pedestrians already exist, both, for type approval purposes and for use in consumer assessment ratings of vehicles. These existing protocols have been used as a basis for the development of a test procedure for the assessment of the protection for VRU in impacts with HGVs [4].

The structural aggressivity index defines two impact zones (adult and child) with 6 areas per zone and 4 regions per area. One region within each area is tested by propelling adult and child headforms (as defined by EEVC WG 17) horizontally at 11.1m/s. Up to 15 tests per vehicle are conducted to assess the structural response. Up to 2 credit-points are assigned to each test area.

Vehicle preparation and marking

The protocol specifies the marking out of the front of the vehicle into two zones, one an adult zone, and the other a child zone. The adult zone is the area where the head of an adult pedestrian is likely to hit and the child zone is the equivalent area for a child pedestrian. The marking procedure includes allowances for changes in ride height of the vehicle and defines the “corner” of the vehicle. The lower boundary of the test zone is defined with the vehicle at its maximum ride height, and the upper boundary with the vehicle at its minimum ride height. The heights of the boundaries are defined based on anthropometric data [5]. Figure 7 shows the marking of the two test zones.

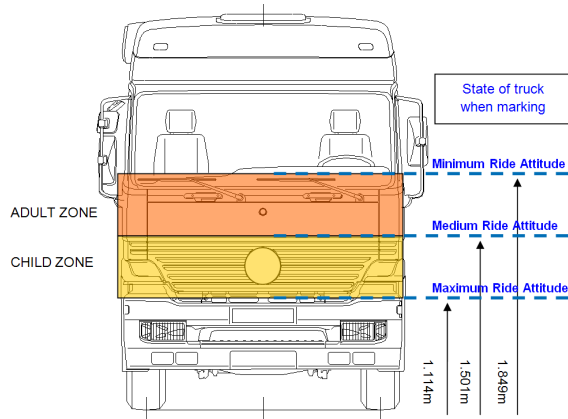


Figure 7. Marking out of test zones accounting for ride height of vehicle.

This approach has been developed based on flat-fronted vehicles, which are the most common HGV design currently in use in Europe. The protocol provides an alternative approach for marking vehicles that are not flat fronted, which allows the wrap-around kinematics to be considered.

Both the child and adult test zones are divided horizontally into six areas. Each area is then subdivided into quarters and labelled as shown in Figure 8.

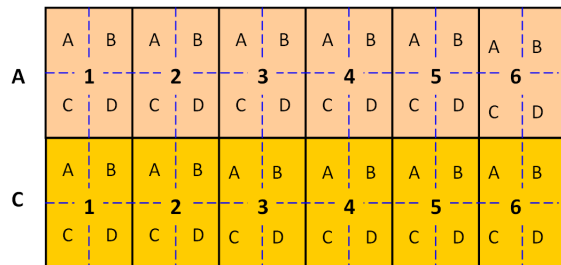


Figure 8. Labelling of test zones.

Impact points

The test points are selected by the test engineer from the testing organisation (as is the case in EuroNCAP pedestrian testing of passenger cars). At least one point must be selected from each test zone (A1, A2.....C5, C6). The test point selected should be expected to be the most injurious within that zone. In some cases, multiple test zones can cover the same structure, which is expected to have equivalent performance (e.g. the windscreen). Where this occurs, the protocol allows for only one test to be performed, with the same result translated to the second (and third etc) test zone.

The vehicle manufacturer may specify up to three additional tests (one per test zone), allowing for a total maximum of 15 tests.

Testing

The testing is carried out with air, spring or hydraulically propelled headforms. The protocol provides details on how to position the headform. The headform is propelled at the vehicle in the x-direction (nominally this is normal to the surface). However, alternative set-up requirements are described where the geometry of the HGV could affect the dynamics of the head impact due to wrap-around kinematics [4].

The testing is carried out using adult headforms for area A and child headforms for area C (Figure 8). The test speed used is 11.1 ± 0.2 m/s selected based on analysis of accident data that showed approximately 50% of fatalities occur at impact speeds up to 40-45 km/h [3].

Assessment criteria

The 15ms Head Injury Criteria (HIC_{15}) is used for the assessment of the structural aggressivity. For each test location, up to two points can be awarded, based on the performance criteria shown in Table 5. The scores for each test zone are combined to give a total of up to 24. This is then linearly scaled to a maximum score of 10.

Table 5. Performance criteria.

HIC	Points	Colour Rating
$0 < HIC < 1000$	2	Green
$1000 < HIC < 1350$	1	Yellow
$1350 < HIC$	0	Red

If additional points are tested (up to 3 extra points), the score for each test location within a zone is weighted to the test zone. For example, if two tests are conducted in zone A6 (Figure 8), with one impact location scoring 1 point and the other scoring 2 points, then the overall score for the area is $(0.5 \times 1) + (0.5 \times 2) = 1.5$.

Example

Figure 9 shows an example of the test locations selected and the associated HIC_{15} category (left) and the scores attributed to each test zone (right).

The left hand figure shows a total of 15 test points. The additional points selected are highlighted with a black border. Also two of the twelve selected points were not tested because there was no expected benefit. These two points are in the adult zone on the

left and right A-pillars. These two points have been assigned a score of 0, because the anticipated headform response is $HIC_{15} > 1350$.

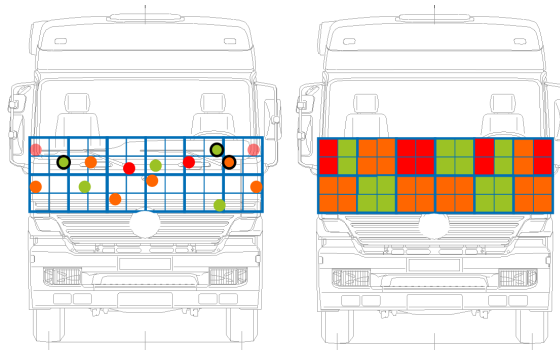


Figure 9. Example of test locations and results (left) and scoring (right).

The figure on the right shows how the overall score is derived. Where an additional test point has been included (for example in zone A1) half of the test zone is rated red and half green. Zone A5 is also rated half red and half green because of the second test point within the zone. The zone A6 was also tested twice, but this zone was rated half amber and half red. The overall score for this vehicle is calculated as shown in Table 6.

Table 6. Calculating the overall score.

	Zone	Score
ADULT	A1	0x0.5 + 2x0.5
	A2	1
	A3	0
	A4	2
	A5	0x0.5 + 2x0.5
	A6	1x0.5 + 0x0.5
	<i>Adult Total</i>	5.5
CHILD	C1	1
	C2	2
	C3	1
	C4	1
	C5	2
	C6	1
	<i>Child Total</i>	8
	<i>Overall Score</i>	$(13.5 / 30 \times 10) = 4.5$

Run-over Index

A virtual testing procedure based on multi-body simulation techniques is used to assess the risk of the VRU being run-over. The HGV is approximated by rigid facet surfaces. A human pedestrian model with and without bicycle is used. In total 21 simulations have to be carried out, covering two accident scenarios (turning and going straight), two road users (bicyclist and pedestrian) and seven impact areas,

depending on the scenario (two on the front and five on side).

The rationale for developing a virtual test procedure is discussed later in the paper.

For the development of the proposed assessment procedure, the following basic objectives were considered: The procedure should remain simple therefore uniform contact characteristics (those of the pedestrian) are assigned to the vehicle, allowing CAD data to be transferred easily. To aid comparison, only one code, one human model and one type/mode of bicycle is currently proposed.

To help achieve these development objectives, the following steps were taken:

- Standard input-decks were developed and used. Only the data describing the outer shape of the specific HGV has to be provided.
- In order to keep the simulation simple, active safety systems were not considered. However, deployable systems can be included in this assessment in the deployed position (deployment of the system will need to be evaluated by additional testing not yet defined).
- The MADYMO multi-body solver was chosen as the common simulation tool, because MADYMO offers a broad variety of pedestrian human models validated with respect to initial impact kinematics. The HGV is represented as a rigid facet model in MADYMO;
- For the purpose of this study, rigid HGVs have been used to demonstrate the assessment procedure. The assessment of HGVs with trailers is also possible but more difficult, because only a certain combination of truck and trailer can be tested. Therefore, it is proposed that a standard trailer should be used.

Accident scenarios and impact locations

To assess the risk of the VRU being run over, a range of accident scenarios were identified from literature and accident data. The outcome of this analysis was the definition of impact locations on the HGV as shown in Figure 10 (for the side) and Figure 11 (for the front).

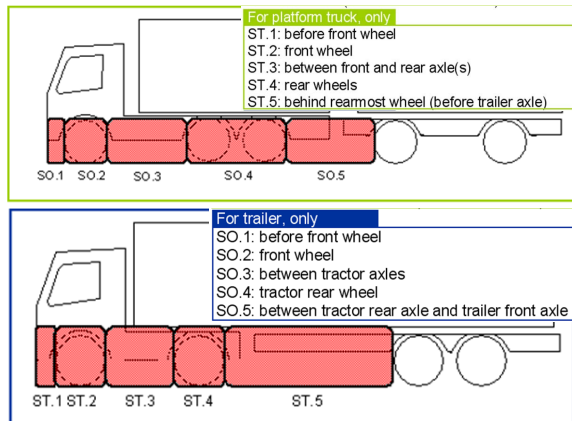


Figure 10. Definitions of impact sub-areas - Side.

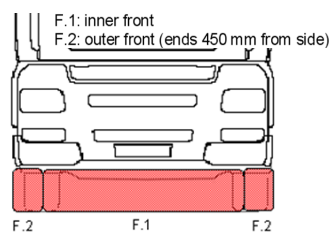


Figure 11. Definitions of impact sub-areas - Front.

The accident scenarios were combined with the relevant impact locations on the HGV. The final simulation matrix for assessing the risk of run over encompasses 21 simulations (Table 7).

Table 7.

Simulation matrix for run-over assessment procedure.

No.	Impact Location	Accident Scenario	Orientation of VRU
1	F.1	HGV turning vs. pedestrian	45°
2	F.2		45°
3	SO.1/ ST.1		0°
4	SO.2/ ST.2		0°
5	SO.3/ ST.3		0°
6	SO.4/ ST.4		0°
7	SO.5/ ST.5		0°
8	F.1	HGV turning vs. cyclist	45°
9	F.2		45°
10	SO.1/ ST.1		45°
11	SO.2/ ST.2		45°
12	F.2		0°
13	SO.1/ ST.1		0°
14	SO.2/ ST.2		0°
15	SO.3/ ST.3		0°
16	SO.4/ ST.4		0°
17	SO.5/ ST.5		0°
18	F.1	Forward driving	90°
19	F.2	HGV vs. pedestrian	90°
20	F.1	Forward driving	90°
21	F.2	HGV vs. cyclist	90°

For the purpose of weighting the impact locations in relation to the frequency of their involvement in real world accidents, it was necessary to combine the impact locations (the data from accidentology do not allow for distinguishing the impact locations to that degree). The sub-areas defined in Figure 10 and Figure 11 are combined into the main areas shown in Figure 12. For one main area to pass the assessment, the associated sub-areas must show that run-over is prevented. The association between the main areas and the sub-areas are shown in Figure 12 and Table 9.

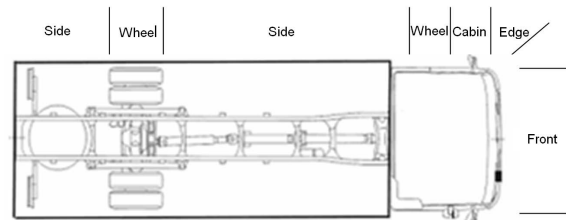


Figure 12. Definition of main impact areas.

Table 8.

Relationships between areas & sub-areas, Part A

Sub area	Turning				
	Front	Edge	Cabin	Wheel	Side
F.1	X				
F.2	X	X			
SO.1/ ST.1		X	X		
SO.2/ ST.2				X	
SO.3/ ST.3					(X)*
SO.4/ ST.4				(X)*	
SO.5/ ST.5					(X)*

(X)* Not relevant for the sub scenario with the HGV turning and the bicyclist on a separate lane

Table 9.

Relationships between areas & sub-areas, Part B

Sub area	Forward driving	
	Front	Edge
F.1	X	
F.2	X	X

Determining risk of run over

The output from the simulations is an assessment of whether or not the VRU is run over by the HGV. For that purpose, run-over is defined in two ways (see Figure 13 and Figure 14). The two definitions of run over are:

- The VRU is run over if one of the body regions coloured red is in contact with a wheel of the HGV (Figure 13); or
- The centre of gravity of the head or the hip is within the critical area defined (Figure 14)

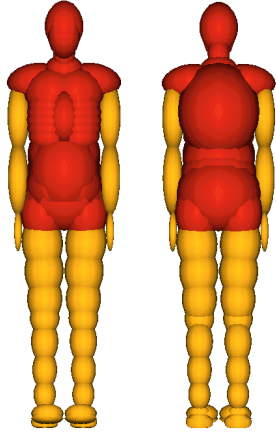


Figure 13. Body regions that must not contact wheels (shown in red).

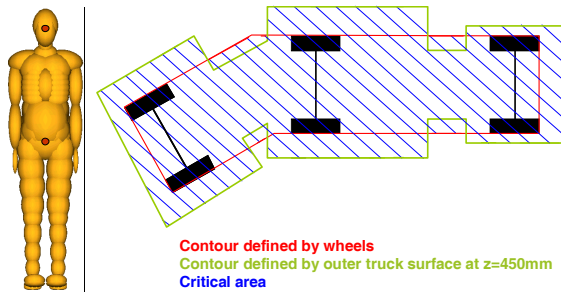


Figure 14. Definition of critical area under HGV.

If the VRU is not run over, there are a number of possible outcomes from the impact. Three types of outcome were defined:

- “Fixing” - the VRU is not run over and subsequently none of the red coloured body regions are involved in the secondary impact with the ground;
- “Isolating” - the VRU is not run over and subsequently the red coloured body regions are involved in the secondary impact with the ground and the HGV;
- “Moving away” – the VRU is not run over and is deflected away from the HGV by the primary impact.

The risk of injury associated with each of these different outcomes can be different. Fixing is considered to result in a lower risk of injury than isolating because the VRU is not pushed over the ground. Moving away is considered to result in a high risk similar to that associated with isolating, because of the uncertainty in relation to the direction and velocity of the secondary impact. The following risk factors are applied depending on the type of protection after the initial impact:

- Fixing = 1
- Isolating = 0.7
- Moving away = 0.7

Weighting factors

The literature and accident analysis has shown the variation in the frequency of the impact scenarios/locations. To allow for the distribution of real world accidents, the scores are weighted as shown in Figure 15 - based on the main areas defined in Figure 12.

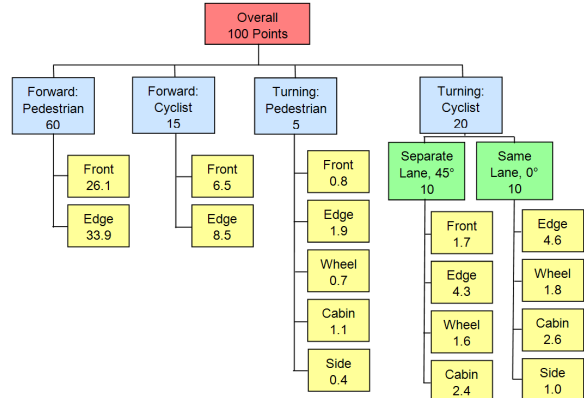


Figure 15. Weighting factors for each accident scenario.

Example

The following figures show a comparison between a flat fronted HGV and an HGV fitted with a “nosecone” [6]. Figure 16 and Figure 17 show simulations where the nosecone prevents run-over, while the flat front does not. Figure 18 and Figure 19 show a scenario where none of the designs prevents run-over. More examples can be found in APROSYS WP2.1 report [7].

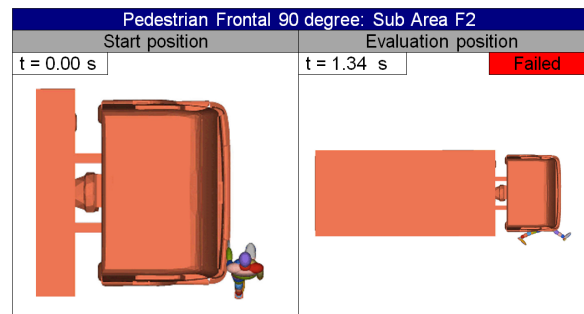


Figure 16. Flat front simulation result: Pedestrian frontal 90 degree - Sub Area F2.

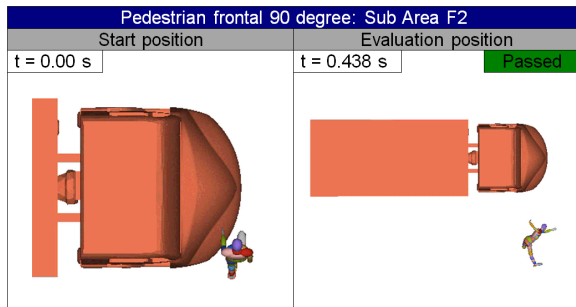


Figure 17. Nosecone simulation result: Pedestrian frontal 90 degree - Sub Area F2.

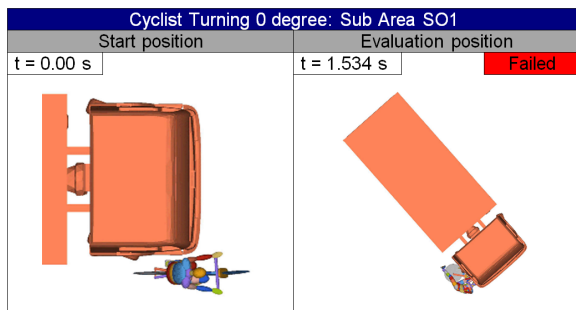


Figure 18. Flat front simulation result: Cyclist with HGV turning 0 degree – sub-area SO1.

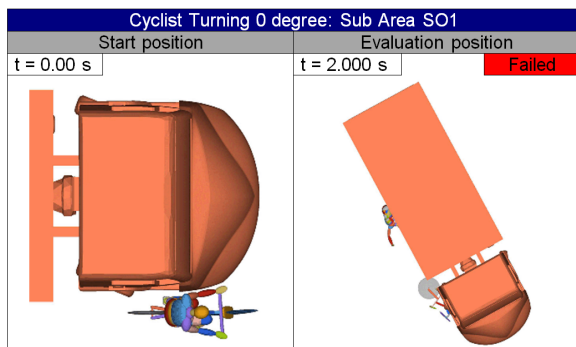


Figure 19. Nosecone simulation result: Cyclist with HGV turning 0 degree – sub-area SO1.

The outcomes from the simulations in terms of run over/not run over and the injury risk associated with the post impact kinematics are entered into a calculation spreadsheet. The spreadsheet returns a score between 0 and 10.

To continue the example of the nose-cone HGV: While the conventional flat front vehicle scores 0.3 points out of 10, the nose-cone HGV reaches 5.5 points.

DISCUSSION

Assessing the protection of VRU is not new to vehicle engineering. Directives 2003/102/EC [1] and 2005/66/EC [2] assess the “structural aggressivity” of

passenger cars and front protection systems (“bullbars”). Revisions of these directives to come, will consider active collision avoidance systems, too. For HGV legislations addressing the protection of VRU are related to the sideguards and the geometry of the front of the HGV in relation to protrusions. Comparable directives to 2003/102/EC and 2005/66/EC do not exist for HGV. Adopting these directives for assessing HGVs would be straightforward. However, assessing the “structural aggressivity” only, will fail to address a large number of low-speed fatalities that result from accidents involving HGVs [3].

The HVAI, developed by APROSYS, addresses these low-speed accidents by assessing the field of view around the vehicle and the risk of the VRU being run-over. Analysis of accident data has shown that a “structural index” has to concentrate on the front of the vehicle (including the vehicle’s corners). The pedestrian is most frequently impacting the HGV front (64 to 75 % [3], [8, 9], [10]). For cyclists, the co-driver side is also highly relevant. However, where the impact is with the side of the HGV, the relative speeds between cyclists and HGV are lower and there is a greater risk of the cyclist being caught/run over by the HGV[8] and therefore this scenario is covered by the run-over index.

In APROSYS [11] major accident scenarios were defined. Table 10 cross-references each part of the AI with the accident scenarios that are most relevant to it (more stars represents closer correlation between the sub-index and the accident scenario).

Table 10.
Heavy Goods Vehicle Aggressivity Index versus accident scenarios

Scenario	Active AI	RunOver AI	Structural AI
1.1 (Turning)	★★★	★★★	
1.2 (Turning)	★★★	★★★	
2.1 (Overtaking, frontal impact)			★★★
2.2 (Overtaking, lateral impact)	★	★	
3.1 (Crossing, pulling away)	★★★	★★★	
3.2 (Crossing)			★★★
4 (Autobahn)			★

Figure 20 shows the accumulated percentage of fatal HGV-pedestrian accidents versus impact speed. The red bars highlight the impact speed range that is

addressed by each of the sub-indexes. It can be concluded, that the HVAI covers a significant range of HGV-VRU accidents and fatalities.

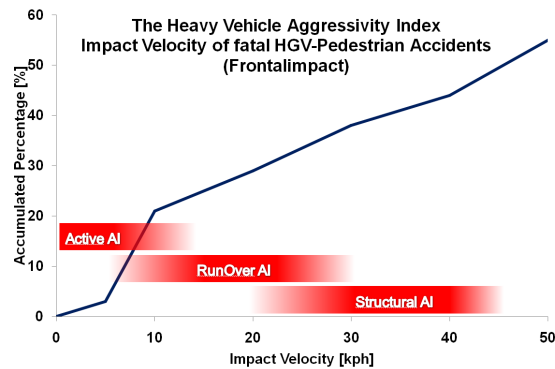


Figure 20. Heavy Goods Vehicle Aggressivity Index versus impact speed.

Presenting the three aspects of the HVAI separately allows the vehicle design to be assessed with respect to each individual component of the AI. Combining the three parts into one overall rating was discussed, however it was decided that presenting the individual results would be easier to understand (have more meaning) and enable designers/engineers to identify which aspects of the vehicle design to focus on in relation to the protection of VRU. A single overall score might distort the vehicle's performance.

The current index is a starting point and should be used as the basis to motivate further discussions and developments in the field of VRU protection of HGV.

Active Index

Vehicle blind spots and the driver's field of view from the cab of HGVs are often cited as contributory factors in a range of accident scenarios. The most recent changes in legislation requiring the fitment of close proximity mirrors to the front and nearside of the vehicle, have been intended to help reduce the number of casualties that are attributed to blind spot accidents. However, legislation provides a minimum performance requirement and does not account for the overlap of direct and indirect views. VRU are a group of casualties that are often severely or fatally injured in accidents caused by a driver's blind spot impaired field of view. Examples of accidents involving VRU casualties are those where the HGV is turning to the nearside and collide with a pedal cyclist or where the HGV is held up in stop-start traffic and a pedestrian crosses close to the front of the vehicle. This active AI aims to identify and

encourage vehicle designs that can help to reduce the number of VRU casualties through improved visibility or the use of active safety systems.

The active index promotes areas that are covered by both direct and in-direct view consecutively, through the use of modifiers. The driver's view to the co-driver's side with its dangerous blind spot areas has a strong influence/effect.

By applying weighting factors improvements to the direct field of view are promoted. Of course, improved vision can be provided by mirrors as well, however, mirrors have a number of drawbacks:

- Mirrors need to be correctly set and adjusted to provide the view that is required by legislation:
- The number of mirrors fixed to current HGV makes it hard for the driver to correctly use these mirrors:
- Identification of objects in the mirrors is sometimes hard, as only parts of the VRU are shown (e.g. the legs of a cyclist).

The calculated values for the vehicles analysed while developing this methodology ranged from 2.4 to 9.2. From the 14 vehicles analysed, 10 of the vehicles reach only an index value between 2.4 and 4.0. Comparison of the active index result with the height of the lower edge of the windscreen from the ground showed some correlation, particularly for the lower scoring vehicles. There are already some designs on the market which achieve a good result for the active index despite a very high lower edge of the windscreen and vice versa. Therefore the lower edge of the windscreen is not the only factor that influences the visibility.

Further development of the active AI should consider the following issues:

- Evaluation of electronic vision aids is not implemented yet. Currently there are a number of such system under development, e.g. by Hino Motors [12] or Volvo [13], that overcome some of the limitations of mirrors.
- The current version of the active AI considers mandatory mirror areas only. However, mirror systems may exceed the requirements set by legislation. Also the new class VI mirror was not considered, yet.
- Obstructions caused by internal structures such the steering wheel and dashboard were not considered.

Run-over Index

For the development of the protocol assessing the run over aggressivity of HGVs several basic requirements were considered. The main objective was to offer a quantitative value representing the ability of an HGV to prevent the VRU from being run over when hit by a HGV. The assessment value has to reflect the influence of a broad variety of possible design modifications whilst ensuring that the biofidelity of the VRU is appropriately represented.

A number of approaches can be used to assess the risk for VRU being run over:

- experimental test;
- directive requiring simply measurable attributes (e.g. geometry or strength);
- combination of experimental testing combined with numerical simulation; or
- test procedure based mainly on numerical simulation.

Each of these approaches was assessed for their advantages and disadvantages against a range of criteria [7].

At the start of the project it was acknowledged that any proposed assessment protocol should be developed with minimal costs associated with any testing. Clearly, that aim was contradictory to experimental testing for assessing the risk of run-over due to potential damage to the dummies and HGV. Also, reproducibility and costly test set-ups of such experiments are an issue. For a test procedure that is based on numerical simulation, the effort is acceptable with respect to time effort and costs.

Also, virtual models of the VRU already exist while the development of experimental dummies for HGV vs VRU accidents would still require an extensive effort.

In parallel to the run-over index a new HGV front shape was developed, reducing the risk for run-over. This “nose cone” (see Figure 21) was tested at 20 and 30kph. In both tests, the pedestrian was deflected to the side and a run-over was prevented (see Figure 22).



Figure 21. Nose cone



Figure 22. Experimental testing of nose cone

Structural Index

The current proposal has been based on head impacts with the HGV, particularly because it is one of the most frequently injured body regions and there are test tools currently existing for evaluating those impacts. Future developments of the structural index could include the development and inclusion of new test tools, for example to assess impacts with the thorax of the VRU.

Currently the structural AI is addressing the primary contact only (the contact with the truck front). However, numerical studies and experiments [14] have shown the severity of the secondary impact makes it a highly relevant aspect for future consideration. Studies of the “nose cone” [6] indicated not only a reduced likelihood for run-over, but also a reduced severity of the secondary impact (prevent forward-projection of pedestrian).

Existing test methods for passenger cars are continually under development, such as the research into rotational acceleration as an assessment method.

The future development of the structural index should be based on the lessons learned from existing test methods.

CONCLUSIONS

Legislation relating to the protection of VRU in impacts with HGVs is very limited, currently only covering the fitment of sideguards and geometric requirements for structures on the front of the HGV in relation to protrusions.

A set of assessment criteria to assess the risk posed by HGVs to pedestrian and cyclists were developed by APROSYS WP2.1. The index is a combination of physical and virtual testing. Each sub-index is returning a value between 0 and 10.

The active AI evaluates the field of view of 50th percentile driver. Weighting factors are applied to promote improvements to the direct field of view. Modifiers are applied to promote the overlap of direct and in-direct fields of view within the PAI.

The run-over AI is based on multi-body simulation techniques using 21 simulation set-ups

The structural AI defines two impact zones (adult, child). Up to 15 tests per truck are conducted to assess the structural response using EEVC WG 17 headform impactors.

A separate score is reported for each of the three sub-indices, which prevents the masking of important design features within a single score. The presentation of the individual scores also shows the assessment in a way which is considered to be easy to read and understand (see Figure 1).

The HVAI could be developed for future legislation/consumer testing or could be used by manufacturers during the development of future vehicle designs. The current index is a starting point and should be used as the basis to motivate further discussions and developments in that field.

LIMITATIONS

Where available, accident data was used to define the so-called weighting factors. In case of the run-over index the weighting factors are based on accident data. However, in other cases, (e.g. Active Index) arbitrary weighting values were applied- based on experience from accident researchers and expert opinion.

REFERENCES

- [1] European Parliament. Directive 2003/102/EC of the European Parliament and of the Council of 17 November 2003 relating to the protection of pedestrians and other vulnerable road users before and in the event of a collision with a motor vehicle and amending Council Directive 70/156/EEC. 15-25. 6-12-2003. Brussels, Belgium, European Parliament and Council. Official Journal of the European Union L 321.
- [2] European Parliament. Directive 2005/66/EC of the European Parliament and of the Council of 26 October 2005 relating to the use of frontal protection systems on motor vehicles and amending Council Directive 70/156/EEC. 37-40. 25-11-2005. Brussels, Belgium, European Parliament and Council. Official Journal of the European Union L 309.
- [3] APROSYS WP 2.1. Summary of UK Accident Data. Smith, T. and Knight, I. AP-SP21-0038, 1-24. 24-1-2005. Transport Research Lab.
- [4] APROSYS WP 2.1. AP-SP21-0090: Technical Report on Structural Aggressivity Index. Barrios, J. M. and Aparicio, A. AP-SP21-0090, 1-32. 13-6-2008. APROSYS - Subproject 2 - Workpackage 2.1.
- [5] TNO MADYMO BV., MADYMO: Human Models Manual: Version 6.2, pp. 1-197, TNO MADYMO BV., Delft 2004.
- [6] S. Faßbender, M. Hamacher, R. Puppini, F. Feist and J. Gugler. AP-SP21-0077 D2.1.3 Demonstrator Module for New Design Concepts. 2007. Aachen, Deutschland, Institut für Kraftfahrzeugwesen (IKA), RWTH Aachen.
- [7] APROSYS WP 2.1. AP-SP21-0091: Technical Report on Run-Over Aggressivity Index. Faßbender, S. and Hamacher, M. AP-SP21-0090, 1-52. 28-3-2008. APROSYS - Subproject 2 - Workpackage 2.1.
- [8] W. Niewöhner, F. A. Berg and Nicklitsch. Innerortsunfälle mit rechts-abbiegenden LKW und ungeschützten Verkehrsteilnehmern. 20-10-2004. Neumünster, Germany, Dekra/VDI. Dekra/VDI Symposium.
- [9] W. Niewöhner and F. A. Berg. Gefährdung von Fußgängern und Radfahrern an Kreuzungen durch rechtsabbiegende Lkw. 1-84. 2004. Bergisch Gladbach, Germany, Bundesanstalt für Straßenwesen. Berichte der Bundesanstalt für Straßenwesen, Fahrzeugtechnik, F54.
- [10] C.-N. Strub. Lastwagenkollisionen mit Fußgängern und Radfahrern im Kanton Zürich

- (1984 – 1986). 1990. Insitut für Rechtsmedizin: Universität Zürich.
- [11] APROSYS WP 2.1. AP-SP21-0065: Enhanced HV Aggressivity Index. Feist, F., Smith, T., Avalue, M., Chirwa, C., Knight, I., Puppini, R., Franzen, M., and Mayrhofer, E. AP-SP21-0065, 1-99. 7-6-2007. APROSYS - Subproject 2 - Workpackage 2.1.
- [12] K. Akiyama and H. Enomoto. Advanced Safety Truck - A Proposal for Driver Assistance in Visibility. Proceedings of the Symposium on "Safety of Commercial Vehicles" , 1-9. 9-10-2008. Neumünster, Germany, DEKRA.
- [13] Steine + Erde, Ausgabe 06/08: Das neue Fahrzeugprogramm von Volvo Trucks. <http://www.steine-und-erden.net/se608/volvo.html> . 2009. 17-3-2009.
- [14] F. Feist, C. Arregui, C. Deck, R. Willinger, E. del Pozo de Dios and F. Lopez-Valdes. Pedestrian collisions with flat-fronted vehicles: injury patterns and importance of rotational accelerations as a predictor for traumatic brain injury (TBI). Proceedings of the 21st International Technical Conference on the Enhanced Safety of Vehicles (ESV) , 1-19. 2009. Stuttgart, Germany, National Highway Traffic Safety Administration.

DESIGN ANALYSIS OF A SANDWICH HOOD STRUCTURE FOR PEDESTRIAN PROTECTION

Qi Liu

Yong Xia

Qing Zhou

State Key Laboratory of Automotive Safety and Energy Department of Automotive Engineering,
Tsinghua University, China

Jenne-Tai Wang

General Motors Research & Development, Warren, Michigan, USA

Paper Number 09-0356

ABSTRACT

Besides functioning as an engine compartment cover, the hood of modern vehicles can also help manage the impact energy of a pedestrian's head in a vehicle-pedestrian impact. However, a hood's ability to absorb impact energy may be impeded by the proximity of the hood to components packaged inside the engine compartment, i.e., by its underhood clearance. For example, for a given hood design, the hood's ability to absorb impact energy through deformation can be significantly reduced when the hood and engine block are in close proximity. Therefore, a large underhood clearance would be preferred for pedestrian protection. However, it could negatively affect driver visibility, as well as a vehicle's aerodynamics and aesthetic appeal. This paper presents a sandwich hood design that has a potential to improve the hood's ability to absorb the impact energy of a pedestrian's head with a relatively small underhood clearance. Using nonlinear finite element and the EEVC headform impactor models, a design analysis was conducted with an underhood clearance target of 60 mm and 75 mm for the child head impact area and the adult head impact area, respectively. A set of design parameters of the sandwich hood was optimized. The analysis shows that out of the 12 impact points covering the main hood area, about half of the impact points achieved Head Injury Criterion (HIC) values less than 800 and the others yielded HIC values between 800 and 1000.

INTRODUCTION

The hood of modern vehicles can help manage the impact energy of a pedestrian's head in a vehicle-pedestrian impact. European Enhanced Vehicle-Safety Committee (EEVC) Working Group 10 (WG10), followed by Working Group 17 (WG17), has recommended component test procedures so as to perform the pedestrian protection verification tests for vehicles^{[1][2][3][4]}. The pedestrian protection

performance rating reported by European New Car Assessment Program (EuroNCAP)^[5] is one of the consumer metrics taking advantage of the component test procedures. The EuroNCAP pedestrian protection rating is determined by four types of component tests: adult headform and child headform impacting the hood, upper legform impacting the hood leading edge, and the lower legform impacting the bumper. The focus of this paper is on the first two, in which the adult headform (AH) and the child headform (CH) are used to impact with specified hood areas with an impact angle of 65° and 50°, respectively, at an impact speed of 40 km/h. The Head Injury Criterion (HIC) calculated from the resultant acceleration is adopted as the injury index with a threshold of 1000 by the EuroNCAP.

To meet the HIC threshold, the hood must be designed to manage the impact energy of a pedestrian's head. However, a hood's ability to absorb energy may be impeded by the proximity of the hood to components packaged inside the engine compartment, i.e., by its underhood clearance. For a given hood design, the hood's ability to absorb energy through deformation will be significantly reduced when the hood and engine compartment components, like engine block, battery, etc., are in close proximity. Therefore, a large underhood clearance would be preferred for pedestrian protection. However, a large underhood clearance may negatively affect driver visibility, as well as a vehicle's aerodynamics and styling.

Otubushin and Green^[6] reported that the theoretical minimum intrusions in the impact direction, which determines the amount of the required underhood clearance for a 40 km/h headform impact to meet HIC 1000 and 800, are 51.1 mm and 59.3 mm, respectively. However, the head acceleration-time history waveform corresponding to the theoretical minimum intrusions requires infinite head

acceleration at time zero as implied by Figure 1, which is practically impossible to achieve.

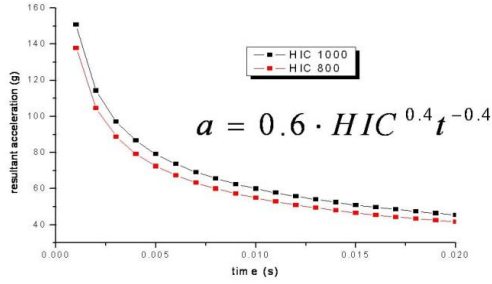


Figure 1. Ideal acceleration waveform for the theoretical minimum intrusion [6].

More recently, Wu and Beaudet^[7] compared several acceleration waveforms analytically and proposed a compromise waveform as the target for pedestrian head impact to achieve with HIC<1000. According to their study, with the parameters as shown in Figure 2, the theoretical intrusion in the impact direction will be as small as 67.9 mm, while meeting the requirement of HIC<1000. However, the authors didn't provide any hood designs that could result in such a performance.

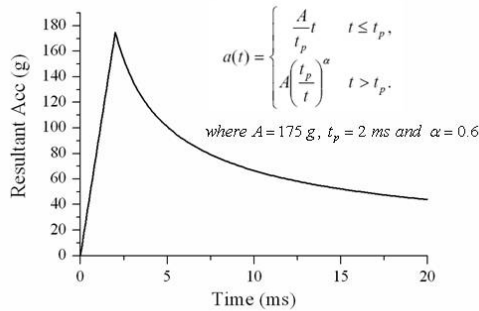


Figure 2. A compromise acceleration waveform to achieve HIC<1000 [7].

This paper presents a sandwich hood design that could improve the hood's ability to absorb the impact energy of a pedestrian's head with a relatively small underhood clearance. The sandwich structure consists of three layers of substructures. Using nonlinear finite element and EEVC headform impactor models, a design analysis is presented.

PRELIMINARY CONSIDERATIONS

Definition of underhood clearance

Figure 3 shows the geometrical relationship of a headform impacting a hood, with an impact angle γ

and a local hood angle θ , which may vary at different hood locations depending on hood design.

Underhood clearance Δ is defined as the vertical distance between the hood outer surface and the engine compartment upper limit. Intrusion in the impact direction, I , and its vertical component, I_z , are also shown in Figure 3. One should pay special attention between the vertical component of intrusion I_z and underhood clearance Δ . The relationship among them is shown in EQ 1. Notice that I_z depends on the impact angle γ while Δ depends on both angles γ and θ , and that the underhood clearance Δ is always greater than the vertical component of intrusion I_z because of the hood angle θ . Only when the hood angle θ is zero, does the underhood clearance Δ equal the vertical component of intrusion I_z . Should one confuse the underhood clearance with the vertical component of intrusion, it may lead to a design with insufficient underhood clearance since the former is always greater than the latter.

$$\begin{aligned} I_z &= I \sin \gamma \\ \Delta &= I_z + I \cos \gamma \tan \theta \end{aligned} \quad (1).$$

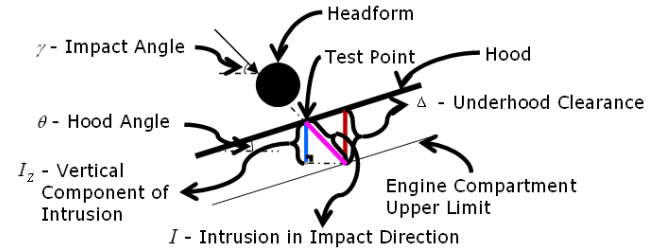


Figure 3 Relationship among underhood clearance, intrusion and its vertical component.

Target HIC threshold

A 20% safety margin for the HIC threshold, i.e., a HIC threshold of 800, is chosen as the target for this study to account for possible test variations due to the tolerances of impact speed, impact direction and impact location.

Target waveform shape

Consider a typical 40 km/h headform-hood impact test. On the one hand, a waveform with a high and long duration deceleration during the early stage of the headform impact is preferred to achieve a smaller underhood clearance design. On the other hand, a waveform with such a high and long duration deceleration imposes a high risk of resulting in an undesired high HIC value. We see that a small

underhood clearance and a low HIC value are two competing performance requirements. Therefore, in order to balance these competing performance requirements an ideal headform deceleration pulse should have a waveform with a sudden increase peaking at an appropriate level followed by a quick decrease during the early stage of the impact. Figure 4 depicts such a balanced waveform, which offers an excellent HIC performance of 800 and a 68 mm intrusion in the impact direction. This waveform is generated using a design tool, called the Dual Asymmetrical Triangle Pulse Generator [8]. We use it as the target waveform for our sandwich hood structure.

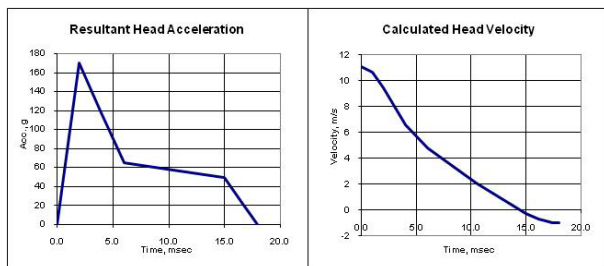


Figure 4. Target waveform using the Dual Asymmetrical Triangle Pulse Generator [8].

MODEL DESCRIPTION

Sandwich hood

A late model mid-sized car, not designed to meet any pedestrian protection requirements, is selected as the study vehicle for the development of the sandwich hood structure. A finite element (FE) model of the sandwich hood, together with other necessary front-end structures and components of the study vehicle, was developed.

Figure 5 shows the exploded view of the sandwich design and Figure 6 shows a sectional view of the sandwich hood. The sandwich hood design consists of three aluminum substructures: the outer hood as an upper layer, the ripple plate as a middle layer, and the support plate as a lower layer. The ripple plate has two sections: the core ripple section in the central area of the hood and the boarder section, in which the ripple gradually diminishes toward the edge of the hood. The support plate is divided into two sections corresponding to CH and AH impact areas, namely CH section and AH section. The outer hood is bonded to the ripple plate with glue strips spread on the upper ridges of the main section of the ripple plate and glue spots in the outlier section of the ripple

plate, as illustrated in Figure 7. The support plate is bonded to the ripple plate with “finite rigid links” (e.g., bolts, rivets or spotwelds), as shown in Figure 8.

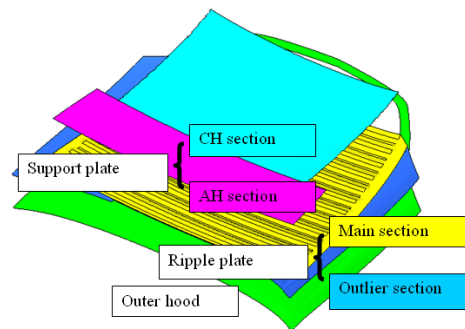


Figure 5. Exploded view of the sandwich design for main hood area with color coded labels (upside-down view of the hood assembly).

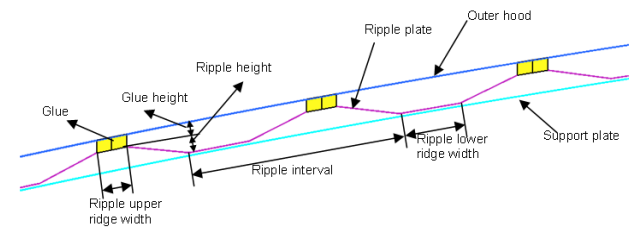


Figure 6. Enlarged sectional view of sandwich hood assembly.

A design optimization analysis of the sandwich hood structure was performed using nonlinear finite element models. The final geometry parameters and material parameters of an optimized sandwich hood are shown in Table 1 and Table 2. The total mass of this sandwich hood design is 11.8 kg, about 27% more than that of the original hood of the study vehicle.

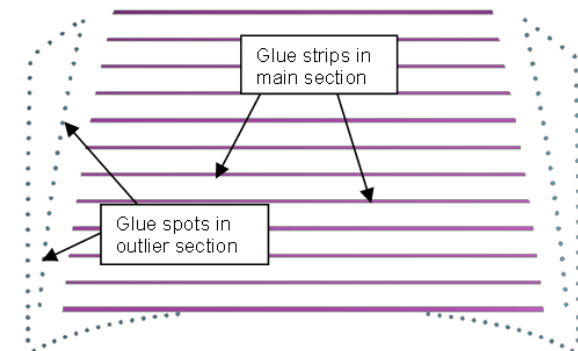


Figure 7. Glue distribution between the ripple plate and the outer hood (top view).

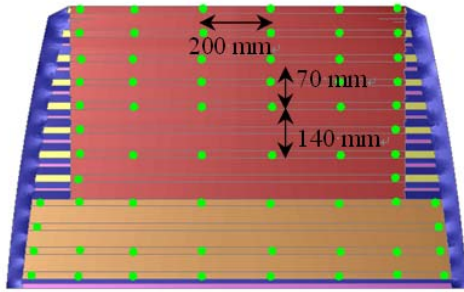


Figure 8 Rigid link distribution between the support plate and the ripple plate (bottom view).

Table 1. Optimized geometry design parameters of the sandwich hood assembly (unit: mm)

Component	Dimension
Outer hood thickness	1.05
Support plate thickness: CH / AH	1.2 / 1.8
Ripple plate thickness	0.5
Ripple upper ridge width	8
Ripple lower ridge width	20
Ripple height	6
Ripple interval	70

Table 2. Material parameters of the sandwich hood assembly

	Material model	Density (kg/mm ³)	Modulus (GPa)	Yielding strength (MPa)
Ripple/support	*MAT_024	2.6e-6	70	200
Glue	*MAT_001	1.27e-6	0.03	/

Other components in the FE model

Besides the hood assembly, the FE model also includes other components shown in Figure 9 near the hood assembly that may be engaged in pedestrian head impacts, including the fenders, the front panel, the bumper stops, the towers, and the cowls, etc. These components constitute a more complete environment for pedestrian head impacts. The lower part of the fenders, the towers and the cowls are all fixed to the vehicle reference frame in the model to provide the necessary boundary condition as shown in Figure 9. The hood assembly is constrained at the latch and hinge positions as a

conventional hood as shown in Figure 10. Specifically, the outer hood is fixed at the latch position and the ripple plate is rigidly linked to the original hinges in the model.

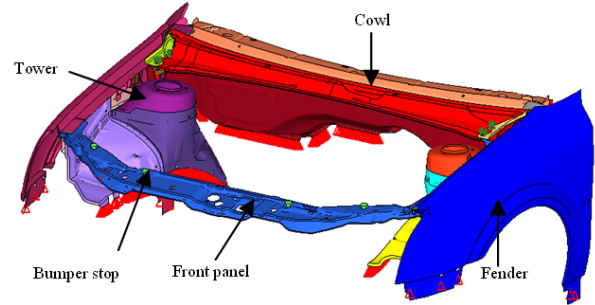


Figure 9. The FE model (hood assembly and underhood rigid wall excluded).

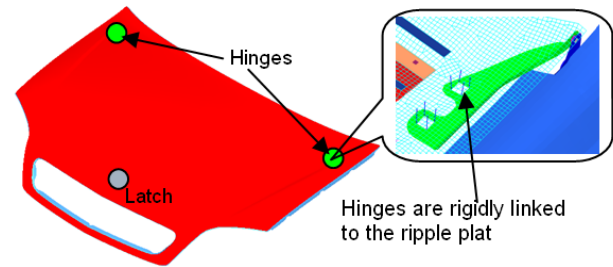


Figure 10. The hood assembly constraints at the latch and the two hinge positions.

Impact area definition

The wrap around distance (WAD) 1500 mm line^[5] of the study vehicle is very close to the hood rear edge and leaves a rather small AH impact area as shown in Figure 11. To provide adequate AH impact area for the purpose of this study, we artificially reduce the CH area and increase the AH area as shown in Figure 12. A base point ($x=0$ or x_{base}) is set at $WAD=1400$ mm. Line $x=0$ separates CH area and AH area. Three impact points for AH and nine impact points for CH are selected as marked in Figure 13.

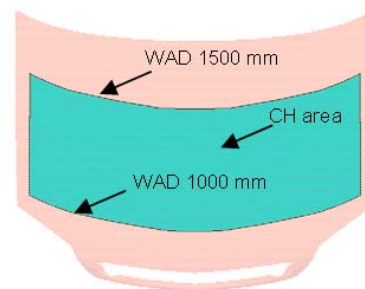


Figure 11. Baseline hood CH area definition according to EuroNCAP.

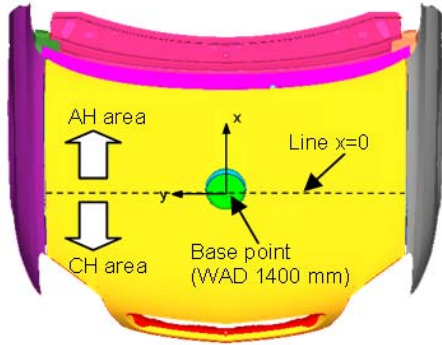


Figure 12. CH and AH area definition for analyses in this study.

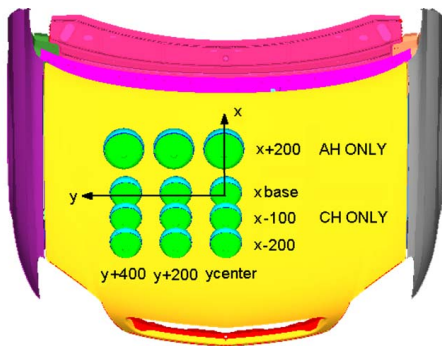


Figure 13. CH and AH impact cases in the main hood area.

Target underhood clearance

An underhood clearance target of 60 mm and 75 mm is selected for the CH area and the AH area, respectively, as shown Figure 14 and Table 3. A rigid wall of the same curvature as the outer hood at the specified vertical distance beneath the outer hood is used in the FE model to represent underhood components, such as an engine block.

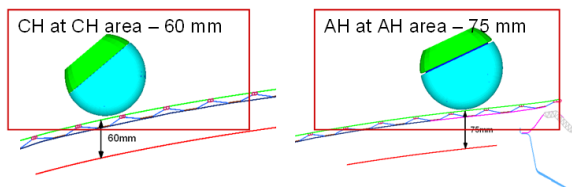


Figure 14. Underhood clearance set for different impact areas.

Table 3. Underhood clearance required for HIC<800

Headform requirement	Underhood clearance (mm)
CH 2.5 kg, 40 km/h, HIC<800	60
AH 4.8 kg, 40 km/h, HIC<800	75

SIMULATION RESULTS AND DISCUSSIONS

The results of all the 12 impact cases are summarized in Table 4. As shown, HIC<1000 has been achieved for all the impact points. Of these, all five impact points along the centerline of the hood achieve HIC<800. For the impact points away from the centerline of the hood, the HIC value becomes higher. Rigid wall contact is observed from simulations at all the four “ycenter” points and four “y+200” points. No rigid wall contact occurs in any of the four “y+400” cases. This means that at these “y+400” impact points, the given underhood clearance is not fully utilized, which implies that there is room for further improvement for these impact points.

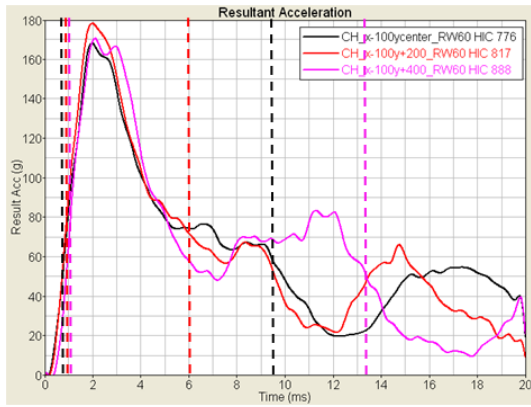
Table 4. Simulation results

Area	Underhood clearance (mm)	Impact point	HIC		
			y+400	y+200	ycenter
AH	75	x+200	841	703*	764*
CH	60	xbase	973	872*	751*
		x-100	889	817*	776*
		x-200	934	874*	788*

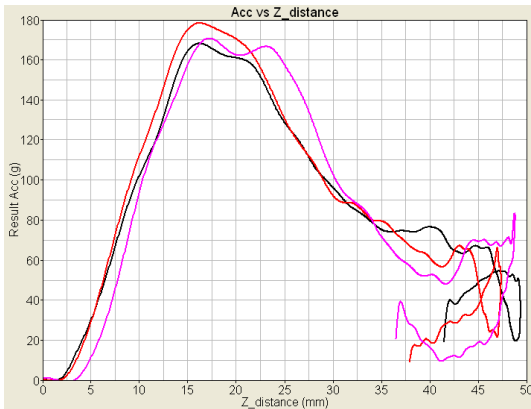
* Contacted with the underhood rigid wall.

Impact results in the CH area

Taking the three cases of “CH x-100” in Figure 15 as example, “CH x-100ycenter” and “CH x-100y+200” cases have similar resultant acceleration waveform shapes. The latter has a higher first peak, probably due to the effect of discontinuity of the scattered lower links, while the former has the biggest intrusion (represented by the Z_distance in Figure 15 (b)). “CH x-100y+400” case has a similar first peak to that in “CH x-100ycenter” case.



(a)

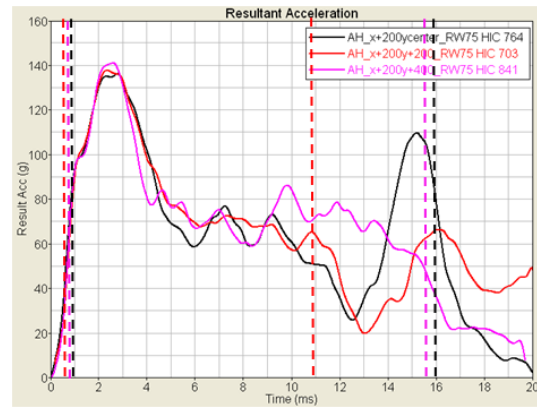


(b)

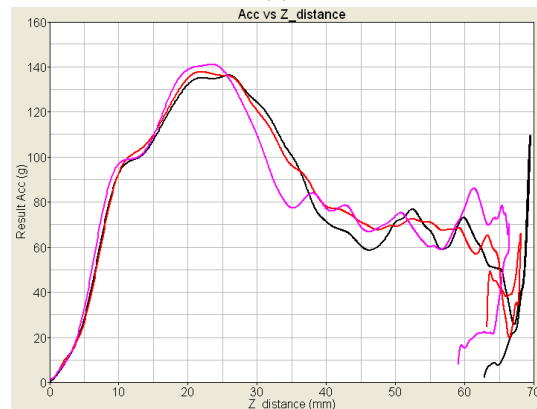
Figure 15. Simulation results of “CH x-100” impact points.

Impact results in the AH area

The simulation results of AH at “x+200” points where the underhood clearance is set as 75 mm are shown in Figure 16. All the three cases achieve HIC below 900. Note that the first acceleration peaks for the three AH cases are lower than those of CH cases in the last sub-section. Actually, without considering CH, the hood can be optimized for AH to reach less underhood clearance required for HIC 800. However, such optimized hood will be too strong and may have too much active mass for CH impact, causing high first peak of acceleration and generating HIC greater than 800. Therefore, the hood must be designed somewhat softer for satisfying CH impact, and yet the softened hood needs larger underhood clearance for AH impact.



(a)



(b)

Figure 16. Simulation results of “AH x+200” impact positions.

SUMMARY

A sandwich hood structure is proposed for improving the hood’s ability to absorb the impact energy of a pedestrian’s head with a relatively small underhood clearance. A design optimization analysis for the sandwich hood structure is performed using a study vehicle and FE models. The total mass of this optimized sandwich hood design is about 27% more than that of the original hood of the study vehicle. An underhood clearance of 60 mm and 75 mm is achieved for the child headform impact area and the adult headform impact area, respectively. Of the 12 impact positions covering the main hood area, about half of the impact points meet the HIC<800 and the others achieve HIC from 800 to 1000. However, no attempt was made to assess manufacturability of the sandwich structure in this study. Further developments to address all safety requirements, including performance in real-world crash events, are also necessary before implementing this feature in a production vehicle.

REFERENCES

- [1] European Enhanced Vehicle Safety Committee (EEVC) Working Group 17. Improved test methods to evaluate pedestrian protection afforded by passenger cars (December 1998 with September 2002 updates), 2003, <http://eevc.org/publicdocs/publicdocs.htm>.
- [2] The European Parliament and the Council of the European Union, Directive 2003/102/EC, Official Journal of the European Union, L 321: 15-25.
- [3] Commission of the European communities. Proposal for a Regulation of the European Parliament and of the Council on the protection of pedestrians and other vulnerable road users. 2007, <http://ec.europa.eu/enterprise/automotive/pagesbackground/pedestrianprotection/index.htm>.
- [4] Commission of the European communities. Commission working document on the measures necessary to implement the proposed regulation on pedestrian protection. 2008, <http://ec.europa.eu/enterprise/automotive/pagesbackground/pedestrianprotection/index.htm>.
- [5] European New Car Assessment Programme (EuroNCAP) Assessment Protocol and Biomechanical Limits, Version 3, April 2001.
- [6] Otubushin, A. and Green, J., "An Analytical Assessment of Pedestrian Head Impact Protection," Proceedings of The 16th International Technical Conference on the Enhanced Safety of Vehicles (ESV), Windsor, Ontario, Canada, May 31 - June 4, 1998.
- [7] Wu, J. P. and Beaudet, B., "Optimization of head impact waveform to minimize HIC," SAE Paper No. 2007-01-0759.
- [8] Cheng, C.-S. and Wang, J. T., "An Analytical Study of Pedestrian Headform Impacts Using a Dual Asymmetrical Triangle Function," GM R&D Publication No. R&D-9326, May 2002; Conference Proceedings of Crashworthiness, Occupant Protection and Biomechanics in Transportation Systems, the 2002 ASME International Congress, New Orleans, La.

PEDESTRIAN INJURY CHARACTERISTICS FOLLOWING ROAD TRAFFIC COLLISIONS

Rebecca Cookson

Richard Cuerden

David Richards

TRL

Harry Rutter

SEPHO

United Kingdom

Paper Number 09-0429

ABSTRACT

The paper outlines the nature and severity of the injuries suffered by pedestrians in motor vehicle accidents in England. Pedestrian admissions to hospitals in England as recorded in the Hospital Episode Statistics (HES) over a nine year period were compared with accidents recorded in Great Britain's national road casualties database (STATS19). Alongside this, the most frequently injured regions and individual injuries of the pedestrians were investigated. The relationship between individual injuries and the length of time spent at hospital was investigated. The changes in frequency of individual injuries were investigated to see whether recent changes in vehicle design could have altered the types of injuries received by pedestrian casualties.

The HES data from April 1998 to March 2007 in England contained details of 82,811 pedestrian admissions following accidents involving motor vehicles. In the same time period there were 65,526 killed or seriously injured pedestrians recorded in the STATS19 database. It was found that over the nine year period, the number of pedestrian casualties in HES remained relatively constant, while the number in STATS19 has reduced. In this period, HES data shows that tibia and femur fractures have reduced slightly. This could be due to a number of factors including improved vehicle design.

The nature of the HES data means that very little information is included about the characteristics of the accident, which prevents possible causes of pedestrian injuries to be studied using the HES dataset by itself. However, this paper shows the potential of hospital data as an important tool in accident research, as the injury information can give evidence of the effects of the changing vehicle fleet, along with other road safety interventions. Further, through an in-depth understanding of the frequency and consequences of different injuries, future injury prevention strategies can be prioritised.

INTRODUCTION

Every year in the UK thousands of people are killed and tens of thousands are seriously injured in traffic accidents. As well as the personal tragedy of these events, road traffic accidents have economic implications. An understanding of how injuries occur in accidents is sought in order to implement ideas to try and mitigate them, and a major part of gaining this understanding is looking at national level statistics. The importance of these statistics is such that they can affect Government and local authority initiatives, policy, spending and legislation, and even vehicle manufacturing decisions. Hence the need for them to be accurate and reliable is prevalent.

This project presents an opportunity to investigate two such sources of national statistics: the data recorded by the Police (STATS19) and the data recorded by the hospitals (Hospital Episode Statistics). While the purpose of STATS19 is to record traffic accidents, recording details of traffic casualties is only a small part of the Hospital Episode Statistics (HES). As such, only limited accident analysis has been performed using HES in the past. This paper provides the opportunity to investigate how HES can be used in accident investigation, and how it relates to STATS19.

Hospital Episode Statistics (HES)

Hospital Episode Statistics are compiled by the Department of Health and record details of all hospital admissions, finished consultant episodes and hospital discharges for England. Data of this type has been collected since 1989, with its main purpose being to ensure correct funding of hospitals from their Primary Care Trust (PCT) [1]. HES contain data such as age, sex, dates of admission and discharge, diagnoses, operations and procedures, place of residence and ethnicity, with approximately 12 million new records being added each year. Information regarding the diagnosis of injury and its causation is coded using the 'International Classification of Diseases' (ICD), of which the latest version ICD-10 has been used since 1995. Injuries

sustained in road traffic accidents can easily be identified when coded in this way. It should be noted that HES do not include details of any casualties treated in Accident and Emergency (A&E) that are not admitted to hospital [2].

Great Britain's National Road Casualties Database (STATS19)

STATS19 data is comprised of the details of road traffic accidents attended by the police in Great Britain. The Police are required to attend every road traffic accident that involves an injury and whilst on scene, officers fill out a series of standard forms. Officers make a judgement, often without further information from hospitals, and record the severity of the injured casualties and the overall accident as 'slight', 'serious' or 'killed'. This data is then collected, collated and analysed by the UK's Department for Transport (DfT).

STATS19 is, in principle, the national database in which all traffic accidents that result in injury to at least one person are recorded, although it is acknowledged that some injury accidents are missing from the database and a few non-injury accidents are included [3]. The database primarily records information on where the accident took place, when the accident occurred, the conditions at the time and location of the accident, details of the vehicles involved and information about the casualties. Approximately 50 pieces of information are collected for each accident [4].

The accidents that are recorded in STATS19 are summarised annually in the DfT "Road Casualties Great Britain" (RCGB) series.

Overview Of Accidents In Great Britain

The number of killed and seriously injured road casualties per year has been decreasing for pedestrians from 1996 to 2006 (see Figure 1); however the decrease has been less from 2004 to 2006. This trend is the same for pedal cyclist and car user casualties. Motorcyclist casualties increased between 1996 and 2003, decreasing back to the 1994-98 average by 2006.

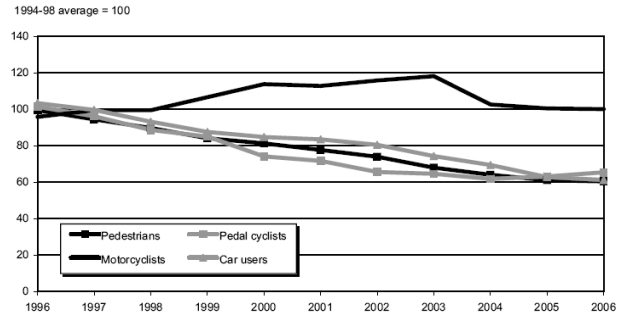


Figure 1. Trend of road casualties in Great Britain by road user type [5].

In 2006, 1.2% of all road user casualties suffered fatal injuries. Both pedestrians and motorcyclists had above average rates of fatalities with 2.2% and 2.6% of those injured being killed respectively [4]. In total, of all the fatally injured casualties on Britain's roads in 2006, 675 (21%) were pedestrians. Of all the killed or seriously injured casualties, 7,051 (22%) were pedestrians.

Apart from being a large group of the road casualties in Great Britain, there are a number of reasons for investigating pedestrians in HES and STATS19. Arguably, compared to car occupants, the injury epidemiology and characteristics of pedestrians are less well understood, because of the lack of large pedestrian-focused accident studies.

Supported by the European Commission (EC), the European Enhanced Vehicle-safety Committee Working Group 10 (EEVC WG10) and 11 developed testing methods and standards for pedestrian protection in frontal impacts with cars. These new standards have been introduced in a 2-stage approach, the first of which was the EC Directive 2003/102/EC. This directive introduced a number of tests, including limits on the results of impacts between a lower leg form and the bumper, and a head form to the bonnet top. This new pedestrian legislation has meant that the design of cars has and will continue to change, so it is important to find any corresponding change in pedestrian injury epidemiology.

In addition to the pedestrian regulation, Euro NCAP undertakes pedestrian sub-system impactor tests. Leg forms impact with the bumper and the bonnet leading edge and the head forms (child and adult) strike the bonnet at a variety of locations. As of 2009, the pedestrian tests have become an integral part of the new overall score given by Euro NCAP for any new car [5].

Pedestrian casualties are amongst the most vulnerable road users. Children have a large exposure to traffic as pedestrians, especially on their journey to and

from school. Elderly people, who may not have another form of transport available to them, are also exposed and at greatest risk of serious injuries if they are involved in an accident. These are also the two groups of pedestrians who are proportionally less well equipped for the road-crossing task.

Previous studies [3] have found that the difference in the number of casualties recorded in HES and STATS19 is greatest for vulnerable road users. Vulnerable road users include pedal cyclists and pedestrians; the relationship between HES and STATS19 for pedal cyclists has already been explored [4].

METHODOLOGY

This section explains some of the systems that were used to analyse the databases which are referred to later in the paper.

International Statistical Classification of Diseases (ICD) - In HES, injuries are recorded in 14 fields (7 before April 2002), which contain information about a patient's illness or condition [6]. The first of these fields contains the primary diagnosis and the other fields contain secondary/subsidiary diagnoses. The codes are defined in the International Statistical Classification of Diseases, Injuries and Causes of Death [7]. HES records currently use the tenth revision (ICD-10). Diagnosis codes start with a letter and are followed by two or three digits.

The ICD-10 codes are recorded in HES in both their 3-character and 4-character formats. The first 3 characters of the ICD-10 code provide the core classification of the injury, whereas the first 4 characters of the code provide a more specific injury description. An example of this would be a 3-character code of "S01 – an open wound of the head" [7]. When split into its 4-character codes it could be any of the following:

- S01.1 – Open wound of eyelid and periocular area
- S01.2 – Open wound of nose
- S01.3 – Open wound of ear
- S01.4 – Open wound of cheek and temporomandibular
- S01.5 – Open wound of lip and oral cavity
- S01.7 – Multiple open wounds of head
- S01.8 – Open wound of parts of head
- S01.9 – Open wound of head, part unspecified

Operation Codes - There are twelve fields in HES (four prior to April 2002), which contain information about a patient's surgical operations. The first code contains the main (i.e. most resource intensive) procedure. The other fields contain secondary procedures. The codes are defined in the Tabular List of the Classification of Surgical Operations and Procedures. The current version is OPCS4 [8]. Procedure codes start with a letter and are followed by two or three digits. The third digit identifies variations on a main procedure code containing two digits. A single operation may contain more than one procedure.

RESULTS

This section of the paper presents an overview of the two datasets, and compares the datasets where possible. Comparisons include the number of pedestrian casualties in both databases, the vehicles involved in the accidents, and the age and gender of the pedestrian casualties. The data analysed for this report included all pedestrian casualties contained in HES from April 1998 to March 2007 in England, and all the killed or seriously injured pedestrian casualties in STATS19 from April 1998 to March 2007 in England. The period of April to March is referred to as a 'financial year'.

It is expected that the majority of pedestrian casualties recorded in HES should be present in STATS19. This is because of the definition of a "serious" casualty in STATS19, which includes "detention in hospital as an in-patient, either immediately or later" [9]. Most of these should be in HES, which contains all patients "admitted" to hospital. The reverse is not true: there are likely to be many pedestrians in STATS19 who would not appear in HES. This could be because they had an injury which did not require admission to hospital, or because they died at the scene so were not admitted to hospital.

Summary of Casualties

Hospital Episode Statistics - In HES there were 82,908 admissions and 80,116 patients in the original dataset, which shows that some of the patients were admitted more than once. However, some of these admissions were duplicated in the dataset due to coding errors, once these were removed, there were 82,811 unique admissions for the 80,116 patients. This is summarised in Table 1.

Table 1.

Number of admissions and patients in HES

Number of admissions in original dataset	82,908
Number of patients in original dataset	80,116
Number of unique admissions, after duplicate records removed	82,811
Number of patients, after duplicate records removed	80,116

These admissions were then broken down by their accident type classification, using their 4 digit causation code. From these codes the admissions which were described as non-traffic or unspecified non-traffic were eliminated for comparison with STATS19. This resulted in 72,878 admissions for analysis.

Police Statistics (STATS19) - The pedestrian casualties used for analysis in STATS19 were selected to be only those who were killed or seriously injured as only these pedestrians could have been admitted to hospital and therefore be in the HES dataset. In the same 1998 to 2007 time period there were 64,233 pedestrian accidents in England recorded in STATS19. This consisted of 64,253 vehicles and 65,526 pedestrian KSI casualties. The casualties in this dataset were only those of fatal or serious severity, the 65,526 casualties consisting of 6,000 fatalities and 59,526 seriously injured pedestrians.

Accident Characteristics

Admission Date - The year in which the patient was admitted is recorded in HES and is compared, in this section, to the year of accident in STATS19. Figure 2 shows the number of HES admissions per year split by the type of accident as recorded by 4 digit causation code. As described earlier, from these codes the admissions which were described as non-traffic or unspecified non-traffic were eliminated for comparison with STATS19. From this figure it can be seen that the number of pedestrians recorded in HES who were selected for analysis decreased from 8,907 admissions in 1998 to 7,726 in 2003, but has been at a fairly constant level of around 7,800 admissions from 2003 to 2007. STATS19 data shows pedestrian accidents to have been on a steady decrease throughout the financial year groups decreasing from 8,888 in 1998/99 to 6,132 in 2006/07.

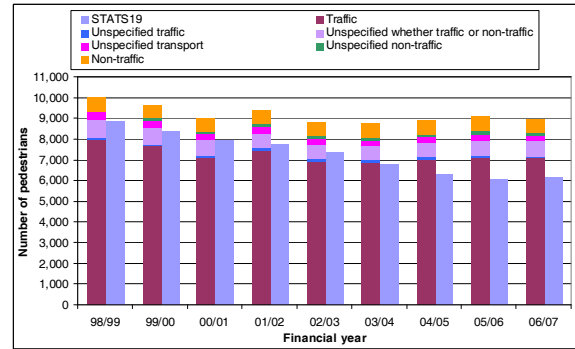


Figure 2. Number of pedestrian casualties from 1998 to 2007 in HES and STATS19

This shows that at the beginning of the years analysed, the numbers of pedestrian accidents recorded were very similar in both datasets, however, in recent years the numbers have become less similar. These fluctuations could be due to a number of reasons. It should be noted that a warning is given on the HES website about the admission date data stating:

“Fluctuations in the data can occur for a number of reasons, e.g. organisational changes, reviews of best practice within the medical community, the adoption of new coding schemes and data quality problems that are often year specific. These variations can lead to false assumptions about trends.” [6].

Vehicle Type - The accidents recorded in both STATS19 and HES were broken down by the vehicle type that struck the pedestrian. The vehicle type categories were selected based on the codes used in HES.

From analysis of the HES data, it was found that the majority, 84%, of the pedestrians admitted were struck by vehicles in the “Car/pickup/van” category compared to 86% of those in STATS19. The percentage of pedestrians struck by a pedal cycle in HES was 3% which is higher than the 1% of those in STATS19, in contrast, the number of pedestrians struck by “Heavy transport vehicles” in STATS19 was 8%, which was higher than the 6% of pedestrians in HES. Overall the distributions of the vehicle types that struck pedestrians look very similar.

Casualty Characteristics

Gender - The difference between the gender percentages in STATS19 and HES were minimal. Males were the most frequent in both datasets with 61% of STATS19 pedestrians and 63% of HES pedestrians being male.

Age - The age of pedestrian casualties peaked for 5-20 year olds in both datasets, with around 19% of casualties aged 10-15 in both datasets. For the younger age groups (particularly the 0-9 year olds), the percentage of casualties in STATS19 was lower than the percentage in HES. Overall the distribution of age in the datasets looks similar.

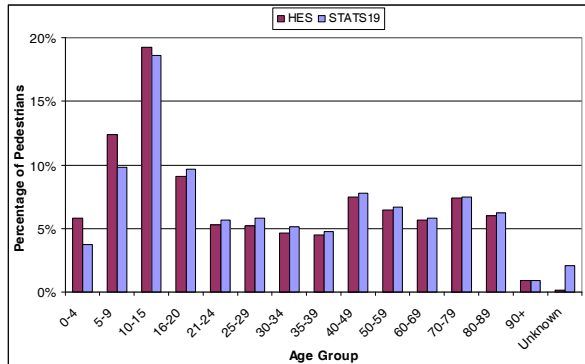


Figure 3. Age of pedestrian casualties in HES and STATS19.

When split by gender, a second peak was seen for females of 70 to 89 years of age (Figure 5), whereas males aged over 20 years peaked in pedestrian casualties at the age of 40-49 (Figure 4). These peaks occurred at the same ages for both HES and STATS19 datasets.

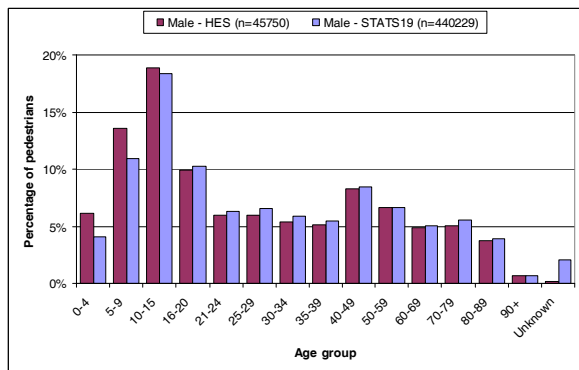


Figure 4. Age of male pedestrians by gender in HES and STATS19.

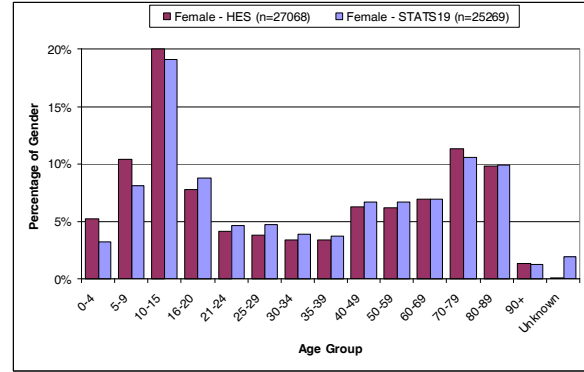


Figure 5. Age of female pedestrians by gender in HES and STATS19.

Injury Characteristics

Analysis in this section used the ICD-10 diagnosis codes to analyse the most frequent injuries, injury regions and numbers of injuries received by pedestrians in HES. Also investigated in this section, is the number and type of operations received by pedestrians as classified in OPCS4. ICD-10 and OPCS4 are described in the methodology section of this paper.

Overall Severity - STATS19 records the overall severity of the injuries received by the pedestrian which has been analysed in this section.

Overall, 91% of KSI pedestrian casualties in STATS19 were recorded to be serious and 9% fatal. From Figure 6 it can be seen that males proportionally suffered more fatal injuries when involved in pedestrian accidents than females.

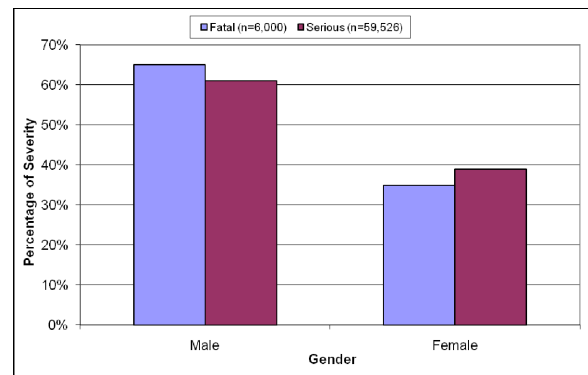


Figure 6. KSI pedestrians' severity split by gender in STATS19.

Figure 7 shows that younger pedestrians received a higher proportion of serious injuries, with older pedestrians being those that were killed more frequently in pedestrian accidents.

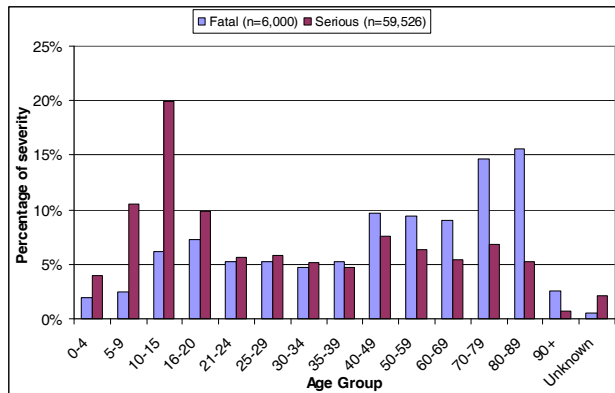


Figure 7. Severity split by age group for KSI pedestrians in STATS19.

ICD Analysis - The most frequently injured regions coded as primary injuries in HES using 3-character ICD10 codes are shown in Figure 8. The most frequent injury, received by 12,442 of the pedestrians in HES was a fracture to the lower leg including ankle, followed by 9,345 with unspecified injuries of the head. Of these most frequent injuries, a large proportion were other injuries to the head and legs.

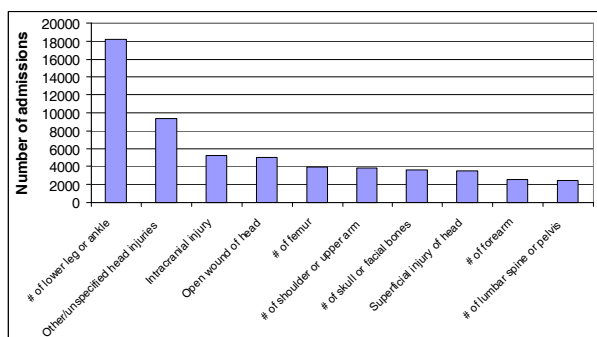


Figure 8. Most frequent primary injuries (using 3-character code) in HES.

The injuries coded using the 4-character codes were then analysed and are shown in Figure 9. The most frequent primary injury in this field was an unspecified injury to the head, which 9,051 pedestrians had. Fractures to the shaft of the tibia were present in 6,987 of the pedestrians. The next two top injury categories were also fractures to the tibia, with 3,526 pedestrians receiving fractures to the lower end of the tibia and 3,054 with fractures to the upper end of the tibia.

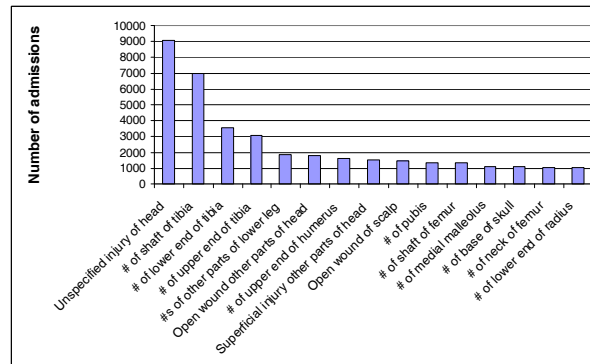


Figure 9. Most frequent primary injuries (using 4-character code) in HES.

When grouped into body regions it was found that 38% of pedestrians had head injuries as their primary diagnosis and 29% had knee and lower leg injuries.

When all the injuries for each pedestrian were combined (i.e. the primary injury and all secondary/subsidiary injuries recorded) and the region of these injuries defined, the head and neck was the most frequently injured region still with 38% of the injuries being to this region. The next most frequently injured region was the lower limb region (does not include pelvis) with 32% of the injuries occurring here.

Operations - From analysis of the number of operations each pedestrian underwent, it was found that 52% of the 72,878 pedestrians had no operations after their accidents. Of those that had operations, the most common number of operations to have was three; 16% of pedestrians had three operations and 38% had three or more operations.

The areas of the primary operations recorded in HES for pedestrians were also analysed. After the “no operation” category, the most frequent operation area was “other bones and joints” with 21,066 pedestrians having an operation in this area. “Other bones and joints” includes any bones and joints other than those in the neck and spine.

Assuming that the majority of primary operations were carried out on the primary injury regions, most (75%) of the other bones and joints operations were performed on those with leg injuries. Arm injuries were the next highest injury category with 18% of other bones and joints operations correlated with this region.

Injury Numbers - The number of injuries recorded in HES for each pedestrian was calculated and is presented in Figure 10. It should be noted that the increase in the number of injuries which could be recorded in the HES dataset increased from 7 in 2002

and therefore only 3% had 7 or more injuries. Pedestrians with only one injury made up 33% of the sample, the percentage of pedestrians then decreased with the increasing number of injuries.

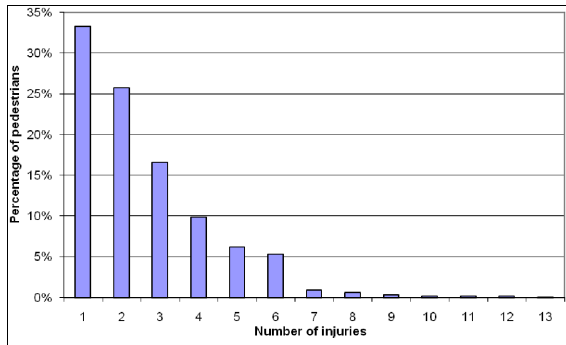


Figure 10. Number of recorded injuries for pedestrian casualties in HES.

Injuries with respect to age - The percentage of pedestrians with head injuries decreased with increasing age, as can be seen in Figure 11. Hip and thigh injuries were fairly constant for all ages until 59 years of age, after which the percentage of the age group with injuries in that region increased from 5% for 50-59 to 16% for those over 90. Knee and lower leg injuries had the opposite trend, decreasing from 30% for 60-69 year olds to 23% of over 90 year olds. Injuries in the shoulder and arm region were particularly low for those aged up to 9 years, but were then fairly constant for all other age groups.

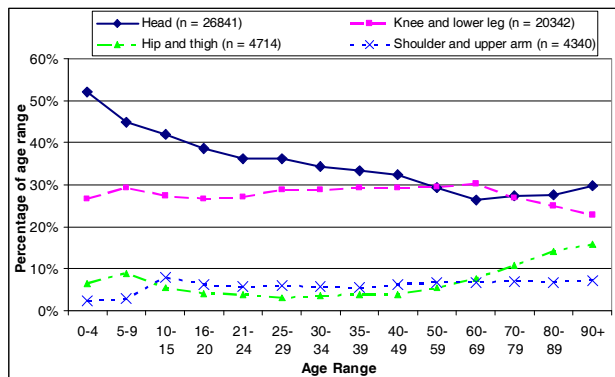


Figure 11. Relationship between the most frequent injuries and age of pedestrians, as a percentage of pedestrians in each age range in HES.

Injuries related to striking vehicle - Knee and lower leg injuries were the most common injury regions for pedestrians struck by all vehicle types apart from 2/3 wheel motor vehicles for which wrist and hand injuries were slightly more frequent. Pedestrians hit by heavy transport vehicles received

the highest rate of injuries to multiple body regions, the abdominal region and the shoulder. Pedestrians struck by pedal cycles received the highest rate of ankle and foot, and thorax injuries.

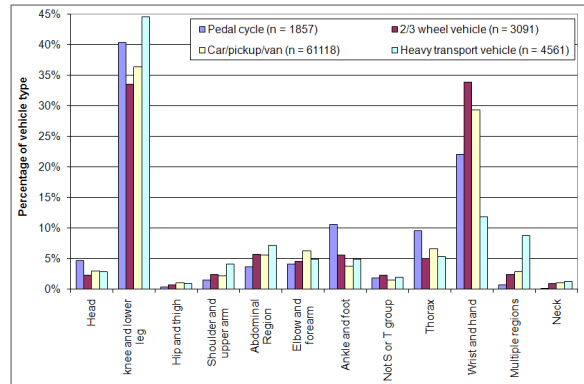


Figure 12. Pedestrian injuries caused by different vehicle types in HES.

Injuries related to time in hospital - It can be seen in Figure 13 that the number of pedestrians who stay in hospital for 0 days increased from 745 in 1998/99 to 1,345 in 2006/07. This may be due to the improvement in treatment over this time period or could be due to changes in admission procedures. It could also potentially be due to an increase in traffic congestion and therefore lower impact speeds so lower severity injuries or the better and/or different vehicle designs. The number of pedestrians in hospital for 2 or more days has decreased from 5,093 to 3,494, but the stays of 1 day (and unknown stays) remained fairly constant at about 2,000 pedestrians per year.

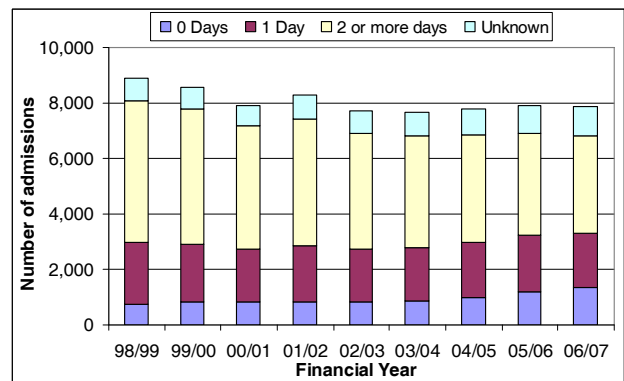


Figure 13. Number of pedestrian admissions from 1998-2007, and duration of stay in HES.

The duration of stay for pedestrians peaked with 25% of pedestrians staying for 1 day. The next two most frequent lengths of stay were 0 or 2 days both accounting for 11% of pedestrians.

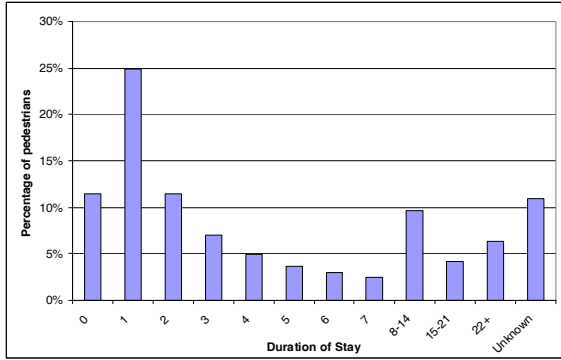


Figure 14. Duration of stay as a percentage of the number of pedestrians in HES.

When comparing primary injury regions with duration of stay, it can be seen that the length of stay for those with head injuries peaked at 1 day, whereas those with knee and lower leg injuries peaked at 2 days. Patients who were admitted for 2 days or more, most commonly had leg injuries compared to head injuries.

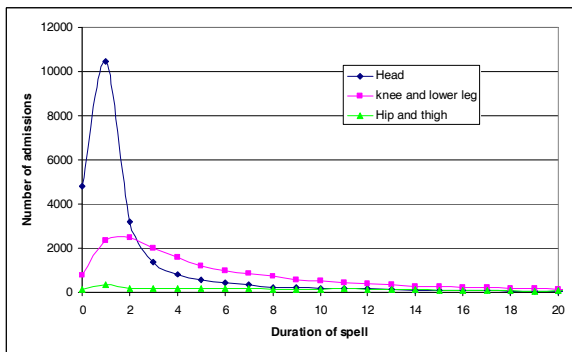


Figure 15. Duration of stay at hospital for pedestrians with the three most frequently injured body regions in HES.

Figure 16 is a box plot which shows how primary injuries in different regions related to the length of time spent in hospital. The central horizontal line within the bars gives the median duration of stay, and the bars themselves give the upper and lower quartiles. The lines extending from the bars contain approximately 99% of the pedestrians. The circles and stars outside these lines are outliers. The body regions themselves are sorted by the mean duration of stay, descending from the left. The mean duration of stay for the different injury regions is shown in Table 2.

Primary injuries to the hip and thigh were associated with the longest mean and median duration of stay in hospital. There were a lot of outlying points for injuries to all body regions, where the pedestrian had been in hospital for a relatively long time. This was especially true for injuries to the head, where the

quartiles of the duration of stay were close together, but there were a lot of outliers who were in hospital for much longer. This seems to be because a large number of pedestrians had relatively minor head injuries, and were only in hospital for one day, compared to a relatively small sub-set who spent over 5 days in hospital with serious or life threatening head injury.

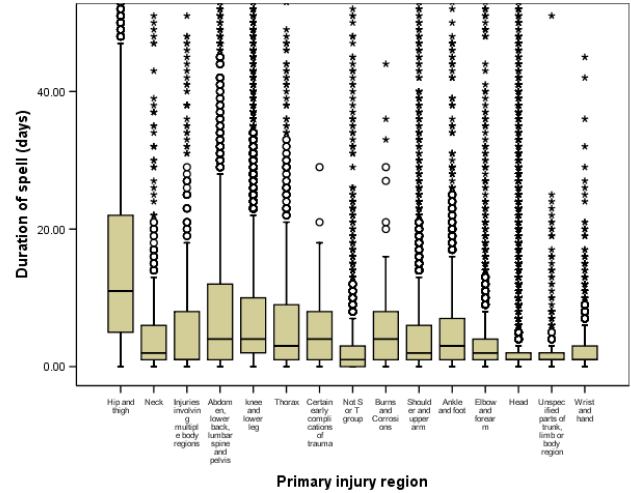


Figure 16. Mean duration of stay, by region of primary injury in HES.

Table 2. Mean duration of stay by primary injury region in HES

Primary injury region	No. of pedestrians	Mean duration of stay (days)
Hip and thigh	4714	16.7
Neck	695	15.1
Injuries involving multiple body regions	732	10.4
Abdomen, lower back, lumbar spine and pelvis	4085	10.2
knee and lower leg	20342	8.9
Thorax	1670	8.1
Certain early complications of trauma	100	6.7
Not S or T group	2183	6.4
Burns and Corrosions	122	6.3
Shoulder and upper arm	4340	6.1
Ankle and foot	2355	5.9
Elbow and forearm	2964	4.7
Head	26841	3.7
Unspecified parts of trunk, limb or body region	481	3.4
Wrist and hand	1212	2.6

These injuries were then broken down into the more specific injuries as shown in Figure 17, which gives the 10 injuries with the highest mean duration of stay, received by at least 100 pedestrians. The injuries are coded using the 4 character ICD code, the descriptions of which are given in Table 3. The longest mean duration of stay was 68 days for those pedestrians with fractured cervical vertebra. This large mean duration was due to two pedestrians who received this injury and were in hospital for 1,082 and 2,878 days.

The majority of other injuries which led to long durations of stay were fractures of the legs. As with the other body region injuries, there was a large spread in the duration of stay of the pedestrians suffering lower limb injuries.

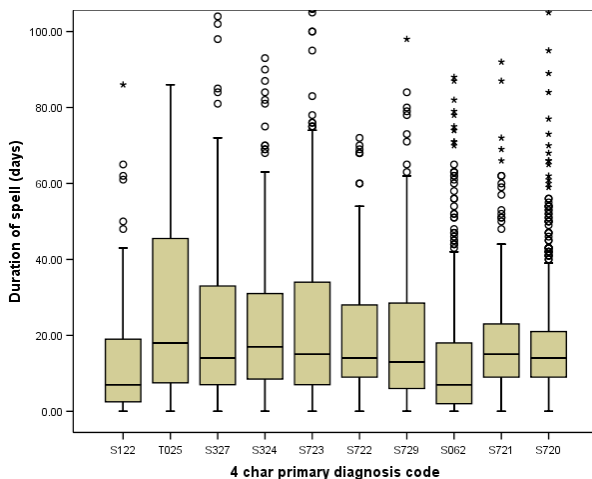


Figure 17. Mean duration of stay for injuries suffered by at least 100 pedestrians in HES.

Table 3. Descriptions of 4 character primary diagnosis codes in HES

4 char code	Injury description	No. of pedestrians	Mean stay duration (days)
S122	Fracture of other specified cervical vertebra	101	67.5
T025	Fractures to multiple regions of both legs	100	33.9
S327	Multiple fractures of lumbar spine and pelvis	150	25.3
S324	Fracture of acetabulum	308	24.4
S723	Fracture of shaft of femur	1335	21.9
S722	Subtrochanteric fracture of femur	154	20.9
S729	Fracture of femur, part unspecified	336	20.3
S062	Diffuse brain injury	924	19.1
S721	Petrochanteric fracture of femur	379	18.6
S720	Fracture of neck of femur	1067	17.5

Changes Over Time

The large amount of data present in the HES dataset from 1998-2007 enabled some variations in pedestrian injuries over time to be investigated.

Table 4 compares the ten most frequent injuries recorded in 2006/2007, using the 3-character ICD codes.

Table 5 compares the most frequent 4-character ICD codes recorded in 2006/2007. In these tables, the percentage point difference to the 1998/1999 figures for that injury are presented in brackets.

Although the most frequent injuries have changed very little, the changes in the proportion of pedestrians receiving these injuries paint an interesting picture. With the exception of “fractures of other part of lower leg”, all of the injuries which have increased in proportion are relatively minor, while those that have decreased are fractures and other serious injuries. This suggests that pedestrians received less severe injuries in 2006/2007 compared to those in 1998/1999.

Table 4.
Most frequent 3-character ICD codes, 2006/2007 in HES

Injury description	No. of pedestrians	% of pedestrians
Fracture of lower leg, including ankle	1867	23.7 (-1.6)
Other and unspecified injuries of head	816	10.3 (-4.1)
Open wound of head	616	7.8 (+1.9)
Intracranial injury	524	6.6 (-1.4)
Superficial injury of head	519	6.6 (+2.7)
Fracture of shoulder and upper arm	400	5.1 (-0.5)
Fracture of femur	383	4.9 (-1.3)
Fracture of skull and facial bones	382	4.8 (-0.6)
Fracture of lumbar spine and pelvis	268	3.4 (-0.2)
Fracture of forearm	266	3.4 (-)

Table 5.
Most frequent 4-character ICD codes, 2006/2007 in HES

Injury description	No. of pedestrians	% of pedestrians
Unspecified injury of head	791	10.0 (-3.8)
Fracture of shaft of tibia	646	8.2 (-2.4)
Fracture of lower end of tibia	367	4.7 (-)
Fracture of upper end of tibia	298	3.8 (-0.4)
Open wound of other parts of head	233	3.0 (+0.7)
Fractures of other parts of lower leg	215	2.7 (+0.2)
Superficial injury of other parts of head	198	2.5 (+0.9)
Open wound of scalp	179	2.3 (+0.8)
Fracture of upper end of humerus	157	2.0 (-0.5)
Superficial injury of head, part unspecified	150	1.9 (+0.9)
Fracture of pubis	140	1.8 (-0.3)
Fracture of shaft of femur	100	1.3 (-1.2)
Intracranial injury, unspecified	40	0.5 (-1.5)

Figure 18 shows the change with respect to time of two of the injuries which were shown to have reduced in frequency between 1998/1999 and 2006/2007. These were the fractures to the shaft of the tibia and femur. This graph shows that there has been a steady decline in these injuries over the last few years.

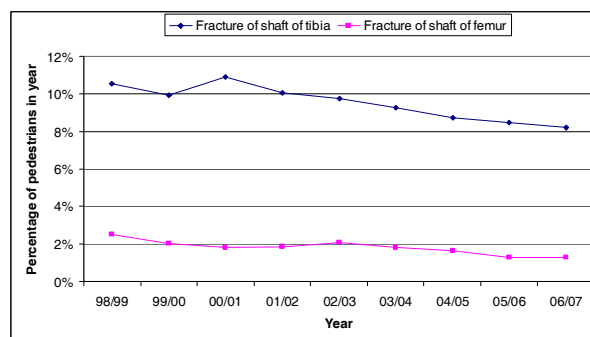


Figure 18. Distribution of pedestrians receiving tibia and femur fractures in HES by year.

Figure 19 compares the distribution of the primary injuries for the pedestrians admitted in 1998/1999 and 2006/2007. There was a small decrease in the proportion of head and/or neck and lower limb injuries, and a slight increase in the proportion of upper limb and thorax injuries.

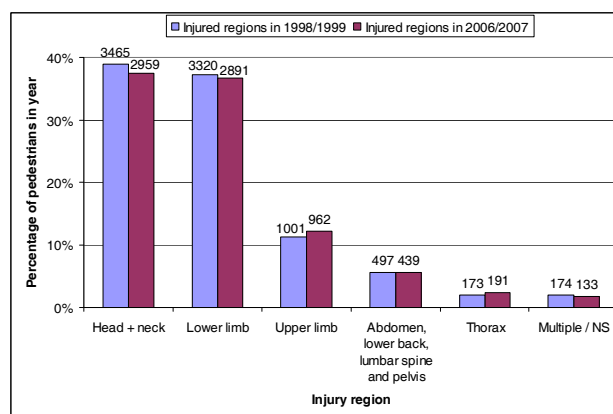


Figure 19. Distribution of injury regions in 1998/1999 and 2006/2007 in HES.

Figure 20 compares the age distribution in 1998/1999 and 2006/2007 of the pedestrians in the HES dataset. This shows that the largest difference was a reduction in the number of 5-9 year old pedestrian casualties. The most significant proportional increase was for pedestrians aged 40-49 years.

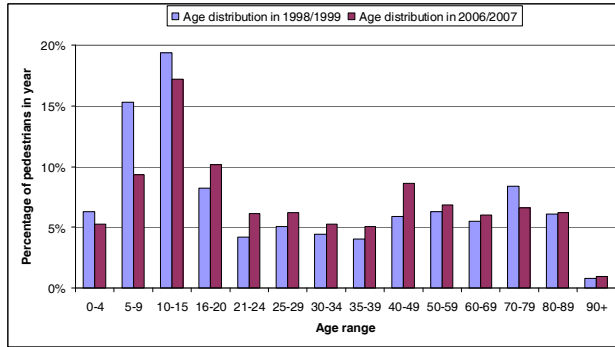


Figure 20. Age distribution of HES pedestrian casualties in 1998/1999 and 2006/2007 in HES.

Figure 21 shows how the proportion of pedestrians aged 5-9 and 40-49 varied from 1998/1999 to 2006/2007. This shows that the change in the proportion of both 5-9 and 40-49 years olds has been relatively constant since 1998/1999. Figure 22 shows that a reduction in the proportion of 5-9 year olds was also present in STATS19. This suggests that the change in the proportions of these pedestrians was related to some real change, and not just statistical variation or changes in recording practices, and this will correlate with injury changes.

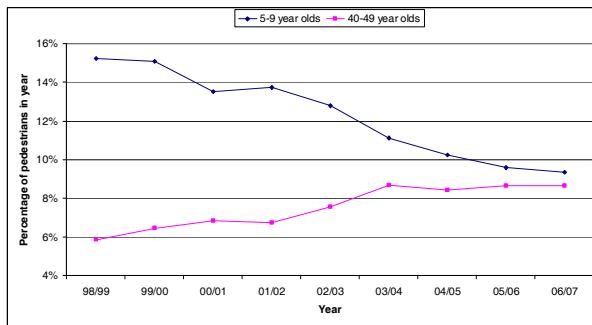


Figure 21. Change in time of proportion of pedestrians aged 5-9 and 40-49 years in HES.

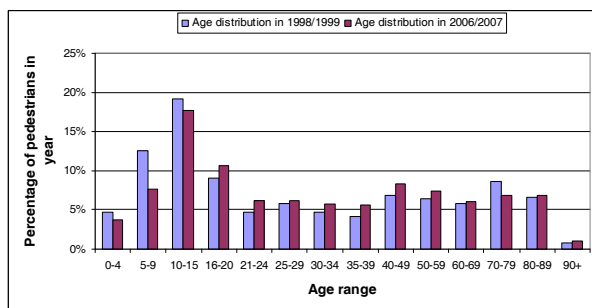


Figure 22. Age distribution of pedestrian casualties in 1998/1999 and 2006/2007 in STATS19.

In addition to age, the variation in the gender of the pedestrians over time was analysed in both datasets.

This showed that there was very little change in the proportion of pedestrians who were male or female from 1998/1999 to 2006/2007.

The change in the distribution of the vehicles involved in the pedestrian accidents in 1998/1999 and 2006/2007 was also analysed in STATS19 and HES. There was a slight increase in the proportion of pedestrians impacted by heavy transport vehicles, and a slight decrease in the proportion of pedestrians struck by cars/pickups/vans.

Figure 23 shows how the proportion of pedestrians struck by heavy vehicles and cars varied in the HES dataset from 1998/1999 to 2006/2007. The proportions of the two vehicles are shown on different scales because of the large difference between them. This figure shows that the proportion of pedestrian accidents involving heavy vehicles has been steadily increasing. The proportion due to impacts with cars/pickups/vans decreased from 1998/1999 to 2003/2004, but since then remained relatively constant.

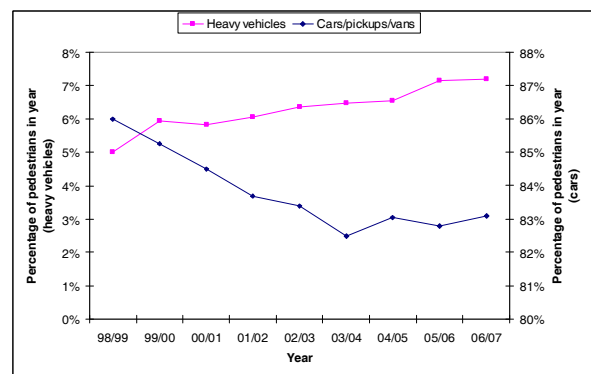


Figure 23. Change in time of proportion of pedestrians struck by heavy vehicles and cars in HES.

DISCUSSION

Comparing the number of pedestrians recorded in HES and STATS19 from 1998 to 2007 showed that while the number of pedestrian admissions in HES has remained relatively constant, the number of killed and seriously injured pedestrians recorded in STATS19 has reduced considerably from 1998 to 2007. This may be due to a number of reasons. Possibly the most important is the warning that HES gives on its data stating that fluctuations can occur due to such factors as organisational changes, reviews of best practice within the medical community, the adoption of new coding schemes and data quality

problems that are often year specific. STATS19 may also be subject to variations in the number of pedestrian accidents recorded per year due to factors such as the number of pedestrian accidents that are actually reported to the police. Reasons for these differences have been discussed previously by other authors [10, 11, 12, 13].

Comparisons of age and gender showed that in general the two datasets are very similar with respect to these casualty characteristics. The largest difference is an increase in the proportion of pedestrians in HES aged 0-9 years old. At the time of writing the reason for this difference is not clear, but potentially could be associated with under-reporting by the police of these collisions, due to their characteristics.

STATS19 can also be used to distinguish between killed and seriously injured pedestrians, information which was not contained in the HES data. This shows that males were slightly more likely to be involved in fatal accidents, and that children were more likely to survive the impact than older pedestrians. This is believed to be because of their greater tolerance to injury and their different sizes and potentially crash types.

Injuries

The most valuable part of the HES dataset is the injuries it records for pedestrians, data which is not available in any other database on such a large scale.

The most frequent injuries recorded for the pedestrians in HES are head and lower leg injuries. This is true whether the 3-character or the more detailed 4-character ICD codes are used.

Using the 4-character ICD codes, the most frequent injury is “unspecified injury of head”, however, we do not know the severity of this injury due to the ICD coding system not including a measure of injury severity. This also means that different injuries can not be compared with respect to their severity.

The next four most frequent injuries are all fractures of the lower leg, and the majority of the top ten most frequent injuries are head and leg injuries. This agrees with previous studies on smaller samples of pedestrians [14].

The relationship between the age of the pedestrian and the proportion of injury in the four most frequently injured regions was investigated. This showed that the rate of head injuries decreases with age, and the rate of hip and thigh injuries increases with age. The rate of hip and thigh injuries increases most above the age of 60, which would coincide with

the decreasing bone density and strength of older people, especially women. This would help to explain why the number of female pedestrian casualties increases above the age of 70.

The incidence of head injuries was greatest for young children (0-9), which is likely to be because they will receive a more direct contact to the head from the front of the vehicle, because of their height. From the age of 16 and older, the proportion of pedestrian casualties with a head injury remains relatively constant. It might be expected that elderly pedestrians would also see an increase in head injuries because they are generally less tolerant to injury. However, it may be that these pedestrians are being seriously injured at lower impact speeds (receiving leg fractures), which may counterbalance their reduced tolerance to head injuries. Some knowledge of impact type and speeds involved would be required to determine whether or not this was true.

Duration of Stay

The duration of the stay in hospital is one way in which the HES data can be used to estimate the cost to the hospital of different injuries and the severity with respect to the affects on the casualties' life. Overall the duration of stay in hospital of the pedestrian casualties in HES is a very skewed distribution, with a large number of pedestrians staying for only one day, and a very small number of pedestrians remaining in hospital for very long periods of time. This distribution is a similar shape when individual injuries are investigated. For this reason, the relationship between individual injuries and the duration of stay in hospital has been investigated using the mean stay in hospital, and box-plots showing the distribution of the length of stay for different injuries.

Measuring the mean duration of stay shows that injuries to the hip and thigh and neck result in the longest average stay in hospital. Injuries to the hip and thigh are also some of the most frequent so, combined with the long duration of stay in hospital, injuries to this region will be some of the most costly. This could, however, also be due to the hip and thigh injuries frequently being associated with older women who generally stay in hospital longer for all injuries.

Looking at individual injuries shows that a fracture of the cervical spine leads to the longest mean duration in hospital, but this is mainly due to one pedestrian who received this injury and remained in hospital for almost eight years. Apart from this spinal injury, multiple fractures of the lower legs led to the longest

mean stay in hospital. The remainder of the ten longest mean durations of stay in hospital are mostly made up of fractures to the femur.

There are a number of limitations to using this method of determining which injuries are most costly to the hospitals. The first is that it only takes into account the primary injury, and not any other injuries sustained. Secondly, it does not take into account other costs, such as operations and procedures in the hospital, post-hospital care, and the effect on quality of life. These are things which could be investigated, but would need information other than that in the HES data.

The HES data provided to TRL covers a period of nine years, and the large number of pedestrians recorded in each year has enabled some of the changes over time to be investigated. Some injuries, such as fractures to the shaft of the tibia and fibula, show a small but steady decline over the ten year period. This could be evidence that improved car design in recent years has reduced the rate of these injuries. However, further evidence would be required relating to the characteristics of the crashes and injury mechanisms before this could be known.

The most startling change over the 9 years of HES data is the way that the distribution of the age of the pedestrian casualties has altered. Specifically, the proportion of pedestrians aged 5-9 years has dropped from 15% to 10%, and the proportion of pedestrians aged 40-49 years has increased from 6% to 9%. It is not clear why these changes have occurred.

Previously it was shown that the proportion of 5-9 year olds was different in STATS19 and HES, which could have meant that the reduction in 5-9 year olds is caused by something which affects the HES data only. However, a drop in the proportion of 5-9 year old pedestrian casualties is also seen in STATS19. This is evidence that it is a real effect, which could perhaps be related to a reduction in the exposure of children to traffic, for example if fewer children walk to school. Or it could be related to road safety schemes aimed at this age group, such as the UK's THINK! campaign [15] proving effective.

Other changes over the nine years were a reduction in the proportion of casualties who were in impacts with cars, and a reduction in the proportion of casualties who lived in the 10% most socially and economically deprived areas of England.

CONCLUSIONS

TRL successfully collaborated with the South East Health Observatory (SEPHO) who provided Hospital Episode Statistics (HES) data for pedestrian casualties admitted to hospitals in England from April 1998 to March 2007. This data was analysed, along with STATS19, to explore what the dataset contained, how it could be used in the field of accident research, and how it compared to STATS19. A multi-disciplinary team of researchers designed the research study and undertook the work programme.

While the number of pedestrian casualties in HES remains relatively constant, the number of killed and seriously injured casualties in STATS19 has reduced over the last nine years. This difference matched the observations in previous research which looked at all road users.

In general, the distribution of age, gender, and striking vehicle were similar in STATS19 and HES. Apart from date, these were the only variables which could be directly compared.

The most frequent injuries recorded for pedestrians in the HES datasets were head and lower leg injuries. The most frequent individual recorded injury was "unspecified injury of head", followed by four different types of lower leg fractures.

The proportion of head injuries decreased with age, while hip and thigh injuries increased with age.

The duration of stay in hospital was used as a measure to determine which injuries resulted in the highest cost to the hospital. With the exception of the relatively infrequent cervical spine fractures, the injuries which resulted in the longest stay in hospital were leg injuries, especially fractures of the femur.

Leg injuries seem to be the area with the greatest potential for injury prevention. Tibia fractures were among the most frequent injuries, and femur fractures led to some of the longest mean durations of stay in hospital, so preventing these injuries may have the largest benefit in terms of cost to the hospitals.

There has been a large decrease in the proportion of 5-9 year olds in the HES and STATS19 datasets over the last nine years.

ACKNOWLEDGEMENTS

The work described in this report was carried out in the Accident Research Group of the Transport Research Laboratory.

TRL would also like to acknowledge the contributions of Harry Rutter, Steve Morgan, Jo Watson and Bryony Tatem of the South East Public Health Observatory who supplied the data and information required for the analysis of the HES data, and provided help and advice throughout.

REFERENCES

- [1] Department for Transport (2007), *Road accident statistics in Great Britain: Levels of reporting*. A summary note on levels of reporting of road accidents statistics in Great Britain.
- [2] Department for Transport (2006), *Road accident casualties: a comparison of STATS19 data with Hospital Episode Statistics*.
- [3] Ward H, Lyons R, Thoreau R (2006), *Under-reporting of Road Casualties – Phase 1*. A report for the Department for Transport, with the Centre for Transport Studies - University College London and the Centre for Health information, Research and Evaluation – Swansea University.
- [4] Department for Transport, Scottish Executive, National Assembly for Wales (2007), *Road Casualties Great Britain 2006*.
- [5] EuroNCAP (2009), www.euroncap.com (retrieved on 12th March 2009)
- [6] HES (2009), <http://www.hesonline.nhs.uk> (retrieved on 12th March 2009)
- [7] World Health Organisation (1992), *International Statistical Classification of Diseases and Related Health Problems – Tenth Revision: Volume 1*. World Health Organisation.
- [8] Surginet (2009), OPCS4 search engine <http://www.surginet.org.uk/coding/opcs4.php> (retrieved on 12th March 2009)
- [9] Department for Transport (2004), *STATS20: Instructions for the completion of road accident report form STATS19*. <http://www.dft.gov.uk/pgr/statistics/datatablespublications/accidents/casualtiesgbar/> (retrieved 12th September 2008)
- [10] Goldacre M J, Gill M, Yeates D G (2006), *Changes in safety on England's roads: analysis of hospital statistics*. BMJ
- [11] Simpson H F (1996), *Comparison of hospital and police casualty data: a national study*. TRL Report TRL173. Crowthorne: Transport Research Laboratory.
- [12] Department for Transport (2006), *Road accident casualties: a comparison of STATS19 data with Hospital Episode Statistics*.
- [13] Department for Transport, Scottish Executive, National Assembly for Wales (2007), *Road Casualties Great Britain 2006*.
- [14] Cuerden R W, Richards D C, Hill J (2007), *Pedestrians and their survivability at different impact speeds*, Proceedings 20th International Technical Conference on the Enhanced Safety of Vehicles 2007.
- [15] Department for Transport (2009), Think campaigns, Children – pedestrians. http://www.dft.gov.uk/think/focusareas/children/childpedestrians?whoareyou_id (retrieved on 10th March 2009)

BENEFIT OF “DYNAMIC USE CASES” TO EARLY DESIGN A DRIVING ASSISTANCE SYSTEM FOR PEDESTRIAN/TRUCK COLLISION AVOIDANCE

Hélène Tattegrain,
Arnaud Bonnard,
Benoit Mathern,
LESCOT, INRETS
France
Paper Number 09-0489

ABSTRACT

The common approach to express Driving Assistance Systems (DAS) functionalities is often based on use cases that explain driving context and required assistance. However, DAS design requires temporal consideration of driving situation evolution when using the assistance, in order to define when the assistance is activated and which decision criteria is used. Driving situation complexity and its temporal progress cannot be easily appreciated without tools taking into account all actors (pedestrians, driver, vehicles...) and assistance effects on the scenario evolution.

This paper describes a software application that offers designers a light and simple way to early design, tune and test DAS functioning on progressing situations. This tool is developed in the VIVRE 2 project to support the early design of a DAS that warns truck drivers to avoid pedestrian collisions. In this context, the tool permits to test the DAS functioning by running “dynamic use cases” (static use cases enriched with additional inputs to reflect the temporal evolution). It allows the designer to build scenarios with specific parameters about driver, truck, pedestrians and assistance. It also proposes replay and trace features that help the analysis of the “dynamic use cases” combination. These iterative tests and adjustments of DAS allow determining decision criteria that works in all targeted situations.

To further efficient early design, the tool must stay light and easy to use. As a consequence, the temporal evolution models of actors are kept simple. Once the DAS functioning is validated, another design phase in more realistic conditions is required; to make sure that no unanticipated behaviour occurs, which may reduce the functioning.

This approach is crucial for early designing of a DAS to bring continuity to the use cases and to evaluate the consequences of any decision criteria modification on the global functioning in order to ensure driver warning efficiency.

INTRODUCTION

The approach to design assistance systems is most of the time based on “use case” (UC). These UC are developed to share a common view of system functioning between all partners in charge to design, to develop and to test the driving assistance. In fact, the functioning can not be easily defined by rules but has to be replaced in its context of use to understand the real wanted performance and the different factors which can influence or modify the final running. Some projects have defined some format to describe UC. For example, in AIDE project (which goal was to design a system to manage the information flow to the driver), the UC described the road context, the signals to be send, and the expected system functioning. For this application, the time constraints are not precise and a textual description was enough. But for others systems which have to deliver some urgent warnings like anti-collision warning, the time constraints are very important and textual description can only give qualitative functioning like “if a pedestrian is in front of the vehicle, the warning is diffused by auditive mode . In order to refine the functioning rules with quantitative values, some simulations are needed.

The purpose of this article is to present an approach developed in the VIVRE2 project. This approach was used during the design phase to tune a driver’s assistance system which warns truck drivers to avoid pedestrian collisions. This approach combines different use cases with different driver behaviours and different system tunings.

CONTEXT

The truck traffic increase is particularly critical in urban areas where the cohabitation between as different users as pedestrian and trucks creates a lot of critical situations. From a technical point of view, a lot of sensors are designed to run in less

complex road situations like on highways or in rural areas where mobile entities are easier to detect (big size) and where the number of objects to detect is limited. From a user's point of view, the pedestrian situation awareness is often incorrect due to his lack of knowledge about truck driving [1]. To evaluate risks, the pedestrian uses his driving knowledge which results from his experience as a car driver. He doesn't know the place and the size of dead zones around the truck. For example, the dead zone just in front of the vehicle can mask a too close pedestrian. A car front blind zone is small and can not mask objects taller than 50 cm. A truck front blind zone is higher and can mask objects taller than 1m like a child. Pedestrians do not realize that the trajectory of the backward part of the truck during a turn does not follow the trajectory of the front wheels and he can be surprised by the nearness of this part. A pedestrian does not picture the truck inertia and its braking length and he may make the decision to cross the road too late according to the truck speed and distance. Another aspect concerns the different situation awareness of actors depending on whether one considers the pedestrian's or the truck driver's point of view. In urban areas, trucks have to give way to pedestrians and pedestrians think that trucks have to stop. In this case, if the truck driver cannot or does not perceive the danger, the pedestrian will be quite within his rights but dead.

In the VIVRE2 project, a driving assistance system (DAS) was developed to prevent collisions with vulnerable users in urban areas, especially during delivery truck manoeuvres. This kind of truck has to drive into cities to deliver goods and must manoeuvre on urban roads.

In this project a truck driver needs study done by project partners (LEACM, INRETS, Renault TRUCKS) gives some information to determine the most critical situations and a set of classical Use Cases including the expected system functioning.

OBJECTIVES

To design this DAS, these Use Cases (UC) give the main functionalities to be included in the system (temporal sequences of warning display according to the road situation) but did not take into account all possible sequences.

The objective of this work is to create a tool and a method that take into account most of the possible case of assistance that system can provide in all different situation. It permits to synthesize and to harmonize all the needs of assistance in most of the target situations.

This is a way to enrich the classic Use Case generally used in DAS design.

DYNAMICS USE CASE DESCRIPTION

The main advantage of the DUC is to add easily variability to driving situation. It is composed by some elements coming from classical Use Case like a driving context (infrastructure, dangers to avoid); by the initial position and speed of major actors. But some other components, like a driver behaviour model, allow to increase the number of expected assistance system functioning variant according to the driver reaction at some system warning.

For the dynamic use case, a lot of variations can be added to test the DAS in several situations. The initial value of the truck speed can be 0 to 10 km/h. The initial pedestrian speed can be from 0 to 10, and the initial position can be on the road or on the walkway, at 1.5 or 10 meters

Then the functioning of the system is different. At 1 meter in front of the truck this is a start inhibit situation. At 10 meters in front of the truck, if the pedestrian is moving quickly enough not to be hit by the truck, the alarm will not go off. This shows that different combinations or variable values induce very different system functioning. Temporal aspects must be taken into account to efficiently design a driving assistance system.

The complexity of combinations of all parameters requires the use of a tool to generate the DUC but also to run them.

“DYNAMIC USE CASE RUNNER” ARCHITECTURE

This tool is composed of two principal parts (Figure 1):

- The generic part is composed of several modules focused on DUC temporal deployment.
- The specific part concerns the driving system assistance itself.

The main tool functionalities are:

- To define the scenario.
- To manage all objects involved in the UC. It concerns the equipped vehicle, the different actors like pedestrians, bicycles, cars, trucks.

To deploy the UC dynamic at each time step, the generator has to:

- Calculate the position of all mobile objects including the equipped vehicle. The dynamic of the equipped vehicle is also defined by driver reaction given by a driver behaviour model.

- Run the driving assistance (DA) on this time step.
- Use the DA decision to modify the equipped vehicle dynamics (acceleration, orientation) to be use into the next time step.
- Display the information to be sent to the truck driver.
- Display curves which describe the temporal evolution of the situation.

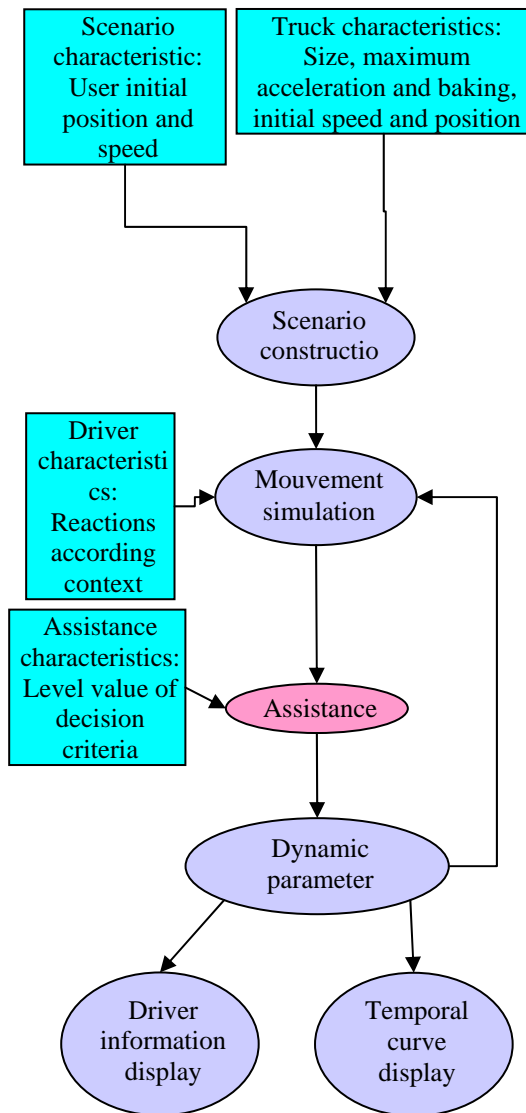


Figure 1. “Dynamic Use Case Runner” architecture

“DYNAMIC USE CASE RUNNER” PARAMETERIZATION

To run the UC, some parameters can vary to describe different UC variants. These parameters

are classified in several categories according to their use by the generator.

For the first module which creates the UC, the parameters are:

- Truck characteristics like size, acceleration maximum, braking maximum, initial position, initial speed.
- Scenario characteristics like position and speed of mobile object (vulnerable user, other vehicle).

For the module which simulates the mobile dynamics, the variable parameters concern:

- The driver characteristics which include the desired speed, the desired acceleration and some behaviour modifications according to Assistance System information like “stop acceleration after 1 second when warning occurs”.
- The trucks characteristics like acceleration maximum, ...

For the module which calculates the driving assistance decision, the variable parameters concern the different criteria of decision levels.

Another constraint was induced by this project. The system had to be validated on truck simulator with final users. The system integration on simulator had to be taken into account at the beginning of the project [2]. But the time necessary to develop the simulator database did not allow us to test the system functioning at an early stage; hence the “dynamic use case runner” was created to permit parallel developing of the database and of the system design phase.

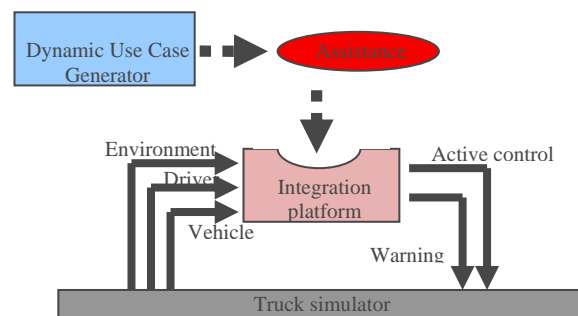


Figure 2 : integration principle

An integration platform (Figure 2) was then designed to manage the interaction between the truck driving simulator and the assistance system. Moreover, to avoid software translation problems and to gain some time, it was decided to use the same code for the “dynamic use case runner” and the integration platform.

This integration platform allows us to collect data, to replay data and to connect the driving assistance to the truck driving simulator.

“DYNAMIC USE CASE RUNNER” OUTPUT

The assistance is based on using several areas around the truck. Some of them monitor the front of the truck, others the truck rear and some of them the truck’s right side. The presence of a vulnerable user in one of these areas is transmitted to the decision module. This module also uses the driver activity analysis to adapt the warning level to make the decision.

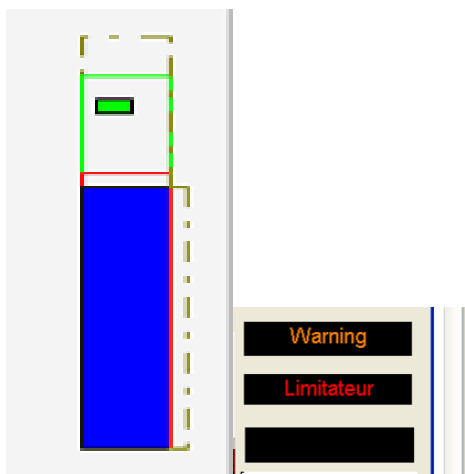


Figure 3. DUC runner Output

The tool presents (Figure 3) the truck on the road (blue rectangle) and displays the survey areas around the truck. The nearest is the “Braking zone” (red solid line), the further is the “speed limiter” zone (dotted line) and the intermediate is the “warning” zone (green solid line) . One “warning” zone is also in the right side of the truck

The Assistance decision is display when active controls or warnings occur.

“DYNAMIC USE CASE RUNNER” INTERFACE

The software window (Figure 4) is split in three parts:

- The first one concerns the DUC description including the driver, truck, assistance and scenario parameters.
- The second one represents the context situation which *changes over time*.
- The third one displays the temporal curves. The first two curves display the truck speed and the maximum acceleration authorised by the assistance. The last two curves display the level of

assistance in terms of active control (no control, speed limiter and urgency braking) and warning level (no information, danger indication or warning).

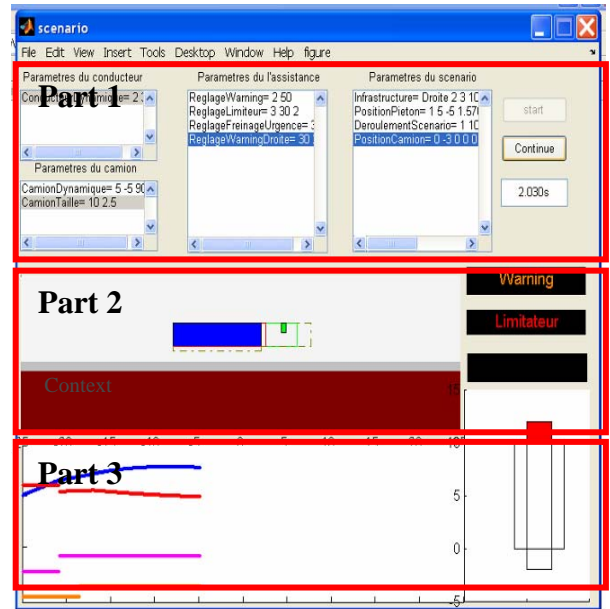


Figure 4. Software interface

DYNAMIC USE CASE RUNNING

The DUC used in these examples is located on a straight on line with walk side. The pedestrian is on the walkway and is heading for the road when the truck starts. In the first example, the pedestrian speed is 5 Km/h and in the second one it is 2km/h. These two examples are different variant of the same DUC.

Example 1: Speed limitation.

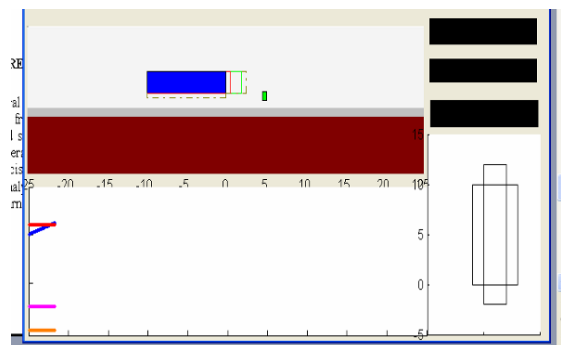


Figure 5: Speed limitation UC step 1

At the beginning (Figure 5), the pedestrian is on the walkway and is heading for the road at 5 km/h. The truck has just started and its initial speed is 0 Km/h.

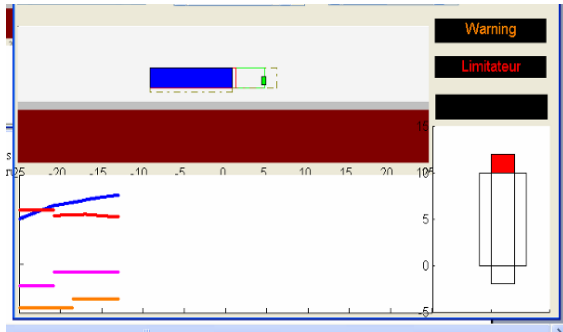


Figure 6: Speed limitation UC step 2

The pedestrian is then in the warning and speed limiter areas (Figure 6). The maximum acceleration allowed by the system is decreased and the active control and warning levels are increased.

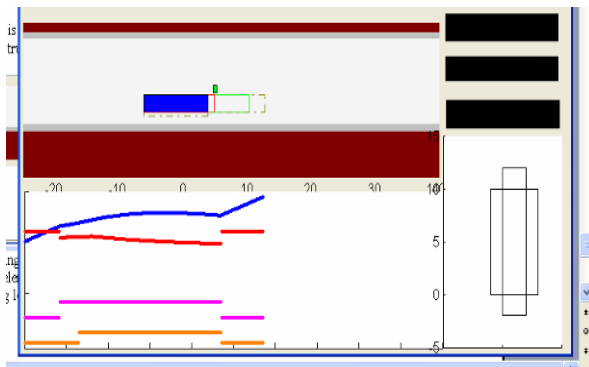


Figure 7: Speed limitation UC step 3

The speed limitation was sufficient to avoid the collision and all warning and active control have now disappeared (Figure 7).

Example 2: Urgency Braking

The same UC is running except that the pedestrian speed is adjusted to walk slowly at 2 km/h.

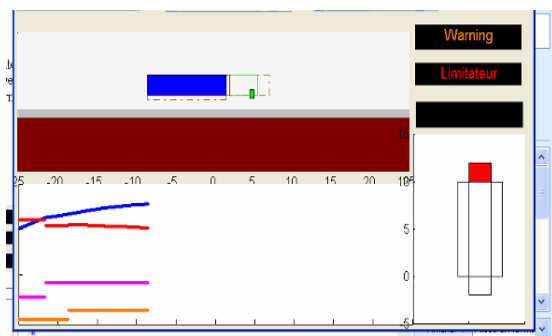


Figure 8. Urgency braking UC step 1

The beginning is the same as in example 1 (Figure 8). The pedestrian enters in the warning and limitation zone.

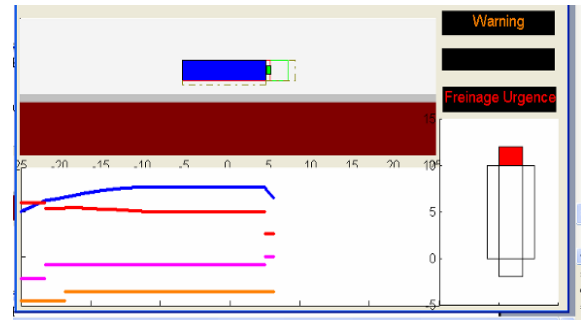


Figure 9. Urgency braking UC step 2

But the pedestrian is not walking quickly enough to leave the “Urgency Braking” area and the hard braking goes off (Figure 9).

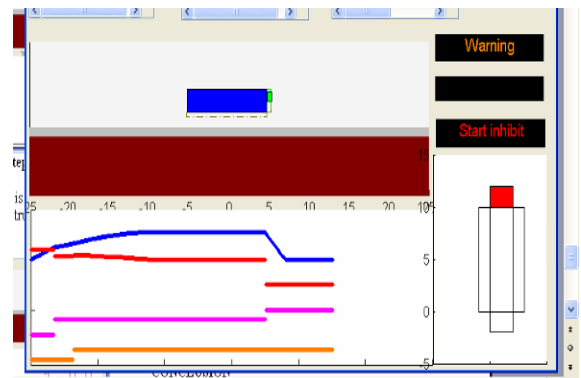


Figure 10. Urgency braking UC step 3

The “start inhibit” system is active since the pedestrian is just in front of the truck (Figure 10).

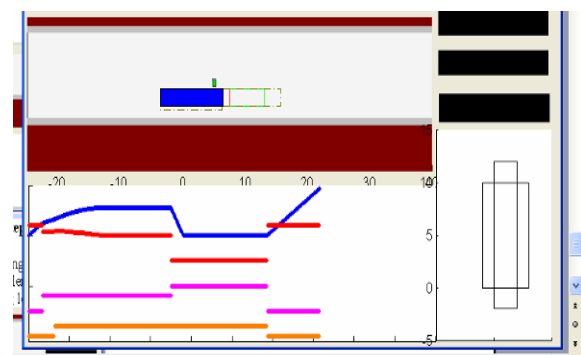


Figure 11. Urgency braking UC step 4

When the pedestrian leaves the zone, the warning message goes out (Figure 11).

Example 3: DUC on Intersection

Several types of infrastructure (figure 12) can be used in the DUC.

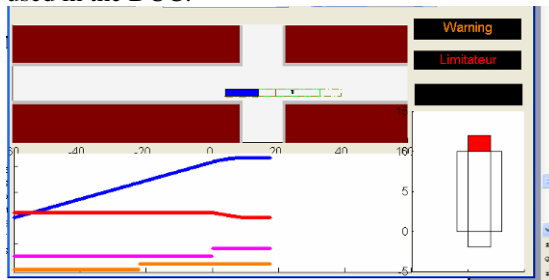


Figure 12. UC on intersection

DISCUSSION

As shown in the examples, a change in just one parameter value (in the example, the pedestrian speed) may induce a different system functioning. All these changes cannot be described in classical Use case, due to too high a number of use cases. But most of the combinations have to be tested to validate the global system functioning. This tool allows to create “Dynamic Use Case” with several variants and testing for each of them, whether the real functioning corresponds to the expected one or not.

The DUC temporal aspect can be analysed using the curves. Moreover, additional functionalities like “pause” or “scenario speed” allow the designer to run the DUC either slowly to show some details or quickly to analyse long sequences.

Another advantage of this tool is to tune the driving assistance system. For example, the parameters which define the areas in front of the truck can be easily changed and all DUC variant can be validated with the new values. This set of variants can be considered as unitary tests to be applied after any change in the driving assistance system.

EXPERIENCE FEEDBACK

We have used this tool to design and develop a Driving assistance System. The early design phase was completed using this DUC generator and all major concepts were correctly designed. The software transfer into the implementation platform was immediate and the time gain was successful as planned. But some unexpected problems appeared. The first one concerns the dynamic model of the truck. The simple model used in the generator was not precise enough and some adaptation had to be done to take into account some truck specificity, especially to calculate the urgency braking distance. This problem was solved in one day during the implementation phase. The second

problem affects the parameters used to describe driver activity. The driver model outputs were not the same as simulator one. For example, the gear box type (manual to automatic) can induce different driver actions. This problem was impossible to anticipate due to the fact that it was linked to the simulator model implementation. The last point concerns the system tuning. In the DUC generator the phase chain was correctly designed. But the final absolute values of the driving assistance system parameters had to be set according to the recommendation of ergonomics experts made during an expertise of the system before the final evaluation.

CONCLUSION

This design of Driving Assistance System (DAS) shows the contribution of a Dynamic Use Case generator which allows us to apprehend driving situation complexity and its temporal progress by taking into account all actors (pedestrians, drivers, vehicles...) and assistance effects on the scenario evolution.

This generator offers a light and simple way to early design, tune and test DAS functioning in progressing situations. It was validated by designing a DAS that warns truck drivers to avoid pedestrian collisions. It allowed us to build scenarios with specific parameters about drivers, trucks, pedestrians and assistance. The driver model will be improve to create some DUC variants which can explain some real situations.

To further efficient early design, the tool stays light and easy to use. As a consequence, the actor temporal evolution models are kept simple especially the truck model. Once the DAS functioning was validated, the expertise phase in more realistic conditions allowed finalizing the criteria adjustments in order to ensure the driver’s warning efficiency. The final experiment is currently carried out to evaluate the final DAS with end users.

REFERENCES

- [1] Maincent, A., Brun, L., Martin, R., (2008). « Pedestrians’ representations about risky behaviours in urban areas”, Proceedings of International Conference on Traffic and Transport Psychology, Washington, septembre 2008: Elsevier
- [2] Mathern B, Bonnard A, Tattegrain H, “Method of driving assistance system design to improve human vehicle interaction and safety development for truck”, 21st International Technical Conference on the Enhanced Safety of Vehicles (ESV) Stuttgart, Germany, June 15-18, 2009, paper 09-0472

A STUDY OF BICYCLIST ACCIDENTS IN CHANGSHA OF CHINA AND HANNOVER OF GERMANY

Chunyu Kong, Jikuang Yang

Research Center of Vehicle and Traffic Safety, State Key Lab of Advanced Design and Manufacture for Vehicle Body, Hunan University, Changsha, China

Dietmar Otte

Accident Research Unit, Hannover Medical University, Germany

Paper Number 09-0504

ABSTRACT

Bicyclists represent a population with high risk of traffic injuries since they are unprotected in vehicle collisions. A study was conducted with an in-depth analysis of bicyclist accidents in China and Germany. The analysis is to identify the hazard of bicyclists in Changsha and to propose the way to reduce the number of these accidents and also severity of injuries. The analysis was carried out in terms of the causes of injury, injury severity and distribution and also type of vehicle involved, accident type, road environment, time distribution etc. The accident cases that occurred from 2001 to 2006 were collected from IVAC database in Changsha, China and GIDAS database in Hannover, Germany. Based on specified sampling criteria, 1,013 bicyclist cases and 1806 cases were selected from the two databases, respectively. Statistical analyses and comparative analyses were carried out with the sampling data. The results show that there were similarities and differences regarding bicyclist accidents between Changsha and Hannover, especially for the frequency and age distribution of the fatalities and also the road environment where accidents occurred. The results from this study suggested that there is a great potential for reduction of the accidents and fatalities by safety countermeasures, such as usage of helmet and improvement of road environment in countries like China.

Keywords: bicyclist accidents, statistical analysis, circular distribution analysis

1 INTRODUCTION

The bicyclist accidents are considered to be an important issue regarding urban traffic safety in China. At present it is estimated that in China more than 500 million^[1] bicycles are used. China is a country with the largest number of bicycles over the world. Bicycle is one of the most popular tools for travel in urban areas. The report^[2] states that more than 30% of residents

travel by bicycle - not other transportation modes. Bicyclists represent a population at high risk injuries since they are unprotected in collisions with vehicles.

It is reported^[3] that in China during 2006, about 0.38 million traffic accidents with all together 520,000 casualties (fatalities and injuries), of these were 43,781 (8.4 %) bicyclists, and in this group 8471 (19.3%) were killed.

In comparison in Germany during year 2006, about 2.2 million traffic accidents were registered with altogether 427,000 casualties (fatalities and injuries). Of these 77,054 (18 %) were bicyclists, however only 486 (0.6 %) were killed^[4].

These differences are so significant that we decided to make a comparative study to better understand the factors influencing this situation.

2 METHOD AND MATERIALS

2.1 Accident data collection

The bicyclist accident cases from the IVAC database from Changsha and GIDAS database from Germany were collected based on the following criteria: (1) the accident occurred during the period from 2001 to 2006, and (2) the bicyclist accidents occurred in the urban area.

2.1.1 Accident data from police sector in Changsha

Changsha is the capital city of the Hunan province located in the middle of China, with a population of 2.06 million (6,133,000 including residents in suburb) and 452,809 registered vehicles in 2006^[5].

An ad-hoc working team has been organized in Hunan University in co-operation with traffic authority sectors and hospital in Changsha. In-depth traffic accident investigations are carried out and all information is saved in database (IVAC). The accident data is collected from the traffic authority sectors and hospital in Changsha.

In the current study an analysis on police documentations of bicyclist accidents from 2001 to

2006 was carried out, and the 1013 cases were selected for a statistical study. The information about location and type of an accident, vehicle involved in accident, as well as road environment etc. was considered. In the study we used the three levels of victim's injuries: minor, serious or fatal.

2.1.2 GIDAS accident data from Hannover Medical University

In the district of Hannover a representative sampling of accidents was carried out by Accident Research Unit at Medical University of Hanover in cooperation with the FAT (Automotive Industry Research Association) and BASt (Federal Road Research Institute) since the year 1990. In the area of Hannover nearly 1000 accidents with injured person are collected annually [6]. These accident cases were documented in the database GIDAS (German In-Depth Investigation Accident Study). The 1806 bicyclist accident cases were selected from GIDAS database from the accident occurred between 2001 and 2006.

2.2 Statistical analysis of bicyclist accidents

A statistical study with aim to compare bicyclist accident events was conducted by using the selected cases. A general statistical analysis was carried out using the cases in terms of type and number of vehicle involved in accident, accident time, accident type, injury distributions and injury severity and also age, gender of victim, etc.

2.2.1 The circular distribution analysis method

The time occurrence of bicyclist accidents within a day and night was analyzed using circular distribution method^[7] where a cyclical scale of 0-360° was used. We investigated this distribution and desired to determine if there was some predominant direction (peak time — the time of the day when we can observe maximum number of accidents; and rush hours — time period with heavy bicycle traffic) of time distribution. In circular distribution the mean angle $\bar{\alpha}$ represents the predominant direction. After the mean angle $\bar{\alpha}$ being converted to the time it means the peak time of accidents within a day. The rush hour ranges from $(\bar{\alpha} - S)$ to $(\bar{\alpha} + S)$.

As circular data of accident time were recorded in a frequency table, the following computations are needed for the coordinates (x, y) of the sample mean angle:

$$x = \frac{\sum f_i \cos \alpha_i}{\sum f_i}, \quad y = \frac{\sum f_i \sin \alpha_i}{\sum f_i}$$

and, then get $r = \sqrt{(x^2 + y^2)}$ (1)

where α_i is the midpoint of the recorded measurement's interval, f_i is the frequency of occurrence of the data within the interval, r is the length of the mean vector.

The value of $\bar{\alpha}$ is determined as the angle fulfilling the following equations:

$$\cos \bar{\alpha} = \frac{x}{r}, \quad \sin \bar{\alpha} = \frac{y}{r} \quad (2)$$

Circular standard deviation (S) will be:

$$S = \frac{180}{\pi} \sqrt{-2 \ln r} \quad (3)$$

In our study the r is a measure of concentration of accident over the time. This value varies inversely with the amount of dispersion in the accident data. It has no unit and it may vary from 0 when there is so much dispersion that a mean angle can not be described to 1.0 when all the data are concentrated at same direction. A measure of dispersion can be expressed as: $1 - r$. Lack of dispersion will be if: $1 - r = 0$, and maximum of dispersion if: $1 - r = 1.0$.

The significance of the mean angle was tested by the Rayleigh test. Our hypothesis H_0 is:

H_0 : The accident time distribution in a day is uniformly distributed around the circle.

Rayleigh's Z is utilized for testing the H_0 :

$$Z = nr^2, \quad n = \sum f_i \quad (4)$$

If $Z > Z_{0.05}$ ($Z_{0.05}$ can be found in the statistical table), H_0 is rejected, we may conclude that there is a peak time within a day, and if $Z < Z_{0.05}$, we may conclude that accident time distribution with in a day to be uniform around the circle.

Furthermore, to determine if there was difference between peak times of two cities a test was made by Watson-William method, it was calculated as follows:

$$t = \frac{\sqrt{K(N-2)(R1+R2-R)}}{\sqrt{N-R1-R2}};$$

$$R1 = n_1 r_1; \quad R2 = n_2 r_2; \quad R = Nr \quad (5)$$

where: r_1 and r_2 are the length of the mean vectors of data (from circular distributions analysis) from Changsha and Hannover respectively.

R is the length of the mean vector of data but from the united samples from Changsha and Hannover.

n_1 , n_2 and N are frequencies of these samples.

K is a correction factor.

We were testing the hypothesis:

H_0 : The peak times of bicyclist accidents in Changsha and Hannover are equal.

If $t < t_{0.05}$, H_0 is accepted and we may conclude that the peak times within a day in Changsha and Hannover are significantly same.

3 RESULTS AND ANALYSIS

The results from comparative statistical analysis based on the selected bicyclist accident cases are presented for the frequency of bicyclist accidents, injuries, and injury severities.

Table 1 Distribution of vehicle type in bicyclist accidents

Vehicle	Changsha, China		Hannover, Germany	
	N	%	N	%
Truck	122	12.0	95	5.3
Bus	104	10.3	27	1.5
Passenger car	593	58.5	1157	64.1
Motorcycle	161	15.9	20	1.1
Bicycle	-	-	223	12.4
Pedestrian	11	1.1	59	3.3
None	1	0.1	223	12.4
Others	21	2.1	2	0.1
Total	1013	100	1806	100

3.1 Analysis of involvement of vehicles

The distribution of vehicle types in bicyclist accidents in Changsha and Hannover is presented in Table 1. In Changsha the passenger cars were involved in 58.5% of the bicyclist accidents, motorcycles and trucks in about 15.9% and 12.0% of these accidents, respectively. In Hannover the passenger cars accounted for 64% of reported bicyclist accidents, which indicated the passenger cars are involved more frequently in bicyclist accidents than in Changsha.

3.2 Injury severity

Among all casualties in Changsha, 5% bicyclists were killed, 5.4% bicyclists were serious injured, 85.6% were slightly injured, and 4% had no injuries (Table 2). In Hannover, the relative frequency of the bicyclist fatalities (0.8%) is much lower than that in Changsha. The relative frequency of the slightly injured bicyclists is on the same level both in Changsha and Hannover.

Table 2 Proportions of bicyclist injury severity

Severities	Changsha, China		Hannover, Germany	
	N	%	N	%
Fatalities	51	5.0	15	0.8
Seriously injured	55	5.4	318	17.6
Slightly injured	867	85.6	1345	74.5
No injuries	40	4.0	128	7.1
Total	1013	100	1806	100

3.3 Age and gender

The distributions of relative involvement in bicyclist accidents by the age and gender are similar in both Changsha and Hannover. In both towns, male had a higher rate of involvement in accidents for example in Changsha: male 60%, and female 30%, unknown 10%; in Hannover: male 57%, and female 43%. Regarding the age, bicyclists ranged from 36-40 years old have a high frequency of involvement compared with other age groups.

Table 3 Age vs. Injury severity

Age	Changsha, China (%)				Hannover, Germany (%)			
	Fatalities	Seriously injured	Slightly injured	No injuries	Fatalities	Seriously injured	Slightly injured	No injuries
0-5	-	-	0.6	-	-	1.3	1.1	3.9
6-10	-	-	0.1	-	-	3.5	3.3	3.1
11-15	3.9	5.5	6.1	10	-	10.7	8.3	12.5
16-20	-	7.3	9.8	20	6.7	4.7	8.0	10.9
21-25	-	3.6	7.2	7.5	-	3.8	7.7	7.8
26-30	9.8	5.5	7.5	7.5	-	4.1	8.0	7.0
31-35	5.9	7.3	7.6	7.5	13.3	7.2	6.8	8.6
36-40	15.7	23.6	10.7	15	6.7	8.2	9.7	7.0
41-45	11.8	5.5	7.8	5	6.7	6.3	7.9	9.4
46-50	13.7	7.3	11.2	7.5	-	5.0	6.8	1.6
51-55	5.9	5.5	7.2	2.5	6.7	5.7	4.8	4.7
56-60	7.8	12.7	4.3	-	6.7	5.7	5.7	3.9
61-65	9.8	5.5	3.1	2.5	6.7	9.1	6.1	0.8
66-70	7.8	3.6	3.5	-	13.3	6.6	5.0	3.1
71-75	2.0	5.5	1.2	2.5	20.0	8.2	4.3	1.6
76-80	2.0	-	0.5	-	6.7	5.3	3.2	3.1
81-85	-	-	0.2	-	6.7	3.8	1.1	-
86-90	-	-	-	-	-	0.6	0.3	-
Unknown	3.9	1.8	11.5	-	-	0.3	1.6	-
Total	100	100	100	100	100	100	100	100

3.4 Age and injury severity

Table 3 shows the distribution of injury severity by different age groups. The frequency of fatalities by the age in Changsha is different from the situation in Hannover. It indicates that in Changsha 41.2% of fatalities were bicyclists 36-50 years old and 21.6% of fatalities were these above 60 years old. In Hannover 53.3% of fatalities were bicyclists above 60 years old.

3.5 Circular distribution analysis with 24-hour accident time

Accident data were divided into 24 (15 degree) bins (Table 4). The mean angles of two samples (212.07 degree in Changsha and 211.02 degree in

Hannover) were found. Rayleigh's test indicated that the distribution was not uniform (in Changsha: $p < 0.05$, $r = 0.2447$; in Hannover: $p < 0.05$, $r = 0.4997$). The results indicated that the most frequently bicyclist accident time of a day was 14:08, the period of rush hour was 7:44 - 20:33 ($\bar{\alpha} \pm S$) in Changsha. In comparison in Hannover the most frequently time was 14:04 and the rush hour ranged 9:34 - 18:34 (Table 5).

Using the Watson-William test method the value of t was calculated according to the Equation (5). We obtained $t = 0.28$ that is lower than $t_{0.05} = 1.96$. That means the most frequently bicyclist accident time in Changsha and Hannover are same.

Table 4 The 24 hours circular distribution analysis

Time	Changsha, China				Hannover, Germany			
	f	α	$f \sin \alpha$	$f \cos \alpha$	f	α	$f \sin \alpha$	$f \cos \alpha$
00:00-00:59	27	7.5	3.5	26.8	16	7.5	2.1	15.9
01:00-01:59	18	22.5	6.9	16.6	3	22.5	1.1	2.8
02:00-02:59	7	37.5	4.3	5.6	2	37.5	1.2	1.6
03:00-03:59	3	52.5	2.4	1.8	3	52.5	2.4	1.8
04:00-04:59	6	67.5	5.5	2.3	3	67.5	2.8	1.1
05:00-05:59	10	82.5	9.9	1.3	7	82.5	6.9	0.9
06:00-06:59	48	97.5	47.6	-6.3	33	97.5	32.7	-4.3
07:00-07:59	94	112.5	86.8	-36.0	111	112.5	102.6	-42.5
08:00-08:59	60	127.5	47.6	-36.5	93	127.5	73.8	-56.6
09:00-09:59	44	142.5	26.8	-34.9	105	142.5	63.9	-83.3
10:00-10:59	54	157.5	20.7	-49.9	127	157.5	48.6	-117.3
11:00-11:59	57	172.5	7.4	-56.5	124	172.5	16.2	-122.9
12:00-12:59	46	187.5	-6.0	-45.6	142	187.5	-18.5	-140.8
13:00-13:59	56	202.5	-21.4	-51.7	121	202.5	-46.3	-111.8
14:00-14:59	57	217.5	-34.7	-45.2	134	217.5	-81.6	-106.3
15:00-15:59	41	232.5	-32.5	-25.0	154	232.5	-122.2	-93.7
16:00-16:59	53	247.5	-49.0	-20.3	133	247.5	-122.9	-50.9
17:00-17:59	62	262.5	-61.5	-8.1	146	262.5	-144.8	-19.1
18:00-18:59	65	277.5	-64.4	8.5	139	277.5	-137.8	18.1
19:00-19:59	43	292.5	-39.7	16.5	73	292.5	-67.4	27.9
20:00-20:59	53	307.5	-42.0	32.3	54	307.5	-42.8	32.9
21:00-21:59	60	322.5	-36.5	47.6	39	322.5	-23.7	30.9
22:00-22:59	27	337.5	-10.3	24.9	22	337.5	-8.4	20.3
23:00-23:59	22	352.5	-2.9	21.8	22	352.5	-2.9	21.8
Σ	1013		-131.6	-210.0	1806		-465.0	-773.4

Table 5 Results of 24 hour circular distribution analyses

	Changsha, China	Hannover, Germany
x	-0.2073	-0.4283
y	-0.1299	-0.2575
r	0.2447	0.4997
$\bar{\alpha}$	212.07	211.02
S	96.14	67.49
Rayleigh's Z	60.64	450.97
$\bar{\alpha} \pm S$	7:44÷20:33	9:34÷18:34

3.6 Road line type

Comparing the accident ratio on intersections, bicyclist accidents took place more frequently in Hannover (56%) than in Changsha (13.2%) where the most common place of accident was straight road (81.4%). We can say that for this accident place the situation in Changsha is opposite to that in Hannover.

Table 6 The distribution of bicyclist accidents vs. road line type

Road line type	Changsha, China		Hannover, Germany	
	N	%	N	%
Straight	825	81.4	545	30.2
Slope	39	3.8	40	2.2
Intersection	134	13.2	1011	56.0
Others	15	1.5	210	11.6
Total	1013	100	1806	100

3.7 Type of bicyclist accidents

The type of bicyclist accidents is shown Table 7. It can be found that the most common types of bicyclist accidents were lateral impact and front impact, in both Changsha and Hannover city area. However the frontal impact is 50% more common in Hannover than in Changsha.

Table 7 Type of bicyclist accidents

Accident type	Changsha, China		Hannover, Germany	
	N	%	N	%
Lateral impact	527	52.0	871	48.2
Front impact	213	21.0	629	34.8
Rear Impact	60	5.9	75	4.2
Scratching	133	13.1	-	-
Fall	-	-	103	5.7
Roll over	1	0.1	45	2.5
Others	79	7.8	83	4.6
Unknown	1013	100	1806	100

3.8 Distribution of injuries by body regions

Table 8 shows that the lower extremities, head and upper extremities were found to be the most frequently

injured. The total 345 bicyclist cases which were used in the Table 8 were all registered in police data in Changsha, while bicyclist accidents cases with no registered injury regions were ignored. In these police data only one main injured body part was registered for each case, but in Hannover data there are multiple injuries registered regarding the bicyclist casualties. So Changsha data can only be appropriate in the preliminary comparative analyses.

Table 8 Distribution of body regions

	Changsha, China (N=345)	Hannover, Germany (N=1806)
	RF *, %	RF, %
Head	31.3	37.5
Neck	0.3	4.6
Thorax & Back	2.3	22.0
Up limbs	12.8	42.1
Waist & Abdomen	2.0	5.3
Pelvis	-	12.5
Low limbs	51.3	54.1

* RF=the number of bicyclists injured a certain part / total of casualties N

Table 9 shows that the frequency of fatalities and injuries in urban bicyclist accidents by main body parts including the head, the lower extremities and the upper extremities. It indicates that the head is most common part of the bicyclist body when injuries are classified as serious or fatal. In Changsha, 25.9% of bicyclists suffered fatal head injury. In Hannover, only 1% of these were fatal. In Changsha some limbs injuries also led the bicyclist's dead. The possible reason is that the criteria of injury severity used by Chinese policeman are rude.

Table 9 Distribution of injuries by head, low limbs and up limbs for bicyclist accidents

	Changsha, China (N=345) (%)				Hannover, Germany (N=1806) (%)				
	Slightly injured	Seriously injured	Fatalities	Total	Slightly injured	Seriously injured	Fatalities	No injuries	Total
Head	53.7	20.4	25.9	100	76.1	18.4	1.0	4.4	100
Up limbs	86.4	9.1	4.5	100	91.5	7.0	-	1.6	100
Low limbs	89.8	9.6	0.6	100	88.8	9.8	-	1.3	100

4 DISCUSSION

The present study is based upon an analysis of 1013 bicyclist accidents in urban area of Changsha in China and 1806 cases in the area of Hannover in Germany. The evaluation method is described in methodology section and the available accident data were analyzed. The quality of data is acceptable in this preliminary study. The presented methodology of comparison of different in-depth accident studies could

be used for evaluation of the injury risk and injury outcome in different countries. Such methodology can be used for further studies with new accident data in the area of special research issues.

4.1 Involvement of vehicle

Table 1 shows that passenger cars are most frequently involved in bicyclist accidents in both Changsha and Hannover. For this reason the safety

design of passenger cars considering bicyclists is vital for reducing the injury risk of bicyclists. It is also found that in Changsha compared to Hannover motorcycles, trucks and buses are more frequently involved in bicycle accidents. In addition we have to say that there are differences also in vehicle types. Most motorcycles registered in police data in Changsha are three-wheel light motorcycles when in Hannover are heavy motorcycles. Due to the difference of involved vehicles between countries, the priority of safety countermeasures should be given considering the frequency of involved vehicles.

4.2 Bicyclist injuries

The bicyclist accident is a common problem in both motorized countries and motorizing countries, which occur frequently in city area. The all results of the analysis of the two different areas of China and Germany show major resources for further countermeasures on car safety developments.

It was found that both in Changsha and Hannover the male bicyclist had a higher rate of accidents than the female one. It can be explained by the fact that male had more opportunities to work or travel by bicycle. We also found that bicyclists ranged from 36-40 years old have a higher percentage compared with other age groups. It is directly related to the fact that they are exposed to traffic more frequently when working and taking part in social activities.

The injury severity and risk to die in accident for bicyclists in Hannover can be seen as much lower as in Changsha. One possible reason of this high relative frequency is related to the layout of urban traffic network^[8]. The design of road traffic system in most of cities in China doesn't consider bicyclists as road users. Consequently bicyclists are more frequently exposed to a mixed traffic situation including motor vehicles. Therefore the risk of bicyclist fatalities is high. The other reason is due to that the bicyclists travel in Changsha without using any helmets. The protection effect of helmets in bicycle accident is known since 1980's. For example, a conclusion was made by Kroon et al.^[9] that bicycle helmets, even simple ones, could be recommended for cyclists of all categories as they protect against head injuries, at least against head injuries of minor severity. Another report^[10] stated that the risks of serious head injuries had reduced by 85% with wearing helmets in vehicle-bicyclist accidents.

As it was shown in Table 3, frequency distribution of fatalities by the age in Changsha is quite different from that in Hannover. The possible reason for this situation is that bicycles are used differently in these two countries. In China, bicycles is one of the most popular means for living and work and are often chosen by middle aged people. In Germany, bikes are usually

used by young and the elderly for pleasure, trip and besides commuting purpose.

The findings of the distribution of bicyclist injuries were compared in our study between the results from both cities. As a common tendency, the head, lower extremities and upper limbs have been found to be the most frequently injured body regions. This confirmed the findings from several studies performed already at 80's and 90's in European countries^[11, 12].

4.3 Accident time

Initial approaches using a linear scale were not fruitful. For this reason 24-hour time distribution of accidents was analyzed by circular distribution method. The most frequently bicyclist accident time of a day was proved to be existed by Rayleigh's Z test and the rush hours of bicyclist accidents in Changsha and Hannover were tested to be identical by Watson-William method. Whereas the period of heavy traffic in a day in Changsha is longer than that in Hannover: 7:44-20:33 versus 9:34-18:34.

4.4 Accident type & road line type

Lateral impact is the most frequent type of bicyclist accident. According to results from the study we can see that most accident cases in Hannover occurred at intersection. However in Changsha the main accident places is straight road. These results indicate that it is a potential to improve the bicyclists safety in both cities.

4.5 Limitations

It has to be noticed that the limitations existed in the study. The data sources partly reflect the real situations of bicyclists in traffic accidents in Changsha and Hannover and not in the whole country. Compared to this the data of GIDAS are comprehensive and give information on every issue of accident and injury details.

Another problem existed with the police records in Changsha: they provided data on the injury severity that seldom included exact details of the locations and severity of the injuries. Therefore it make difficult to compare them with the injuries coded according to the AIS. This problem can be solved by further in-depth studies using detailed accident data collected from hospital and police sectors, as well as on-site and retrospective investigations.

5 CONCLUSIONS

Bicyclists represent a group of vulnerable road users with high risk of injuries, therefore a priority

should be given to this road user group in research of safe urban transportation.

There are some similarities regarding bicycle accidents in developed country (Hannover, Germany) and developing one (Changsha, China). Male bicyclist shows a higher involvement rate in vehicle-to-bicycle accidents than female one. Passenger cars are most frequently involved in bicyclist accidents. The most bicyclist cases occurred at the same time of a day. The study confirmed that head, lower extremity and upper limbs injuries are dominant. The head injuries are the main cause for the high frequency of bicyclist fatalities especially in Changsha.

There are also some differences between the two cities,. It was found that in Changsha the frequency of bicyclist fatalities is much higher, more often young bicyclists are involved in fatal accidents and the time period of rush hour is longer, besides accident place in Changsha is opposite to that in Hannover.

There are different possibilities to reduce the number and the risk of bicyclist fatalities in Changsha. One of the possible solutions is to make the use of helmets popular because it has good protection effect.

The further in-depth study is needed to develop efficient counter-measures for improvement of bicyclist safety.

6 ACKNOWLEDGEMENTS

The study in Changsha (China) is sponsored by the Education Ministry of China in “111 program” No. 111-2-11, the GM Research & Development Center RD-209. The study in Hannover (Germany) is financed by Federal Road Research Institute (BAST) in cooperation with Research association of Automotive Manufactures (FAT). The authors would like to thank Mr. Chao Zhang, and Mr. Zhimin Liu, the Director of Traffic Police Section in Changsha, and Joachim Nehmzow, Hannover Medical University, for providing accident data, Dr. Janusz Kajzer (Sweden) for valuable advice.

REFERENCE

- [1] Qiao WG. (2005). Study of the Accident Modalities and the Protective Methods about Motorcycle, Bicycle, Pedestrian Collisions. Thesis for the Degree of Doctor. Wuhan University of Technology. (in Chinese)
- [2] Li S. (2007). A Study on Head-Brain Protections of Cyclists in Vehicle-Bicycle Collisions. Thesis

for the Degree of Master. Hunan University. (in Chinese)

- [3] Traffic Administration (2006). Statistics of Road Traffic Accidents in P.R. of China. Ministry of Public Security. (in Chinese)
- [4] Statistical Bureau (2006). Statistical Data from Germany, Wiesbaden.
- [5] Kong CY, Yang JK, Li L, Li WQ, Zhao Z, Otte D. (2006). In-Depth Investigation of Vehicle Traffic Injuries in Changsha of China, International Conference on Expert Symposium on Accident Research (ESAR), Hannover, Germany. pp.38-46.
- [6] Otte D, Krettek C, Brunner H, Zwipp H. (2003). Scientific Approach and Methodology of a New In-Depth-Investigation Study in Germany so called GIDAS, Proceedings of the 18th ESV Conference, Nagoya, Japan, Paper No. 03-161.
- [7] Jin PH. (2003). Methods of Statistics in Medicine. Fudan University. ISBN: 730903653. Issue.2. pp.211-217. (in Chinese).
- [8] Liu Q. (2006). Effective Urban Roads System in Germany. Urban Planning International. (in Chinese).
- [9] Kroon PO, Bunketorp O, and Romanus B. (1986). The Protective Effect of Bicycle Helmets - A Study of Paired Samples in a Computer – Based Accident Material in Gothenburg, Sweden. International Conference on the Biomechanics of Impact (IRCOBI). pp249.
- [10] Fatality Facts: Bicycles. Insurance Institute for Highway Safety, 1999. Web sitS: http://www.highwaysafety.org/safety_facts/fatality_facts/bikes.htm.
- [11] Otte D. (1980). A review of different kinematic forms in two-wheel-accidents-their influence on effectiveness of protective measures. Society of Automotive Engineers, Inc., 24th Stapp Car Crash Conference, Troy, Michigan, USA. pp.575.
- [12] Otte D. (1989). Injury mechanism and crash kinematic of cyclists in accidents-An analysis of real accidents. Society of Automotive Engineers, Inc., 33rd Stapp Car Crash Conference, Washington, DC, USA. pp. 3-5.